# COPPER PHOTOSENSITIZERS IN PHOTOCATALYTIC HYDROGEN PRODUCTION

---

**Dissertation**

zur

**Erlangung der naturwissenschaftlichen Doktorwürde (Dr. sc. nat.)**

vorgelegt der

**Mathematisch-naturwissenschaftlichen Fakultät**

der

**Universität Zürich**

von

**Johannes Windisch**

von

**Densbüren AG**

**Promotionskommission**

Prof. Dr. Roger Alberto (Vorsitz)

Dr. Benjamin Probst (Leitung)

Prof. Dr. Peter Hamm

Prof. Dr. Greta Patzke

Zürich, Februar 2017

*To my family*

## Zusammenfassung

Die vorliegende Doktorarbeit legt ihren Hauptfokus auf die Synthese von Kupfer(I) bis-Phenanthrolin Photosensitiser (PS) und deren Anwendung zur photokatalytischen Wasserstoffproduktion in Verbindung mit Kobalt-basierten Wasser-Reduktions-Katalysatoren (WRC). Solch ein edelmetallfreies System konnte erfolgreich realisiert werden, mithilfe eines Elektronen-Mediators zwischen PS und WRC, der den notwendigen Elektronentransfer erst ermöglicht. Durch eine detaillierte mechanistische Untersuchung des katalytischen Zyklus konnten die limitierenden Faktoren des Systems aufgezeigt werden. Ein wichtiger Punkt scheint die Zersetzung des PS während der Katalyse zu sein, was auf den Verlust mindestens eines Liganden zurückzuführen ist. Die Behebung dieser Stabilitätsprobleme stellt den zweiten Hauptteil der voliegenden Arbeit dar. Verschiedene Strategien und Synthesen in Richtung eines tetraedrischen Käfigliganden, der eine perfekte Umgebung für Kupfer(I) bieten würde, werden beschrieben. Auch wenn dieses Molekül bisher nicht isoliert werden konnte, gab es trotzdem einige vielversprechende Zwischenprodukte und zahlreiche Erkenntnisse, die eine zielgerichtete Fortführung des Projekts ermöglichen.

## Summary

The thesis at hand focuses on the synthesis of copper(I) bis-phenanthroline photosensitizers (PS) and their incorporation into a system for photocatalytic hydrogen evolution by combining them with cobalt based water reduction catalysts (WRC). The viability of such a noble metal-free system was successfully demonstrated by introducing an electron relay, which is necessary to enable the electron transfer between the PS and WRC. A detailed mechanistic analysis of the catalytic cycle allowed for the identification of performance limiting factors. Most strikingly, the PS was shown to decompose during catalysis, due to ligand decomplexation. These stability issues were addressed in the second major part of the thesis. Various strategies and syntheses towards a cage-like ligand with a tetrahedral pocket, which would be perfect to accommodate copper(I), are described. Although such a molecule remained elusive so far, promising intermediates were isolated and important insights were gained to further pursue this goal in a more directed manner.

## Objective

The overall goal of this thesis was to replace noble metal-based photosensitizers commonly used in molecular photocatalytic hydrogen evolution with more abundant materials, namely first row transition metals. This is an important step, in order to make artificial photosynthesis for energy production economically more viable. In particular, the focus will be on $Cu^{I}$ bis-phenanthroline complexes, due to their promising photophysical properties. After establishing a general understanding of these compounds, they will be incorporated into a three component system for hydrogen evolution.

Furthermore, new ligands will be synthesized, tailored to improve photocatalytic performances. Since a low stability of the $Cu^{I}$ complexes turned out to be a major issue, the preparation of a tetrahedral cage ligand will be the main goal of these synthetic efforts, besides efforts to increase the solubility of the compounds.

## Abbreviations

| | |
|---|---|
| $AscH_2$ | Ascorbic acid |
| bpy | 2,2‘-Bipyridine |
| btmopp | 2,9-Bis(3,4,5-trimethoxyphenyl)-1,10-phenanthroline |
| BuLi | Butyllithium |
| COD | 1,5-Cyclooctadiene |
| DBU | 1,8-Diazabicyclo[5.4.0]undec-7-en |
| DCM | Dichloromethane |
| DMAP | *N*,*N*-Dimethylpyridin-4-amine |
| DME | 1,2-Dimethoxyethan |
| dmesp | 2,9-Dimesityl-1,10-phenanthroline |
| DMF | *N*,*N*-Dimethylfromamide |
| dmp | 2,9-Dimethyl-1,10-phenanthroline |
| dpotmp | 2,9-Dipropan-3-ol-1-yl-3,4,7,8-tetramethyl-1,10-phenanthroline |
| dsbdpp | 2,9-Di-*sec*-butyl-4,7-diphenyl-1,10-phenanthroline |
| dsbdspp | 2,9-Di-*sec*-butyl-4,7-bis(sulfonatophenyl)-1,10-phenanthroine |
| dsbp | 2,9-Di-*sec*-butyl-1,10-phenanthroline |
| dsbtmp | 2,9-Di-*sec*-butyl-3,4,7,8-tetramethyl-1,10-phenanthroline |
| dtbp | 2,9-Di-*tert*-butyl-1,10-phenanthroline |
| EtOAc | Ethyl acetate |
| Fc | Ferrocene |
| HPLC | High pressure liquid chromatography |
| HV | High vacuum |
| LAH | Lithium aluminium hydride |
| MeCN | Acetonitrile |
| MeOH | Methanol |
| MOMCl | Chloro(methoxy)methane |
| $MPP^+$ | *N*-Methyl-4-phenylpyridinium |
| Ms | Mesyl |
| NMP | *N*-Methyl-2-pyrrolidone |

| | |
|---|---|
| OTf | Trifluoromethanesulfonate |
| phen | 1,10-Phenanthroline |
| PS | Photosensitizer |
| rt | Room temperature |
| TBA | tetra-*n*-Butylammonium |
| TBS | *tert*-Butyl-dimethylsilyl |
| TEA | Triethylamine |
| THF | Tetrahydrofuran |
| TLC | Thin layer chromatography |
| Ts | Tosyl |
| WOC | Water oxidation catalyst |
| WRC | Water reduction catalyst |

# Compounds

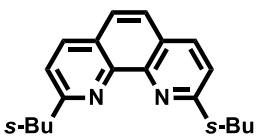


1
dsbp

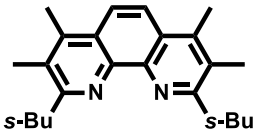


2
dsbtmp

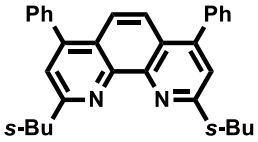


3
dsbdpp

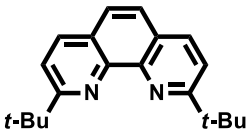


4
dtbp

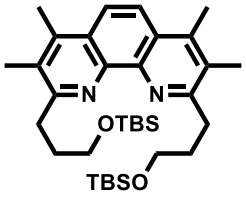


5

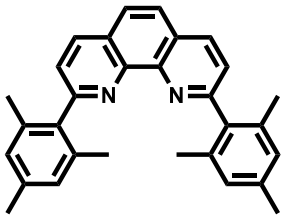


6
dmesp

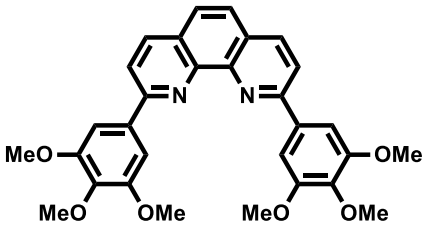


7
btmopp

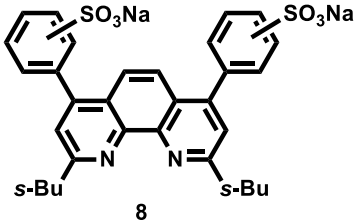


8
dsbdspp

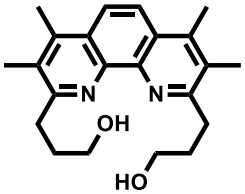


9
dpotmp

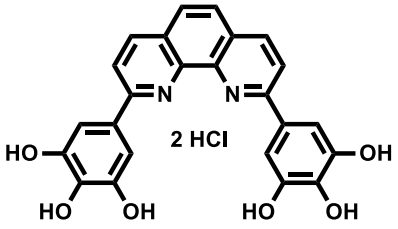


10
bthopp

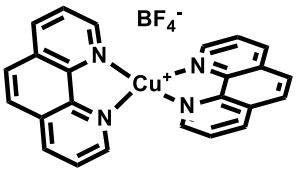


11
$[Cu(phen)_2]BF_4$

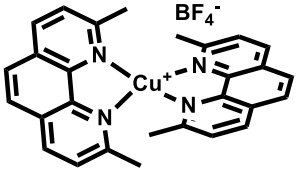


12
$[Cu(dmp)_2]BF_4$

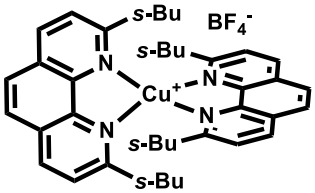


13
$[Cu(dsbp)_2]BF_4$

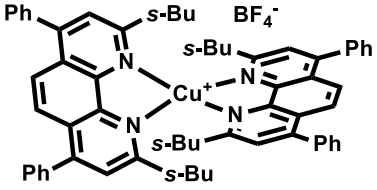


14
$[Cu(dsbdpp)_2]BF_4$

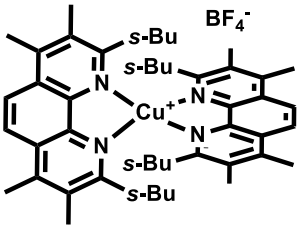


15
$[Cu(dsbtmp)_2]BF_4$

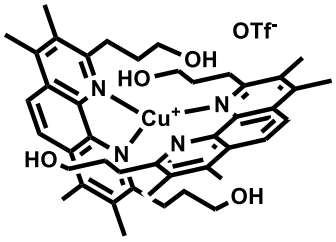


16
$[Cu(dpotmp)_2]OTf$

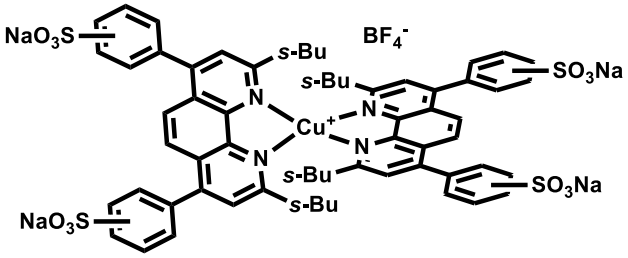


17
$[Cu(dsbdspp)_2]BF_4$

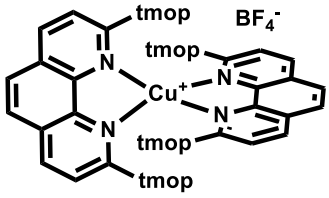


18
$[Cu(btmopp)_2]BF_4$

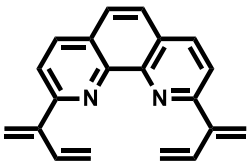


19

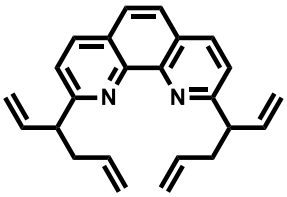


20

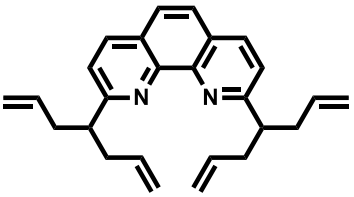


21

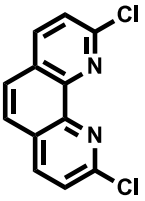


22

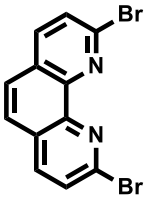


23

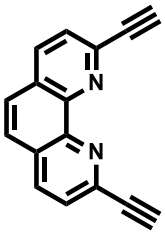


24

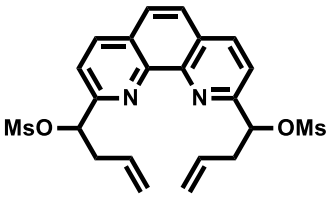


25

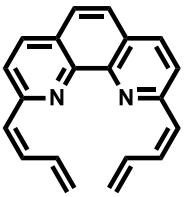


26

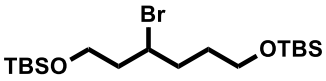


27

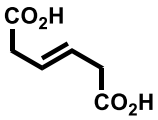


28

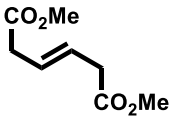


29

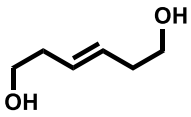


30

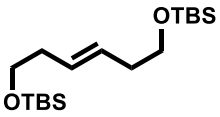


31

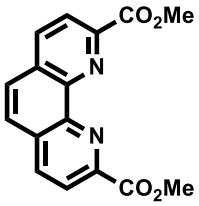


32

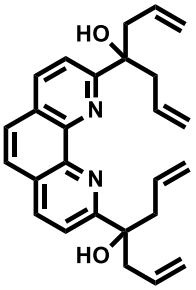


33

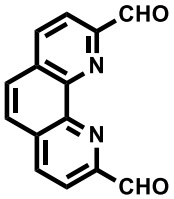


34

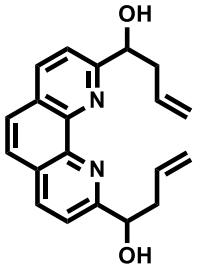


35

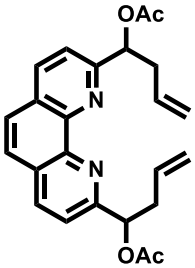


36

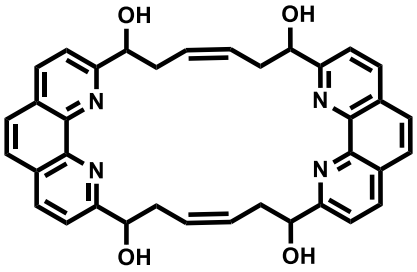


37

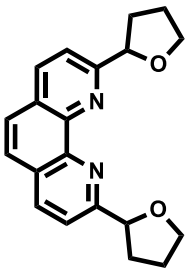


38

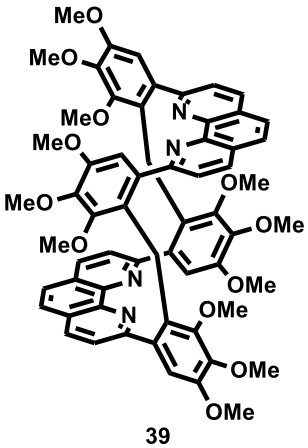


39

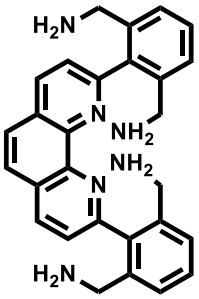


40

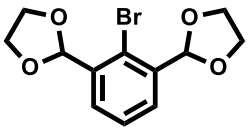


41

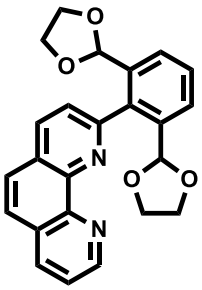


42

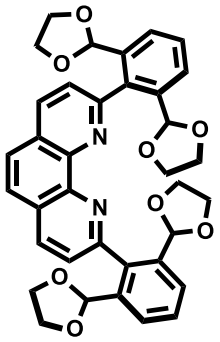


43

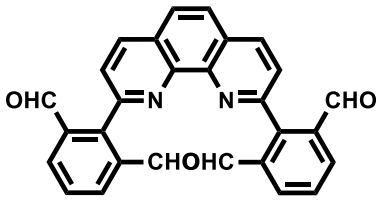


44

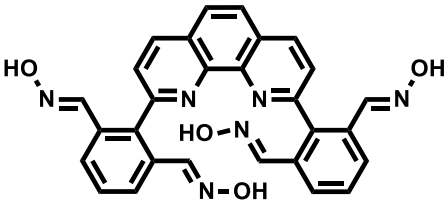


45

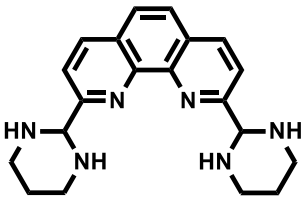


46

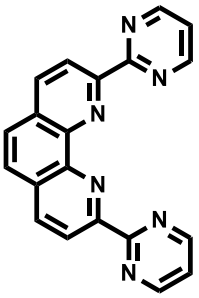


47

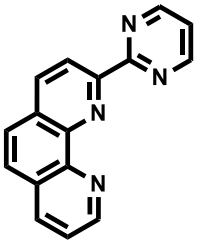


48

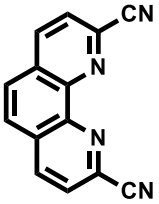


49

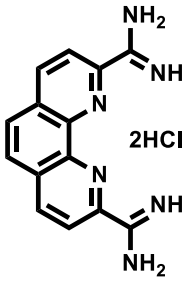


50

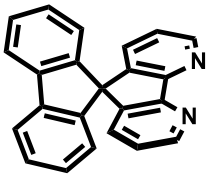


51

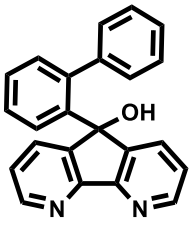


52

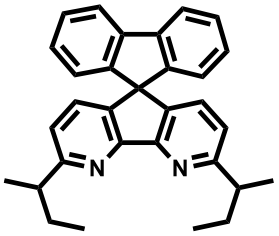


53

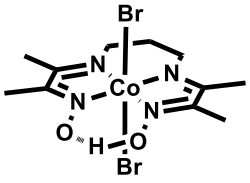


54

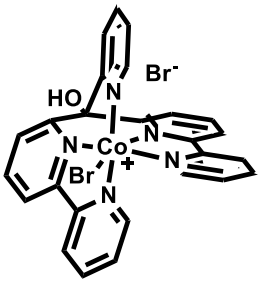


55

## Table of Contents

# 1. Introduction

## 1.1. Current Energy Situation

The demand of energy has rapidly increased over the last few decades, as reflected by the development of the world's total primary energy supply (Figure 1).[1] From 1971 to 2014, the amount has more than doubled to reach a value in 2014 of 13700 Mtoe (Mtoe = megatons of oil equivalent). This corresponds roughly to the impact energy of 13700 meteors forming Barringer craters,[2] it is equivalent to 573 exajoules ($5.73 \cdot 10^{20}$ J) or 160 PWh, which is twice the total electric energy produced by all nuclear power plants since 1954.[3] In other words, the amount of energy is inconceivable.

A closer look at the fuel composition of the energy supply shows that nowadays 86% are provided by non-renewable sources (coal, oil, natural gas, nuclear), which is virtually the same as in 1971 (88%). Considering the finite reserves, this clearly calls for the expansion of other energy sources, which today contribute to the total energy mix with only 1.4%.

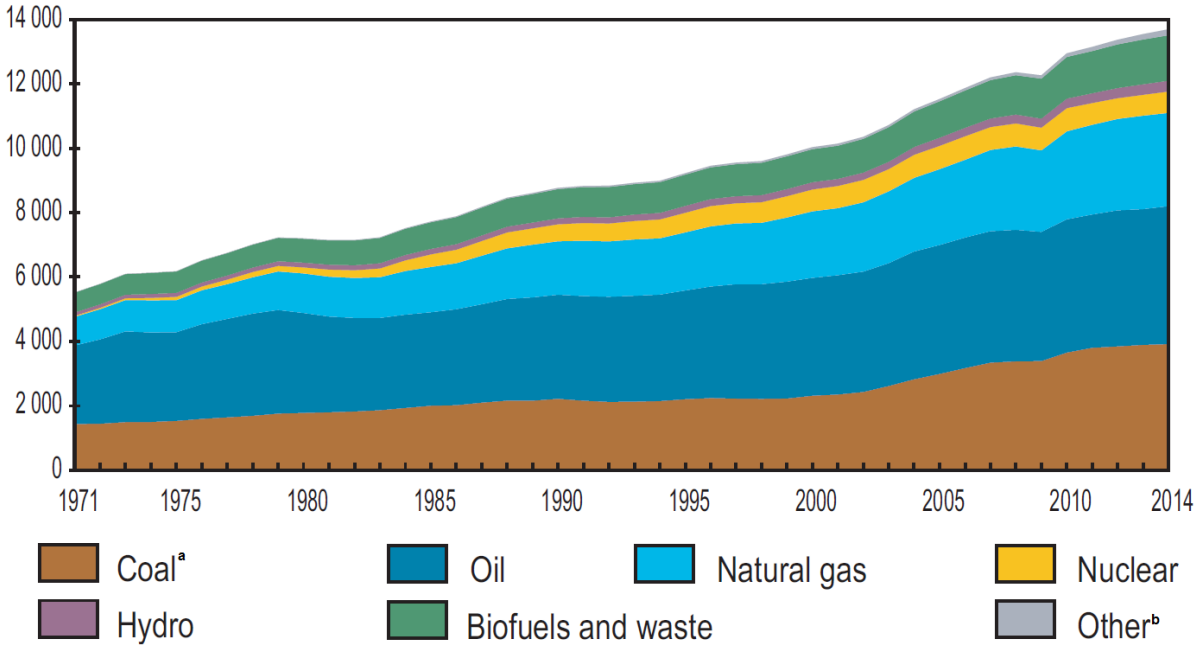


**Figure 1:** World's total primary energy supply (TPES) from 1971 to 2014 in megatons of oil equivalent (Mtoe) by fuels. [a] includes peat and oil shale; [b] includes geothermal, solar, wind, tide / wave, heat.[1]

Apart from the issue of limited resources, the burning of fossil fuels as well as the power generation by nuclear fission are accompanied by major environmental and social problems: The emission of large quantities of $CO_2$ into the atmosphere over the last century led to an atmospheric concentration of currently 400 ppm, which is the highest concentration ever observed.[4] Climate change as a consequence of the

growing $CO_2$ level has been identified as a very critical challenge facing mankind and requires immediate action.[5] Nuclear power generation was hit by major accidents in Chernobyl (1986) and more recently Fukushima (2011), which both led to the radioactive contamination of large areas and many people. Understandably, this raised many safety concerns and e.g. led to the intended nuclear power phase-out of Germany until 2022, which is also under consideration in many other countries. Furthermore, the disposal of radioactive waste is a complex issue, mostly due to the very long half-life of certain radionuclides.

Additionally aggravating is the projected increased energy demand in the future (Figure 2). This is not necessarily caused by the wasteful use of energy but mainly by the development of new industrial nations, which inherently have higher energy throughputs, as well as simply by the ever-growing population. Even when considering very conservative scenarios, as shown in Figure 2, the TPES is expected to increase significantly until 2040, with the major portion still being provided by non-renewable sources.

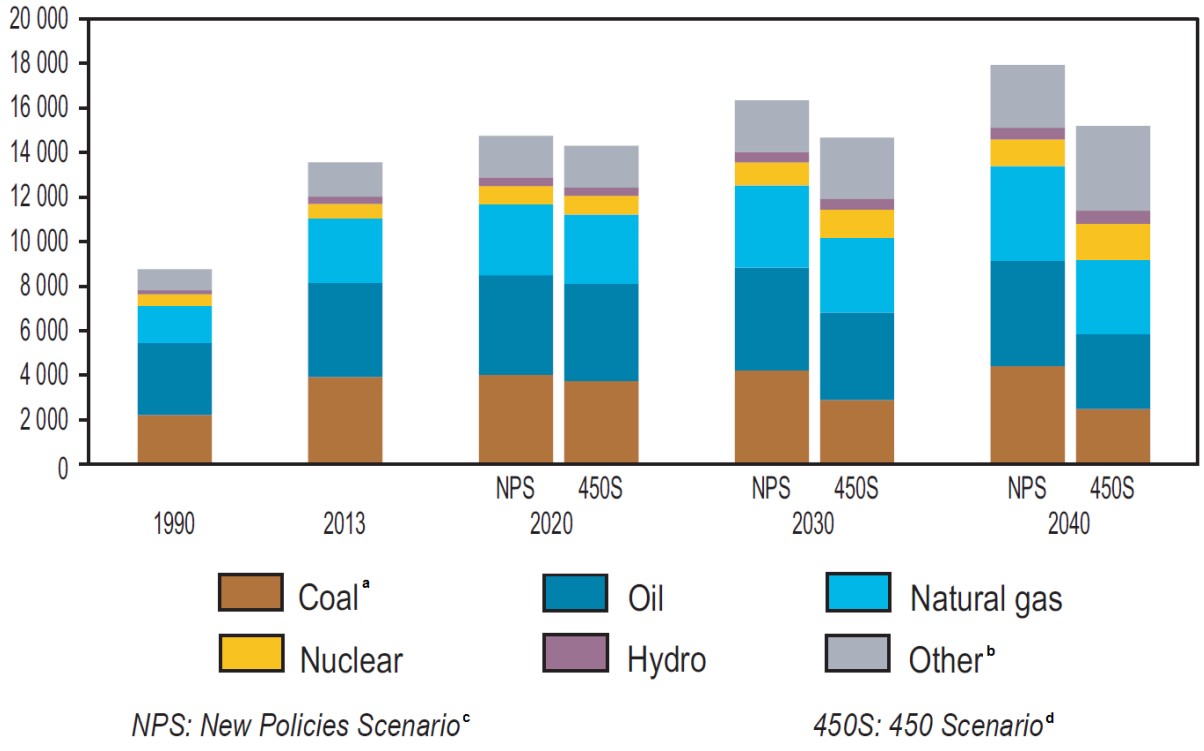


**Figure 2:** World's TPES in Mtoe for the past and projected for the future accounting for two different scenarios. [a] includes peat and oil shale; [b] includes biofuels and waste, geothermal, solar, wind, tide / wave, heat; [c] based on policies under consideration; [d] based on plausible post-2015 climate policy framework[5a] to stabilise the long-term concentration of global greenhouse gases at 450 ppm $CO_2$-equivalent.[1]

In order to design a strategy for the supply of energy from renewable resources, it is also crucial to consider the final consumption of different fuels (Figure 3). A mere 18% are used as electricity, which emphasizes the importance to produce the energy in the

form of a convenient storage material. This is especially true for mobile applications, such as transportation.

When comparing the different renewables (solar, geothermal, wind, tide / wave, biofuels and waste), clearly the solar approach has the most potential:[6] In one hour roughly the same amount of energy reaches the earth as is used by mankind in one year.[7] It would be sufficient to only harness a small fraction of this energy.

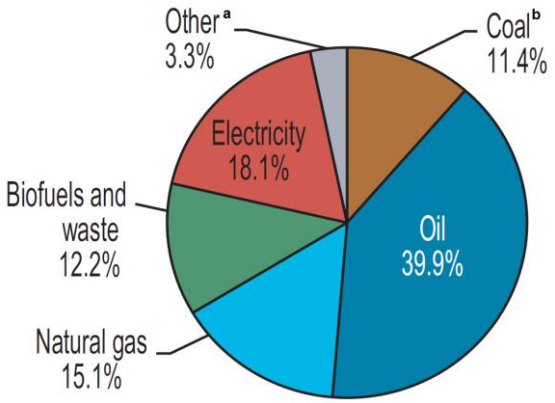


**Figure 3:** Fuel shares of world's total final energy consumption in 2014. [a] includes geothermal, solar, wind, tide / wave, heat; [b] includes peat and oil shale.

However, solar energy is also subject to some major disadvantages. Geographical and thereby climatic differences, as well as seasonal and day / night cycles complicate the continuous supply of energy, which is required. Therefore, efficient conversion into a storable fuel is necessary. A somewhat obvious solution is to use the solar energy to split water, forming hydrogen as an energy carrier and oxygen as a (desirable) side product. The combination of these two highly abundant resources would provide an essentially inexhaustible source of energy.

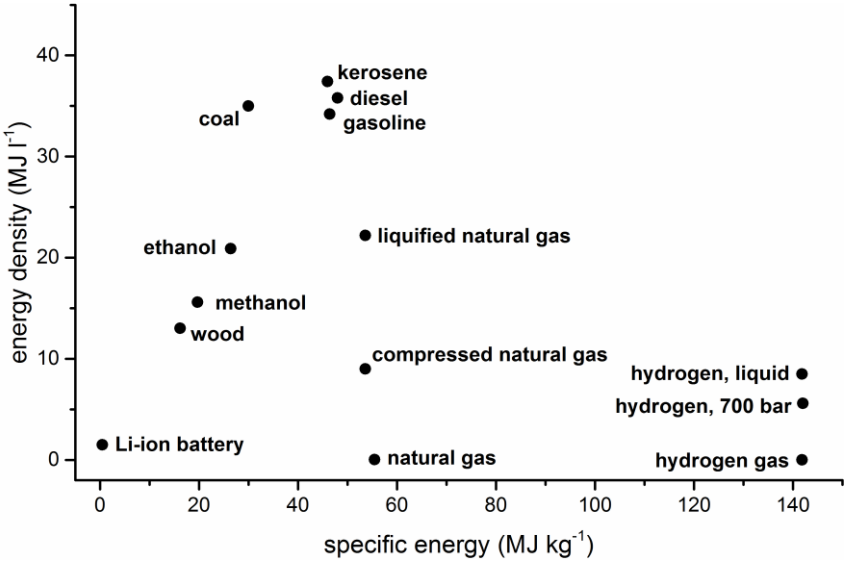


**Figure 4:** Energy density plotted versus the specific energy of selected energy storage materials.[8]

Although this approach seems exclusively beneficial, the resulting fuel (hydrogen) is far from ideal in terms of energy density (MJ $l^{-1}$, Figure 4). Despite its very high specific energy (142 MJ $kg^{-1}$), it cannot compete with today's prime energy carriers for mobile applications (kerosene, diesel, gasoline), simply due to the large volume necessary for storage. The problem can be slightly mitigated by compressing or liquefying the hydrogen, making it actually viable for these applications.[9] Another approach would be the conversion of hydrogen into a liquid fuel, e.g. production of hydrocarbons via the Fischer-Tropsch process, even a methanol based economy has been proposed.[10] Apart from an increased energy density, a liquid fuel would also fit better into the existing infrastructure (combustion engines, filling stations, etc.), making a commercialization much easier.

## 1.2. Photocatalytic Water Splitting

There exist many ways to convert solar energy into hydrogen, e.g. coupling of photovoltaic cells with an electrolyser, integrated devices (photoelectrochemical cells) or even photobiologically by using hydrogen producing algae. The most direct way however, would be the photocatalytic splitting of water in homogeneous solution, often also referred to as artificial photosynthesis. Generally, such a system consists of three components (Scheme 1): A photosensitizer (PS), which absorbs the sunlight and thereby produces high energy electron hole pairs, a water reduction catalyst (WRC), which uses the electrons to reduce protons thereby forming hydrogen, and a water oxidation catalyst (WOC), which closes the catalytic cycle by making use of the leftover holes for oxygen production.

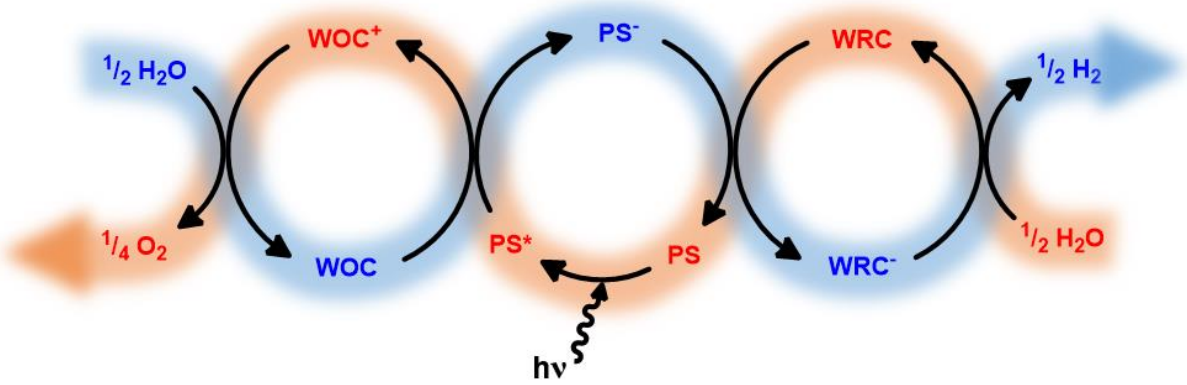


**Scheme 1:** Hypothetical overall water splitting scheme in homogeneous solution with molecular catalysts. Highlighted in blue and red are the pathways of the electron and hole, respectively. WOC = water oxidation catalyst, PS = photosensitizer, WRC = water reduction catalyst.

A major drawback of this approach is the possibility of many unintended side reactions to occur, in particular the recombination of the initially formed electron hole pair. In principle, almost all species in blue (Scheme 1) may react with the species in red in an unproductive manner. Due to this, a full homogeneous water splitting system has not been described yet. Consequently, the two half-reactions (water oxidation and water reduction) are usually studied separately by replacing the corresponding other half with a sacrificial electron acceptor and sacrificial electron donor, respectively.

### 1.2.1. Water Oxidation Catalysis

Although the product of water oxidation is not of immediate interest as an energy carrier, the importance of this reaction for the overall water splitting process is indisputable. As implied in Scheme 1, the WOC needs to accumulate four holes in order to release one molecule of $O_2$, which makes the search for suitable catalysts very challenging. The first molecular catalyst for water oxidation was the so called “Blue

Dimer" by T.J. Meyer and was relying on ruthenium (Scheme 2, left).[11] Thereafter many other reports appeared with catalysts mainly based on ruthenium, iridium and manganese,[12] however, also other metals, such as cobalt, nickel, iron and copper were considered.[12b, 13] A key issue of these molecular catalysts is the stability of their ligands towards oxidation under the very harsh conditions. Often secondary species or metal oxides are suspected to be responsible for oxygen evolution rather than the original catalysts. To circumvent this problem, an interesting class of compounds, the polyoxometalates (POMs), were extensively investigated.[14] These are basically molecular analogues of metal oxides.

Benchmarking of the various WOCs is usually performed by electrocatalysis or frequently also by chemical oxidation with ceric ammonium nitrate (CAN). Photocatalytic essays are generally performed using $[Ru(bpy)_3]^{2+}$ as a photosensitizer and peroxodisulfate ($S_2O_8^{2-}$) as sacrificial electron acceptor.

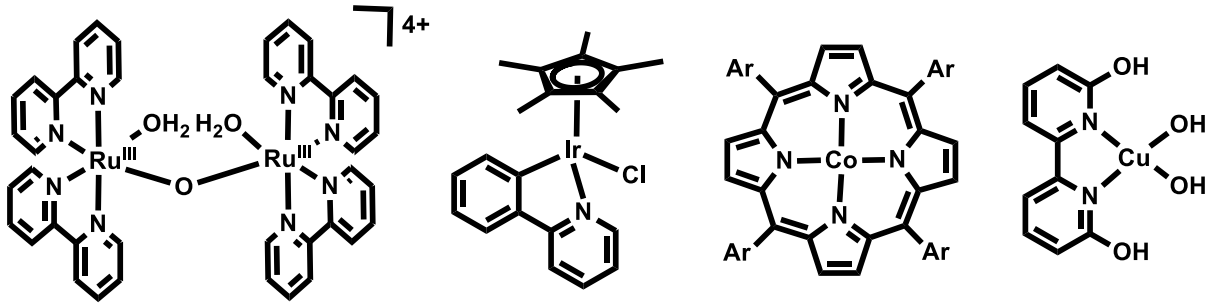


**Scheme 2:** Molecular structures of selected water oxidation catalysts, based on ruthenium,[11] iridium,[15] cobalt[16] and copper.[17]

### 1.2.2. Water Reduction Catalysis

From Scheme 1 it becomes clear, that the WRC needs to accumulate two electrons in order to produce one molecule of hydrogen. Although this is still a challenging process, it is more easily achieved than the accumulation of four holes in water oxidation. Unsurprisingly, there exist many more WRCs with good activity and stability than WOCs. The first example of a completely molecular system was reported by Lehn and Sauvage in 1979, employing a rhodium based WRC (Scheme 3).[18] Thereafter, many other rhodium[19] and platinum[20] based catalysts emerged, with increased activity and stability. More recently, the development shifted away from these noble metal based catalysts, towards complexes with more abundant metals, such as cobalt, nickel, iron or molybdenum.[21]

Our group has been especially active in the development of new cobalt based molecular catalysts. Starting from simple cobaloximes with relatively fragile dioxime

ligands and thereby low catalytic stability,[22] the research evolved towards more stable complexes with polypyridine based ligand scaffolds (Scheme 3).[23] The latter show equal or even superior performances compared to the noble metal based catalysts.

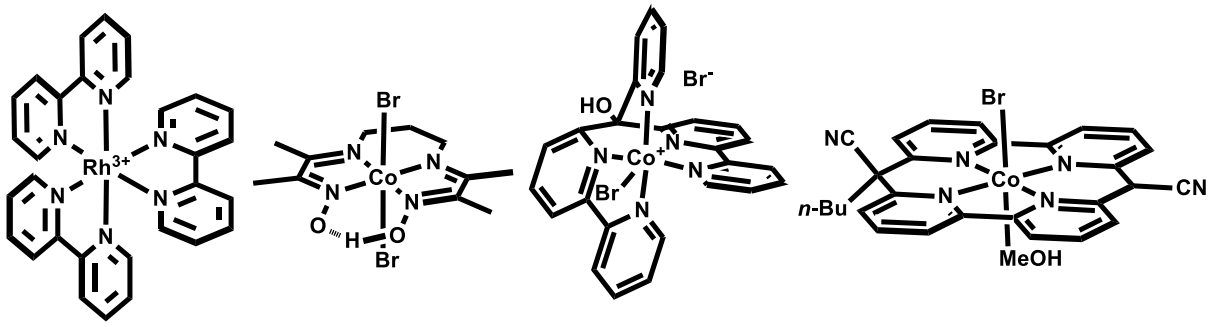


**Scheme 3:** Molecular structures of molecular WRCs. The first rhodium based example (left), followed by cobalt based examples, which were used and / or developed in our group.

### 1.2.3. Photosensitizers

The photosensitizer plays a central role in both water oxidation and water reduction catalysis. It absorbs the visible light and transforms this energy into a chemical potential, which can be used to drive either reaction. For homogeneous applications, apart from the absorption of visible light, an important prerequisite for a good photosensitizer is a long excited state lifetime. At least a few nanoseconds are necessary, to allow for diffusion controlled bimolecular reactions with e.g. the WOC or WRC. Most often used is $[Ru(bpy)_3]^{2+}$ (Scheme 4, left), which belongs to the extensively studied family of $Ru^{II}$-polypyridine complexes.[24] However, also other noble metal compounds based on platinum,[25] iridium[26] or rhenium[22b, 27] were investigated for their photoredox activity. A major drawback of all these compounds is their dependence on rare metals, which increases the overall price of a photocatalytic system. Therefore, significant efforts towards photosensitizers based on more abundant materials were made. Successful systems were reported employing Eosin Y,[28] fluorescein,[29] Al-,[30] Zn-[31] and Sn-porphyrins,[32] as well as quantum dots.[33]

Of particular interest for this thesis are the reports on photosensitizers based on earth abundant copper. Already in 1984, Sauvage et al. applied $Cu^{I}$ bis-phenanthroline complexes for light driven hydrogen evolution.[34] In recent years these compounds experienced renewed attention, which led to the development of photosensitizers based on copper with very nice photophysical properties. The group of Castellano reported on $[Cu(dsbtmp)_2]^{+}$ (Scheme 4, middle), which has a the longest emission lifetime in room temperature solutions ever observed for homoleptic $Cu^{I}$

bisphenanthroline complexes .[35] Moreover, the lifetime is almost independent of the solvent, which is very atypical. More recently, replacement of the *s*-butyl with *i*-propyl groups on the phenanthroline ligand produces a complex with almost identical properties.[36]

The group of Beller replaced one of the phenanthrolines with a bidentate phosphine ligand, to produce highly emissive heteroleptic $Cu^{I}$ complexes (Scheme 4, right).[35a, 37]

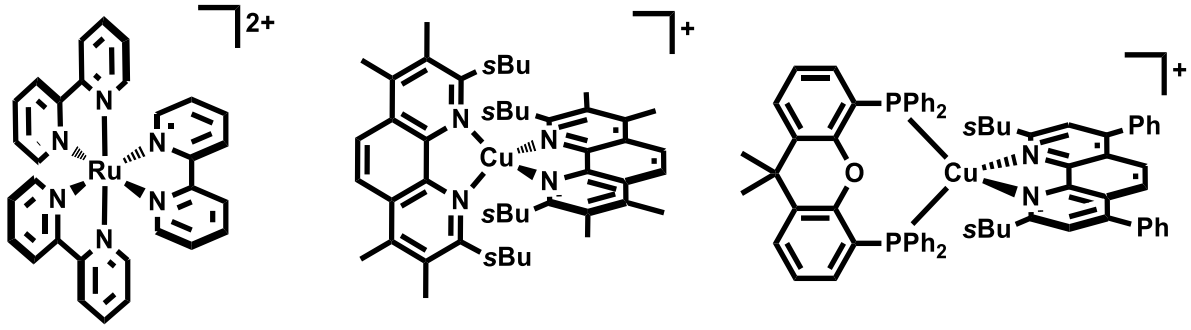


**Scheme 4:** Molecular structures of the famous ruthenium based photosensitizer $[Ru(bpy)_3]^{2+}$ (left) as well as examples of copper based alternatives developed in the groups of Castellano (middle) and Beller (right).

Although the heteroleptic compounds show very long excited state lifetimes, they only absorb at the blue edge of the visible region (~390 nm), similar to rhenium based photosensitizers (see Figure 5). In contrast, the homoleptic bis-phenanthroline complexes show a better overlap with the solar spectrum, similar to $[Ru(bpy)_3]^{2+}$, and are therefore chosen here for further investigation. For comparison, also the spectrum of a water soluble tin-porphyrin ([$SnCl_2$TPPC]) is shown in Figure 5, which has nice absorption features, deep into the visible region. This dye was investigated in the course of the thesis but is not discussed herein.[32b]

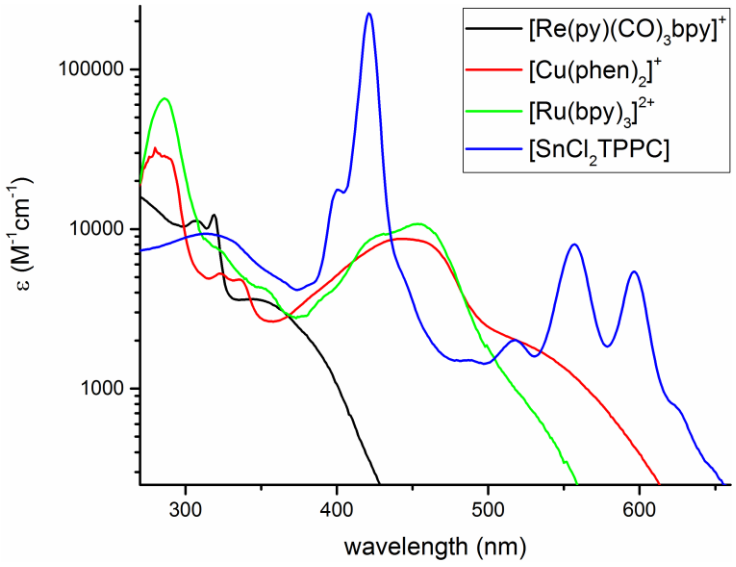


**Figure 5:** Comparison of the UV/VIS absorption spectra of different chromophores.

## 1.3. Copper Bis-Phenanthroline Complexes

The first synthesis of $Cu^{I}$ bis-phenanthroline complexes was reported in 1933 by Tartarini.[38] He obtained the compounds either by reducing $Cu^{II}$ salts in the presence of the ligand or by simply mixing $Cu^{I}$ salts with the chelator. Subsequently, owing to the deep red colour of these compounds, phenanthroline ligands were proposed as reagents for the spectrophotometric determination of small copper ion concentrations in solution.[39] In particular 2,9-dimethyl-1,10-phenanthroline (dmp), since it is unable to form octahedral complexes and is therefore specific for copper also in the presence of other metals.

Some years later McMillin and co-workers discovered the photoredox activity of $Cu^{I}$ bis-phenanthroline complexes. When irradiating mixtures of $[Cu(dmp)_2]^+$ and various $Co^{III}$ compounds with visible light, they observed electron transfer from the copper- to the cobalt-species.[40] Only a few years later, they first described the room temperature luminescence of $[Cu(dmp)_2]^+$.[41] This was the starting point for extensive research on this class of compounds.

Soon, the importance of structural factors, determining absorption and emission properties of the complexes, was recognized.[42] This is fairly different from e.g. $[Ru(bpy)_3]^{2+}$, where mainly electronic effects are at play. Most influential are the substituents in the 2- and 9-position of the phenanthroline scaffold (Scheme 5, left). Their size and chemical nature has a heavy impact on the complex-geometry in the ground and excited sate. E.g., bulky alkyl substituents force a tetrahedral geometry, since they clash upon flattening, whereas aryl substituents lead to a flattened geometry, due to ππ stacking interactions between opposite phenanthroline moieties (Scheme 5, middle and right).

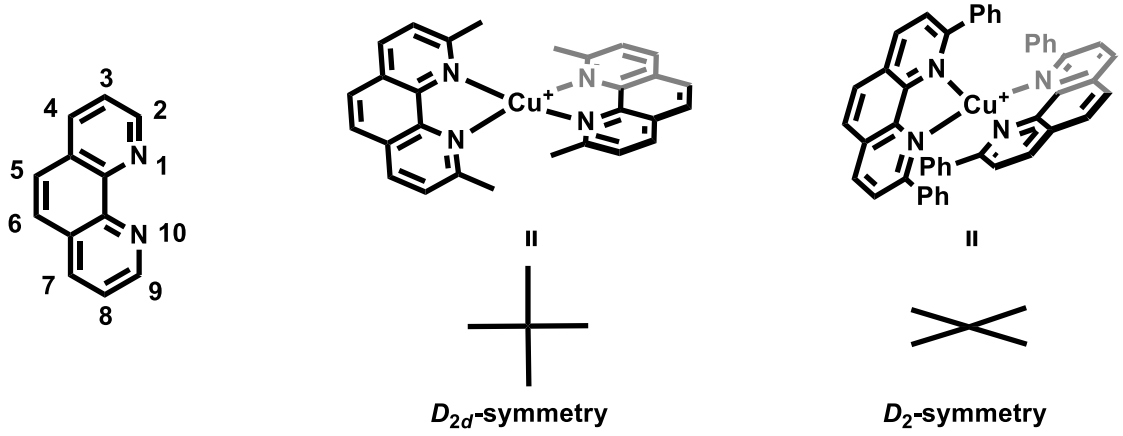


**Scheme 5:** Left: Numbering scheme for the phenanthroline scaffold; Middle: Perfectly tetrahedral $Cu^{I}$ bis-phenanthroline complex ($D_{2d}$ symmetry) exemplified with $[Cu(dmp)_2]^+$; Right: $Cu^{I}$ bis-phenanthroline complex with a strong flattening distortion ($D_2$ symmetry), exemplified with $[Cu(dpp)_2]^+$ (dpp = 2,9-diphenyl-1,10-phenanthroline).

The symmetry of the ground state has great consequences for the absorption features in the visible region. In general, there are three overlapping MLCT absorption bands (band I-III) between 350 and 600 nm. Band I refers to the lowest energy transition (> 500 nm), which is only allowed in $D_2$-symmetry, whereas bands II and III belong to transitions in $D_{2d}$-symmetry (see $[Cu(phen)_2]^+$ in Figure 5 for an exemplary spectrum).[42b] A detailed assignment of the transitions is given in chapter 2.4.1.2, directly applied to the relevant compounds of this thesis.

Similar arguments are employed to explain the luminescence behaviour of $Cu^I$ bis-phenanthrolines. Upon irradiation, the $Cu^I$ ($d^{10}$) complex undergoes a MLCT process, which formally oxidizes the metal center to $Cu^{II}$ ($d^9$) and moves the electron to the phenanthroline ligand. This comprises the driving force for a flattening distortion towards $D_2$-symmetry in the excited state, opening up the metal center for coordination of additional ligands (e.g. solvent molecules). Thus, non-radiative decay becomes more relevant, due to exciplex quenching. The process of solvent coordination upon light excitation, as well as other early dynamics processes (internal conversion, intersystem crossing, geometrical distortions, etc.) have been studied recently by applying ultrafast spectroscopic techniques.[43] However, the emissive properties can be enhanced by introducing bulky substituents. On the one hand, they help preserving the tetrahedral geometry and on the other hand, they additionally shield the metal center from solvent molecules. The influence of various substituents on the emission properties is discussed in chapter 2.4.1.3.

Similar to the formal oxidation of $Cu^I$ bis-phenanthroline complexes upon light irradiation, also the electrochemical oxidation is heavily influenced by the ligand substituents. Large groups hinder the desired flattening motion and thereby make the removal of an electron much more difficult (see 2.4.1.4 for examples).

The group of Sauvage initially used $Cu^I$ bis-phenanthroline complexes as a template to produce various macromolecular assemblies, such as catenanes, rotaxanes and molecular knots, in a very elegant way (Scheme 6).[44]

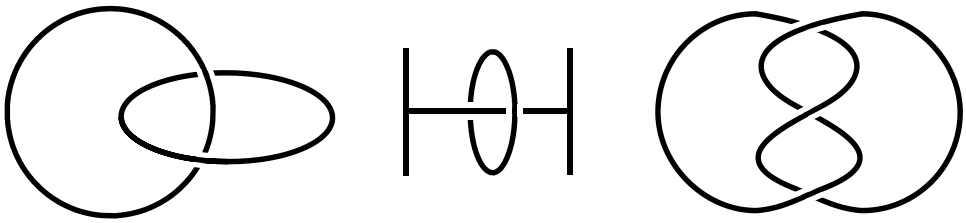

**Scheme 6:** Simplified representation of the linking principle of catenanes (left), rotaxanes (middle) and knots (right).

Especially the so formed catenanes seemed very interesting with respect to the aforementioned importance of steric constraints around the copper center (Scheme 12, left). Therefore, their photophysical properties were investigated and compared to the simple homoleptic $Cu^{I}$ bis-phenanthroline complexes.[44c, 45] Indeed, increased luminescence lifetimes were observed, however, the effect was much less pronounced than expected. In contrast, a very marked feature was the enhanced kinetic stability of the compounds, which is atypical for the usually highly labile $Cu^{I}$ complexes. Still, the achieved small improvements do not seem to justify the synthetic efforts, which are necessary to prepare these elaborate macrocycles. Especially with the emergence of the aforementioned much simpler $Cu^{I}$ complexes, developed in the group of Beller and Castellano, it is unsurprising that the catenanes did not find applications in photocatalysis.[35-37, 46] However, these compounds found many applications in the field of molecular machines, which earned Jean-Pierre Sauvage the Nobel prize in chemistry 2016, jointly with Sir J. Fraser Stoddart and Bernard L. Feringa.[47]

# 2. Results and Discussion

In this chapter the main findings of the thesis are described and interpreted. Starting with the synthesis of a series of substituted phenathroline ligands (2.1) and their $Cu^{I}$ complexes (2.2), followed by more elaborate ligand synthesis towards a tetrahedral cage ligand (2.3). In the last subchapter (2.4), the development of a working photocatalytic system for hydrogen evolution is detailed.

## 2.1. Ligand Syntheses

### 2.1.1. Syntheses of 1,10-Phenanthroline Ligands

1,10-phenanthroline ligands were mainly derivatized in the 2- and 9-position. One strategy to achieve this is based on the nucleophilic attack of organolithium reagents in the *ortho*-positions of the phenanthroline-nitrogens, giving the respective unsaturated adducts. Subsequently, re-aromatization of the intermediate species is achieved through oxidation with $MnO_2$ during workup (Scheme 7). This is a well-known literature procedure and was already applied to produce a plethora of phenanthroline-derivatives.[48]

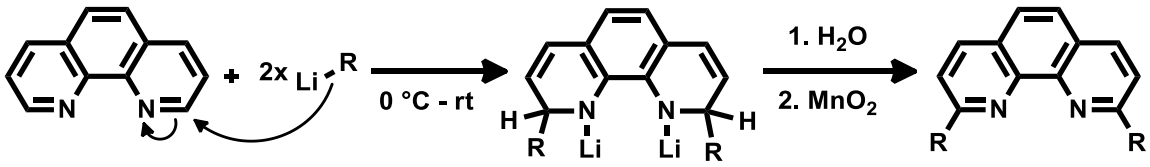


**Scheme 7:** General approach for the synthesis of 2,9-disubstituted 1,10-phenanthrolines.

The reaction does not only work with bare 1,10-phenanthroline, but also with substituted derivatives thereof, of course providing that the 2- or 9-position is free. Ligands **1** - **4** were prepared in one step using this method, applying commercially available starting materials. It is important to use anhydrous phenanthroline, since the presence of crystallization water completely disrupts the reaction, giving a complex mixture of unknown products. All *s*-Bu-substituted derivatives were isolated and used without separation of the diastereoisomers. The solvent of choice for this reaction is dry toluene. In other solvents, which are commonly used in conjunction with organolithium reagents ($Et_2O$, THF), the conversion to the 2,9-disubstituted products is incomplete and mainly the monosubstituted compounds are obtained. The strong solvent influence could be exploited advantageously for the preparation of unsymmetrically substituted derivatives. However, in toluene some care should be taken to control the stoichiometry of the reaction, since already a slight excess (2.2

eq.) of lithium-reagent leads to small amounts of tri- and tetrasubstituted products, as observed by UPLC-MS in case of ligand **1**.

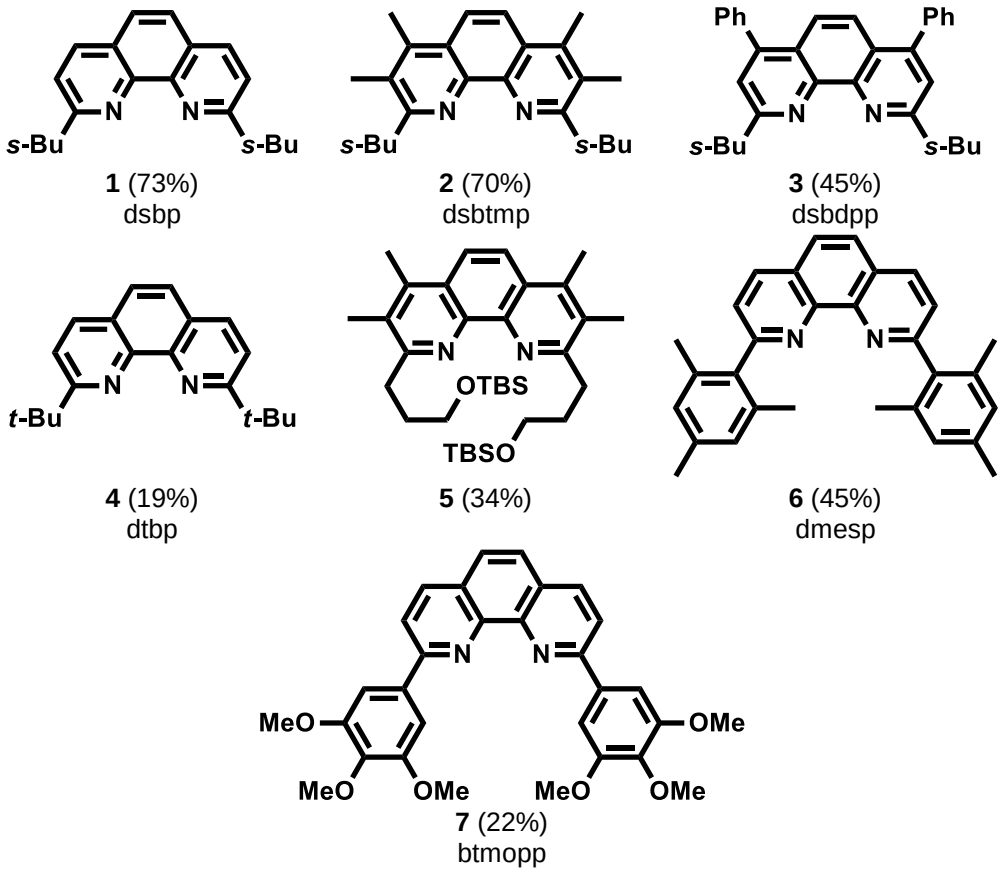


**Scheme 8:** Molecular structures of ligands prepared according to the general method with the yields given in parentheses.

The required organolithium reagents for the syntheses of ligands **5**, **6** and **7** were prepared in situ from the corresponding bromo-precursors.[49] These lithiation procedures are described to work in dry $Et_2O$ and therefore the ligands **5** - **7** were prepared over two steps in this solvent. After the first substitution, the intermediates were isolated through an aqueous workup and precipitation from DCM by the addition of hexane. Without further purification, the same reaction conditions as in the first step were applied to yield the disubstituted products.

For all ligands **1** - **7** the reactions run smoothly and HPLC does not show the formation of significant amounts of side products. However, purification procedures were usually necessary, due to the presence of unknown impurities. The crude products were generally subjected to column chromatography on neutral alumina for purification, ligands **4** and **7** were additionally recrystallized. For derivatives **5** and **6** however, only minimal purification was necessary, which makes it difficult to explain the low yields.

### 2.1.2. Ligand Modifications for Water Solubility

Water solubility of all components of a homogeneous photocatalytic system is a prerequisite in order to function in water as solvent. Thus, ligand modifications towards the goal of increasing the solubility of the resulting complexes by the introduction of polar groups on the 1,10-phenanthroline derivatives were performed. Treatment of ligand **3** with fuming $H_2SO_4$ gave the disulfonated product **8** in 75% yield, as confirmed by UPLC-MS. However, the exact sulfonation-position at the phenyl substituent is unknown, a previous report even suggests reaction in the 5,6-position on a similar phenanthroline ligand.[37c]

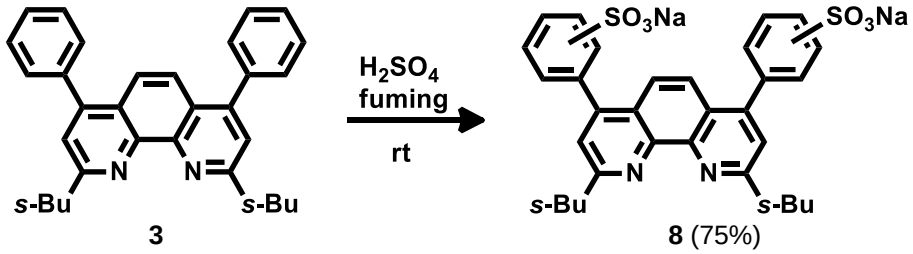


**Scheme 9:** Sulfonation of **3** to give the water soluble ligand **8**.

Another approach to improve the water solubility of phenanthroline ligands is the introduction of hydroxyl groups, as was demonstrated elsewhere.[50] Similarly, after deprotection of ligands **5** and **7**, the water soluble analogues **9** and **10** were obtained.

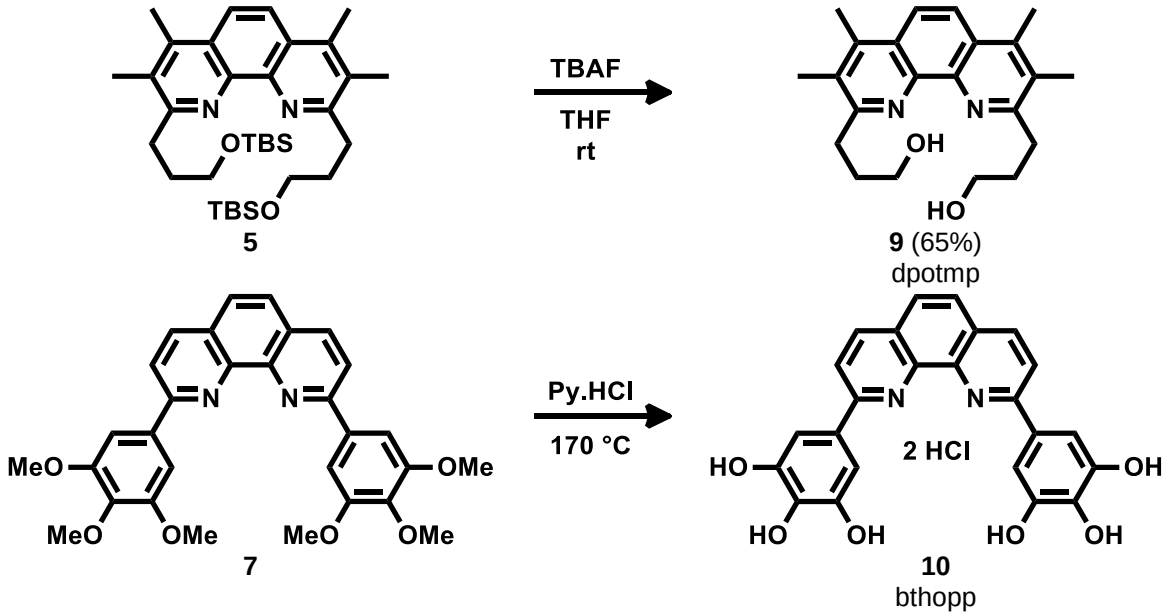


**Scheme 10:** Synthesis of water soluble ligands **9** and **10** via deprotection of the corresponding precursors.

Some efforts were also made to prepare a water soluble version of ligand **2**. However, when applying the same sulfonation conditions as for **8** (fuming $H_2SO_4$ at rt), only starting material is recovered. Even at elevated temperatures (up to 180 °C) the compound does not react as desired, indicating that the sulfonation at the 5,6-position

is not favoured. Similarly, the ligand seems to be inert towards standard nitration conditions ($H_2SO_4$, $HNO_3$ at 160 °C), which generally yields the 5-nitro compound, when applied to other phenanthroline derivatives. The reluctance of **2** to undergo an electrophilic aromatic substitution seems surprising from an electronic point of view. The positive inductive effect of all the alkyl substituents should have an activating influence on the system. Therefore, steric inaccessibility of the 5- and 6-position of **2** is likely to be the disabling factor.

## 2.2. Syntheses of $Cu^{I}$-Complexes

A very versatile precursor for the synthesis of $Cu^{I}$-compounds is the tetrakisacetonitrile complex $[Cu(MeCN)_4]X$. Its synthesis is achieved via comproportionation of $CuX_2$ and $Cu^0$-powder in MeCN, whereby a variety of anions X are accessible by simply choosing the corresponding $Cu^{II}$-source.[51] In this manner $[Cu(MeCN)_4]BF_4$ and $[Cu(MeCN)_4]OTf$ were prepared and isolated as colorless solids. Both compounds are sensitive to oxygen and take on a blue color upon oxidation. Where the former takes a few weeks to completely oxidize, the latter turns blue within hours, therefore both compounds were stored under nitrogen in a glove box.

The synthesis of homoleptic $Cu^{I}$-bisphenanthroline complexes is straightforward (Scheme 11) and well described in the literature.[52]

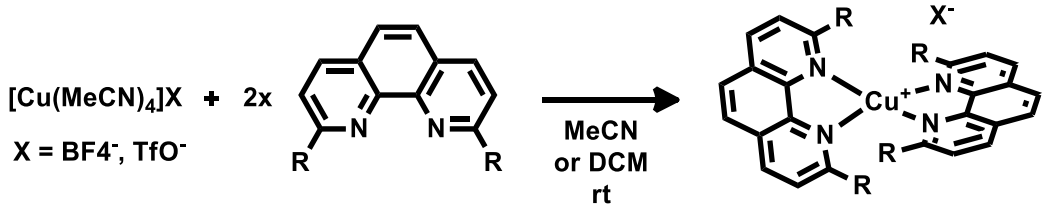


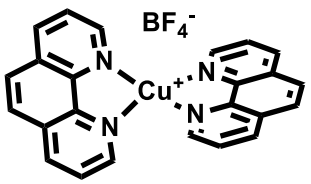

**11**
$[Cu(phen)_2]BF_4$

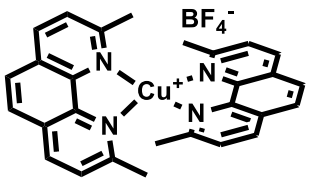

**12**
$[Cu(dmp)_2]BF_4$

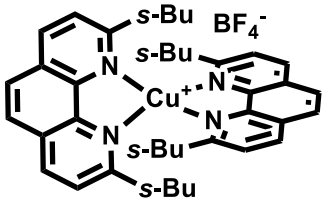

**13**
$[Cu(dsbp)_2]BF_4$

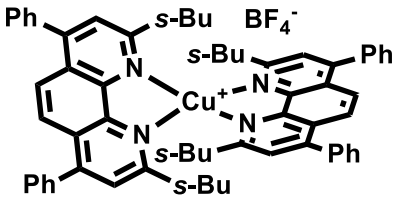

**14**
$[Cu(dsbdpp)_2]BF_4$

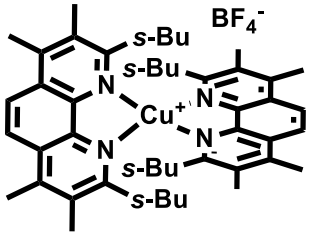

**15**
$[Cu(dsbtmp)_2]BF_4$

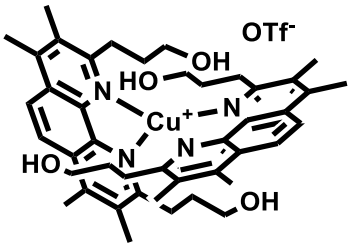

**16**
$[Cu(dpotmp)_2]OTf$

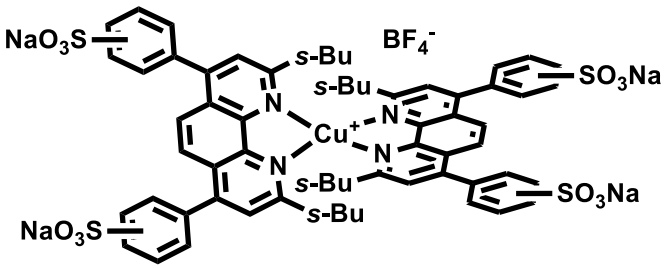

**17**
$[Cu(dsbdspp)_2]BF_4$

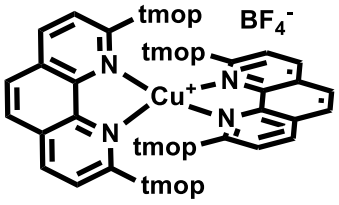

**18**
$[Cu(btmopp)_2]BF_4$

**Scheme 11:** Structures of homoleptic $Cu^{I}$-bisphenanthroline complexes prepared according to the general approach.

Mixing 1 equivalent of $[Cu(MeCN)_4]X$ with 2 equivalents of various 1,10-phenanthroline ligands at room temperature in MeCN or DCM under oxygen free conditions yields deeply red colored solutions within seconds. Upon addition of a nonpolar solvent ($Et_2O$, toluene) the desired homoleptic complexes usually precipitate and can be isolated as bench stable solids. Using this general method complexes **11** - **16** were prepared. For complexes **16** and **18** single crystals suitable for X-ray diffraction were obtained and their structure could be resolved (Figure 6 and Figure 23). In contrast, all complexes containing *s*-Bu groups did not yield single crystals, likely due to the presence of diastereoisomers. The general preparation method is no longer applicable, if the substituents in the 2,9-position of the phenanthroline ligand are too bulky, as is the case for dtbp (**4**) and dmesp (**6**). However, these sterically demanding ligands are very useful to prepare heteroleptic mixed phenanthroline complexes, a concept which was termed HETPHEN.[53] Whereas homoleptic complex $[Cu(dmesp)_2]^+$ has never been reported, it is possible to obtain $[Cu(dtbp)_2]^+$ by providing $Cu^I$ in an very non-coordinating environment (oxidation of $Cu^0$ by AgX in acetone, where X is $BF_4^-$, $SbF_6^-$ or $BAr^F{}_4^-$).[54]

Since the sulfonated ligand **8** is insoluble in DCM and MeCN, a slightly modified procedure for complex formation was applied. The ligand was dissolved in water and $[Cu(MeCN)_4]BF_4$ was added as a solution in MeCN. Purification was achieved by removal of the solvents and precipitation of complex **17** from MeOH by the addition of MeCN.

Complex formation was attempted for ligand **10** as well, however, the desired homoleptic product could not be isolated. Instead a mixture of unknown products was observed by ESI-MS during the reaction. Possibly, the coordinating ability of the hydroxy-groups inhibits clean complex formation.

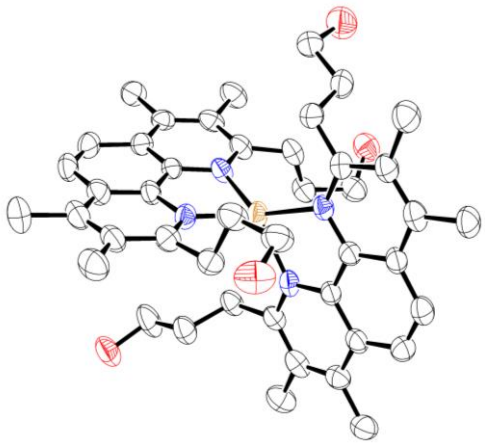

**Figure 6:** ORTEP drawing of **16** at 50% probability level. Hydrogen atoms, solvent molecules and anions as well as a second complex molecule, which is part of the asymmetric unit, are omitted for clarity.

## 2.3. Syntheses Towards a Tetrahedral Cage Ligand

As will be evident from chapter 2.4, the stability of copper bis-phenanthroline complexes still presents a major challenge. It is not only crucial to improve the long term performance in photocatalysis, i.e. prevent ligand decomplexation, but also to increase luminescence lifetimes even in very polar media, i.e. fix the tetrahedral geometry and shield the metal center from quenching interactions. Therefore a tetradentate ligand with an inherent tetrahedral geometry would be highly desirable.
In this sub-chapter the different strategies and attempts towards the synthesis of such a tetrahedral cage ligand are described.

### 2.3.1. General Considerations

The need to increase the ligand denticity and therefore the stability of copper bis-phenanthroline complexes was recognized already in the 1980's. The problem was addressed by catenating two phenanthroline-containing macrocycles, mainly by the group of Sauvage.[44a, 44b, 55] With this approach, metal decomplexation is much more unlikely, since the two intertwined macrocycles can be considered as one tetradentate ligand, rather than two separate bidentate ligands. However, the catenane structure still allows for a lot of flattening distortion in the excited state, which restricts its applicability for photocatalysis.[44c, 45] Hence, a different approach combining both properties was sought. Consequently, linkage of the phenanthroline moieties in a more direct fashion was proposed, as is shown in Scheme 12 on the right. With this approach, not only the two aforementioned properties would be fulfilled, but also the metal center would be completely surrounded by the macrocycle and therefore solvent coordination in the excited state would be prevented. This would enable the excited complex to still have some structural flexibility, i.e. flattening distortions, while preserving a long excited state lifetime.

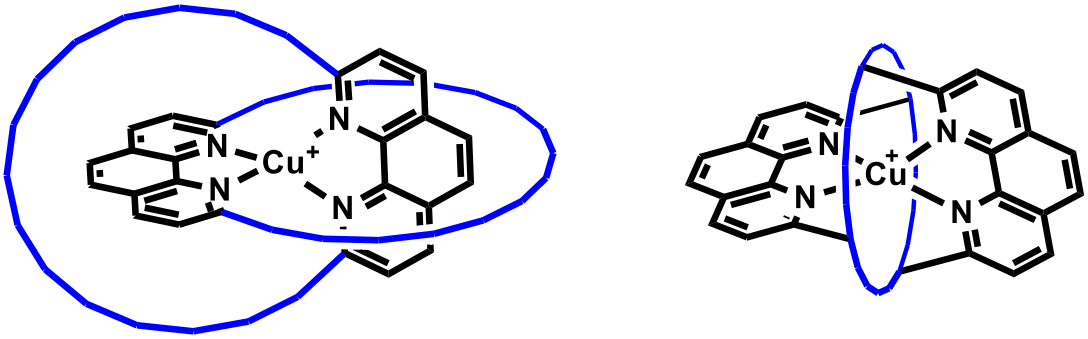


**Scheme 12:** Generalized molecular structures of tetradentate bis-phenanthroline ligands, such as the previously reported catenane type (left), as well as the proposed cage type (right).

In the following, some of the employed strategies for the synthesis of such a cage like ligand are described. For illustrative purposes, the parts that are predetermined to form the linking macrocycle are colored blue.

### 2.3.2. Terminal Diene Approach

One strategy for the formation of a tetrahedral cage ligand is based on either ring closing metathesis or radical polymerization. At least for the former reaction a lot of precedent for the formation of macrocycles exists.[56] Therefore, a series of ligands was envisioned (Scheme 13), where the terminal dienes function as the linking moieties for cyclization.

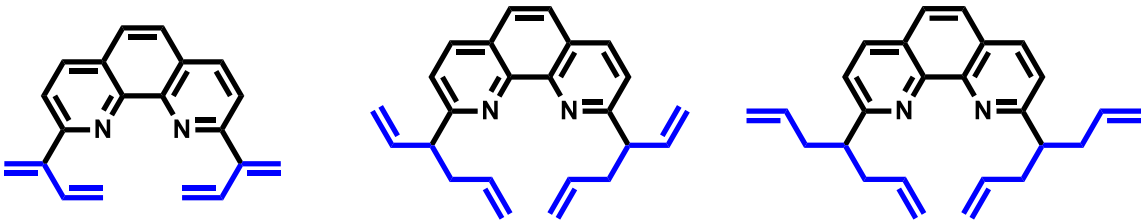


**19** **20** **21**

**Scheme 13:** Molecular structures of envisioned phenanthroline derivatives for cage ligand formation.

Ligand **19** would serve as the precursor for radical polymerization, yielding a 16-membered macrocycle, similarly ligands **20** and **21** would serve as precursors for ring closing metathesis, yielding 16- or 20-membered macrocycles respectively. Preferentially the cyclization reactions are performed with the preorganised homoleptic copper complexes to avoid polymerization into open chains. Scheme 14 exemplifies the formation of C-C bonds via radical recombination, which yields the fully formed macrocycle.

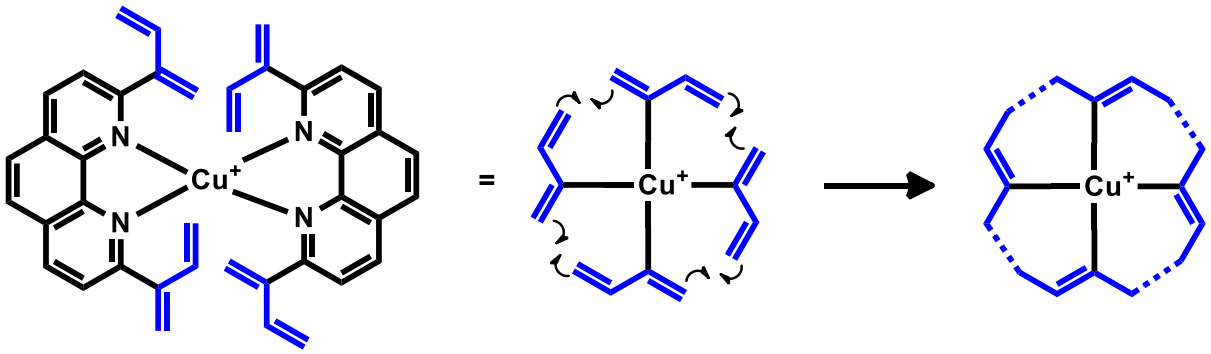


**Scheme 14:** Envisioned macrocycle formation by polymerization after radical initialization (e.g. by light).

### 2.3.2.1. Towards a 16-Membered Macrocycle via Polymerization

The synthetic strategy to produce ligand **19** is outlined in Scheme 15. The chlorinated starting material **22** was prepared according to a known literature procedure in three steps.[57] Subsequent treatment of this with $PBr_3$ yields the corresponding bromide compound **23**.[58] For the Sonogashira coupling a literature procedure suggests very mild conditions ($Pd(PPh_3)_2Cl_2$, CuI, *i*-$Pr_2NH$, THF, rt), however, in our hands no product formation was observed, even under rigorous exclusion of moisture and oxygen.[59] However, by running the reaction in DMF at 90 °C using TEA as the base, the desired product **24** was obtained in an overall yield of 40% with both the chloride and the bromide starting materials.[60] The success of the latter reaction conditions might be attributable to the better solubility of reactants (**22**, **23**) in DMF, but also using a tertiary amine over a secondary one, could have an influence.

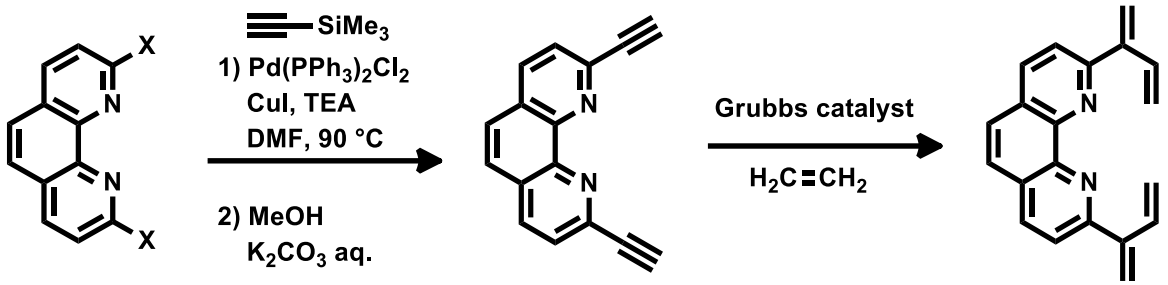


**22** (X = Cl)
**23** (X = Br)

**24** (40%)

**19**

**Scheme 15:** Synthetic strategy for ligand **19**.

With diyne **24** in hand, suitable conditions for the ene-yne cross-metathesis reaction to form **19** were screened. The varied parameters included catalyst type (Grubb's 2nd generation, Hoveyda-Grubb's 2nd generation), solvent (DCM, toluene), temperature (rt, 50 °C, 80 °C), ethylene pressure (1.1-1.9 bar) and reaction time (20-60 h). Unfortunately, even in the best case only product traces were observed by UPLC-MS (*m/z* 307.2 $[M+Na]^+$) along with unreacted starting material and intermediate (Figure 7). This infers fast catalyst deactivation, probably due to coordination of the substrate to the ruthenium center. Possibly, the formation of open-chain polymers also prevents accumulation of the desired product.

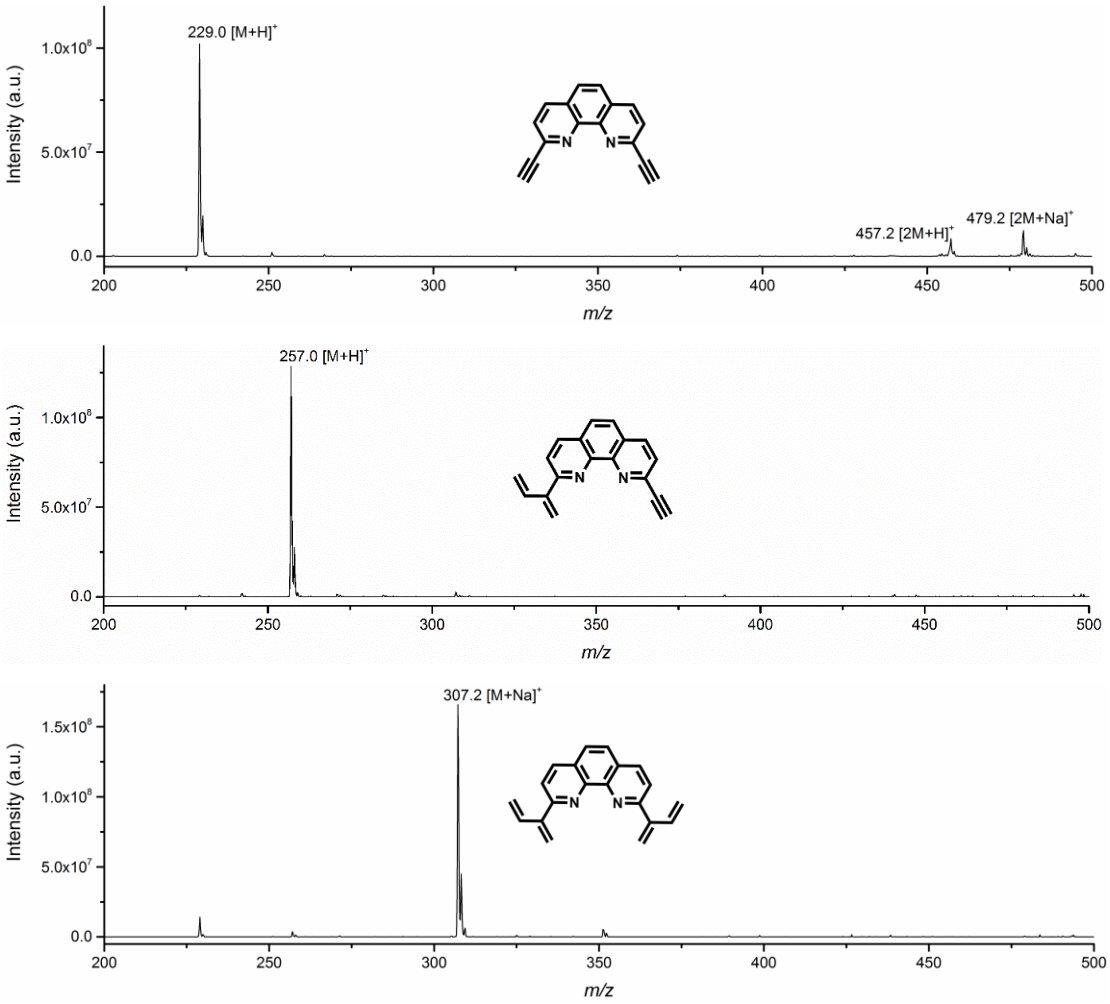


**Figure 7:** Mass spectra of different species observed in the conversion of **24** to **19**.

Since the synthesis of **19** proved to be very difficult, some efforts towards the preparation of the slightly different ligand **26** were made, which would be able to form the macrocycle similarly to **19**, yielding a final product with the double bonds shifted by one position. Indeed, diene **26** is accessible by elimination of mesylate from **25** (synthesis described in 2.3.2.3) under basic conditions (observed by UPLC-MS *m/z* 285.2 $[M+H]^+$, Scheme 16).

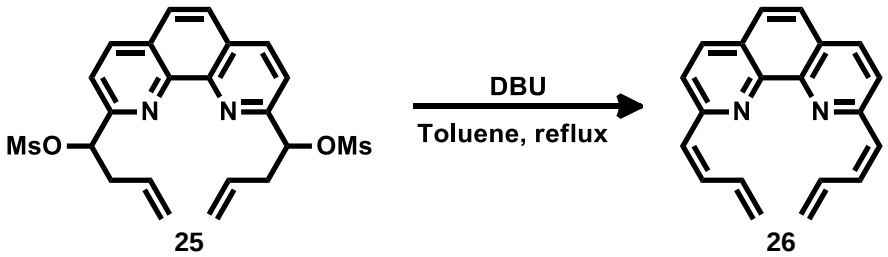


**Scheme 16:** One step synthesis of ligand **26**.

However, all attempts to isolate and characterize the product resulted in polymerization. Nevertheless, it was possible to obtain the homoleptic copper complex $[Cu(\mathbf{26})_2]^+$ in situ by reacting the crude product of **26** (after minimal workup) with

$[Cu(MeCN)_4]BF_4$. The successful formation of the complex was evidenced by the distinct color-change to orange, which is typical for copper(I) bis-phenanthrolines, as well as by UPLC-MS (*m/z* 631.3 $[M]^+$). In order to achieve cyclization, the MeOH solution of the in situ formed complex was irradiated for several days with visible light (slide projector). The reaction was continuously monitored by UPLC-MS as well as direct injection ESI-MS, however, at no point the formation of the macrocyclic product or any intermediates was observed.

### 2.3.2.2. Towards a 16-Membered Macrocycle via Methathesis

The strategy for the synthesis of ligand **20** was based on the same approach as for diene **26**, i.e. introduction of the terminal double bonds by elimination of a good leaving group (Scheme 17). For this purpose, significant efforts were made to prepare the up to date unknown building block **27** (Scheme 18).

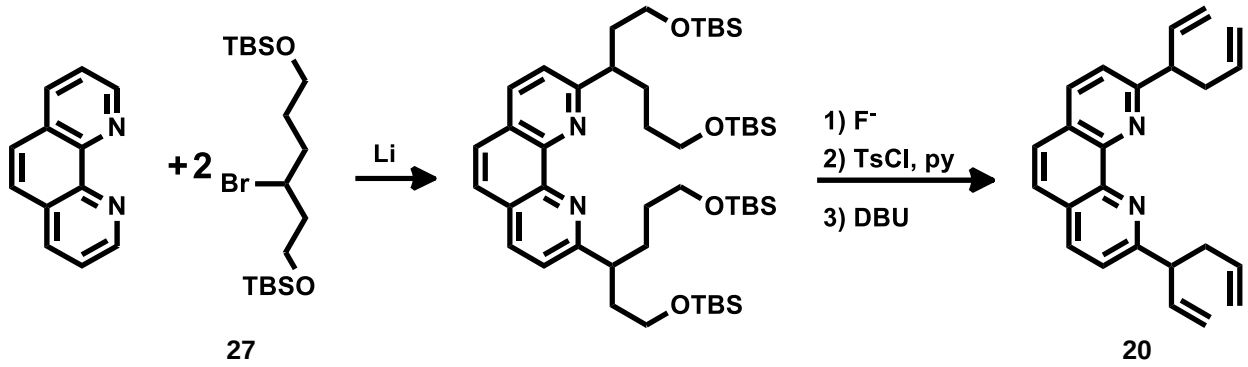


**Scheme 17:** Synthetic strategy for the preparation of ligand **20**.

Starting from commercially available **28**, intermediate **31** was obtained in three steps with an overall yield of 64% by following a literature procedure.[61]

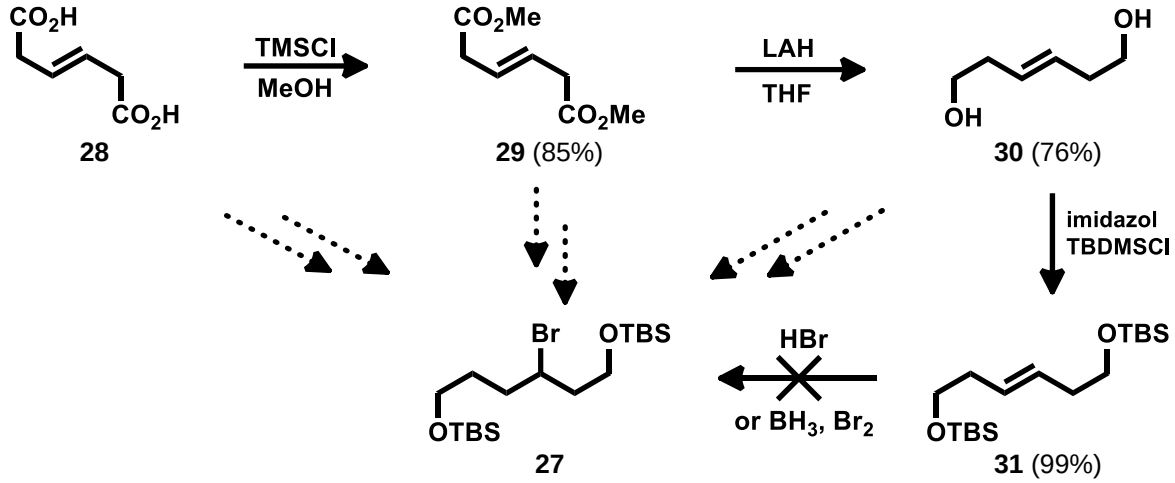


**Scheme 18:** Synthetic approach for the preparation of building block **27**.

Introduction of the bromide at the double bond was attempted either directly, using HBr (33% in AcOH) or via hydroboration with $BH_3$·THF followed by the addition of $Br_2$. All

intermediates **28** - **31** were subjected to the aforementioned conditions, yielding either unreacted starting material or undesired, however somewhat expected side products, e.g. the hydrolysed ester in case of reacting **29** with HBr (33% in AcOH) or replacement of - OH and - OTBS groups by - OAc in case of reacting **30** and **31** respectively with HBr (33% in AcOH). Eventually, the efforts towards the synthesis of building block **27** and consequently also towards ligand **20** were stopped, in favour of more promising strategies, which will be described later.

#### 2.3.2.3. Towards a 20-Membered Macrocycle via Methathesis

The dialdehyde **34** is accessible by oxidation of commercially available neocuproine with $SeO_2$ and serves as the starting material for the synthesis of ligand **21** (Scheme 19).[62] Initially, direct conversion was attempted using allyltrimethylsilane and catalytic amounts of $YbCl_3$. These reaction conditions were reported previously for similar substrates, however in this case only starting material was recovered.[63] After screening different conditions for this reaction type, the best results were obtained with $BF_3 \cdot Et_2O$ (2.2 eq.) as the Lewis acid, allyltrimethylsilane (4.2 eq.) as the nucleophile and DCM as the solvent. Under these conditions the disubstituted product **35** was obtained as a 1:1 mixture of diastereoisomers, unfortunately further substitution did not occur, even under more rigorous conditions (i.e. larger excess of Lewis acid and / or nucleophile). Also after isolation and purification of **35**, substitution of the alcohol by allyl groups was not successful under various conditions reported for similar substrates.[64] Therefore the hydroxyl group was functionalized into a better leaving group, e.g. - OMs or - OAc, to be subsequently replaced by the desired allyl moiety. While the leaving group formation worked well employing standard conditions, substitution was not achieved under the given reaction conditions.

An alternative target structure to **21** would be ligand **33**, which additionally contains two tertiary alcohols. To access this molecule, first diester **32** was prepared by oxidation of dialdehyde **34** to the corresponding dicarboxylic acid, followed by esterification, with an overall yield of 90%. Subjecting **32** to a variation of reagents, all being synthons for an allylic anion, did not yield any useful products (see below).

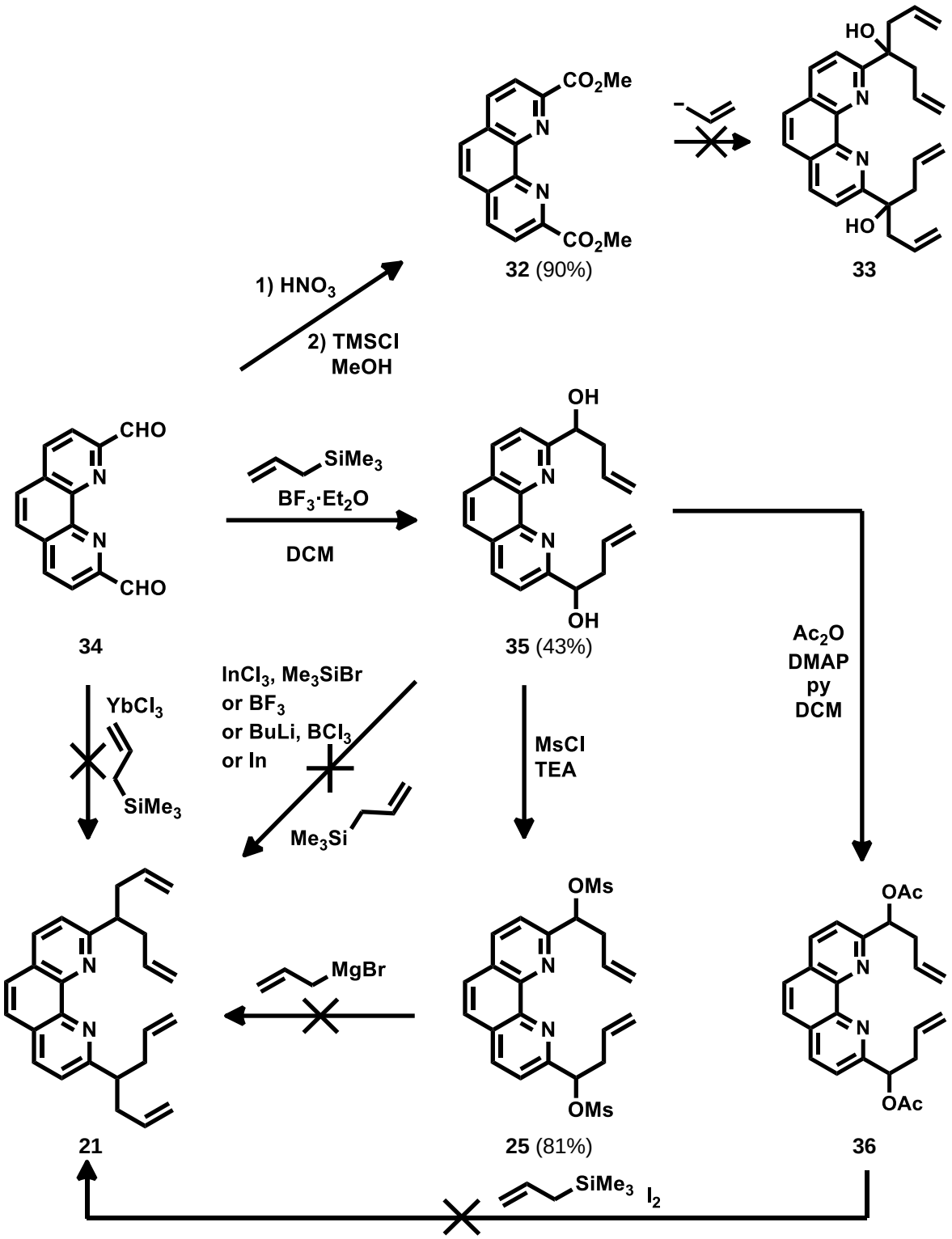


**Scheme 19:** Explored pathways towards the synthesis of ligand **21** and the structurally similar ligand **33**.

The employed reagents include several organometallic species, such as allyl Grignard, allyl lithium, allyl cyanocuprate as well as allyl bromide activated by indium metal. Although diester **32** could be perceived as a versatile starting material for 2,9-functionalized phenanthrolines, it is very scarcely used throughout the literature. This could be explained by the apparent non-classical reactivity behaviour of the ester groups, at least towards nucleophiles.

Since ligands **21** and **33** proved to be inaccessible by the employed strategies, focus was put on the intermediate **35**, which by itself offers a lot of opportunities to approach the ultimate goal of a tetrahedral cage ligand. As was mentioned previously, two diastereoisomers of **35** were obtained, on one hand the racemic mixture of (*R*,*R*)- and (*S*,*S*)-isomers and on the other hand the (*R*,*S*)-*meso* form (Scheme 20).

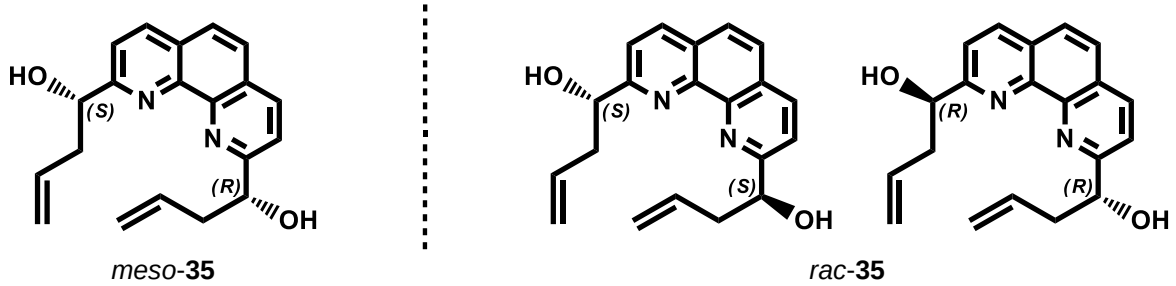


*meso*-**35** *rac*-**35**

**Scheme 20:** Different isomers of compound **35**.

The diastereoisomers were separable by preparative TLC or also partially by recrystallization from EtOH, where the racemate crystallizes preferentially. However, for the following reactivity tests, usually the mixture of diastereoisomers was employed. Under very dilute conditions (2 mM of substrate) **35** was transformed into the dimer **37** by a cross metathesis reaction, as was evidenced by UPLC-MS (Figure 8).

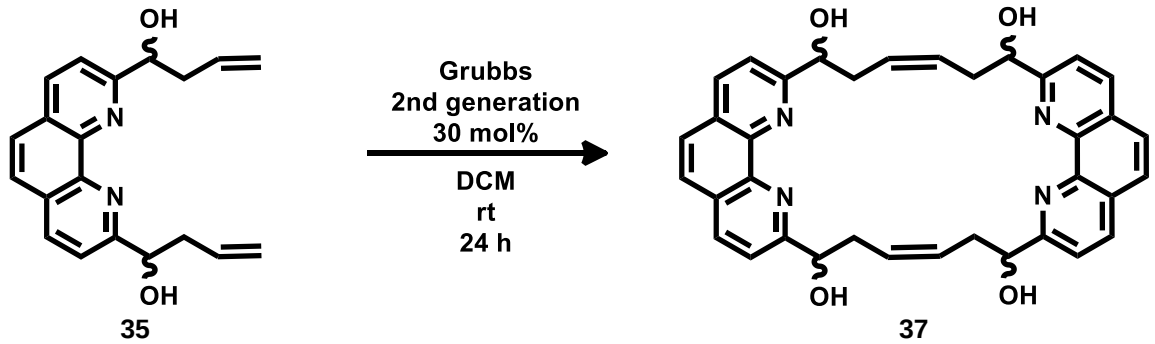


**35** **37**

**Scheme 21:** Dimer formation via cross metathesis of **35** under highly dilute conditions.

However, all isolation and purification attempts of the dimer failed so far, which is especially unfortunate since the remaining hydroxyl groups could serve as a handle for further modification towards the desired macrocycle.

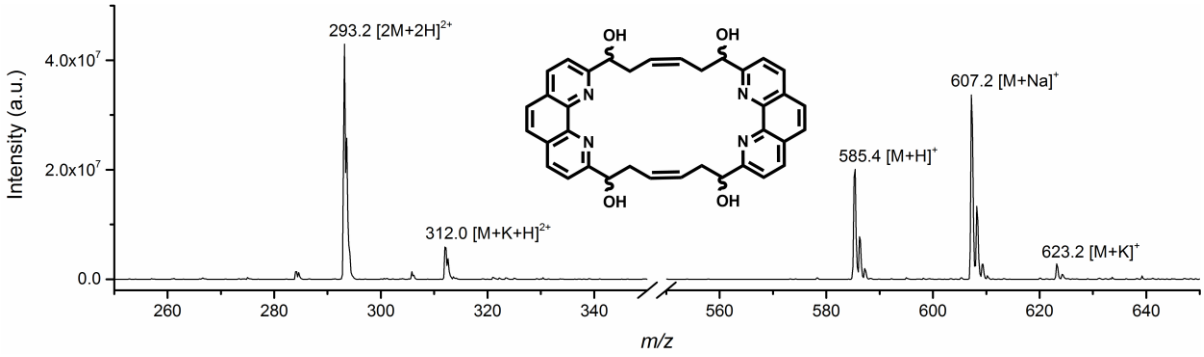


**Figure 8:** Mass spectrum of dimer **37**, as observed by UPLC-MS.

In a more direct approach **35** was first coordinated in situ to $Cu^{I}$ in 1,2-dichloroethane as the solvent, where the formation of the homoleptic complex $[Cu(\mathbf{35})_2]^+$ was confirmed by direct injection ESI-MS (*m/z* 703.4 $[M]^+$). Subsequently, this was reacted with AgOTf at 84 °C und exclusion of light, in the hope to initiate hydroalkoxylation between opposite phenanthrolines. However, since intramolecular formation of the five membered ring seems to be much faster, the tetrahydrofuranyl-substituted phenanthroline **38** is the main product of this reaction.

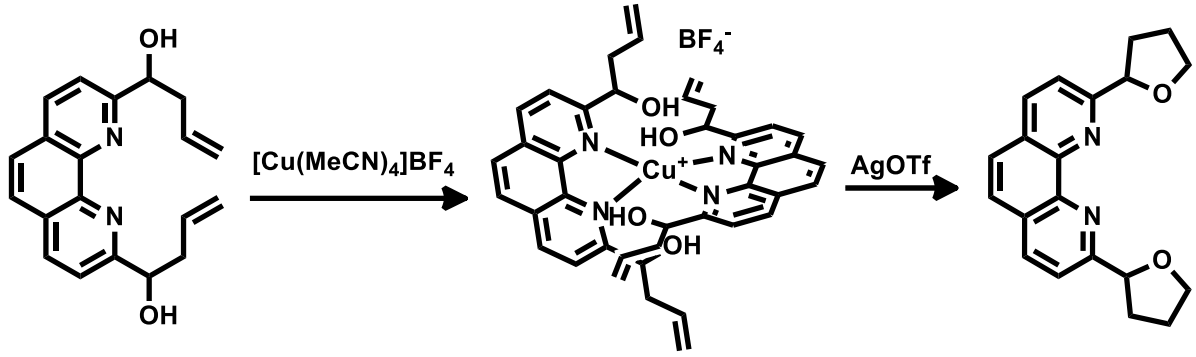


**35** **38**

## 2.3.3. Calixarene Inspired Approach

Another main approach towards a tetrahedral cage ligand was inspired by a well-known class of macrocyclic compounds, the calixarenes and resorcinarenes. Although the structure of these compounds was not understood initially, their preparation has been described already a long time ago, using relatively “simple” reaction conditions (Scheme 22).[65]

In this context, “simple” means the involvement of only small molecules (formaldehyde, phenol / resorcinol, $H^+$), that selectively form the macrocyclic product without the help of bulky catalysts or reagents. However, the formed ring size varies and is greatly dependent on the conditions (reagent concentration, temperature, reaction time), which renders the reaction as a whole by no means “simple”. The formation proceeds through repeating electrophilic aromatic substitutions, followed by elimination of water. The final macrocycles, containing four arene units, can adopt different conformations, one of which is shown in Scheme 22, where all the arene moieties are oriented the same way.

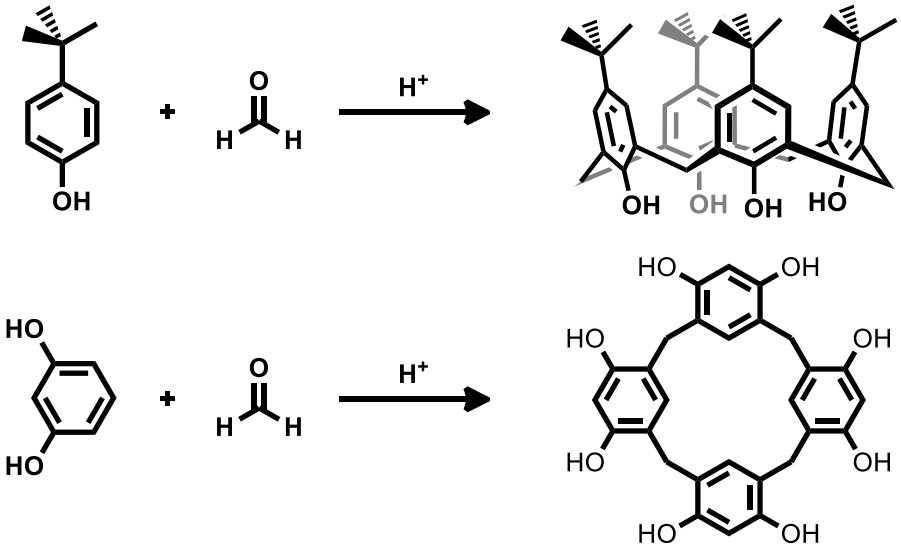


**Scheme 22:** Basic synthesis of a calix[4]arene (top) and a resorcin[4]arene (bottom).

By rotation of these subunits, various other conformations are possible. Most importantly for this approach, the 1,3-alternate conformation (Scheme 23, left), which provides the perfect framework for the desired tetrahedral cage ligand. Replacement of the alcohol groups with bridging phenanthroline units yields the prototypical cage structure. This translates retrosynthetically into ligand **7**, which combines two important properties. First, the electrophilic aromatic substitution is facilitated by the strong electron-donating effect of the methoxy-substituents. Second, only the desired positions at the phenyl-substituents are available for the reaction, whereas all the other positions are blocked by the methoxy-groups. Hence, ligand **7** is the target structure for this approach.

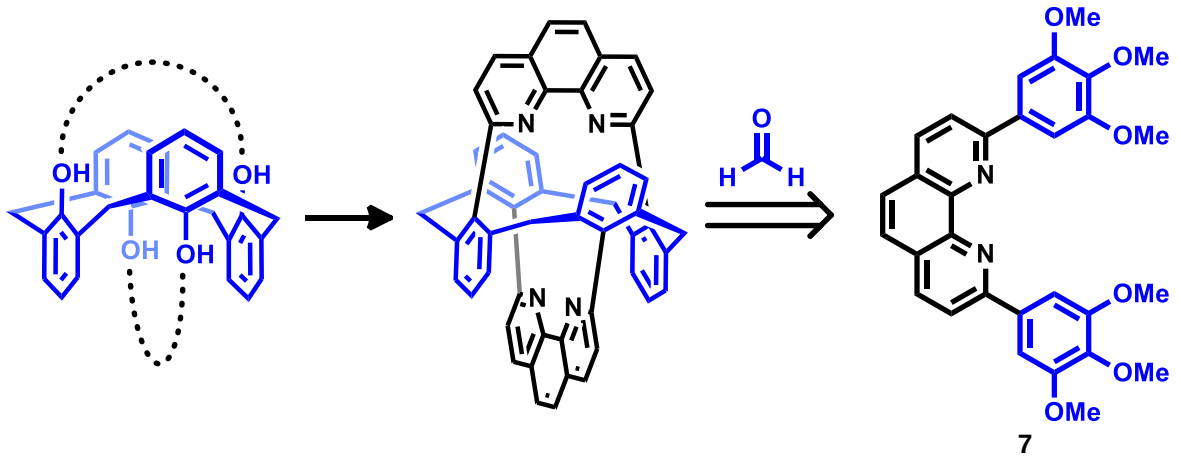


**7**

**Scheme 23:** Derivation of a calixarene inspired cage ligand and the resultant target structure **7**.

### 2.3.3.1. Towards a 16-Membered Macrocycle via Calixarene Formation

The synthesis of **7** followed the general approach for 2,9-disubstituted phenanthrolines and was already discussed in chapter 2.1.1. With the precursor in hand, reaction conditions for cyclization were screened, focusing on paraformaldehyde as the source

for the bridging $CH_2$-group. Various combinations of solvents (DCM, THF, MeCN, $MeNO_2$) and activating agents ($H_2SO_4$, $BF_3 \cdot Et_2O$, $BCl_3$, $SnCl_4$, $P_2O_5$) were applied, however, only traces of both singly bridged dimer (*m/z* 1037.5 $[M+H]^+$) and doubly bridged dimer (*m/z* 1049.5 $[M+H]^+$) were observed by UPLC-MS. Also templated reactions, using the homoleptic $Cu^I$-complex as starting material did not yield the desired cage structure or any intermediates in considerable amounts. The most promising results were obtained, when chloro(methoxy)methane (MOMCl) was used as the $CH_2$-source instead of paraformaldehyde. In this case, the doubly bridged dimer was formed as the main product (UPLC) and could be isolated purely in 16% yield (Scheme 24). Even though traces of the triply bridged dimer were observed, the reaction could not be forced further towards this product, neither by large excess of $SnCl_4$ and MOMCl nor by templating with $Cu^I$ (Figure 9).

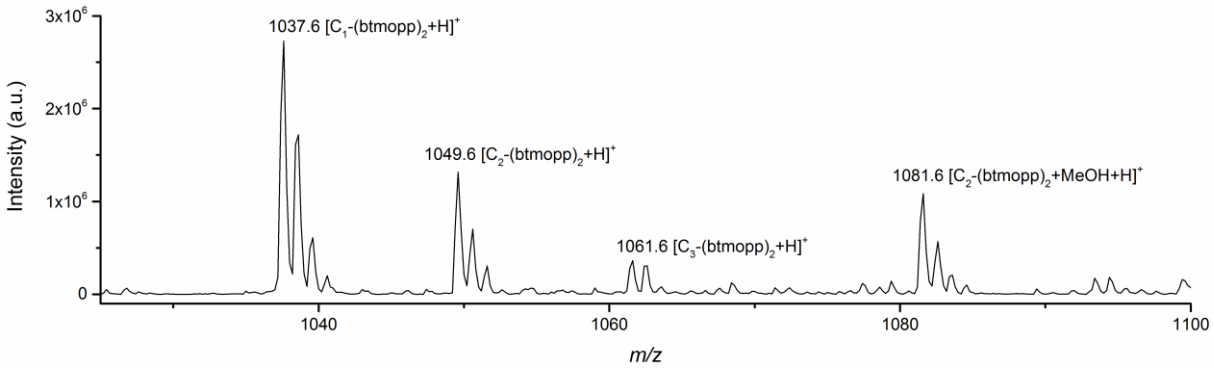


**Figure 9:** Mass spectra of different species observed during the reaction of 7 with MOMCl and $SnCl_4$.

Moreover, subjecting compound **39** again to the same reaction conditions did not lead to further bridging within the already formed dimer. This is unsurprising, if one considers the conformation of **39**, as determined by single crystal X-ray analysis (Figure 10). The two phenanthroline units are not aligned orthogonally as intended, but coplanarly on different heights, with the nitrogens facing towards each other. As long as this alignment is also prevalent in solution, it is obviously not possible to form more $CH_2$-bridges. Similarly, coordination of **39** to $Cu^I$ was not successful due to its unfavorable, non-tetrahedral conformation.

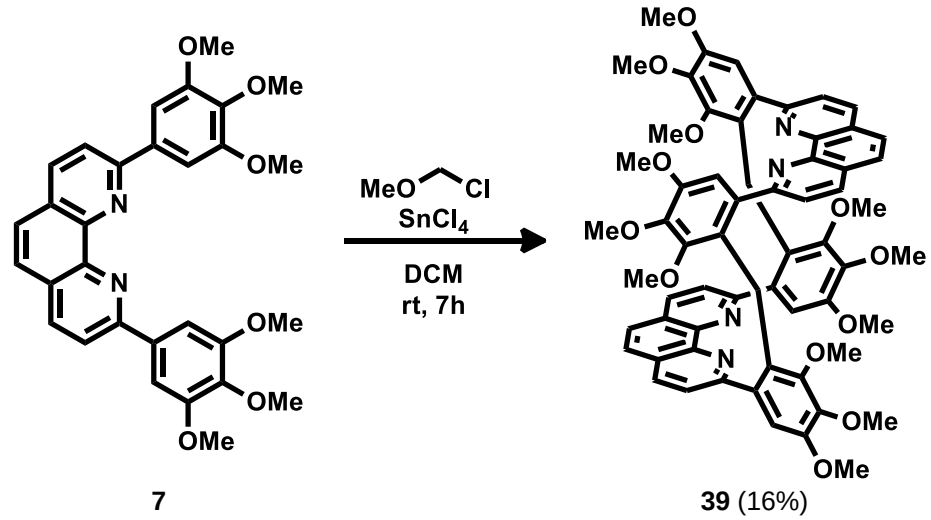


**7** **39** (16%)

**Scheme 24:** Synthesis of doubly bridged ligand **39**.

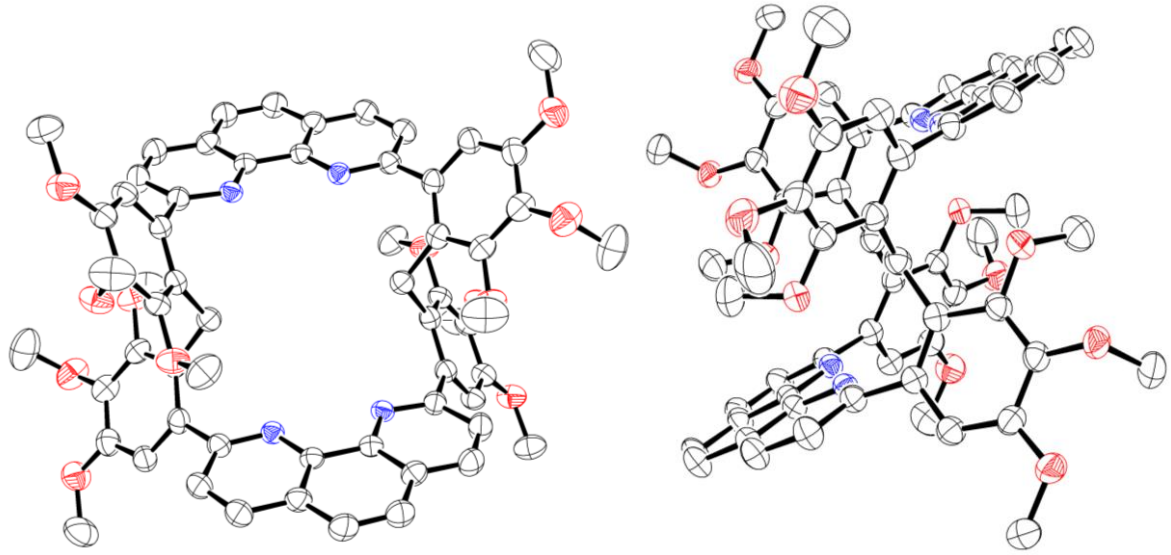

**Figure 10:** ORTEP drawing of **39** at 50% probability level, from two different angles. Hydrogen atoms and solvent molecules are omitted for clarity.

To assess the general coordination ability of **39** to a metal center, it was reacted with 0.5 equivalents $[Ir(COD)Cl]_2$ (COD = 1,5-cyclooctadiene). Indeed, the formation of a new species was observed by UPLC and is tentatively assigned to $[Ir(COD)(\mathbf{39})]^+$ (Figure 11). Hence, metal coordination seems to be possible, despite the large steric constraints imposed by the ligand.

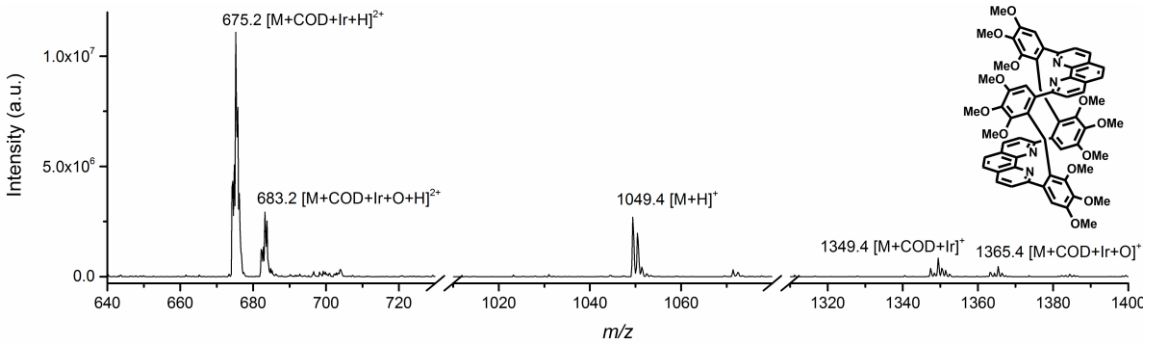


**Figure 11:** Mass spectrum of new species observed by UPLC-MS in the complexation of **39** with $[Ir(COD)Cl]_2$.

### 2.3.4. Imine Condensation Approach

Motivated by the promising results of the calixarene inspired approach, another "simple" reaction type – the imine condensation – was investigated for macrocyclization. In particular, the reaction of primary amines and aldehydes to form imines under the loss of water. These reactions are usually reversible but can be easily driven forwards by removing the eliminated water from the reaction mixture, e.g. using a Dean-Stark trap or adding molecular sieves. Otherwise, no further reagents or catalysts are necessary, which makes the reaction type perfect to form the sterically encumbered cage ligand.

The starting point for this strategy was the already described compound **34**, which provides the aldehyde functionality. Reaction with ethylenediamine under dilute conditions should yield the doubly bridged dimer, containing four imine functionalities, as was described previously.[66] In the presence of more ethylenediamine, the fully formed cage ligand can in principle be formed by nucleophilic attack of the primary amines at the imine-carbons (Scheme 25).

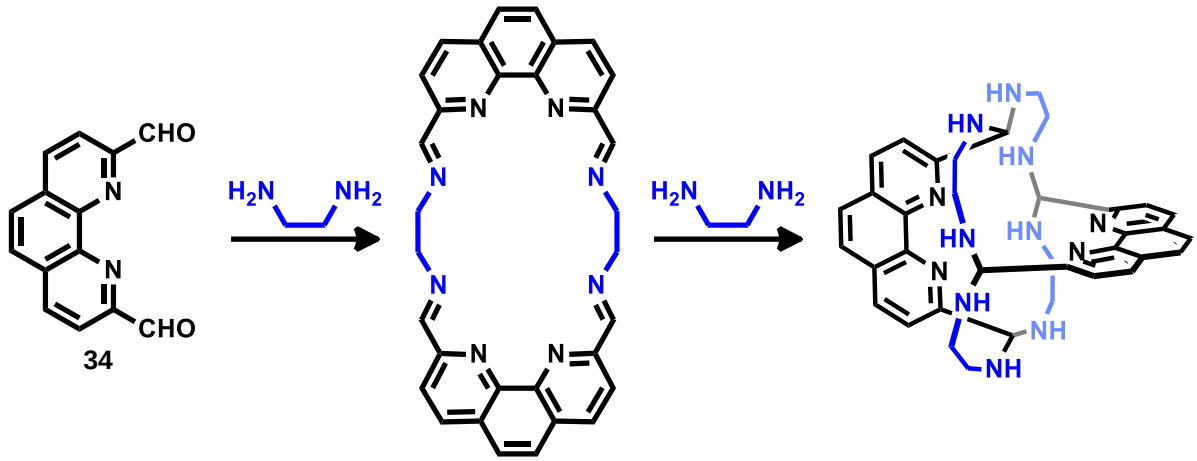


**Scheme 25:** General synthetic principle of the imine condensation approach.

The concept as presented in Scheme 25 is certainly accompanied by various problems. For example the generation of oligomers instead of the desired dimers, or simply the formation of 5-mebered heterocyclic rings (imidazolidinyl). To overcome these problems, ligand **40** was envisioned, which would allow for a more directed synthesis. By incorporating all amine groups into one molecule, only the first reaction step with dialdehyde **34** would have to occur intermolecularly, whereas all subsequent steps are intramolecular. Since compound **40** already bears the phenanthroline moiety, also the first step could be facilitated by templating with $Cu^{I}$ (Scheme 26).

The main difference between the “one-pot” approach and the more directed synthesis is obviously the ring size of the final macrocycle, which is 20 and 16 atoms, respectively.

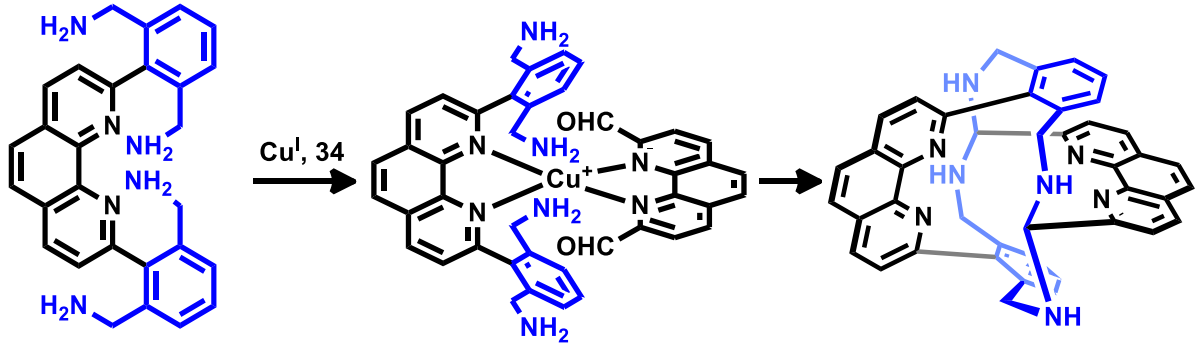


**40**

**Scheme 26:** More directed approach to form the cage ligand via imine condensation, using **40** and **34**.

### 2.3.4.1. Towards a Macrocyclic Cage Ligand via Imine Condensation

After several attempts of reacting **34** with ethylenediamine in a “one-pot” approach, it became clear that the undesired side reactions (oligomer formation, imidazolidinyl formation) predominantly occur over macrocyclization. Even templating with $Cu^{I}$ did not improve the outcome of the reactions. Therefore the synthesis of ligand **40** became the main focus.

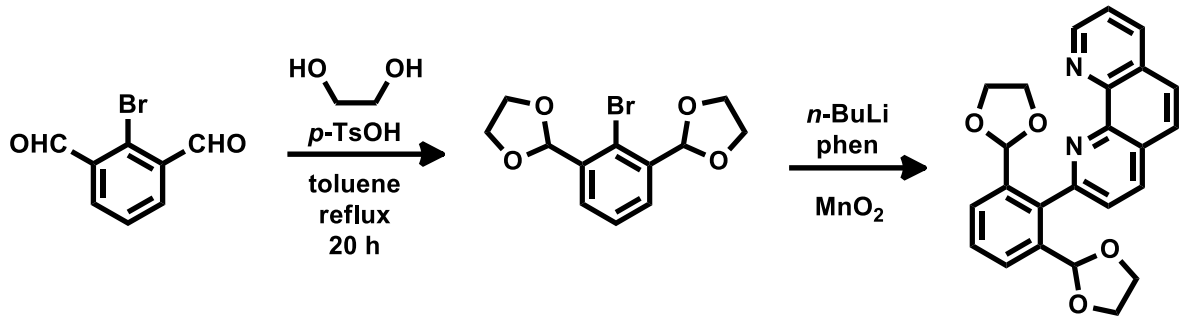


**41** (97%) **42** (68%)

**Scheme 27:** Synthetic pathway to monosubstituted ligand **42**.

To this end, commercially available 2-bromoisophthalaldehyde was protected as 1,3-dioxolane at both aldehyde functions to give **41** in 97% yield.[67] Lithiation of this with *n*-BuLi, followed by reaction with 1,10-phenanthroline leads to monosubstituted ligand **42** in 68% yield (Scheme 27). Subjecting **42** again to the same reaction conditions allows for a second substitution and gives ligand **43** in 49% yield (Scheme 28). Some efforts were made to deprotect **43** using HCl (aq) or *p*-TsOH, and even though tetraaldehyde **44** could be observed by UPLC-MS, it was not possible to isolate the product, probably due to the formation of polyacetals. However, by in-situ trapping of the reactive aldehyde groups using hydroxylamine, tetraoxime **45** could be accessed

directly in one step (75% yield). The reduction of **45** was attempted with $LiAlH_4$ as the reducing agent or via catalytic hydrogenation using palladium on activated charcoal. For the latter method, either too mild conditions (rt for 20 h, atmospheric hydrogen pressure) or too harsh conditions (refluxing MeOH for 20 h, atmospheric hydrogen pressure) were applied, leading to incomplete reaction and over-reduction, respectively. Unfortunately the tetraamine **40** could not be isolated so far, making it impossible to test the viability of this directed approach towards the macrocyclic cage ligand. However, by applying moderate conditions for the catalytic hydrogenation, the synthesis of **40** should be accomplished.

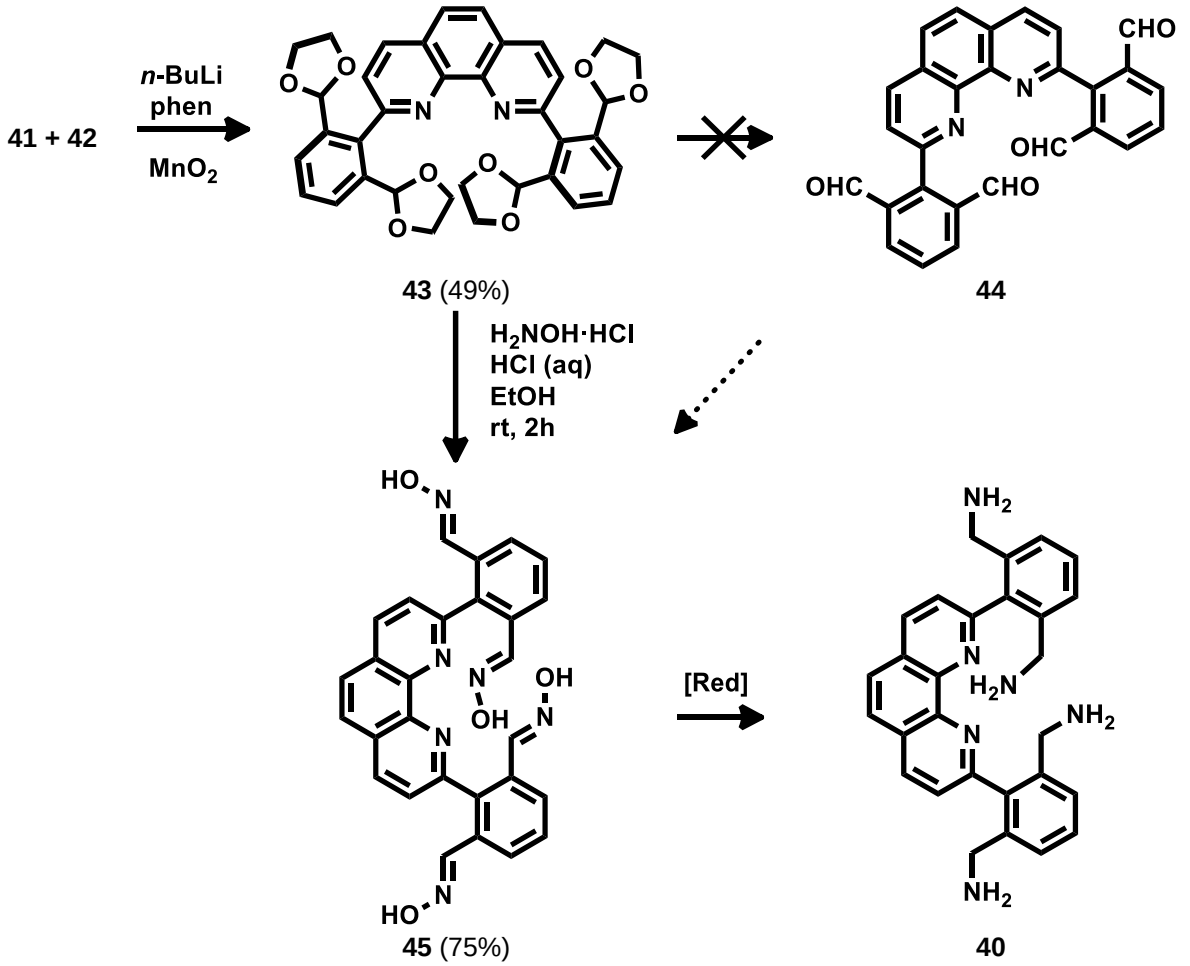


**Scheme 28:** Synthetic pathway leading to ligand **40**.

## 2.3.5. Heterocyclic Substituents Approach

Similar to the calixarene inspired approach, this strategy is based on 6-membered ring substituents at the phenanthroline core. However, the bridging positions are “activated” by a heteroatom, specifically nitrogen. Not only can these be connected by alkyl-chains, but potentially also by metal centers, which makes them much more versatile (Scheme 29). To this end, ligands **46** and **47** were envisioned, bearing hexahydropyrimidyl and pyrimidyl groups respectively.

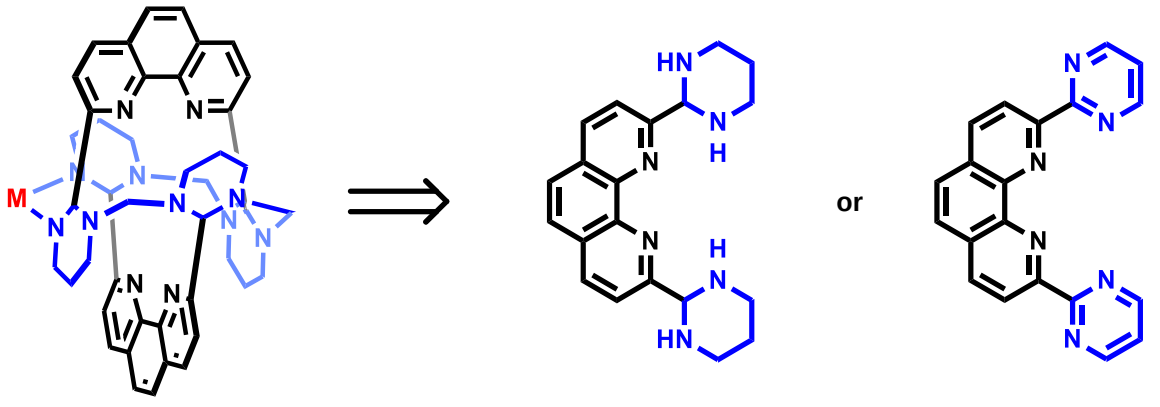


**46** **47**

**Scheme 29:** Left: Generalized structure of a possible tetrahedral cage ligand, showing both bridging possibilities ($CH_2$ and M = metal). Right: Envisioned ligand structures with heterocyclic substituents for this approach.

### 2.3.5.1. Hexahydropyrimidyl Substituents

The synthesis of **46** is easily achieved in one step by reaction of dialdehyde **34** with 1,3-diaminopropane (Scheme 30). The product is relatively prone to hydrolysis, i.e. under HPLC- or UPLC-conditions (acidic aqueous gradients) only decomposition products are observed. However, in solid state or in most organic solvents compound **46** is perfectly stable.

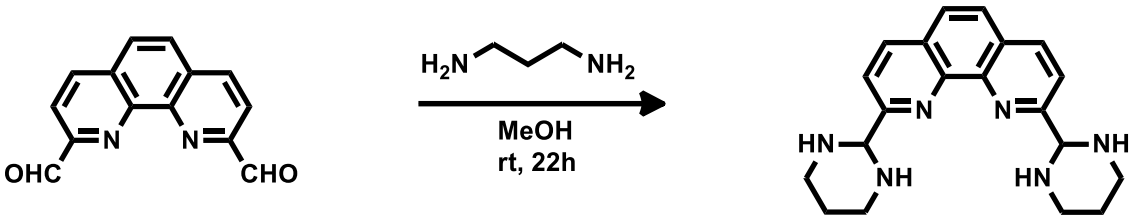


**34** **46** (85%)

**Scheme 30:** Synthesis of ligand 46.

The formation of a homoleptic $Cu^{I}$-complex of **46** would be very desirable, since this would serve as the perfect template to form the cage ligand. Therefore, prior to exploring the bridging between the heteroatoms at the hexahydropyrimidyl substituents, complexation of **46** to $Cu^{I}$ was investigated by reaction with $[Cu(MeCN)_4]BF_4$. Upon combining the two components in DCM, a red solution is obtained, which is indicative of the desired homoleptic compound. Furthermore, a reaction control by ESI-MS shows the formation of various species, including the desired complex $[Cu(\mathbf{46})_2]^+$ as a major component in the mixture (Figure 12). However, the observation of $Cu^{II}$ species as well as the sodium complex $[Na(\mathbf{46})_2]^+$ is indicative of a very low stability of the homoleptic $Cu^{I}$ complex. Nevertheless, bridging attempts were performed with both the free ligand and the in-situ formed complex.

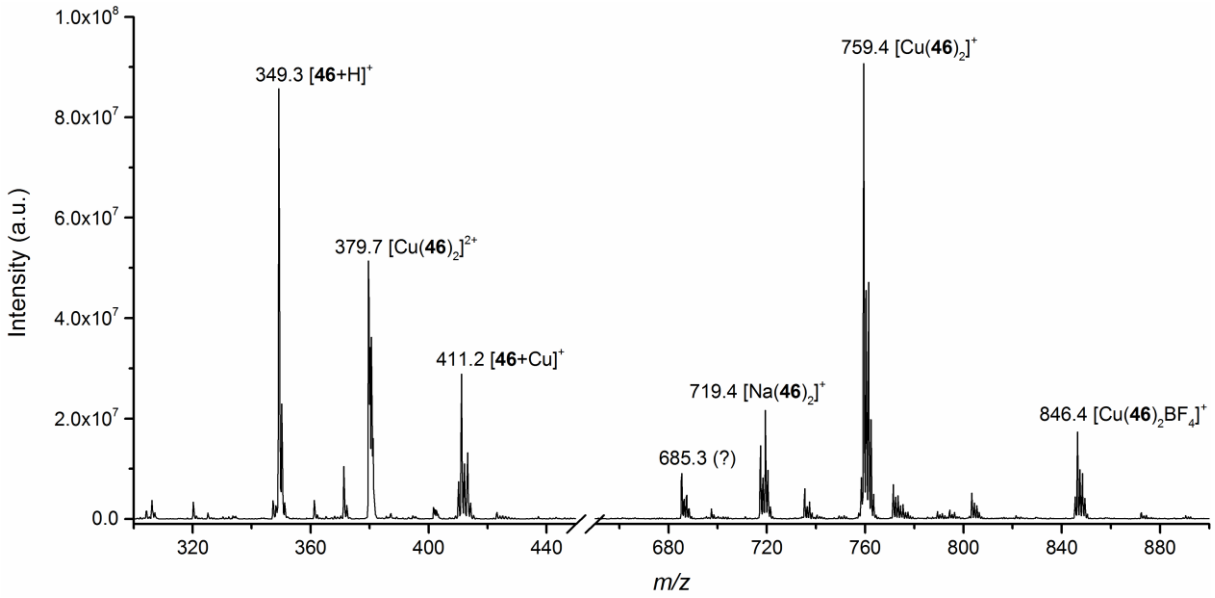


**Figure 12:** Direct injection ESI-MS during the complexation of ligand **46** to $Cu^{I}$ using $[Cu(MeCN)_4]BF_4$ as the metal source. The reaction was performed in DCM, for ESI-MS analysis, the reaction mixture was diluted with MeOH.

Figure 13 shows the result of reacting the in-situ formed $Cu^{I}$ complex with diiodomethane ($CH_2I_2$). The $CH_2$-bridged dimer of ligand **46** (coordinated to copper) is observed as the major product, along with considerable amounts of an unknown species (*m/z* 717.4) and various other minor components. If the same reaction is carried out without the $Cu^{I}$ ion as a template, no formation of the dimeric species or any other desirable product is observed. This clearly validates the templating-approach for this reaction type.

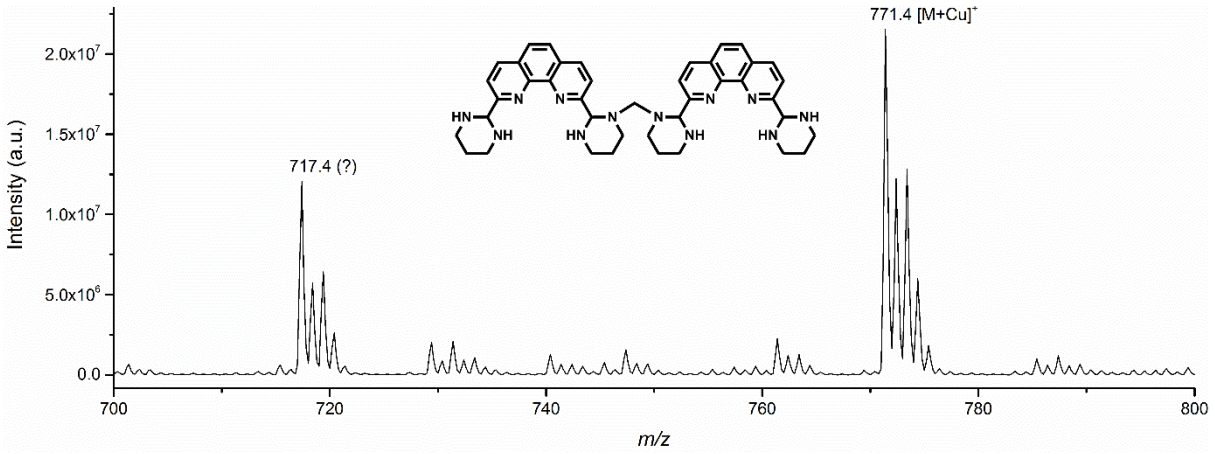


**Figure 13:** Direct injection ESI-MS of a reaction mixture containing **46**, $[Cu(MeCN)_4]BF_4$ and $CH_2I_2$ in MeOH.

Consequently, bridging with a metal center was attempted only with the in-situ formed $Cu^{I}$-complex, which additionally prevents coordination of the bridging metal to the phenanthroline nitrogens. Reaction with $[Pt(COD)Cl_2]$ yields a complex mixture of products, as observed by ESI-MS (Figure 14). Nevertheless, most of the peaks can be reasonably assigned, including mixed metal dinuclear complexes. Unfortunately, in

none of the species the platinum seems to assume a bridging role. This is concluded, since every platinum center is always accompanied by COD and Cl, which saturate three coordination sites, therefore only leaving one open site.

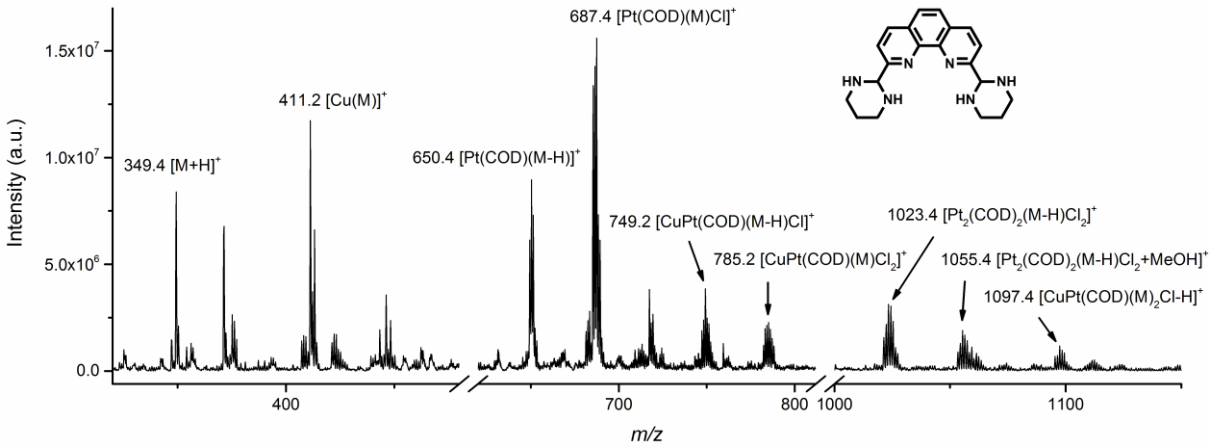


**Figure 14:** Direct injection ESi-MS of a reaction mixture containing 46, $[Cu(MeCN)_4]BF_4$ and $[Pt(COD)Cl_2]$ in DCM.

### 2.3.5.2. Pyrimidyl Substituents

For the synthesis of dipyrimidyl substituted ligand **47**, three strategies were applied (Scheme 31).

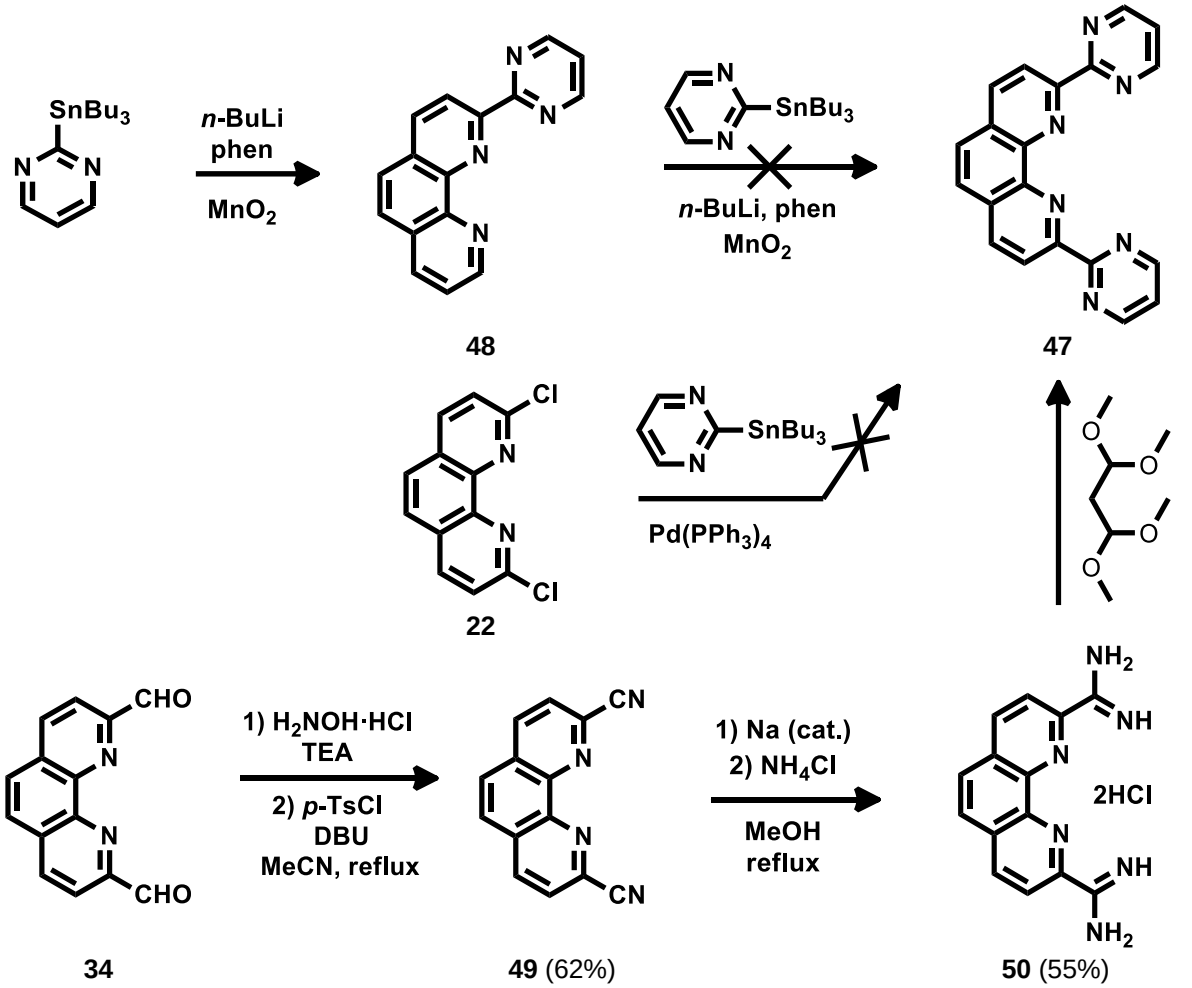


**Scheme 31:** Synthetic pathways towards ligand 47.

In the first approach, 2-lithiopyrimidine was generated by treating the corresponding tributylstannyl-reagent with *n*-BuLi, which was then reacted with 1,10-phenanthroline to give the monosubstituted intermediate **48**. However, further substitution of this, using the same reaction conditions, was not possible. Instead, Stille coupling of **22** with the same stannyl-reagent was explored by screening various reaction conditions. Again, the monosubstituted intermediate **48** was observed by UPLC-MS but further substitution was not achieved.

In the third approach, dialdehyde **34** was transformed into dinitrile **49** in a one pot reaction: Initially the oxime is formed, followed by sulfonation and base-induced elimination in the second step.[68] Dinitrile **49** was then treated with catalytic amounts of sodium (~20 mol%) in MeOH, followed by the addition of $NH_4Cl$ to yield diamidine **50** as the dihydrochloride salt. In the last step, reaction of the amidine groups with malondialdehyde, which was formed in-situ from 1,1,3,3-tetramethoxypropane, should yield the desired ligand **47**. Indeed, according to UPLC-MS clean formation of ligand **47** is observed, accompanied only by minor amounts of side products (Figure 15).

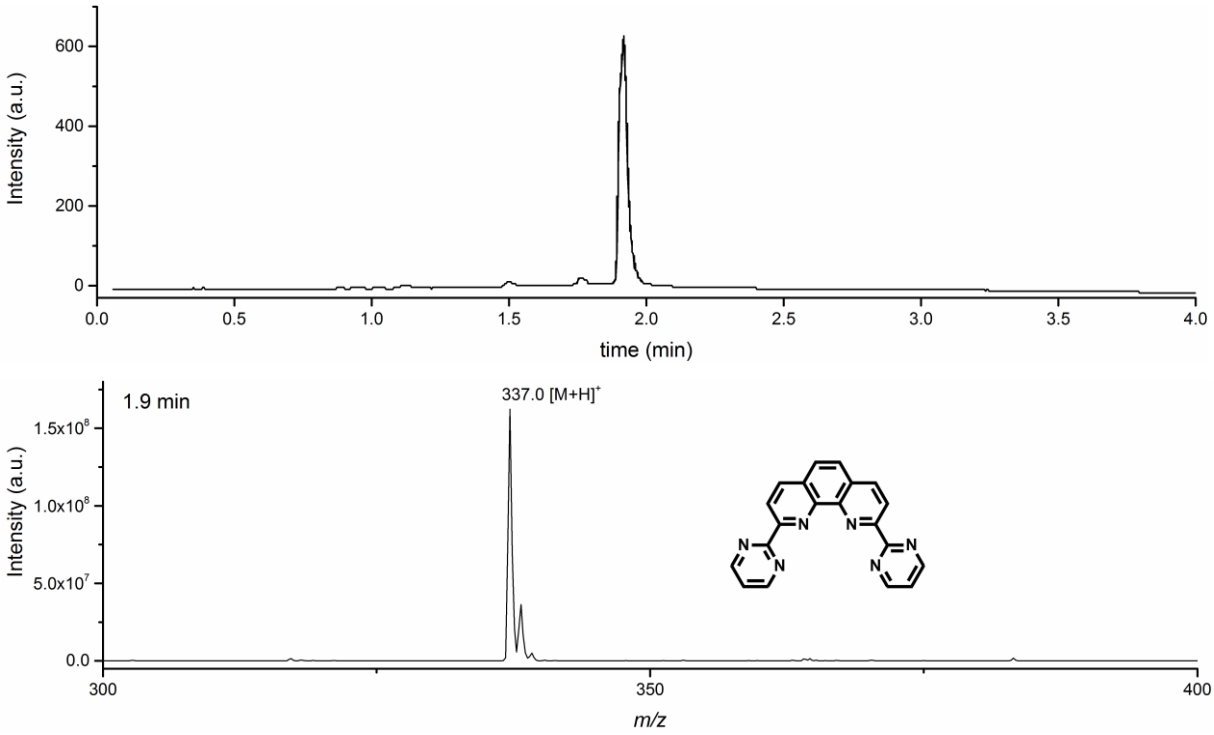


**Figure 15:** UV chromatogram (246 nm) of the crude product after the conversion of **50** to **47** (top) and the corresponding mass spectrum of the main peak at 1.9 min (bottom).

The reaction proceeds optimally under microwave irradiation at 175 °C for 1 h, using *N*-methyl-2-pyrrolidone (NMP) as the solvent. Similarly, some conversion to the product (~5%) can be obtained thermally, by stirring at 190 °C for several hours. However, in order to drive the reaction to completion, probably several days or even

higher temperatures are necessary. Despite the clean transformation as observed by UPLC, the final product seems to be highly contaminated with impurities (dark brown crude), probably originating from excess malondialdehyde. So far no appropriate purification procedure was found and therefore complexation and bridging attempts towards the tetrahedral cage ligand were not performed with this substrate.

### 2.3.6. Diazaspirobifluorene Preliminary Results

All the previously discussed strategies focus on stabilizing the tetrahedral structure by forming a macrocycle in closest proximity to the coordination sites. Even though this has several advantages (see 2.3.1), it is synthetically very challenging, due to the tight space the macrocyclization has to occur in. Therefore a slightly different approach based on 4,5-diazaspirobifluorene (**51**) was considered (Scheme 32). In this case, the tetrahedral geometry is dictated by the spiro-carbon of the ligand itself and the stabilization of the complex is achieved by linear connections between two ligands. However, since $Cu^{I}$ complexes of this ligand type are largely unknown, first the general coordination properties were investigated.

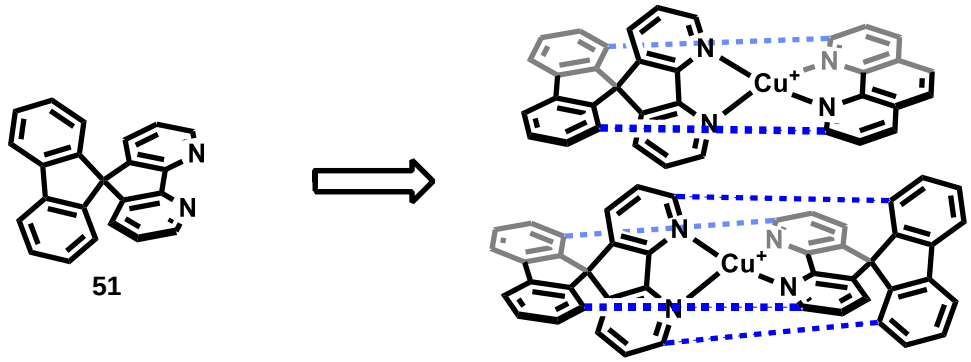


**Scheme 32:** Possible tetrahedral cage ligands based on 4,5-diazaspirobifluorene.

#### 2.3.6.1. Ligand and Complex Synthesis

Ligand **51** was prepared according to a literature procedure, starting from 2-iodobiphenyl, which was transformed to the corresponding Grignard reagent and subsequently reacted with 4,5-diazafluorenone.[69]

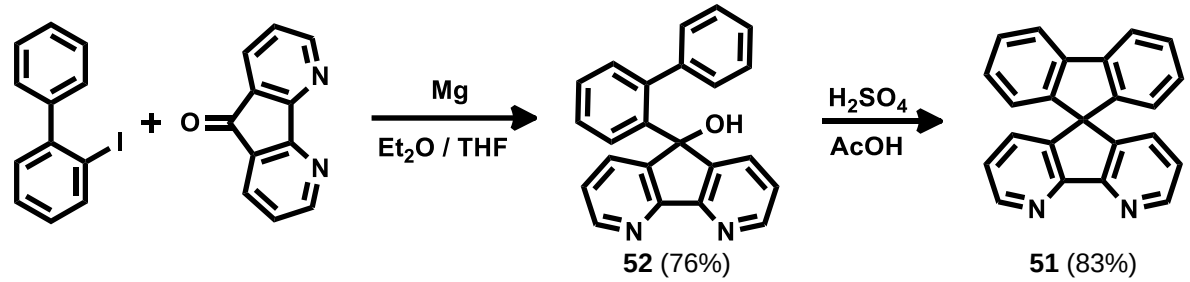


**Scheme 33:** Two-step synthesis of ligand **51**.

The resulting intermediate **52** was then cyclized by treatment with sulfuric acid to give the desired ligand **51** with an overall yield of 63%.

Interestingly, the derivatization of the nitrogen ortho-positions works analogously to phenanthroline (see 2.1.1), as was demonstrated previously with PhLi.[70] Similarly, the introduction of two *s*-butyl groups was achieved in one step using *s*-BuLi, producing ligand **53** as a mixture of diastereoisomers.

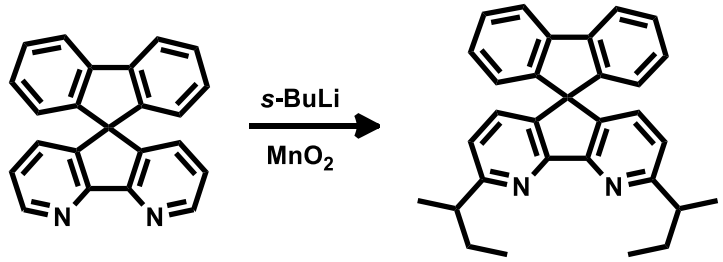


**51** **53** (11%)

**Scheme 34:** Introduction of *s*-Bu groups, using the same method as for phenanthroline derivatives.

Both ligands **51** and **53** were reacted with 0.5 equivalents $[Cu(MeCN)_4]BF_4$ in anticipation of the homoleptic complexes. The reaction with unsubstituted ligand **51** yields an orange solution, which turns green upon exposure to air, probably due to oxidation of the metal center to $Cu^{II}$. Direct injection ESI-MS during the reaction does not show the formation of any coordination compounds, only free ligand is observed. However, slow evaporation of the orange solution under nitrogen atmosphere yields a crystalline product, which was identified as $[Cu(\mathbf{51})_3]BF_4$ by single crystal X-ray analysis (Figure 16).

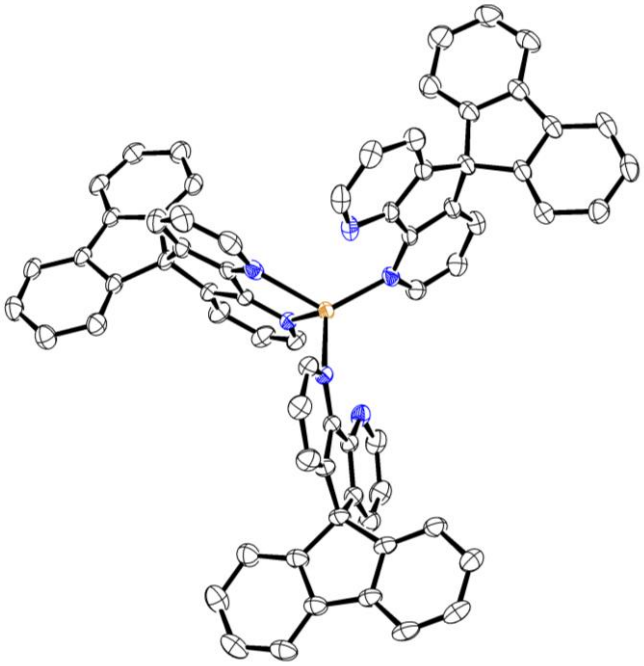

**Figure 16:** ORTEP drawing of $[Cu(51)_3]BF_4$ at 50% probability level. Hydrogen atoms and the anion are omitted for clarity.

For the substituted ligand **53** the homoleptic $Cu^{I}$ complex is observed by ESI-MS (Figure 17). However, the presence of significant amounts of free ligand as well as the sodium complex, indicates a rather high lability of the compound.

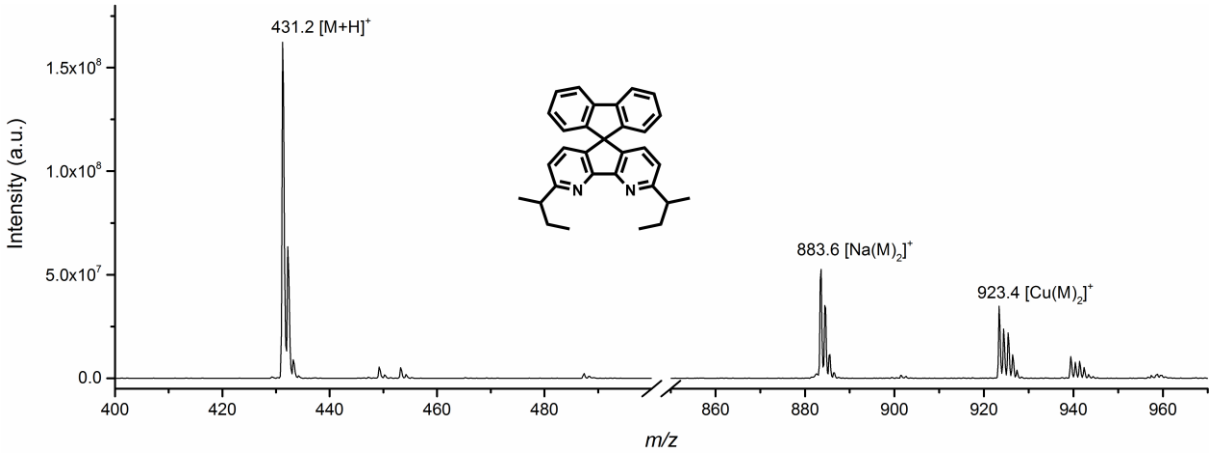


**Figure 17:** Direct injection ESI-MS in MeOH after reacting ligand **53** with 0.5 equivalents $[Cu(MeCN)_4]BF_4$.

Formation of the homoleptic complex in case of ligand **53** is also strongly indicated by $^1$H NMR (Figure 18). All signals are clearly shifted after reaction with $Cu^{I}$ and only traces of free ligand are left. Additionally, a high symmetry is retained, which suggests identical coordination modes of the ligands. Unfortunately, it was not possible to grow single crystals of the complex, which is commonly observed for complexes containing *s*-Bu groups, due to the presence of diastereoisomers.

Apparently, the bulkiness of the *s*-Bu groups prevents the formation of $[Cu(\mathbf{53})_3]^+$, as it was observed for the unsubstituted ligand **51**. This fact in combination with the lack of other coordination partners, probably leads to the formation of the homoleptic complex. This explanation is also consistent with the observations in ESI-MS analysis, where the complex is brought into a more coordinating environment (MeOH).

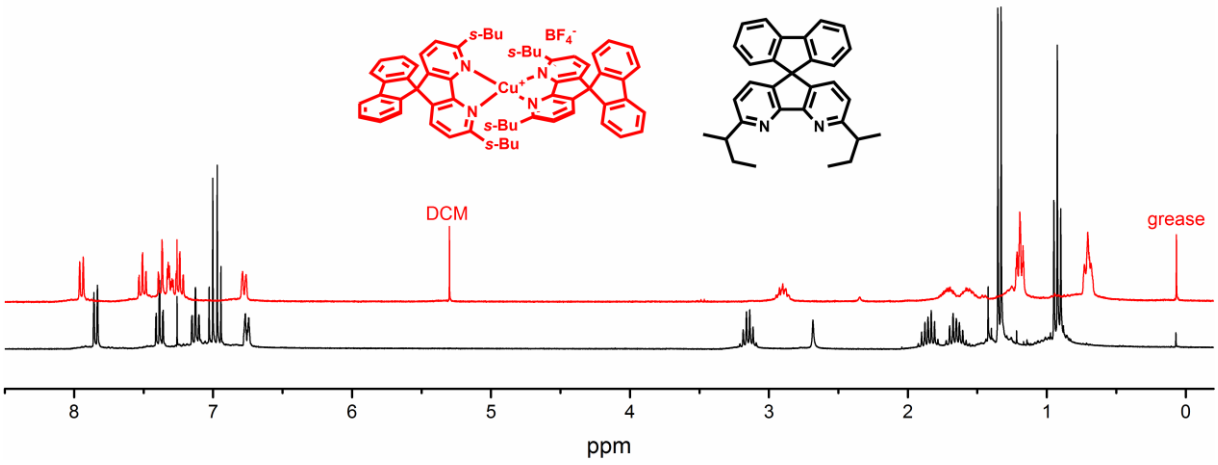


**Figure 18:** $^1$H NMR in $CDCl_3$ of ligand **53** before (black) and after (red) reaction with 0.5 equivalents $[Cu(MeCN)_4]BF_4$.

A comparison of the UV/VIS spectra of ligand **53** and its homoleptic $Cu^{I}$ complex clearly shows the extended absorption into the visible region upon metal coordination (Figure 19). Furthermore, the complex shows photoluminescence when excited at 410 nm with an estimated lifetime of ~60 ns (in deaerated DCM).

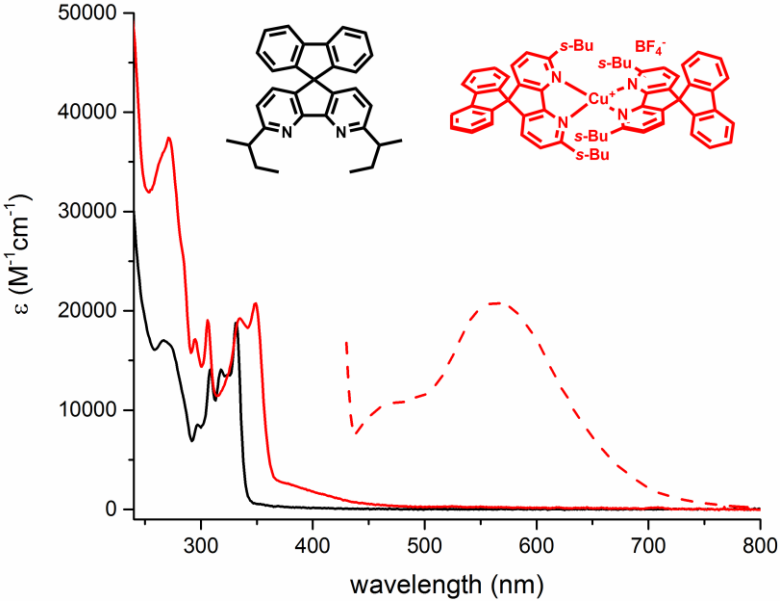


**Figure 19:** UV/VIS absorption spectra of **53** (full black line) and $[Cu(\mathbf{53})_2]BF_4$ (full red line) both 10 µM in DCM and normalized emission of $[Cu(\mathbf{53})_2]BF_4$ (dashed red line) at 100 µM in Ar-degassed DCM after excitation at 410 nm.

# 2.4. System Development with $Cu^{I}$ Complexes

## 2.4.1. Properties of $Cu^{I}$ Complexes

### 2.4.1.1. Stability of CuI-Complexes

In contrast to $[Cu(MeCN)_4]X$ (see 2.2), the homoleptic bis-phenanthroline $Cu^{I}$-complexes are very stable towards oxidation in solid form and – depending on the solvent – also in solution. Even though phenanthroline ligands stabilize copper in the +1 oxidation state, the complexes are kinetically labile in solution and fast ligand exchange reactions can occur.[71] This leads to an equilibrium of various species, highly dependent on the ability of the solvent to solubilize the ligand and to stabilize $Cu^{I}$-ions. This is nicely demonstrated by comparing the UPLC traces of $[Cu(dsbtmp)_2]BF_4$ (**15**) in different solvents after equilibrating for 24 h (Figure 20). In coordinating solvents, such as DMF and MeCN, the chromatograms show a high percentage of free ligand being present in solution (peak at 2.8 min). On the other hand, in a non-coordinating solvent such as DCM, the complex seems to be the favored species (peak at 3.9 min). This is confirmed by $^{1}$H-NMR-analysis of the complex in $CDCl_3$, where only one species is observed. In fact, the free ligand present in the DCM-chromatogram might just be due to ligand exchange during UPLC-analysis, since it is run with a gradient containing MeCN. In MeOH, the complex seems to be surprisingly stable, considering the coordinating ability of the solvent. However, the free ligand is very badly soluble in MeOH, which offers a reasonable explanation for the observed behavior.

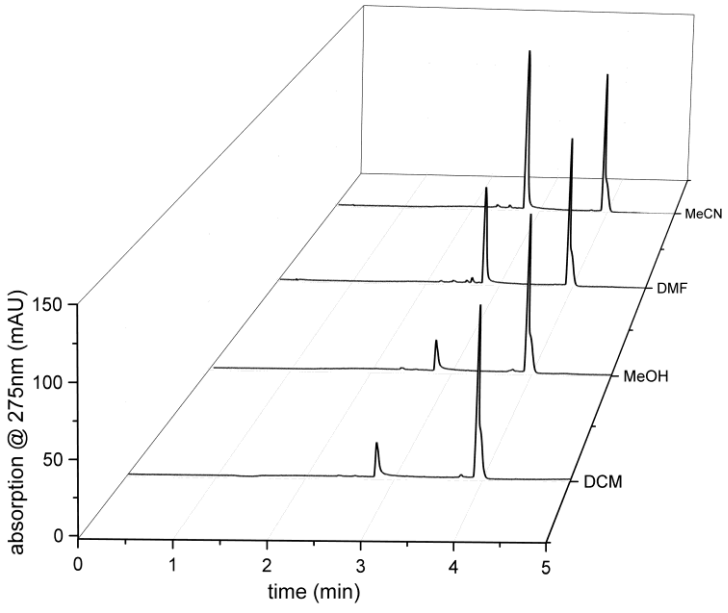


**Figure 20:** UPLC-traces (gradient of MeCN, $H_2O$ / formic acid) of $[Cu(dsbtmp)_2]BF_4$ in various solvents after 24 h of equilibration (100 µM sample concentration). The peak at 2.8 min corresponds to the free ligand dsbtmp, the peak at 3.9 min to the complex $[Cu(dsbtmp)_2]BF_4$. All chromatograms were normalized to the peak at 3.9 min.

### 2.4.1.2. UV/VIS Absorption-Spectra

Figure 21 shows the absorption spectra of complexes **11** - **18** in the near UV and visible region. The bands in the UV (below ~350 nm) originate from ππ* transitions of the phenanthroline ligands, which typically have very high extinction coefficients (ε > 20000 $M^{-1}cm^{-1}$). More interesting, however, are the absorption features in the visible region of the solar spectrum, which are assigned to metal-to-ligand-charge-transfer (MLCT) transitions and can be subdivided into three bands (I-III).[72]

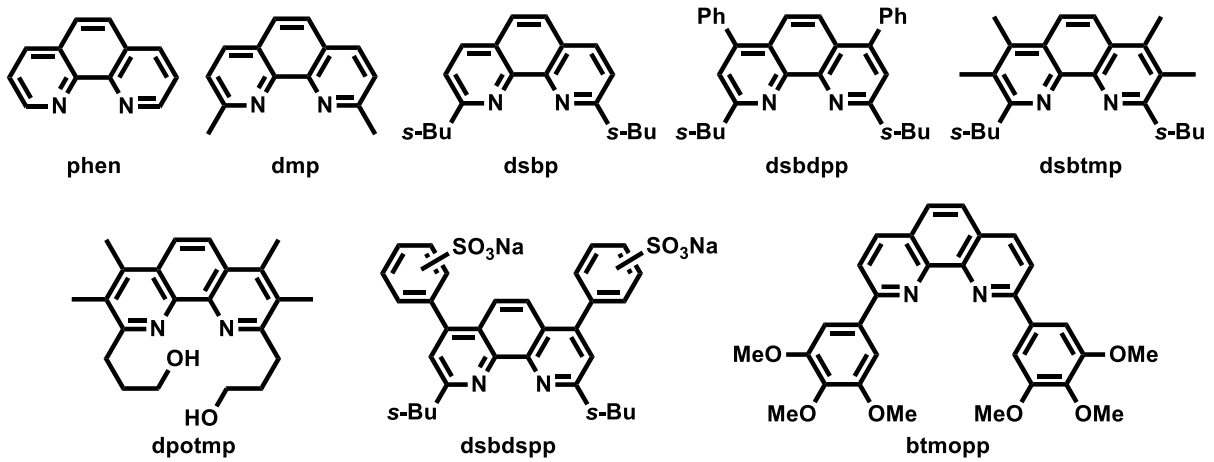


**Scheme 35:** Molecular structures and the corresponding abbreviations of phenanthroline ligands relevant in this chapter.

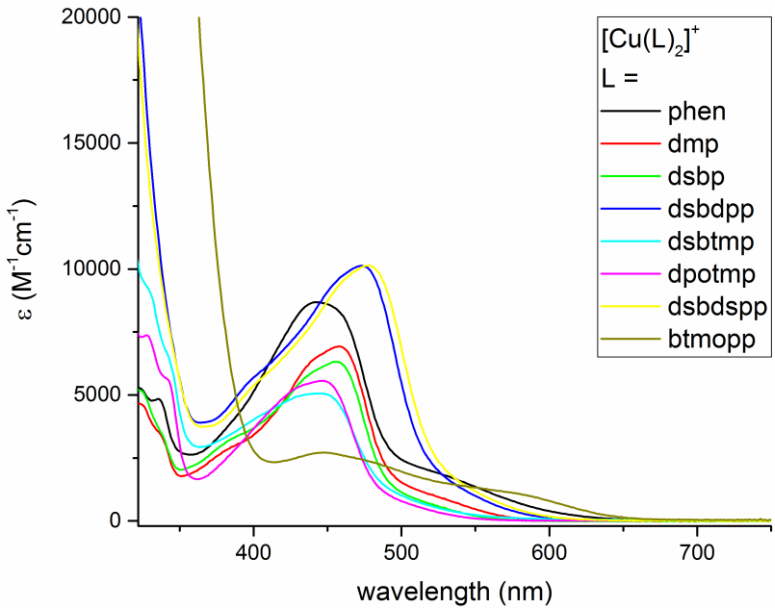


**Figure 21:** UV/VIS absorption spectra for complexes **11** - **18** (0.1 mM). The spectra were recorded in DCM, except for $[Cu(dsbtmp]_2]BF_4$ and $[Cu(dsbdpp)_2]BF_4$ (DMF), as well as $[Cu(dsbdspp)_2]BF_4$ (water).

Band I refers to the lowest energy transition (> 500 nm), which is usually only visible as a shoulder. The most prominent feature between 400 nm and 480 nm is termed band II and the highest energy transition (350 - 400 nm) band III, which is also generally only present as a shoulder. The relative intensity of these three bands is

highly dependent on the symmetry of the complex in solution. From the schematic orbital splitting diagrams for $D_{2d}$-symmetry (perfectly tetrahedral complex) and $D_2$-symmetry (distorted tetrahedral complex), as shown in Figure 22, the absorption behavior of the different complexes can be rationalized.

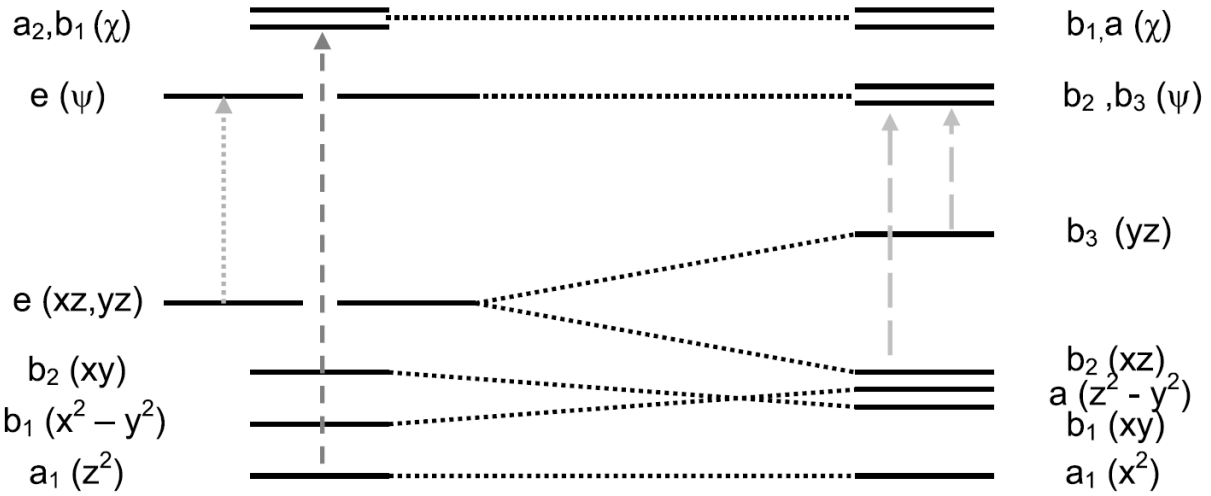


**Figure 22:** Orbital splitting diagram for $D_{2d}$-symmetry (left) and $D_2$-symmetry (right) of homoleptic Cu-bisphenanthroline complexes. Grey arrows indicate the transitions of band I (long dashes), band II (dots) and band III (short dashes).[72]

The mostly dominant band II originates from the e (xz, yz) → e (ψ) transition and the much weaker band III results from the $a_1$ ($z^2$) → $a_2$, $b_1$ (χ) transition, both in $D_{2d}$-symmetry. In contrast, the low energy band I requires a lowered symmetry (towards $D_2$) and is assigned to the $b_2$ (xz) → $b_2$, $b_3$ (ψ) and $b_3$ (yz) → $b_2$, $b_3$ (ψ) transitions.[72] Consequently, the shoulder towards lower energy is a measure for the degree of distortion from a perfect tetrahedral geometry in solution. This effect is nicely observed in the series phen, dmp, dsbp, where the increasingly bulky substituents in 2,9-position force the complex into the tetrahedral geometry and thereby reduce the intensity of band I. The most pronounced low energy transition is observed for $[Cu(btmopp)_2]BF_4$, which is common for 2,9-aryl-substitution due to interligand ππ stacking interactions with the opposite phenanthroline moiety, leading to a flattening distortion towards $D_2$-symmetry (Figure 23). Apart from these symmetry related effects, also the electronic influence of the substituents can be observed. An expanded π-system by introduction of phenyl-substituents in the 4,7-positions leads to a redshift of the absorption maximum up to 478 nm. On the other hand, an increasing amount of σ-donating alkyl-groups leads to a blueshift of the maximum, which is also observed for the electron rich trimethoxyphenyl-substituents in case of $[Cu(btmopp)_2]BF_4$.

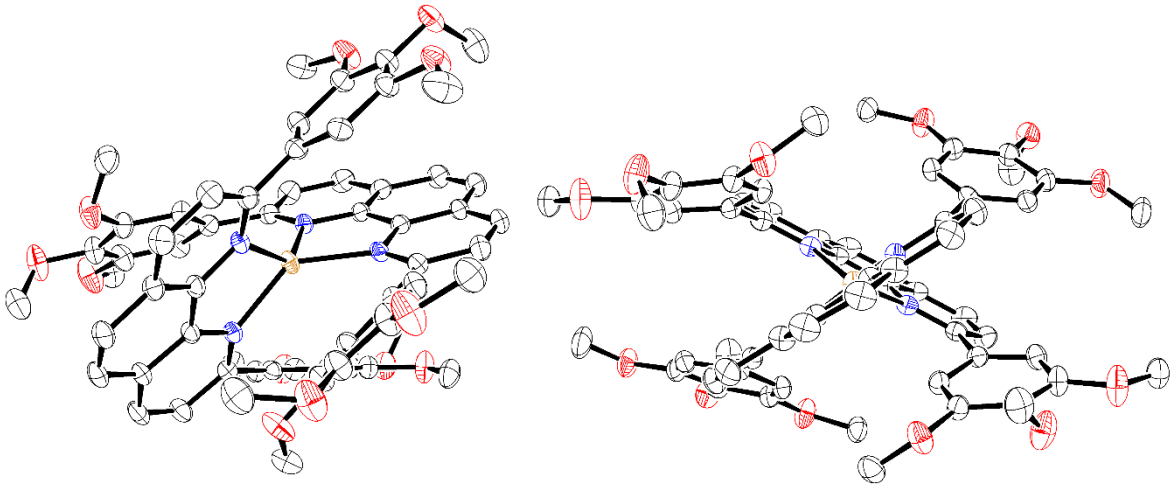

**Figure 23:** ORTEP drawing of **18** at 50% probability level, from two different angles. Hydrogen atoms, solvent molecules and anion are omitted for clarity.

### 2.4.1.3. Emission-Spectra and –Lifetimes

The luminescence spectra are generally dominated by a broad band between 600 and 700 nm, which is due to emission from a MLCT excited state (Figure 24). Previous investigations of the emission properties at variable temperatures showed that this band is a superimposition of phosphorescence from the lowest lying triplet excited state ($T_1$) and E-type delayed fluorescence from the lowest lying singlet excited state ($S_1$).[35b, 73] Very striking is the difference in emission intensity, which ranges from no emission at all for $[Cu(phen)_2]BF_4$ to the highly emissive $[Cu(dsbtmp)_2]BF_4$. This phenomenon is well understood and explained by the presence of bulky substituents in the 2,9-position of the phenanthroline ligands: Since the light absorption is based on a MLCT, the metal center is formally oxidized to $Cu^{II}$, which prefers a different coordination geometry (towards $D_2$-symmetry). This leads to conformational distortions in the excited state and as a result to a decrease in energy of both $T_1$ and $S_1$.[73c] Hence, according to the energy-gap law, a lower emission yield is expected if the structural distortions are severe.[74] Moreover, intermolecular quenching via exciplex formation is greatly facilitated, due to a better accessibility of the metal center for solvent molecules upon geometrical distortion. Both these detrimental effects are minimized by bulky substituents in the 2,9-position, which hinder distortions in the excited state and therefore lead to a more intense luminescence. This substituent effect is nicely demonstrated in the series $[Cu(phen)_2]BF_4$ (no luminescence), $[Cu(dmp)_2]BF_4$ (weak luminescence), $[Cu(dsbp)_2]BF_4$ / $[Cu(dsbdpp)_2]BF_4$ (considerable luminescence) and $[Cu(dsbtmp)_2]BF_4$ (strong luminescence). In the last example, a cooperative steric

influence of the additional methyl-substituents is believed to be the reason for the extraordinary emission properties.[35b]

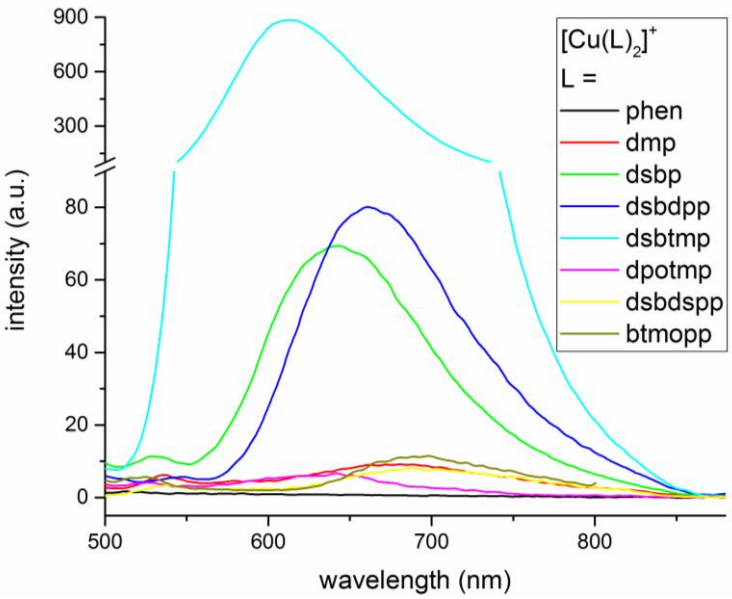


**Figure 24:** Room temperature uncorrected luminescence spectra of complexes **11** - **18** in Ar-degassed DCM-solution, except $[Cu(dsbdspp)_2]BF_4$ (water-solution). Sample concentrations are 10 µM for the most luminescent complexes 13 - 15 and 100 µM for all the others, the excitation wavelength is the absorption maximum of the corresponding complex in the visible region.

Unlike the other *sec*-butyl substituted complexes, $[Cu(dsbdspp)_2]BF_4$ shows only very weak luminescence, which is attributable to the difference in solvent (DCM vs. water). A strong solvent influence is also observed for the other complexes, as is reflected by their luminescence lifetimes in different solvents (Table 1). As mentioned before, the complexes are very prone to exciplex quenching in the excited state, which becomes more pronounced in polar solvents. With increasing steric shielding of the metal center, the effect decreases substantially ($[Cu(dsbtmp)_2]BF_4$).

An unexpected low luminescence intensity is observed for $[Cu(dpotmp)_2]OTf$, considering the bulkiness of the substituents. However, this has been found for similar complexes bearing hydroxy- or ether-groups in proximity of the metal center and was attributed to intramolecular quenching.[73b, 75] Furthermore, the luminescence of $[Cu(btmopp)_2]BF_4$ is quite weak, which likely results from the distortion of the complex already in its ground state, due to interligand ππ-stacking interactions (see 2.4.1.2).

**Table 1:** Summary of absorption-, emission- and electrochemical properties of $Cu^{I}$-complexes **11** - **18**.

| Compd. | $\lambda_{abs}$[a] (nm) | $\varepsilon$[a] ($M^{-1}cm^{-1}$) | $\lambda_{em}$[a] (nm) | $\tau$ (ns) | $E_{ox}$[f] (V) | $E_{red,1}$[f] (V) | $E_{red,2}$[f] (V) | $E^*_{ox}$[j] (V) | $E^*_{red}$[j] (V) |
|---|---|---|---|---|---|---|---|---|---|
| **11** | 443 | 8700 | - | - | -0.35 | -2.04[i] | -2.22[i] | - | - |
| **12** | 458 | 6900 | 675 | [d] 270[a] | 0.15 | -2.10 | -2.32 | -1.69 | -0.26 |
| **13** | 455 | 6300 | 645 | 210[e] 40[b] | 0.46[g] | -2.12 | -2.38 | -1.46 | -0.20 |
| **14** | 473[b] | 10100[b] | 660 | 310[a] 1950[a] | 0.42[g] | -2.00 | -2.22 | -1.46 | -0.12 |
| **15** | 444[b] | 5100[b] | 615 | 1760[e] 1110[b] | 0.43[h] | -2.38[h] | -2.59[h] | -1.59 | -0.36 |
| **16** | 446 | 5600 | 640 | d | d | d | d | d | d |
| **17** | 478[c] | 10100[c] | 690[c] | 40[c] | 0.37[g] | -2.06 | -2.28 | -1.43 | -0.26 |
| **18** | 447 | 2700 | 690 | 150[a] | d | d | d | d | d |

[a] DCM; [b] DMF; [c] $H_2O$; [d] not determined; [e] EtOH/$H_2O$ 8/2; [f] 0.1 M $TBAPF_6$, DMF vs $Fc/Fc^+$ at 0 V; [g] irreversible process, $E_{pa}$ given; [h] 0.1 M $TBAPF_6$, MeCN vs $Fc/Fc^+$ at 0 V; [i] irreversible process, $E_{pc}$ given; [j] minimal excited state potentials were estimated as $E^*_{red/ox} = E_{red/ox} \pm E_{00,min}$ ($E_{00,min}$ is the emission energy at maximum intensity).

### 2.4.1.4. Electrochemistry

The electrochemistry of $Cu^{I}$-bisphenanthrolines has been investigated previously and three processes are generally observed:[76] Towards positive potentials an oxidation, which is metal centered and therefore evidently assigned to the $Cu^{II/I}$ couple. In the cathodic region two closely spaced processes occur, which are assigned to the sequential reduction of both ligands to form radical anions. The redox potentials of complexes **11** - **15** and **17** are summarized in Table 1 and are graphically represented in Figure 25.

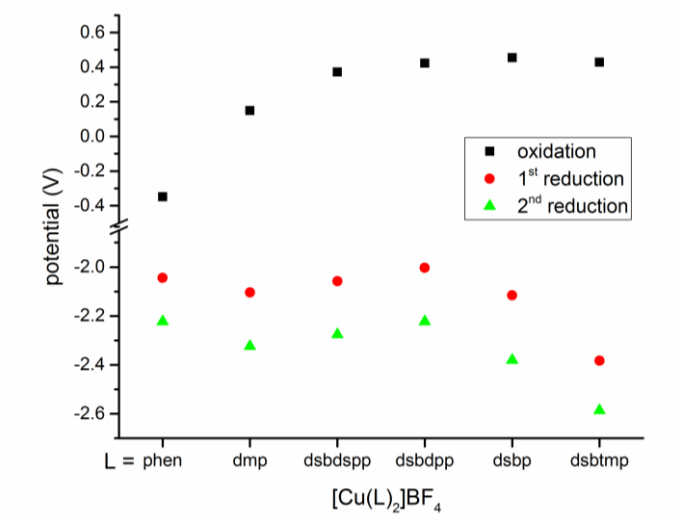


**Figure 25:** Redox potentials of complexes **11** - **15** and **17**. The potentials were determined by CV in DMF with 0.1 M $TBAPF_6$ as supporting electrolyte vs Ag / AgCl and are reported vs $Fc^{+/0}$ as an internal standard. For irreversible processes, the cathodic or anodic peak potentials are given (see Table 1 for details).

A rather large anodic shift of ~0.8 V is observed for the oxidation process, concurrent with increasing bulkiness of the 2,9-substituents of the phenanthroline ligand, which

points to a purely steric effect. Indeed, the bulky substituents lock the tetrahedral conformation, preferred by $Cu^{I}$, in place and as a result disfavor the oxidation process. On the reductive side, the trends mostly originate from electronic effects of the substituents: Introduction of electron rich alkyl-groups shifts both reduction potentials cathodically, whereas introduction of electron poor phenyl-groups leads to an anodic shift.

Both the first and second reduction show high electrochemical reversibility for all complexes as is shown representatively for $[Cu(dsbp)_2]BF_4$ (Figure 26, left). The single exception is the unsubstituted complex $[Cu(phen)_2]BF_4$, which shows an irreversible reduction at 100 mV/s, and becomes quasi-reversible upon increase of the sweeprate (Figure 26, right). The corresponding second reduction does not show any sign of reversibility even at higher sweeprates.

Previous electrochemical investigations of differently substituted bis-phenanthroline $Cu^{I}$-complexes also found the first reduction event to be mostly reversible, however the second reduction is generally reported as irreversible. This is explained with ligand dissociation and formation of $Cu^{0}$ and seems to be dependent on various factors, such as ligand substituents, solvent and supporting electrolyte.[76a-c] Especially the solvent seems to play an important role, since the aforementioned studies were conducted in either MeCN and / or DCM. Whenever the conditions were similar to this study, in particular, when DMF was used as the solvent, the observed reversibility behavior is in better agreement.[76d, 76e] However, so far no explanation could be identified, which is consistent with all observations under these varying conditions.

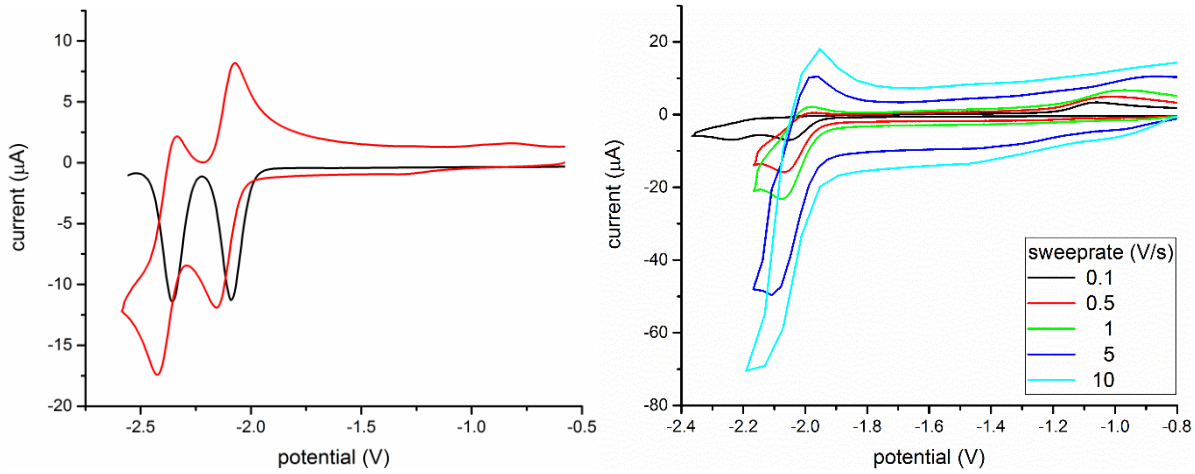


**Figure 26:** Left: Differential pulse voltammetry (black line) and cyclic voltammetry (red line) of $[Cu(dsbp)_2]BF_4$. Right: Cyclic voltammetry of $[Cu(phen)_2]BF_4$ at different sweeprates as given in the legend. Conditions: 1 mM sample, 0.1 M $TBAPF_6$ in DMF under $N_2$. Potentials were measured vs Ag / AgCl and are reported vs $Fc^{+/0}$ as an internal standard.

The reversibility behavior of the oxidation process is shown for selected examples in Figure 27. Clearly, the increased steric bulk on the phenanthroline ligand is concomitant with a decrease in reversibility. Since the complexation strength of sterically encumbered ligands is lower than of their less hindered counterparts, the former tend to dissociate upon oxidation and the open coordination sites are filled by solvent molecules.[76e] In the highly irreversible case of $[Cu(dsbp)_2]BF_4$, the wave in the reverse scan is probably due to the reduction of such a $[Cu(dsbp)(DMF)_x]^{2+}$ species. This effect is more pronounced in polar solvents, due to their better coordination ability, and has been found to be stronger in DMF rather than MeCN.[76a, 76e] Similarly, the complex $[Cu(dsbtmp)_2]BF_4$ shows irreversible behavior in DMF (not shown) but almost full reversibility in MeCN, as shown in Figure 27.

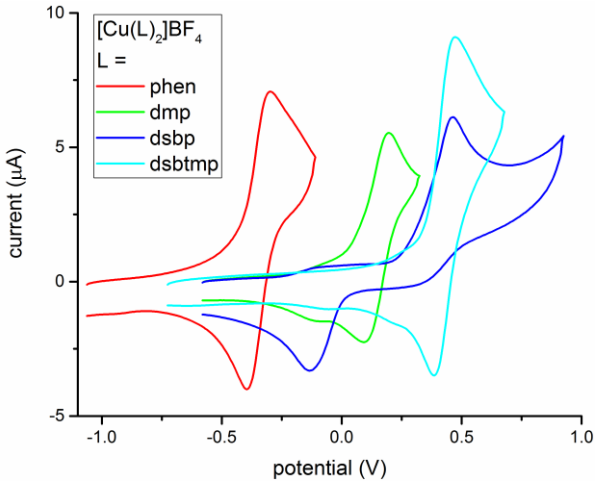


**Figure 27:** Cyclic voltammetry of the oxidation of complexes **11** - **13** and **15**. Conditions: 1 mM sample, 0.1 M $TBAPF_6$ in DMF or MeCN (for $[Cu(dsbtmp)_2]BF_4$) under $N_2$. Potentials were measured vs Ag / AgCl and are reported vs $Fc^{+/0}$ as an internal standard.

## 2.4.2. Quenching Experiments

In the previous chapters, a good understanding of the photophysical and electrochemical properties of $Cu^I$ bisphenanthroline complexes was acquired. This knowledge serves as the basis for implementation of these compounds into a photocatalytic system for hydrogen evolution. To this end, first the absorbed light energy has to be transferred from the photosensitizer to a suitable catalyst for proton reduction. Generally, this is achieved by dynamic quenching of the photosensitizer via one of three pathways: energy-transfer quenching, reductive electron transfer quenching or oxidative electron transfer quenching (Scheme 36). With a given photosensitizer, the assumed pathway is mainly dependent on the type of quencher, furthermore, multiple pathways can be operational at the same time.

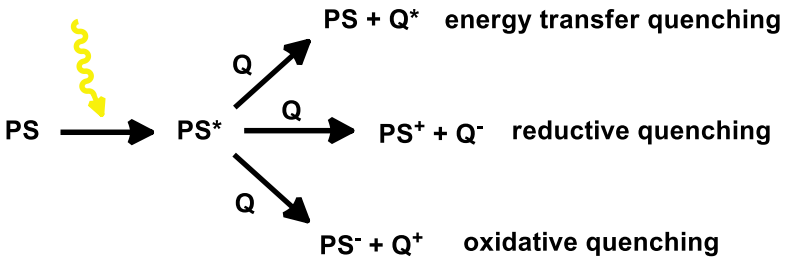


**Scheme 36:** Three possible pathways to quench the excited state of a photosensitizer.

The rate of such quenching reactions can be determined according to the Stern-Volmer relation (Equation 1).

$$\frac{I_0}{I} - 1 = k_q \tau_0 [Q] \quad (1)$$

Where $I_0$ denotes the luminescence intensity without quencher and $I$ the luminescence intensity at a known quencher concentration [$Q$]. Thus plotting ($I_0/I$)-1 versus [$Q$] results in a linear correlation with intercept 0 and slope $k_q\tau_0$. If the lifetime $\tau_0$ of the photosensitizer is known, the bimolecular quench rate $k_q$ can be directly extracted. Even though, this is an easy and elegant method, it is accompanied by a few problems. The luminescence intensity is quite sensitive to other factors, e.g. light absorption by the quencher. Moreover, if the luminescence quantum yield of the investigated photosensitizer is inherently low, the detection of intensity differences becomes very difficult. Therefore, an adapted version of the Stern-Volmer relation was applied, using the ratio of luminescence lifetimes $\tau_0/\tau$, where $\tau$ denotes the lifetime at a given quencher concentration [$Q$] (Equation 2).

$$\frac{\tau_0}{\tau} - 1 = k_q \tau_0 [Q] \quad (2)$$

With this method, the above mentioned problems are largely avoided.

Complexes $[Cu(dsbp)_2]BF_4$ (**13**) and $[Cu(dsbtmp)_2]BF_4$ (**15**) were chosen for investigation of their quenching behavior. Both these compounds show sufficiently long lifetimes (τ = 270 ns and 1950 ns for **13** and **15**, respectively, in DCM) to perform bimolecular reactions in solution. In addition, their excited state redox potentials are significantly different (see Table 1, Figure 28). Excited state redox potentials of $[Cu(dsbp)_2]BF_4$ show a preference for reductive quenching (higher $E^*_{red}$) as compared to $[Cu(dsbtmp)_2]BF_4$, which is better suited for oxidative quenching (lower $E^*_{ox}$).

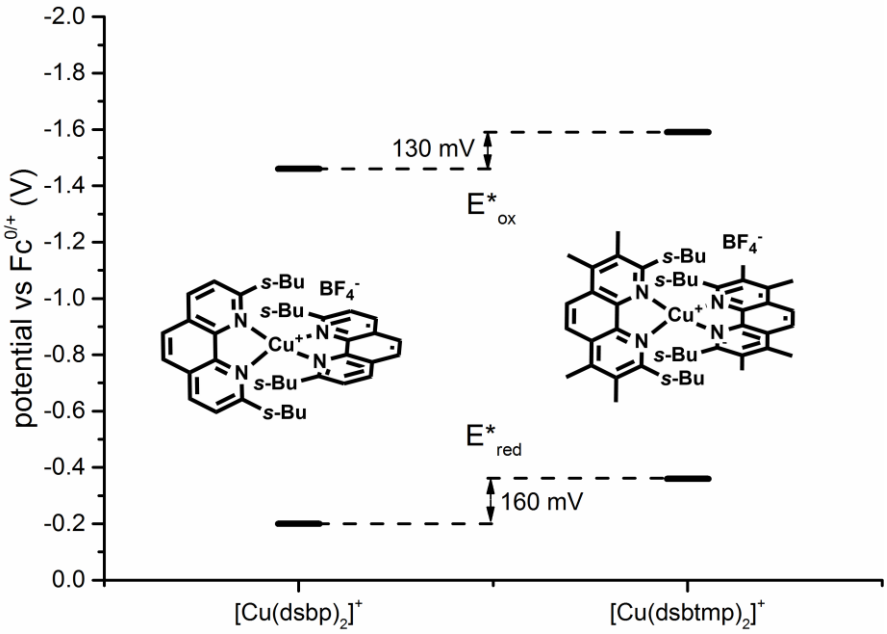


**Figure 28:** Comparison of the excited state redox potentials of complexes **13** and **15**, which were estimated as $E^*_{red/ox} = E_{red/ox} \pm E_{00,min}$ ($E_{red/ox}$ being the ground state reduction and oxidation potential, respectively, and $E_{00,min}$ the emission energy at maximum intensity).

### 2.4.2.1. Quenching of $[Cu(dsbp)_2]BF_4$

The quenching of $[Cu(dsbp)_2]BF_4$ was investigated in a solution of 8/2 EtOH/$H_2$0, which provides a polar environment, but still retains a reasonable lifetime of the photosensitizer (210 ns). This allows the observation of relatively slow quench reactions, compared to e.g. DMF solutions, where the lifetime is already heavily diminished (40 ns) due to unproductive quenching with the solvent.

A series of typical reductive quenchers were assayed for their interaction with $[Cu(dsbp)_2]BF_4$ (Scheme 37).

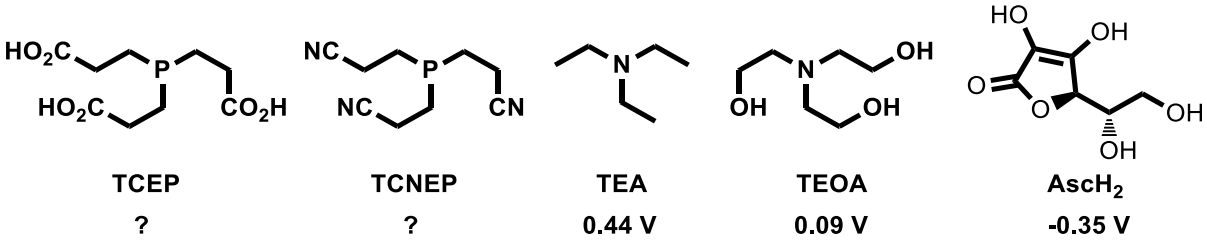


**Scheme 37:** Quencher molecules, screened for reductive quenching of $[Cu(dsbp)_2]BF_4$, along with rough estimates of their respective redox potentials vs $Fc^{0/+}$ as described in the literature: TEA[77], TEOA[78], $AscH_2$[79].

By comparison of the photosensitizer's estimated excited state potential with the estimated potentials of the quencher molecules, electron transfer is only thermodynamically feasible for $AscH_2$. This expectation is fulfilled by the tertiary amines TEA and TEOA, as no quenching is observed with concentrations up to 1 M. Also the tertiary phosphines (TCEP, TCNEP) cannot be oxidized by the excited

photosensitizer. Additionally, slow decoloration of the sample solution is observed upon addition of the phosphines, probably due to their coordination to the metal center in competition with the phenanthroline ligands. Surprisingly, also the addition of up to 0.1 M $AscH_2$ has no effect on the lifetime of the photosensitizer, despite the thermodynamic feasibility of an electron transfer. This might be explained by the presence of an additional kinetic barrier, due to an innersphere reorganization, as it was observed previously.[80] However, the redox potential of $AscH_2$ depends on the protonation state and its oxidation can be easily facilitated by basifying the solution.[79] Deprotonation to $AscH^-$ with up to 1 equivalent TBAOH still does not lead to any observable quenching. However, with further addition of TBAOH (> 1 equivalent), the excited state is quenched by $Asc^{2-}$ with a rate $k_q = 4.7\pm0.4\cdot10^8$ $M^{-1}s^{-1}$. Transient absorption spectra, in comparison with spectroelectrochemical analysis of $[Cu(dsbp)_2]BF_4$ clearly indicate reductive quenching, i.e. electron transfer from $Asc^{2-}$ to the excited state (Figure 29). The depicted transient spectra are after complete decay of the excited state, thereby exclusively showing the reduced PS.

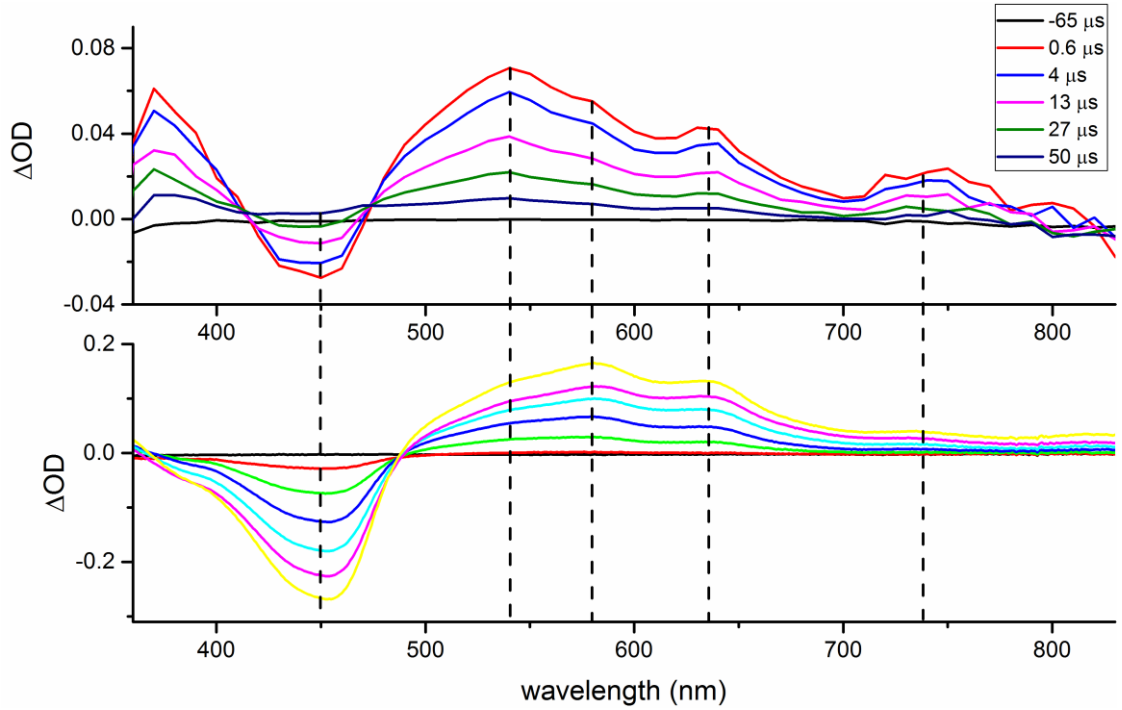


**Figure 29:** Top: Transient absorption spectra at given time delays of a solution containing 0.1 mM $[Cu(dsbp)_2]BF_4$, 0.1 M $AscH_2$ and 0.15 M TBAOH in $EtOH/H_2O$ 8/2. In the first shown spectrum after excitation (0.6 µs), the excited state has decayed completely and only reduced PS is left. Bottom: UV/VIS spectroelectrochemical analysis of 1 mM $[Cu(dsbp)_2]BF_4$ in DMF and 0.1 M $TBAPF_6$, scanning from 0 V to -1.6 V (vs Ag/AgCl).

Even though this is one of the rare examples, where a $Cu^I$ bisphenanthroline complex was quenched reductively, it was not possible to exploit the reduced state for hydrogen evolution, since our groups WRCs generally do not work at elevated pH values.

Given the modest success of reductive quenching with $[Cu(dsbp)_2]BF_4$, the other two pathways were explored. First, oxidative quenching with two cobalt based water reduction catalysts was investigated (Scheme 38). In both cases fast quenching is observed with rates $k_q = 4.7\pm0.6\cdot10^9\ M^{-1}s^{-1}$ and $k_q = 1.7\pm0.1\cdot10^9\ M^{-1}s^{-1}$ for $[Co(DOH)Br_2]$ and [CoBr(apPy)]Br, respectively. However, photocatalytic measurements do not show the formation of hydrogen. This is likely due to the necessity of further reductions of the WRCs, which cannot be achieved by the excited photosensitizer.

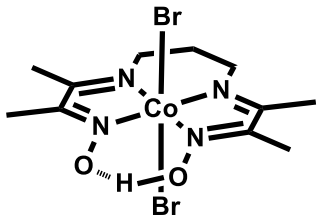


**54**
$[Co(DOH)Br_2]$
$E_{red}(Co^{III/II}) = -0.57$ V

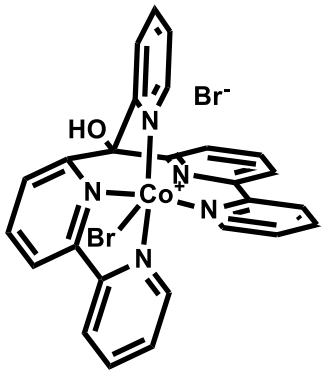


**55**
[CoBr(apPy)]Br
$E_{red}(Co^{II/I}) = -1.40$ V

**Scheme 38:** Molecular structure of cobalt based WRCs, along with their first reduction potential vs $Fc^{0/+}$.

The energy transfer pathway was explored using 9-anthracenecarboxylic acid (9-AC), which was reported to be an efficient quencher of $Cu^I$ photosensitizers.[34] Indeed, a rather fast quench rate $k_q = 1.4\pm0.1\cdot10^9$ was observed. Unlike the previous successful quench reactions, it was possible in this case to exploit the energy transfer for hydrogen evolution. In a EtOH/$H_2O$ 8/2 solution containing 0.5 mM $[Cu(dsbp)_2]BF_4$, 50 mM 9-AC, 0.5 mM $[Co(DOH)Br_2]$ and 0.2 M TEOA as sacrificial electron donor, hydrogen was detected by irradiation at 470 nm. Despite very low turnover numbers (~3 $TON_{Cu}$ (H/Cu)), this experiment proofs the viability of combining $Cu^I$ photosensitizers with Co based WRCs. Scheme 39 shows the proposed mechanism for this system.

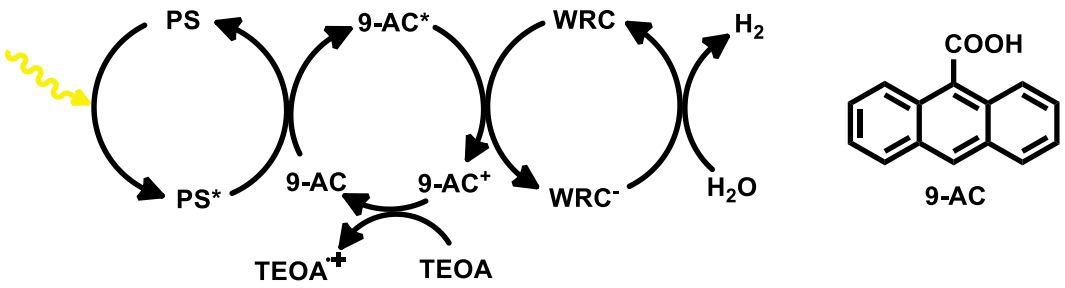


**Scheme 39:** Possible mechanism of the photocatalytic system based on energy transfer to 9-AC.

### 2.4.2.2. Quenching of $[Cu(dsbtmp)_2]BF_4$

Learning from the results for $[Cu(dsbp)_2]BF_4$, where reductive quenching was found to be very difficult, and due to the cathodically shifted excited state redox potentials of $[Cu(dsbtmp)_2]BF_4$, quenching was mainly investigated in the oxidative pathway. Owing to the long lived excited state of $[Cu(dsbtmp)_2]BF_4$ in various solvents, these quench experiments were performed in DMF.

A series of organic electron acceptors as well as Co based water recuction catalysts ($[Co(DOH)Br_2]$, [CoBr(apPy)]Br) were evaluated for their ability to oxidize photoexcited $[Cu(dsbtmp)_2]BF_4$ (Scheme 40, Figure 30).

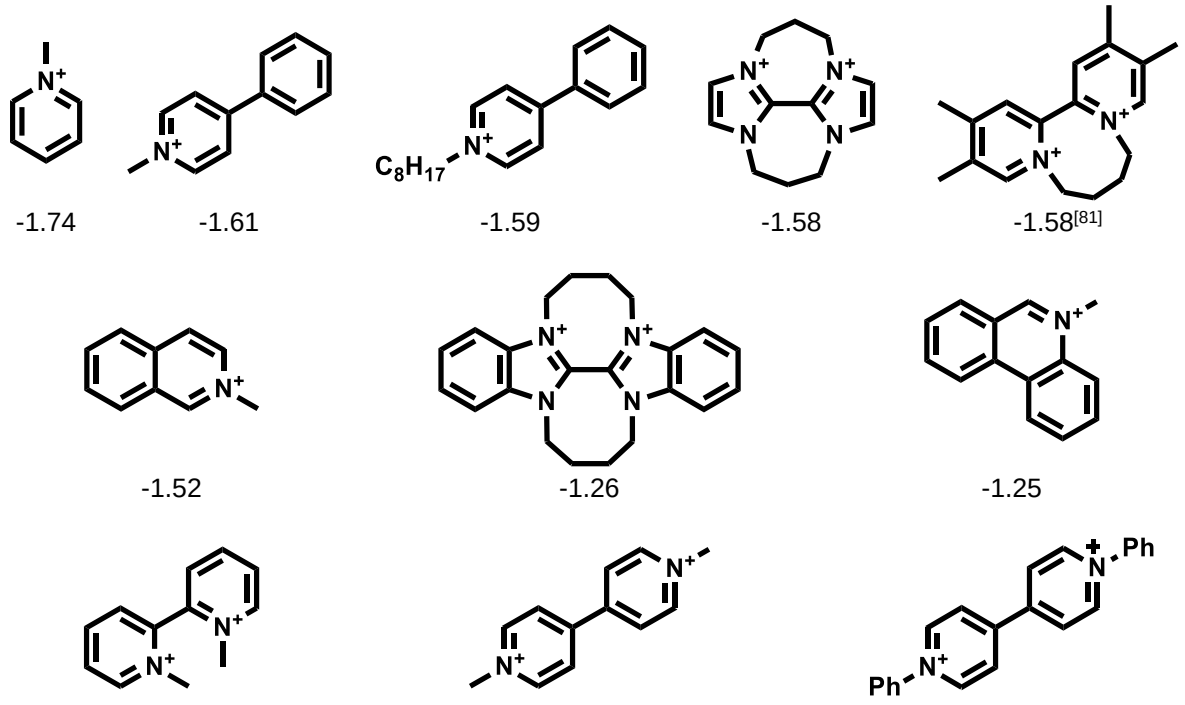


**Scheme 40:** Molecular structures of electron accepting quenchers, along with their respective reduction potentials in V vs $Fc^{0/+}$. The potentials were measured in DMF at 1 mM sample concentration with $TBAPF_6$ as supporting electrolyte on a glassy carbon working electrode or they are taken from the referenced literature.

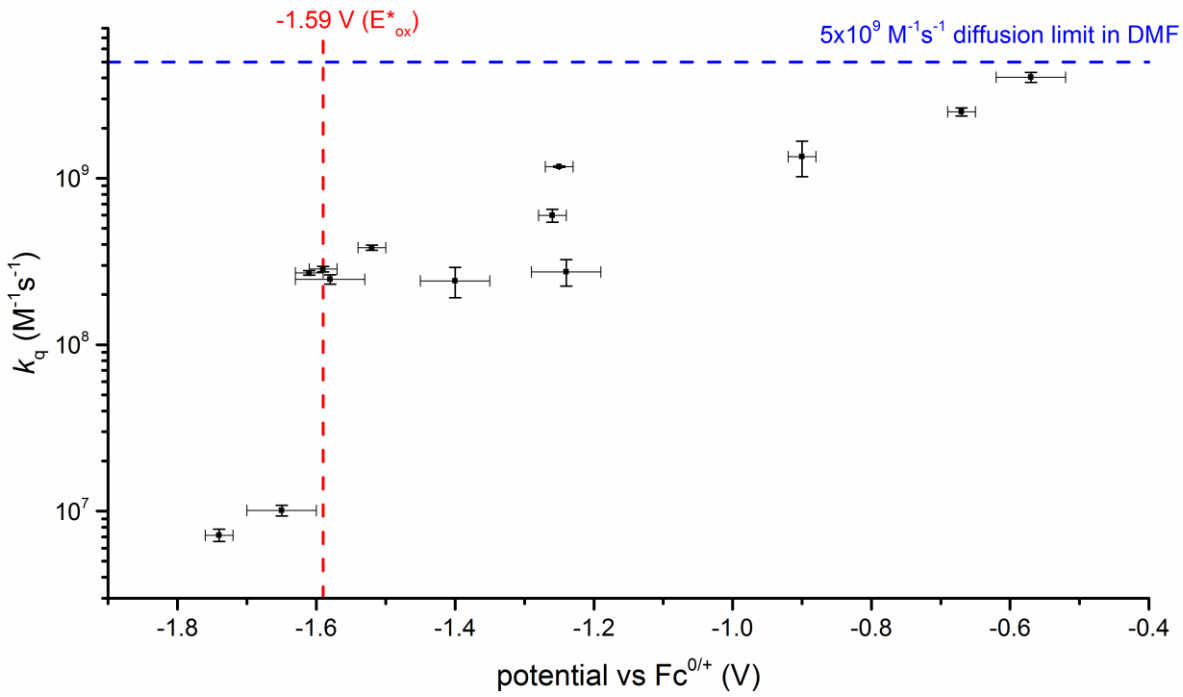


**Figure 30:** Plot of $k_q$ versus the reduction potential of various electron acceptors for $[Cu(dsbtmp)_2]BF_4$ in DMF.

The successful oxidative quenching of $[Cu(dsbtmp)_2]BF_4$ was also exploited for photocatalytic hydrogen evolution. These results are published and are summarized in the next subchapter.

### 2.4.3. Summary of Published Work

This section refers to Appendix I. The publication introduces a new general reaction scheme for photocatalytic hydrogen production, based on oxidative quenching of a homoleptic $Cu^I$ bisphenanthroline photosensitizer ($[Cu(dsbtmp)_2]BF_4$). 1-Methyl-4-phenyl-pyridinium ($MPP^+$) functions as the electron relay between the photosensitizer and various cobalt based water reduction catalysts and the oxidized $Cu^{II}$ species is regenerated by the sacrificial electron donor TEOA. With this scheme a maximum $TON_{PS}$ of 113 (H/Cu) was achieved, as well as 10 turnovers in the relay $MPP^+$. A combination of photocatalytic measurements and UV/VIS transient absorption spectroscopy allowed for detailed insights into the mechanism of the system and thereby also for the identification of the performance limiting factors.

#### 2.4.3.1. Summary of Windisch, J. *et al.*, ChemSusChem 2016, *9*, 1719-1726

From a series of electron acceptors (Scheme 40), $MPP^+$ was identified as the ideal oxidative quencher for $[Cu(dsbtmp)_2]BF_4$. It offers a fast quench rate $k_q = 2.6\pm0.1\cdot10^8$ $M^{-1}s^{-1}$ and a minimal energy loss, since it is reduced at -1.61 V (vs $Fc^{0/+}$), which is very close to the excited state potential of the photosensitizer

$E^*_{ox}$ = -1.59 V (vs $Fc^{0/+}$). The electrochemical reversibility of the oxidation / reduction process further adds to the viability of $MPP^+$ as an electron relay.

Photocatalytic experiments indeed showed the formation of hydrogen when $MPP^+$ was used as an oxidative quencher in a system containing $[Cu(dsbtmp)_2]^+$ as the photosensitizer, $[Co(DOH)Br_2]$ as the WRC, TEOA as sacrificial electron donor and $[HTEOA]BF_4$ as the proton source in DMF. The quantum yields for hydrogen production (<4%) correlate well with the maximal possible quench rates at different $MPP^+$ concentrations (Figure 3 in Appendix I). However, when the quantum yields were corrected for maximal possible quench rates, a constant corrected quantum yield of ~4% was obtained, which indicates a significant loss channel independent of $MPP^+$ concentration. Furthermore, comparative experiments with other photosensitizers ($[ReNCS(CO)_3bpy]$, $[Ru(bpy)_3]^{2+}$) clearly show the ability of the $[Co(DOH)Br_2]$ WRC to produce hydrogen much faster, indicating a limitation in the PS / $MPP^+$ system. In almost all catalytic runs with $[Cu(dsbtmp)_2]BF_4$ the formation of a black precipitate accompanied by discoloration of the reaction solution was observed. The solid was identified as elemental copper by SEM/EDX. From these experiments it was concluded that decomplexation of $[Cu(dsbtmp)_2]BF_4$ and subsequent reduction seem to limit catalysis.

Despite the stability issues, the versatility of the new system was demonstrated by combination with different Co-based WRCs, all showing hydrogen evolution (Scheme 3 and Figure 4 in Appendix I). Blank experiments were conducted to prove the necessity of all components.

Transient absorption experiments in the nanosecond to millisecond timescale were performed and unambiguously confirmed the proposed reaction sequence. In a two component experiment with $[Cu(dsbtmp)_2]BF_4$ and $MPP^+$, clearly the formation of the radical $MPP^{\cdot}$ is observed after oxidative quenching of the excited state. Due to the lack of a sacrificial electron donor, fast recombination of oxidized PS and $MPP^{\cdot}$ is observed. The disappearance of the $MPP^{\cdot}$ signal could be fitted to second order kinetics, giving a rate constant $k_{rec} = 7.2\pm1.2\cdot10^8\ M^{-1}s^{-1}$. Upon addition of TEOA (1 M) as sacrificial electron donor, this recombination process can be partially suppressed, since the oxidized PS is regenerated with a rate $k_{TEOA} = 1.3\pm0.1\cdot10^6 M^{-1}s^{-1}$. In this manner, the radical $MPP^{\cdot}$ is formed with a cage escape yield $\Phi_{cage} \approx 0.6$ after 5 µs. Recombination as well as reaction with decomposition products of oxidized TEOA lead to a decrease in quantum yield, leaving ~20% of the $MPP^{\cdot}$ after 10 ms. Nevertheless, further electron

transfer to a WRC is clearly possible in this time frame, thereby confirming the proposed mechanism.

### 2.4.3.2. Further Observations

A reviewer pointed out that MeCN might be able to stabilize copper ions after decomplexation of the original compound, thereby possibly leading to an overall stabilization of the photocatalytic system. These experiments were performed by adding 0.1 M and 1.9 M MeCN, respectively, to an otherwise standard reaction solution (compare red, blue and black traces in Figure 31). The results clearly indicate a beneficial effect of the MeCN with $TON_{PS}$ increasing from ~35 up to ~140. However, when the standard conditions (without addition of MeCN) were repeated to confirm the improvement, very similar turnovers were obtained. This is attributed to small amounts of MeCN still being present, due to contamination of the setup for photocatalytic measurements from the previous experiments.

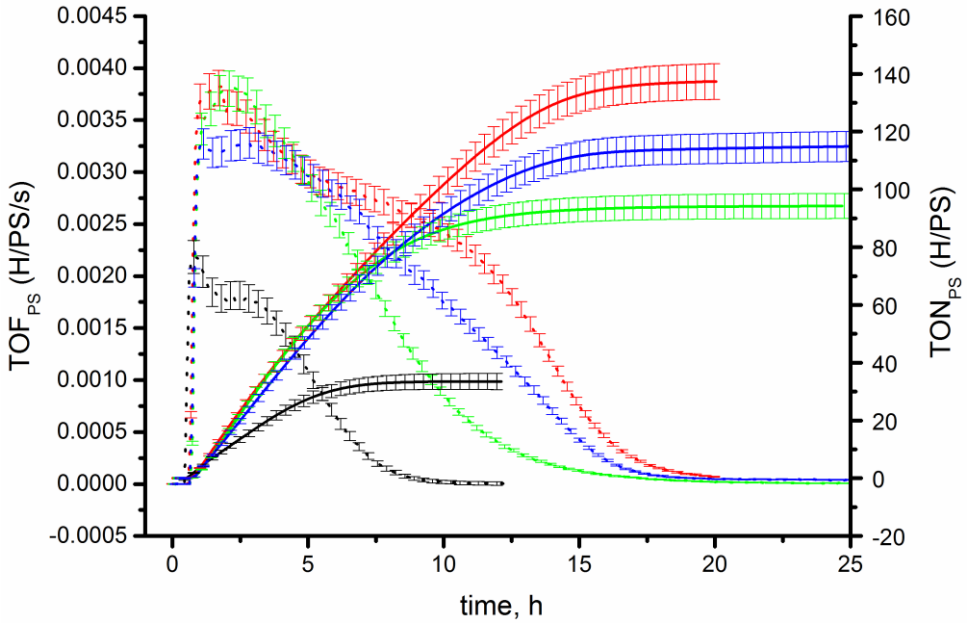


**Figure 31:** $TOF_{PS}$ (dotted lines) and $TON_{PS}$ (solid lines) plotted over time, for photocatalytic experiments containing varying amounts of MeCN: no additional MeCN (black), probably traces of MeCN (green), 0.1 M MeCN (red), 10vol% MeCN (blue). All other conditions were kept constant: DMF, 0.5 mM $[Cu(dsbtmp)_2]BF_4$, 10 mM $[MPP]PF_6$, 1 M TEOA, 0.1 M $HBF_4$, 0.23 mM $[Co(DOH)Br_2]$. Irradiated with a 450 nm LED at a constant photon flux of 0.3±0.04 $\mu Es^{-1}$.

Another interesting observation was made when the concentration and ratio of TEOA and $HBF_4$ in photocatalytic experiments was varied (Figure 32). Although the trend is somewhat ambiguous, it seems that a low concentration of unprotonated TEOA significantly improves the $TON_{PS}$. This suggests the involvement of TEOA in the decomposition of $[Cu(dsbtmp)_2]BF_4$, likely by coordinating the copper ions and thereby deactivating their photosensitizing abilities.

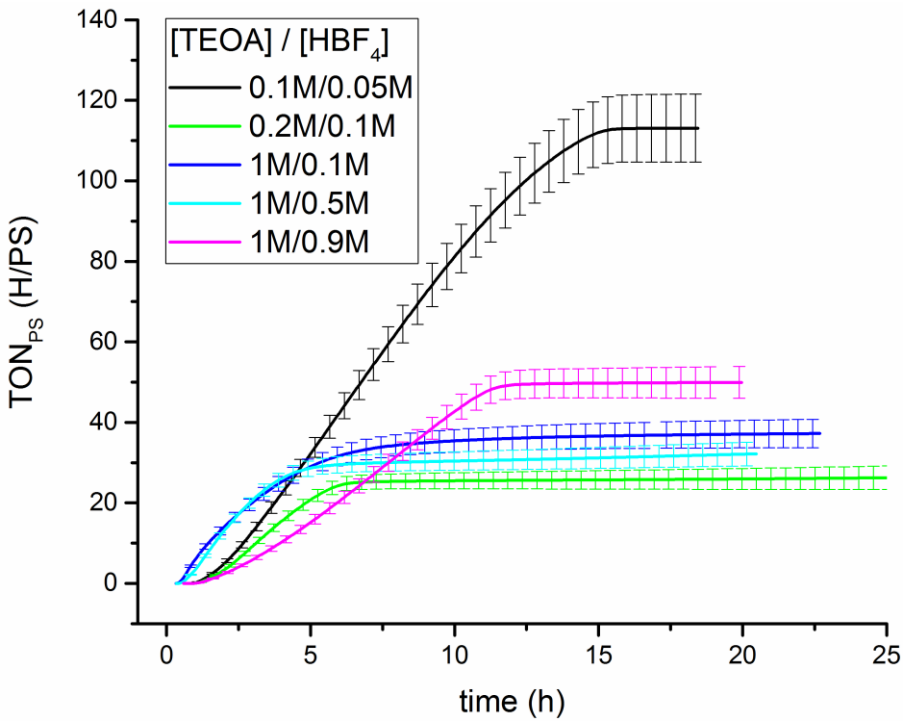


**Figure 32:** $TON_{PS}$ plotted over time of photocatalytic runs with different concentrations and ratios of TEOA and $HBF_4$ as given in the legend. Conditions: DMF, 0.5 mM $[Cu(dsbtmp)_2]BF_4$, 10 mM $[MPP]PF_6$, 0.23 mM $[Co(DOH)Br_2]$. Irradiated with a 450 nm LED at a constant photon flux of 0.3±0.04 $\mu Es^{-1}$.

As mentioned in the discussion of the transient absorption measurements, the decay of the signal attributed to $MPP^{\cdot}$ (at 540 nm) shows a complicated kinetic behaviour (Figure 33).

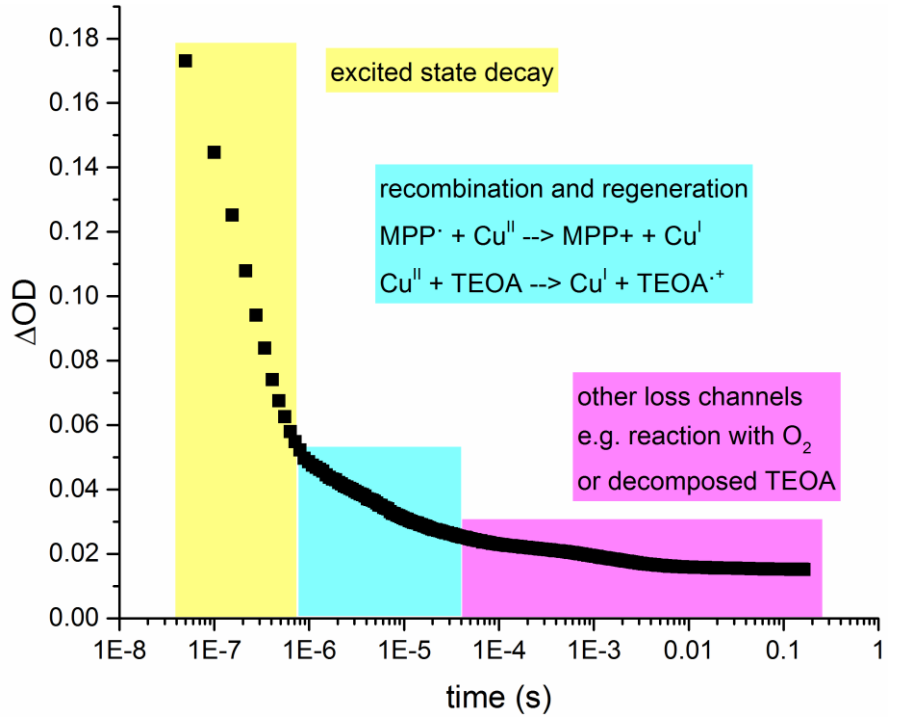


**Figure 33:** Kinetic trace of the transient signal at 540 nm after laser excitation (355 nm) of an Ar-degassed DMF solution containing 0.5 mM $[Cu(dsbtmp)_2]BF_4$, 10 mM $[MPP]PF_6$, 1 M TEOA and 0.1 M $HBF_4$. Different time domains and the presumed processes occurring are marked in color.

The first two time domains are well understood and could be attributed to the shown processes, furthermore it was possible to extract the reaction rates from the data (vide supra). However, for the time domain ranging from ~40 µs up to 200 ms, the reasons for the observed signal decrease are speculative and the data could not be fitted to any simple model. Reactions with trace amounts of oxygen as well as decomposition products of TEOA are likely to be responsible.[23d] Radical dimerization is excluded, since this should occur on a slower timescale according to previous literature reports.[82]

# 3. Conclusion and Outlook

## 3.1. System Development

With the successful incorporation of a $Cu^{I}$ bis-phenanthroline complex as a photosensitizer into a visible light-driven hydrogen evolution system, the main goal of this thesis was achieved. The introduction of an electron relay ($MPP^{+}$) between the photosensitizer and the water reduction catalyst was crucial not only to achieve efficient electron transfer between the two species, and thereby enable hydrogen evolution, but also to make the concept applicable to a manifold of catalysts. Although catalysis was run in an organic solvent (DMF) instead of water, the proof of concept and the identification of performance-limitations represent an important step towards more efficient systems employing copper based photosensitizers.

Of course, the development of such a system entailed the careful study of a series of known, but also new $Cu^{I}$ bis-phenanthroline complexes, with special emphasis on their photophysical and electrochemical properties. An important finding of this analysis was the uncommon redox behavior of the excited state. Unlike most other photosensitizers, $Cu^{I}$ bis-phenanthrolines tend to be oxidized, rather than reduced in the excited state, due to the cathodic shift of both HOMO and LUMO as compared to common photosensitizers. Consequently, the aforementioned catalytic cycle is based on oxidative quenching of the photosensitizer. By systematic screening of various electron acceptors, with a variety of redox potentials, an ideal compromise in terms of low driving force and fast rate was found in $MPP^{+}$ and $[Cu(dsbtmp)_2]^{+}$. Despite this preference, reductive quenching was achieved as well, by employing doubly deprotonated ascorbic acid – a very rare example of this process. However, the reduced species could not be exploited productively.

Hence, further investigations should focus on the oxidative pathway, e.g. searching for more effective electron relays to improve the quantum yield of hydrogen formation. Similarly, the direct attachment of an electron acceptor to the phenanthroline backbone might have a beneficial effect on catalysis, possibly in combination with a directly linked intermediate electron donor. This would accelerate the regeneration of the $Cu^{II}$ species and thereby minimize losses due to decomposition. The stability issues may also be resolved via the synthesis of more durable complexes, e.g. with a tetrahedral cage ligand.

## 3.2. Tetrahedral Cage Ligand Synthesis

Starting with a few attempts on a side note, the synthesis of a tetrahedral cage ligand became a major focus of this thesis. The successful preparation of such a molecule would not only deliver $Cu^{I}$ complexes with potentially highly interesting photophysical properties, but also other metal complexes with possibly peculiar behaviour, due to the very uncommon coordination environment. In addition, these highly symmetric molecular constructs are inherently attractive, simply because of their aesthetics.

The most promising results were obtained with a calixarene inspired approach, where a doubly bridged phenanthroline dimer could be isolated. Since further bridging of this intermediate was not possible, more templated procedures and other precursors should be tested in order to allow the macrocyclic cage to form.

Other promising strategies include the attachment of N-heterocycles to the phenanthroline core, as well as the preorganization of the tetrahedral geometry with diazaspirobifluorenes. The former showed singly carbon-bridged intermediates as well as metal complexation. This could be exploited to assemble the macrocycle through coordination bonds, if an appropriate bridging fragment can be found. Further investigations with these ligands are necessary and advisable. Preliminary results with diazaspirobifluorene seem promising, due to the successful $Cu^{I}$ complex formation and their apparent luminescent properties. This definitely merits further development, especially towards covalent linking of two diazaspirobifluorenes or crosslinking with another bidentate ligand, e.g. phenanthroline.

The approach based on imine condensation still seems viable, at least to serve as a proof of concept. However, with the goal of increased stability in mind, the hydrolytically unstable imine bonds are not ideal.

The least success was achieved with the approach based on terminal dienes. Already during the precursor synthesis, many problems appeared, most prominently the omnipresent polymerization issues. Therefore, further investigations do not seem justified.

Due to the synthetic complexity of a tetrahedral cage ligand, alternative (more pragmatic) concepts to stabilize $Cu^{I}$ photosensitizers should also be considered. Of course, this would not satisfy the aesthetic considerations, however, also simple solutions can have a great impact.

# 4. Experimental

## 4.1. Analytical Methods

**$^{1}$H- and $^{13}$C-NMR** spectra were recorded on a Varian Mercury (200 MHz) or a Varian Gemini-2000 (300 MHz). Chemical shifts are reported relative to residual solvent peaks.[83] s = singlet, d = doublet, t = triplet, q = quadruptlet, bs = broad singlet, m = multiplet.

**UPLC-MS / ESI-MS:** UPLC separation was performed on an Acquity$^{TM}$ Ultra Performance LC with an Acquity UPLC® BEH C18 column (1.7 µm, 2.1 × 50 mm; 0.3 mL/min flow rate) and a gradient of 0.1 % aqueous formic acid and acetonitrile eluents. The mass spectra were recorded on an Esquire HCT from Bruker (Germany), the injection rate was 3 µL/min, the nebulizer pressure was 10 psi, and the dry gas flow rate was 5 L/min at 350 °C. All solvents were of HPLC/LCMS grade.

**HPLC** traces were recorded with a VWR Hitachi Elite LaChrome with a C18-nucleodur or Phenomenex Core Shell column and $H_2O$/MeOH as eluent (gradient starting with 10% MeOH, 0.1% TFA in $H_2O$ to pure MeOH).

**Elemental Analyses** were performed on a Leco CHNS-932 elemental analyzer.

**UV/VIS** spectra were measured using a Cary 50 spectrometer with solution samples in 1 cm quartz cells. For air sensitive samples, cells with silicon septa lids were used to keep samples under an inert gas atmosphere during measurements.

**Luminescence measurements** were performed on a Perkin-Elmer LS50B fluorescence spectrometer with argon-purged solution samples in 1 cm cells.

**Electrochemical measurements** were carried out in DMF or MeCN containing 0.1 M $TBAPF_6$ as conducting electrolyte. A Metrohm 757VA or 797VA Computrace electrochemical analyzer was used with a standard three-electrode setup of glassy carbon working (ID = 2 mm), Pt auxiliary electrode and Ag/AgCl reference electrode. All potentials were referenced to Fc as an internal standard and are given vs. $Fc^{0/+}$.

**Spectroelectrochemical analysis** was performed in an optical transparent thin layer electrolysis (OTTLE) cell in the UV/Vis spectrometer described above. The working electrode was a platinum gauze immersed into the OTTLE cell, auxiliary electrode was a platinum wire, and the reference electrode was an Ag/AgCl electrode. To control the

potential a Metrohm autolab potentiostat (PGSTAT302N) operated with the software NOVA was used.

**Luminescence lifetime measurements** were performed on an Edinburgh Instrument LP920K system equipped with a pumped Q-switched Nd:YAG laser (Continuum Surelite), monochromator (Czerny–Turner with triple grating turret, 300 mm focal length) and a photomultiplier tube.

**Transient absorption spectra** were recorded on the LP920-K system used for luminescence lifetime measurements, additionally equipped with a Xe920 probe lamp (450 W) and an xP920 pulsing unit module. Argon-purged solution samples in 1 cm cells were used.

Alternatively a home-constructed flash photolysis setup was used with a frequency-tripled Nd:YAG laser for sample excitation (355 nm, 6 ns pulse duration) and a two monochromator setup for single-wavelength detection to minimize the sample's exposure to probe light and remove most of the phosphorescence emitted by the photosensitizer. A white-light LED was used as a light source. The probe light was detected with an amplified silicon photodiode (Hamamatsu S3883, spectral response 320–1000 nm, bandwidth 300 MHz) and the signal was digitized with a transient recorder (125 MHz bandwidth, 200 MS $s^{-1}$, 16 bit resolution). Experiments were performed with argon-purged solution samples in a cuvette with a 2 mm path length.

**Hydrogen evolution measurements:** Gas chromatograms were recorded using either an automated Bruker GC-450 or GC-456 gas chromatograph with argon as carrier gas and a 3 m x 2 mm packed molecular sieve 13X 80–100 column. The column and reference gas flow (Ar) was set to 20 $mLmin^{-1}$. The oven was operated isothermally at 100 °C. An argon flow of 6 $mLmin^{-1}$ (adjusted with an onboard electronic flow control device and referenced with a F-200CV-002 from Bronkhorst) was passed through the reaction mixture and into the GC, in which 1 mL gas samples were automatically injected at defined time intervals (usually 5 min) using a 6-Port 2-Position Valve from Vicci. The gases were detected using a thermal conductivity detector operated at 150 °C (filament temperature 170 °C; retention time ~1 min for $H_2$). Calibration was achieved by mixing Ar and $H_2$ in known ratios with two mass flow controllers (Bronkhorst, F-201CV-200 for Ar and F-200CV-002 for H2, 0.51% $H_2$ in Ar (Pangas)). This setup allowed the detection of $H_2$ down to minimum mole fractions of $2 \cdot 10^{-6}$. At Ar flows of 6$mLmin^{-1}$ through the reaction the detection limit was $H_2/s \geq 1 \cdot 10^{-11}$.

**Crystallographic data** were collected at 183(2) K on an Oxford Diffraction Xcalibur system with a Ruby detector using Mo $K_\alpha$ radiation ($\lambda$ = 0.7107 Å) that was graphitemonochromated or an Oxford Diffraction SuperNova dual source system with an Atlas detector using Cu $K_\alpha$ ($\lambda$ = 1.54184 Å) or Mo $K_\alpha$ radiation ($\lambda$ = 0.7107 Å). Suitable crystals were covered with oil (Infineum V8512), placed on a nylon loop that is mounted in a CrystalCap Magnetic™ (Hampton Research) and immediately transferred to the diffractometer. The program suite CrysAlis$^{Pro}$ was used for data collection, multi-scan absorption correction and data reduction.[84] The structure was solved with direct methods using SIR97[85] and was refined by full-matrix least-squares methods on $F^2$ with SHELXL-97.[86] ORTEP representations were created by the program ORTEP-3.[87]

## 4.2. Syntheses

### 4.2.1. General Remarks

Oxygen and water sensitive reactions were carried out under an inert atmosphere (nitrogen or argon) using standard Schlenk techniques. Glassware was dried either by heating in an oven at 120 °C overnight or with a heat gun under HV.

Reactions were generally carried out in at least reagent grade solvents. For moisture sensitive reactions dry toluene was obtained from a MBraun solvent purification system, $Et_2O$ and THF were dried over Na/benzophenone and distilled before use, DMF was dried over $MgSO_4$ and distilled before use, MeCN and MeOH were dried by storing over 3 Å molecular sieves for at least 24 h.

Deuterated solvents ($CDCl_3$, DMSO-$d_6$, acetone-$d_6$, $D_2O$) were purchased from Armar and stored under dry conditions in a desiccator.

For extractions and column chromatography, technical grade solvents (distilled before use) were applied. Water was distilled twice before use.

Column chromatography was performed either using aluminium oxide 90 neutral (neutral alumina) or silica gel 60 (silica), both obtained from Macherey-Nagel. TLC was run either on POLYGRAM-plates of aluminium oxide neutral $F_{254}$ from Macherey-Nagel or on aluminium-plates of silica gel $F_{254}$ from Merck.

All chemicals were of reagent grade and used without further purification. $Cu(OTf)_2$, CuI, MOMCl and TBSCl were obtained from ABCR. Iodomethane, *s*-BuLi and TsCl were obtained from Acros Organics. 1,3-diaminopropane, copper powder, $Cu(BF_4)_2$,

DBU, DMAP, imidazole, $MnO_2$, MsCl, hydroxylamine hydrochloride, $NH_4BF_4$, *o*-phenylenediamine, $PCl_5$, pyridine hydrochloride and $SeO_2$ were obtained from Fluka. 2-Bromoisophthalaldehyde, (3-bromopropoxy)-*tert*-butyldimethylsilane, 4,5-diazafluorenone, allyltrimethylsilane, $NH_4PF_6$, $PBr_3$, 1,10-phenanthroline, TBAF (1 M in THF) and trimethylsilylacetylene were purchased from Fluorochem. $NaHCO_3$, NaOH, ammonia (aq. 25%) and $NH_4Cl$ were obtained from Honeywell. AcOH, $H_2SO_4$, HCl (aq. 32%), $HNO_3$ (aq. 65%) and $K_2CO_3$ were obtained from Merck. $Na_2CO_3$ was obtained from ROMIL LTD. 1,3-Dibromopropane, 1,4-dibromobutane, 3,4-lutidine, 5-bromo-1,2,3-trimethoxybenzene, acetic anhydride, $BF_3{\cdot}Et_2O$, 1-bromododecane, 1-bromooctane, 4,7-diphenyl-1,10-phenanthroline, ethylene glycol, fuming $H_2SO_4$, isoquinoline, LAH, lithium, magnesium, methyl trifluoromethanesulfonate, 2-bromomesitylene, methyl 2,2,2-trichloroacetimidate, $MgSO_4$, NaCl, *n*-BuLi, $NH_4OAc$, glyoxal solution (20%), Pd/C (5 wt%), $POCl_3$, *p*-TsOH, pyridine, $SnCl_4$ (1 M in DCM), sodium, *t*-BuLi, *t*-BuOK, TEA and TMSCl were purchased from Sigma-Aldrich. (*E*)-Hex-3-enedioic acid, 2-iodobiphenyl, 4-phenylpyridine, neocuproine hemihydrate, $Pd(PPh_3)_2Cl_2$, phenanthridine, 1,1''-diphenyl-4,4''-bipyridinium dichloride and 3,4,7,8-tetramethyl-1,10-phenanthroline were obtained from TCI. 1,1'-dimethyl-[2,2'-bipyridine]-1,1'-diium iodide was kindly provided by Dr. Cyril Bachmann.

The procedures are not optimized for yield. In some cases, the syntheses were performed according to (adapted) literature procedures, which are referenced individually.

## 4.2.2. Ligand and Ligand Precursor Syntheses

**2,9-di-sec-butyl-1,10-phenanthroline (dsbp)[48b]**

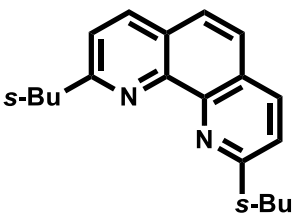

**1**

In a 100 mL Schlenk flask 1,10-phenanthroline (1.233 g, 6.84 mmol) was dissolved in dry toluene (20 mL). At 0 °C *s*-BuLi (1.3 M in hexane, 11.57 mL, 15.05 mmol) was added dropwise to give a deep red solution. After stirring at rt for 40 min, the reaction was quenched by the slow addition of degassed water (35 mL) at 0 °C. The layers were separated, the aqueous layer was extracted with DCM (3x 25 mL) and the combined organic layers were washed with water. To the bright yellow organic layer $MnO_2$ (10 g) was added and the suspension was stirred until deocoloration was observed. $MgSO_4$ was added for drying, the mixture was filtered over celite and the filtrate was concentrated under reduced pressure. The

crude product was purified by column chromatography (neutral alumina, hexane → hexane:DCM 3:1, 0.5% TEA) to give the pure product as a colorless solid (1.449 g, 4.96 mmol, 73%).

**$^1$H NMR** (200 MHz, $CDCl_3$): δ 8.15 (d, *J* = 8.4 Hz, 2H), 7.69 (s, 2H), 7.50 (d, *J* = 8.4 Hz, 2H), 3.43-3.25 (m, 2H), 2.08-1.68 (m, 4H), 1.46 (d, *J* = 7.0 Hz, 6H), 0.99 (dt, *J* = 7.4, 1.2 Hz, 6H); **ESI-MS**: *m/z* = 293.3 $[M+H]^+$ (100%).

**2,9-di-*sec*-butyl-3,4,7,8-tetramethyl-1,10-phenanthroline (dsbtmp)[35b]**

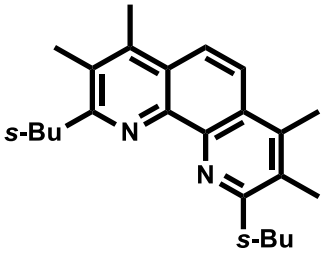

**2**

In a 25 mL Schlenk flask 3,4,7,8-tetramethyl-1,10-phenanthroline was dissolved in dry toluene (7 mL). At 0 °C *s*-BuLi (1.3 M in hexane, 3.59 mL, 4.67 mmol) was added dropwise to give a deep red solution. After stirring at rt for 3 h, the reaction was quenched by the dropwise addition of degassed water (5 mL) at 0 °C. The layers were separated, the aqueous layer was extracted with DCM (3x 20 mL) and the combined organic layers were washed with water. To the bright yellow organic layer $MnO_2$ (8 g) was added and the suspension was stirred until deocoloration was observed. $MgSO_4$ was added for drying, the mixture was filtered over celite and the filtrate was concentrated under reduced pressure. The crude product was purified by column chromatography (neutral alumina, DCM, 0.5% MeOH, 0.5% TEA) to give the pure product as a colorless solid (518 mg, 1.49 mmol, 70%).

**$^1$H NMR** (200 MHz, $CDCl_3$): δ 7.83 (s, 2H), 3.22 (sext, *J* = 6.6 Hz, 2H), 2.58 (s, 6H), 2.41 (s, 6H), 2.18-1.61 (m, 4H), 1.40 (dd, *J* = 6.8, 1.6 Hz, 6H), 0.91 (td, *J* = 7.4, 4.8 Hz, 6H); **ESI-MS**: *m/z* = 349.3 $[M+H]^+$ (100%).

**2,9-di-*sec*-butyl-4,7-diphenyl-1,10-phenanthroline (dsbdpp)[48b]**

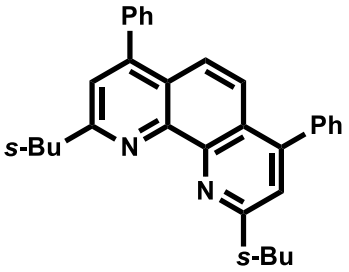

**3**

In a 50 mL Schlenk flask, 4,7-diphenyl-1,10-phenanthroline (332 mg, 1.00 mmol) was dissolved in dry toluene (5 mL). At 0 °C *s*-BuLi (1.3 M in hexane, 1.69 mL, 2.20 mmol) was added dropwise to give a deep red solution. After stirring at rt for 1.5 h, the reaction was quenched by the dropwise addition of degassed water (20 mL) at 0 °C. The layers were separated, the aqueous layer was extracted with DCM (4x 5 mL) and the combined organic layers were washed with water. To the bright yellow organic layer $MnO_2$ (4 g) was added and the suspension was stirred until

deocoloration was observed. $MgSO_4$ was added for drying, the mixture was filtered over celite and the filtrate was concentrated under reduced pressure. The crude product was purified by column chromatography (neutral alumina, hexane:DCM 9:1, 0.5% TEA) to give the pure product as a colorless solid (201 mg, 0.45 mmol, 45%).
**$^1$H NMR** (200 MHz, $CDCl_3$): δ 7.73 (s, 2H), 7.53-7.48 (m, 10H), 7.44 (s, 2H), 3.37 (sext, *J* = 7.0 Hz, 2H), 2.08-1.68 (m, 4H), 1.88 (d, *J* = 7 Hz, 6H), 1.06-0.98 (m, 6H); **ESI-MS**: *m/z* = 445.3 $[M+H]^+$ (100%).

**2,9-di-*tert*-butyl-1,10-phenanthroline (dtbp)[48a]**

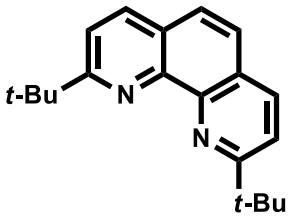

**4**

In a 100 mL Schlenk flask 1,10-phenanthroline (1 g, 5.55 mmol) was dissolved in dry toluene (20 mL). At 0 °C *t*-BuLi (1.7 M in pentane, 7.18 mL, 12.21 mmol) was added dropwise to give a deep red solution. After stirring at rt for 22 h, the reaction was quenched by the dropwise addition of degassed water (20 mL) at 0 °C. The layers were separated, the aqueous layer was extracted with DCM (3x 20 mL), to the combined organic layers $MnO_2$ (10 g) was added and the suspension was stirred until deocoloration was observed. $MgSO_4$ was added for drying, the mixture was filtered over celite and the filtrate was concentrated under reduced pressure. The residue was filtered through a pad of silica (eluent: hexane:DCM 3:1, 0.5% TEA), the filtrate was concentrated under reduced pressure and the crude product was purified by crystallization from hexane to give the pure product as colorless needles (303 mg, 1.04 mmol, 19%).
**$^1$H NMR** (300 MHz, $CDCl_3$): δ 8.16 (d, *J* = 8.5 Hz, 2H), 7.73 (d, *J* = 8.5 Hz, 2H), 7.72 (s, 2H), 1.63 (s, 18H); **ESI-MS**: *m/z* = 293.2 $[M+H]^+$ (100%).

**2-(3-((*tert*-butyldimethylsilyl)oxy)propyl)-3,4,7,8-tetramethyl-1,10-phenanthroline**

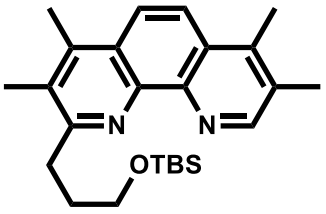


A 25 mL Schlenk flask under argon was charged with lithium (30 mg, 4.32 mmol) and dry $Et_2O$ (2 mL). A solution of (3-bromopropoxy)(*tert*-butyl)dimethylsilane (0.2 mL, 0.86 mmol) in dry $Et_2O$ (2 mL) was added. After stirring this mixture for 2.5 h at rt, the supernatant solution was transferred via syringe to a suspension of 3,4,7,8-tetramethyl-1,10-phenanthroline (68 mg, 0.29 mmol) in dry $Et_2O$ (2 mL). The resulting deep red suspension was stirred for 16.5 h at rt and was then quenched by the addition of water. The aqueous phase was extracted with DCM (2x 5 mL) and the combined organic extracts were stirred with

$MnO_2$ (excess) at rt for 30 min. The black suspension was filtered over a pad of celite, the filtrate was concentrated under reduced pressure and the residue dried under HV. The desired product was obtained as a 3:1 mixture with the 2,9-disubstituted product (75 mg, 0.18 mmol, 64%). The mixture was used for the next step without further purification.

**ESI-MS**: *m/z* = 409.3 $[M+H]^+$ (100%).

**2,9-bis(3-((*tert*-butyldimethylsilyl)oxy)propyl)-3,4,7,8-tetramethyl-1,10-phenanthroline**

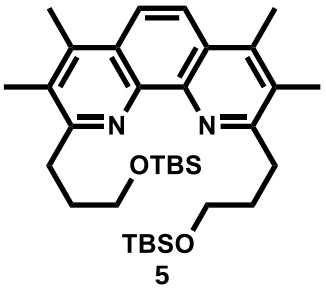

**5**

A 25 mL Schlenk flask under argon was charged with lithium (25 mg, 3.60 mmol) and dry $Et_2O$ (3 mL). A solution of (3-bromopropoxy)(*tert*-butyl)dimethylsilane (0.17 mL, 0.73 mmol) in dry $Et_2O$ (2 mL) was added. After stirring this mixture for 1 h at rt, the supernatant solution was transferred via syringe to a suspension of 2-(3-((*tert*-butyldimethylsilyl)oxy)propyl)-3,4,7,8-tetramethyl-1,10-phenanthroline (75 mg, 0.18 mmol) in dry $Et_2O$ (2 mL). The resulting red suspension was stirred for 30 min at rt and was then quenched by the addition of water. The aqueous phase was extracted with DCM (2x 15 mL) and the combined organic extracts were stirred with $MnO_2$ (excess) for 15 min at rt. The black suspension was filtered over a pad of celite, the filtrate was concentrated under reduced pressure and the residue was dried under HV to give the desired product as a colorless solid (89 mg, 0.15 mmol, 53%).

**ESI-MS**: *m/z* = 581.5 $[M+H]^+$ (100%).

**2-Mesityl-1,10-phenanthroline**[49a]

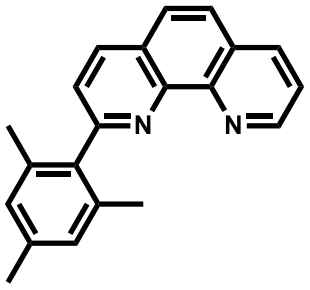


A 250 mL Schlenk flask was charged with 2-bromo-1,3,5-trimethylbenzene (2.55 ml, 16.65 mmol) and dry $Et_2O$ (100 mL). At 0 °C *n*-BuLi (1.6 M in hexane, 10.40 mL, 16.65 mmol) was added and after stirring the mixture for 1 h at this temperature, it was allowed to warm up to rt and stirring was continued for another 6 h. To the white suspension was added 1,10-phenanthroline (2.00 g, 11.10 mmol) and the mixture was stirred at rt for 13 h. Since the reaction was not complete, another portion of mesityllithium (made by stirring 2-bromo-1,3,5-trimethylbenzene (0.85 mL, 5.55 mmol), *n*-BuLi 1.6 M in hexane (3.47 mL, 5.55 mmol) and dry $Et_2O$ (20 mL) at rt for 1.5 h) was added to the mixture and stirring was continued for 1 h. The reaction

was quenched by the addition of water, the aqueous phase was extracted with DCM (2x 50 mL) and the combined organic extracts were stirred with $MnO_2$ (excess) for 1.5 h at rt. The black suspension was filtered over a pad of celite and the filtrate was concentrated under reduced pressure to ~10 mL. An excess of hexane was added to the residue, the newly formed precipitate was filtered off and dried under HV to give the desired product as a colorless powder (1.90 g, 6.35 mmol, 57%).

**ESI-MS**: *m/z* = 299.2 $[M+H]^+$ (100%).

**2,9-dimesityl-1,10-phenanthroline (dmesp)[49a]**

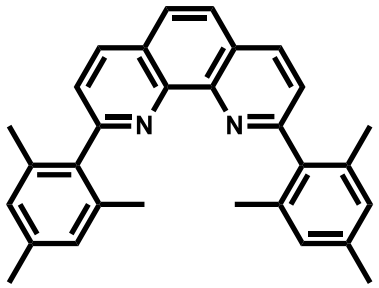


**6**

A 250 mL Schlenk flask was charged with 2-bromo-1,3,5-trimethylbenzene (1.85 mL, 12.07 mmol) and dry $Et_2O$. At 0 °C was added *n*-BuLi 1.6 M in hexane (7.54 mL, 12.07 mmol) and after stirring at this temperature for 15 min, the reaction was allowed to warm up to rt and stirring was continued for 3.5 h. To the white suspension was added 2-mesityl-1,10-phenanthroline (1.80 g, 6.03 mmol) and the resulting brown mixture was stirred at rt for 19 h. The reaction was quenched with water, the aqueous phase was extracted with DCM (2x 50 mL) and the combined organic extracts were stirred with $MnO_2$ (excess) for 1 h at rt. The black suspension was filtered over a pad of celite and the filtrate was concentrated under reduced pressure. The solid residue was triturated with hexane:DCM 10:1 at 40 °C in the ultrasonic bath. Filtration of the suspension, washing of the filtercake with hexane and drying under HV yields the pure product as a colorless powder (1.95 g, 4.68 mmol, 78%).

**$^1$H NMR** (200 MHz, $CDCl_3$): δ 8.30 (d, *J* = 8.2 Hz, 2H), 7.86 (s, 2H), 7.58 (d, *J* = 8.2 Hz, 2H), 6.93 (s, 4H), 2.31 (s, 6H), 2.14 (s, 6H); **ESI-MS**: *m/z* = 417.3 $[M+H]^+$ (100%); **Anal. calcd.** for $C_{30}H_{28}N_2$ (%): C: 86.50, H: 6.78, N: 6.72; Found: C: 86.98, H: 6.73, N: 6.46.

**2-(3,4,5-trimethoxyphenyl)-1,10-phenanthroline**

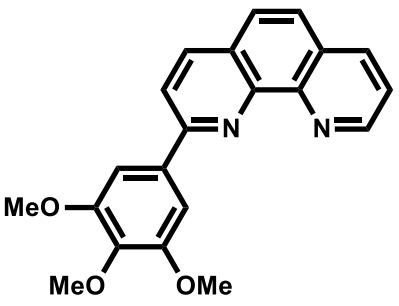


A 100 mL Schlenk flask was charged with 5-bromo-1,2,3-trimethoxybenzene (2.74 g, 11.1 mmol) and dry $Et_2O$. At 0 °C *n*-BuLi (1.6 M in hexane, 6.59 mL, 10.5 mmol) was added slowly. After complete addition, the resulting white suspension was stirred for 30 min at 0 °C, then 1,10-phenanthroline (1.00 g,

5.6 mmol) was added to give a brown suspension. After stirring for 2 h, whilst slowly warming up to rt, the reaction was quenched by pouring into water. The aqueous layer was extracted with DCM (3x 50 mL), the combined organic extracts were dried over $MgSO_4$ and an excess of $MnO_2$ was added. The black suspension was stirred at rt overnight, was filtered over a pad of celite and the filtrate was concentrated to ~5 mL. $Et_2O$ was added to the residue, whereupon a precipitate formed. The mother liquor was decanted off, the solid residue was washed with $Et_2O$ and dried under HV. The product was used without further purification (1.66 g, 4.8 mmol, 86%).

**$^1$H NMR** (300 MHz, $CDCl_3$): δ 9.21 (dd, *J* = 4.3, 1.7 Hz, 1H), 8.32 (d, *J* = 8.4 Hz, 1H), 8.26 (dd, *J* = 8.1, 1.8 Hz, 1H), 8.05 (d, *J* = 8.4 Hz, 1H), 7.81 (q, *J* = 8.8 Hz, 2H), 7.65 (dd, *J* = 8.1, 4.3 Hz, 1H), 7.52 (s, 2H), 4.05 (s, 6H), 3.93 (s, 3H); **ESI-MS**: *m/z* = 347.2 $[M+H]^+$ (100%).

**2,9-bis(3,4,5-trimethoxyphenyl)-1,10-phenanthroline (btmopp)**

In a 50 mL Schlenk flask, 5-bromo-1,2,3-trimethoxybenzene (0.713 g, 2.89 mmol) was dissolved in dry $Et_2O$ (20 mL) and at 0 °C *n*-BuLi (1.6 M in hexane, 1.71 mL, 2.74 mmol) was added. After stirring the resulting white suspension at 0 °C for 15 min, 2-(3,4,5-trimethoxyphenyl)-1,10-phenanthroline (0.5 g, 1.44 mmol) was added and the mixture was stirred for 4 h, whilst slowly warming up to rt. The reaction was quenched by pouring into water and the aqueous layer was extracted with DCM (2x 70 mL). To the combined organic extracts an excess of $MnO_2$ was added and the black suspension was stirred at rt for 30 min. Filtration through a pad of celite yielded a yellow solution, which was concentrated under reduced pressure and the residue dried under HV. The crude product was purified by column chromatography (neutral alumina, DCM, TEA 0.1% → DCM, 0.5%) to give the product still containing small impurities of starting material (0.367 g, 0.72 mmol, 50%). Further purification was achieved by crystallization from hot EtOAc to yield the pure product as crystalline yellowish solid (0.182 g, 0.36 mmol, 25%).

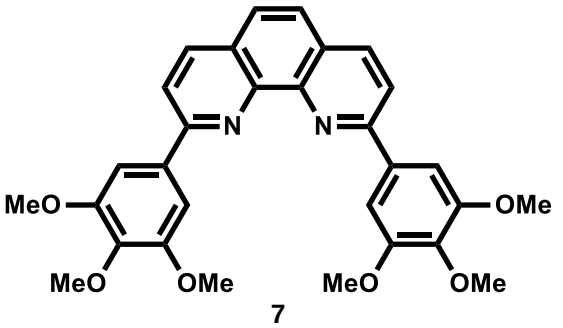

**7**

**$^1$H NMR** (300 MHz, $CDCl_3$): δ 8.31 (d, *J* = 8.4 Hz, 2H), 8.09 (d, *J* = 8.5 Hz, 2H), 7.80 (s, 2H), 7.69 (s, 4H), 4.04 (s, 12H), 3.95 (s, 6H); **ESI-MS**: *m/z* = 513.3 $[M+H]^+$ (100%); **Anal. calcd.** for $C_{30}H_{28}N_2O_6$ (%): C: 70.30, H: 5.51, N: 5.47; Found: C: 69.98, H: 5.53, N: 5.31.

**Sodium 2,9-di-*sec*-butyl-4,7-bis(sulfonatophenyl)-1,10-phenanthroline (dsbdspp)[88]**

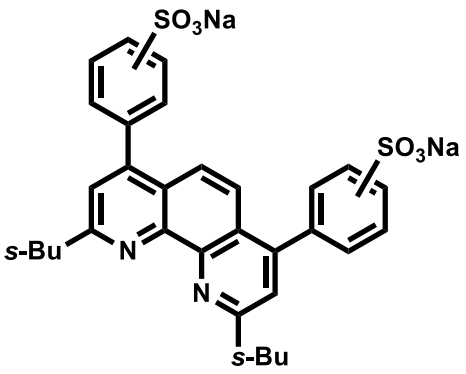

**8**

In a 10 mL round bottom flask 2,9-di-*sec*-butyl-4,7-diphenyl-1,10-phenanthroline (64 mg, 0.14 mmol) was dissolved in fuming sulfuric acid (20% $SO_3$, 0.2 mL). After stirring for 4 h at rt sat. aq. $Na_2CO_3$ was added dropwise until neutral pH. The solvent was boiled off on a heating plate, the residue was extracted with hot ethanol (3x 10 mL). The combined extracts were concentrated under reduced pressure, the residue was dried under HV overnight to give the product as a yellowish solid, which was used without further purification (70 mg, 0.11 mmol, 75%).

**$^1$H NMR** (200 MHz, $D_2O$): δ 7.89-7.81 (m, 4H), 7.56-7.22 (m, 8H), 3.22-3.07 (m, 2H), 1.82-1.55 (m, 4H), 1.40-1.25 (m, 6H), 0.86-0.75 (m, 6H); **ESI-MS**: *m/z* = 605.2 $[M-2Na+3H]^+$ (100%).

**2,9-dipropan-3-ol-1-yl-3,4,7,8-tetramethyl-1,10-phenanthroline (dpotmp)**

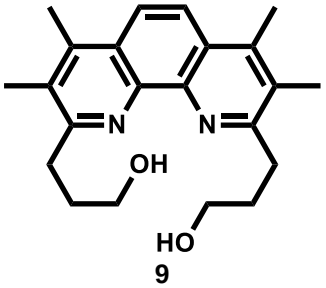

**9**

A 25 mL Schlenk flask was charged with 2,9-bis(3-((*tert*-butyldimethylsilyl)oxy)propyl)-3,4,7,8-tetramethyl-1,10-phenanthroline (56 mg, 0.10 mmol) and dry THF (3 mL). To the orange solution was added TBAF (1 M in THF, 0.10 mL, 0.10 mmol), whereupon the color immediately changed to green. After stirring for 5 h at rt, the solvent was removed under HV and the residue was purified by column chromatography (neutral alumina, DCM 0.5% MeOH → DCM 3% MeOH) to give the pure product as a colorless solid (22 mg, 0.06 mmol, 65%).

**$^1$H NMR** (300 MHz, $CDCl_3$): δ 7.97 (s, 2H), 3.77-3.71 (m, 4H), 3.38-3.32 (m, 4H), 2.70 (s, 6H), 2.50 (s, 6H), 2.21-2.11 (m, 4H); **ESI-MS**: *m/z* = 353.3 $[M+H]^+$ (100%).

**2,9-bis(3,4,5-trihydroxyphenyl)-1,10-phenanthroline (bthopp)**

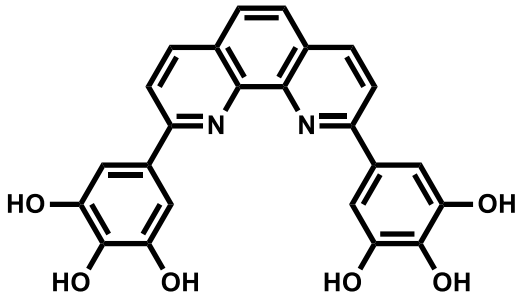

**10**

A 10 mL Young Schlenk flask was charged with 2,9-bis(3,4,5-trimethoxyphenyl)-1,10-phenanthroline (24 mg, 47µmol) and pyridine-1-ium chloride (162 mg, 1.405 mmol). The flask was sealed and heated to 170 °C for 20 h. After cooling down to rt, the solid residue was suspended in water and neutralized, using 1 M aq. NaOH. The red precipitate was filtered off, washed with water and dried under HV to give the desired product.

**$^1$H NMR** (300 MHz, DMSO-$d_6$): δ 8.63 (s, 2H), 8.22 (d, $J$ = 8.1 Hz, 2H), 8.03 (s, 2H), 7.45 (s, 4H), 3.54 (bs); **ESI-MS**: $m/z$ = 429.2 $[M+H]^+$ (100%); **Anal. calcd.** for $C_{24}H_{18}Cl_2N_2O_6$ (M+2HCl, %): C: 57.50, H: 3.62, N: 5.59; Found: C: 57.66, H: 3.74, N: 5.61.

***N,N'*-trimethylene-1,10-phenanthrolinium dibromide[57]**

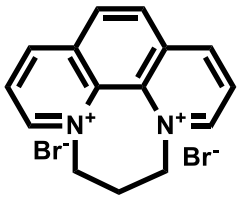


In a 100 mL two neck round bottom flask, equipped with a reflux condenser, 1,10-phenanthroline hydrate (3 g, 15.13 mmol) was dissolved in chlorobenzene (20 mL) at 70 °C. 1,3-Dibromopropane (7.68 mL, 76.00 mmol) was added drowise and after complete addition, the mixture was heated to 120 °C for 3 h. After cooling down to rt, the newly formed orange precipitate was filtered off, washed with hexane and dried under HV. The product (5.09 g, 13.32 mmol, 88%) was used in the next step without further purification.

**$^1$H NMR** (200 MHz, $D_2O$): δ 9.66 (d, $J$ = 5.8 Hz, 2H), 9.45 (d, $J$ = 8.4 Hz, 2H), 8.45-8.61 (m, 4H), 5.14 (t, $J$ = 7 Hz, 4H), 3.42 (quin, $J$ = 6.9 Hz, 2H).

**3,6,7,9-Tetrahydro-5*H*-[1,4]diazepino[1,2,3,4-*lmn*][1,10]phenanthroline-3,9-dione[57]**

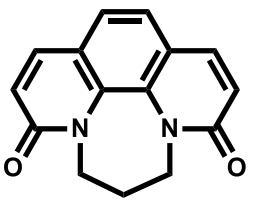


In a 250 mL round bottom flask, *N,N'*-trimethylene-1,10-phenanthrolinium dibromide (2 g, 5.23 mmol) was suspended in *t*-BuOH (40 mL). At 40 °C and air was bubbled through the suspension and *t*-BuOK (2.349 g, 20.94 mmol) was added portionwise. After complete addition, the mixture was stirred at 40 °C for 4 h with air bubbling through the suspension and afterwards over night without the airflow. The formed yellow precipitate was filtered off, the filtercake was

suspended in water and was extracted with DCM (4x 20 mL). The combined organic extracts were dried over $MgSO_4$, the solvent was removed under reduced pressure and the brown residue was dried under HV. The product (0.934 g, 3.70 mmol, 71%) was used without further purification.

**$^1$H NMR** (200 MHz, $CDCl_3$): δ 7.72 (d, *J* = 9.5 Hz, 2H), 7.36 (s, 2H), 6.80 (d, *J* = 9.5 Hz, 2H), 4.32 (t, *J* = 6.7 Hz, 4H), 2.46 (quin, *J* = 6.4 Hz, 2H).

**2,9-Dichloro-1,10-phenanthroline[57]**

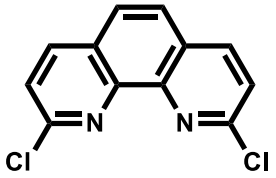

**22**

A 250 mL two neck round bottom flask equipped with a reflux condenser was charged with 3,6,7,9-Tetrahydro-5*H*-[1,4]diazepino[1,2,3,4-*lmn*][1,10]phenanthroline-3,9-dione (2.973 g, 11.79 mmol), freshly distilled $POCl_3$ (36 mL) and $PCl_5$ (4.91 g, 23.57 mmol). After heating the mixture to reflux for 8 h, the excess $POCl_3$ was distilled off under reduced pressure and the residue was suspended in ice-cold water. At 0 °C, the mixture was neutralized with aq. ammonia (25%), which led to the formation of a yellow precipitate. The solid was filtered off and dried under HV. To the residue was added refluxing MeOH (250 mL), the resulting suspension was filtered hot and the filtrate was cooled to -20 °C overnight. The formed crystals were filtered off and dried under HV. A second crystallization from the mother liquor yielded another portion of product, which was also dried under HV and combined with the first fraction (2.09 g, 8.37 mmol, 71%).

**$^1$H NMR** (200 MHz, $CDCl_3$): δ 8.21 (d, *J* = 8.5 Hz, 2H), 7.82 (s, 2H), 7.65 (d, *J* = 8.4 Hz, 2H); **ESI-MS**: *m/z* = 249.0 $[M+H]^+$ (100%).

**2,9-Dibromo-1,10-phenanthroline[58]**

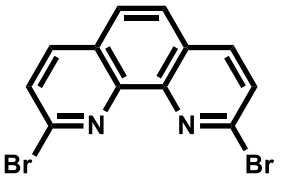

**23**

A 100 mL two neck round bottom flask, equipped with a reflux condenser, was charged with 2,9-dichloro-1,10-phenanthroline (480 mg, 1.93 mmol) and $PBr_3$ (3 mL, 31.90 mmol). The resulting suspension was stirred at 170 °C for 8.5 h and subsequently at rt overnight. The reaction mixture was quenched by addition of ice and the brown suspension was neutralized with sat. aq. $NaHCO_3$. After filtration and drying of the precipitate, the resulting brown solid was dissolved in DCM:MeOH 50:1 and filtered through a plug of silica. The filtrate was concentrated under reduced pressure and the residue dried under HV to give the product as a yellow solid (446 mg, 1.32 mmol, 69%).

**$^1$H NMR** (200 MHz, $CDCl_3$): δ 8.09 (d, *J* = 8.4 Hz, 2H), 7.83 (s, 2H), 7.79 (d, *J* = 8.4 Hz, 2H).

**2,9-Bis((trimethylsilyl)ethynyl)-1,10-phenanthroline[60]**

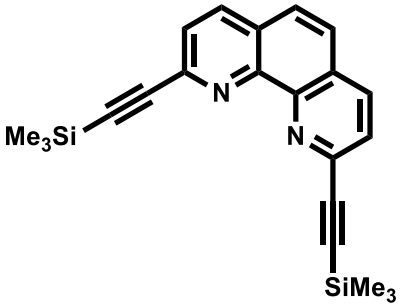


A 10 mL Young Schlenk flask was charged with 2,9-dibromo-1,10-phenanthroline (105 mg, 0.31 mmol) (or 2,9-dichloro-1,10-phenanthroline (77 mg, 0.31 mmol)), CuI (1.8 mg, 9.6 µmol), $Pd(PPh_3)_2Cl_2$ (2.8 mg, 4.0 µmol), which were suspended in dry DMF (1 mL). Ethynyltrimethylsilane (100 µL, 0.7 mmol) and TEA (100 µL, 0.7 mmol) were added, the contents were degassed, the flask was sealed and the mixture was heated to 90 °C for 22 h. After cooling down to rt, the reaction was quenched by the addition of water. The aqueous layer was extracted with DCM (5x 10 mL). The combined organic layers were dried over $MgSO_4$ and concentrated under reduced pressure. Residual DMF was removed under HV to give the crude product. After purification by column chromatography (silica, DCM) the pure product was obtained as a colorless solid (72 mg, 0.19 mmol, 62%).

**$^1$H NMR** (200 MHz, $CDCl_3$): δ 8.17 (d, *J* = 8.2 Hz, 2H), 7.55 (s, 2H), 7.52 (d, *J* = 8.2 Hz, 2H), 0.31 (s, 18H); **ESI-MS**: *m/z* = 373.3 $[M+H]^+$ (100%), 395.2 $[M+Na]^+$ (5%).

**2,9-diethynyl-1,10-phenanthroline[59]**

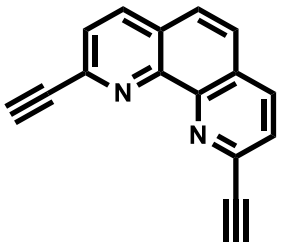


**24**

A 50 mL round bottom flask was charged with 2,9-bis((trimethylsilyl)ethynyl)-1,10-phenanthroline (691 mg, 1.85 mmol) and MeOH (16 mL). $K_2CO_3$ (308 mg, 2.23 mmol) was added to the solution and the resulting suspension was stirred for 18 h at rt. The reaction was quenched by the addition of water (40 mL) and MeOH was removed under reduced pressure. The water was extracted with DCM (3x 20 mL), the combined organic layers were dried over $MgSO_4$ and were evaporated under reduced pressure. The residue was purified by column chromatography (silica, DCM:MeOH 100:1) to give the pure product as a colorless solid (247 mg, 1.08 mmol, 58%).

**$^1$H NMR** (300 MHz, $CDCl_3$): δ 8.21 (d, *J* = 8.4 Hz, 2H), 7.79 (d, *J* = 8.4 Hz, 2H), 7.79 (s, 2H), 3.30 (s, 2H); **ESI-MS**: *m/z* = 229.0 $[M+H]^+$ (100%).

**(1,10-phenanthroline-2,9-diyl)bis(but-3-ene-1,1-diyl) dimethanesulfonate**

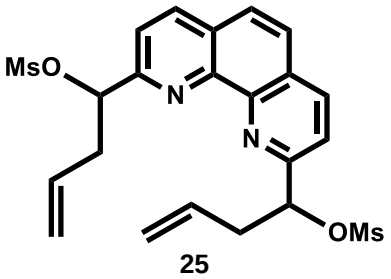

25

A 50 mL Schlenk flask was charged with 1,1'-(1,10-phenanthroline-2,9-diyl)bis(but-3-en-1-ol) (192 mg, 0.60 mmol) and DCM (10 mL). TEA (0.21 mL, 1.50 mmol) was added and the resulting solution was cooled to 0 °C. At this temperature methanesulfonyl chloride (0.10 mL, 1.32 mmol) was added slowly, the mixture was stirred at 0 °C for 30 min and an additional 2.5 h at rt. The reaction mixture was diluted with DCM (10 mL) and was washed with 1 M aq. HCl. The organic layer was then washed with sat. aq. $NaHCO_3$, was dried over $MgSO_4$ and evaporated under reduced pressure. The residue was dried under HV to give the desired product as a colorless solid (230 mg, 0.48 mmol, 81%), which was used without further purification.
**$^1$H NMR** (300 MHz, $CDCl_3$): δ 8.33 (d, *J* = 8.4 Hz, 2H), 7.85-7.81 (m, 4H), 6.15-6.08 (m, 2 H), 6.01-5.87 (m, 2 H), 5.28-5.27 (m, 1H), 5.22-5.20 (m, 2H), 5.19-5.16 (m, 1H), 3.22-2.92 (m, 4H), 3.18 (s, 3H), 3.17 (s, 3H); **ESI-MS**: *m/z* = 417.2 $[M+H]^+$ (100%).

**1,10-Phenanthroline-2,9-dicarboxylic acid[89]**

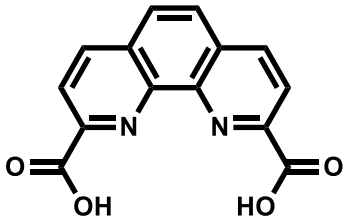


In a 50 mL round bottom flask, 1,10-phenanthroline-2,9-dicarbaldehyde (501 mg, 2.12 mmol) was dissolved in nitric acid 65% (10 mL) and the mixture was heated to reflux for 3 h. After cooling down to rt, the mixture was poured onto ice, whereupon a yellow precipitate formed. The solid was filtered off, washed with water and dried under HV to give the pure product (514 mg, 1.92 mmol, 90%).
**$^1$H NMR** (300 MHz, DMSO-$d_6$): δ 8.73 (d, *J* = 8.3 Hz, 2H), 8.41 (d, *J* = 8.3 Hz, 2H), 8.21 (s, 2H), 3.50 (bs, 2H); **ESI-MS**: *m/z* = 269.0 $[M+H]^+$ (100%).

**Dimethyl 1,10-phenanthroline-2,9-dicarboxylate**

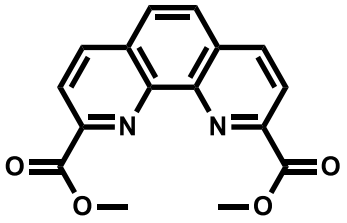

32

A 25 mL Schlenk flask was charged with 1,10-phenanthroline-2,9-dicarboxylic acid (100 mg, 0.37 mmol) and MeOH (5 mL). To the suspension was added at 0 °C chlorotrimethylsilane (0.1 mL, 0.75 mmol), the mixture was allowed to warm up to rt and was then heated to reflux for 3.5 h. The resulting clear solution was allowed to cool down to rt, the solvent was

removed under reduced pressure and the residue was dried under HV to yield the pure product as beige solid (110 mg, 0.37 mmol, 100%).

**1,10-phenanthroline-2,9-dicarbaldehyde[90]**

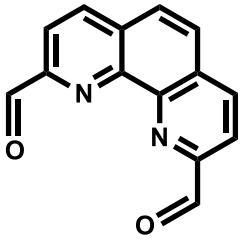

**34**

In a 1000 mL three-neck round-bottom flask, equipped with a reflux condenser and an addition funnel, selenium dioxide (11.24 g, 101 mmol) was suspended in 1,4-dioxane (250 mL) and water (5 mL). The mixture was heated to reflux until all solids dissolved. A solution of 2,9-dimethyl-1,10-phenanthroline hemihydrate (10 g, 46 mmol) in 1,4-dioxane (200 mL) was slowly added via the addition funnel and the resulting red suspension was refluxed for 1.5 h. The suspension was filtered hot, upon cooling a yellow solid precipitated, which was filtered off and dried in vacuo. The residue was triturated with two consecutive portions of refluxing chloroform (2x 200 mL), with filtration after each trituration step. The combined filtrates were concentrated under reduced pressure and the residue was dried under HV to give a beige, fluffy solid (7.08 g, 30 mmol, 65%).

**$^1$H NMR** (300 MHz, $CDCl_3$): δ 10.57 (s, 1H), 8.63 (d, *J* = 8.1 Hz, 2H), 8.3 (d, *J* = 8.1 Hz, 2H), 8.06 (s, 2H); **ESI-MS**: *m/z* = 237.0 $[M+H]^+$ (100%); **Anal. calcd.** for $C_{14}H_8N_2O_2$ (%): C: 71.18, H: 3.41, N: 11.86; Found: C: 71.49, H: 3.43, N: 11.79.

**1,1'-(1,10-phenanthroline-2,9-diyl)bis(but-3-en-1-ol)**

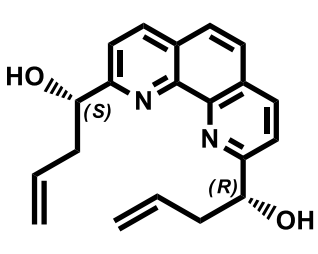

*meso*-**35**

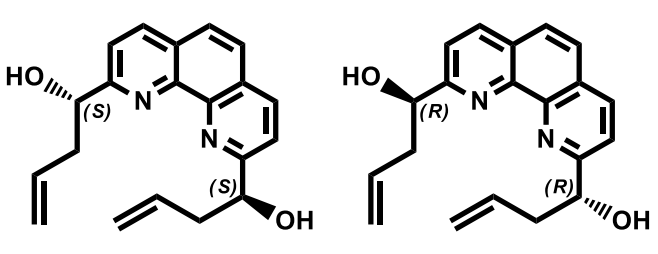

*rac*-**35**

A 500 mL two-neck round-bottom flask was charged with 1,10-phenanthroline-2,9-dicarbaldehyde (1 g, 4.23 mmol) and DCM (200 mL). To the resulting suspension boron trifluoride diethyl etherate (1.18 mL, 9.31 mmol) was added dropwise, after complete addition allyltrimethylsilane (2.8 mL, 17.62 mmol) was added and the mixture was stirred for 16 h at rt. The reaction was quenched by the addition of sat. aq. $NaHCO_3$, the layers were separated, the organic layer was washed with brine, was dried over $MgSO_4$ and concentrated under reduced pressure. The residue was purified by column chromatography (neutral alumina, DCM:MeOH 100:1, 0.1% TEA) to give

the pure colorless product as 1:1 mixture of diastereoisomers (579 mg, 1.81 mmol, 43%).

**$^1$H NMR** (300 MHz, $CDCl_3$): δ 8.16 (d, *J* = 8.1 Hz, 2H, *meso*), 8.05 (d, *J* = 8.4 Hz, 2H, *rac*), 7.74 (s, 2H, *meso*), 7.65 (s, 2H, *rac*), 7.60 (d, *J* = 8.4 Hz, 2H, *meso*), 7.54 (d, *J* = 8.4 Hz, 2H, *rac*), 6.04-5.87 (m, 2H, *rac* / *meso*), 5.58 (br s, 2H, *rac* / *meso*), 5.20-5.05 (m, 6H, *rac* / *meso*), 2.86-2.64 (m, 4H, *rac* / *meso*); **ESI-MS**: *m/z* = 321.3 $[M+H]^+$ (100%), 343.3 $[M+Na]^+$ (5%); **Anal. calcd.** for $C_{20}H_{20}N_2O_2$ (%): C: 74.98, H: 6.29, N: 8.74; Found: C: 74.62, H: 6.15, N: 8.46.

The diastereomers could be separated by preparative TLC (neutral alumina, DCM:MeOH 10:1, 0.2% TEA). The faster eluting compound was identified (chiral HPLC) as the 1:1 racemic mixture of the (*R*,*R*)- and (*S*,*S*)-isomer (*rac*-**35**), the slower eluting compound was identified as the (*R*,*S*)-meso-form (*meso*-**35**). After two recrystallization steps of the diastereomeric mixture from hot EtOH, the pure (~95%) racemate could be isolated as a colorless crystalline solid, whereas the mother liquor still contained a mixture of racemate and *meso*-form.

**(1,10-Phenanthroline-2,9-diyl)bis(but-3-ene-1,1-diyl) diacetate**

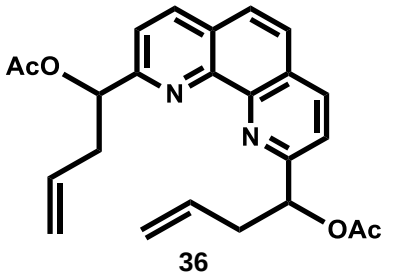

**36**

A 10 mL round bottom flask was charged with 1,1'-(1,10-phenanthroline-2,9-diyl)bis(but-3-en-1-ol) (mixture of diastereoisomers, 15 mg, 0.05 mmol), DCM (0.5 mL), acetic anhydride (100 µL, 1.06 mmol), pyridine (50 µL, 0.62 mmol) and DMAP (tip of a spatula) and this mixture was stirred at rt for 2.5 h. The reaction was quenched by the addition of sat. aq. $NaHCO_3$. The aqueous phase was extracted with DCM (2x 10 mL), the combined organic extracts were dried over $MgSO_4$ and the solvent was removed under reduced pressure. The residue was dried under HV to give the product as a mixture of diastereoisomers.

**$^1$H NMR** (300 MHz, $CDCl_3$): δ 8.23 (d, *J* = 8.3 Hz, 2H), 7.77 (s, 2H), 7.66 (d, *J* = 8.4 Hz, 2H), 6.41-6.30 (m, 2H), 6.00-5.83 (m, 2H), 5.22-5.04 (m, 4H), 3.15-2.85 (m, 4H), 2.26-2.19 (m, 6H); **ESI-MS**: *m/z* = 405.3 $[M+H]^+$ (100%).

**$^1$H NMR** (300 MHz, DMSO-$d_6$): δ 8.74 (d, *J* = 8.3 Hz, 2H), 8.42 (d, *J* = 8.4 Hz, 2H), 8.22 (s, 2H), 4.03 (s, 6H); **ESI-MS**: *m/z* = 297.1 $[M+H]^+$ (100%), 319.1 $[M+Na]^+$ (5%).

**$C_2$-(btmopp)$_2$**

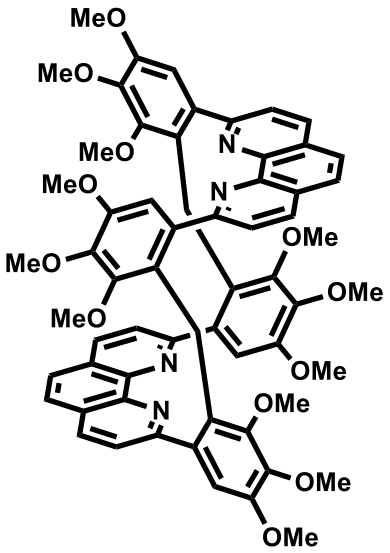

**39**

A 25 mL Schlenk flask was charged with 2,9-bis(3,4,5-trimethoxyphenyl)-1,10-phenanthroline (25 mg, 49 µmol), DCM (5 mL) and chloro(methoxy)methane (15 µL, 195 µmol). To this solution was added dropwise 1 M $SnCl_4$ in DCM (195 µL, 195 µmol) and the mixture was allowed to stir for 7 h at RT. MeOH was added and the reaction mixture was poured into water. The aqueous phase was extracted with DCM (2x 20 mL), the combined organic extracts were dried over $MgSO_4$ and the solvent was removed under reduced pressure. The residue was suspended in MeOH, the solids were filtered off and dried under HV to give the desired product as colorless solid (4 mg, 4 µmol, 16%). Crystals suitable for x-ray diffraction were grown by vapor diffusion of MeOH into a concentrated DCM solution of the product.

**$^1$H NMR** (300 MHz, $CDCl_3$): δ 8.43 (d, *J* = 8.3 Hz, 4H), 7.96 (d, *J* = 8.3 Hz, 4H), 7.89 (s, 4H), 6.57 (s, 4H), 4.95 (s, 4H), 3.75 (s, 12H), 3.72 (s, 12H), 2.62 (s, 12H); **ESI-MS**: *m/z* = 1049.5 $[M+H]^+$ (60%), 525.3 $[M+2H]^{2+}$ (100%).

**2-(2,6-di(1,3-dioxolan-2-yl)phenyl)-1,10-phenanthroline**

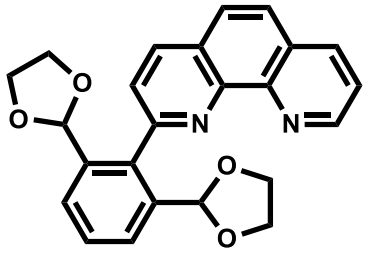

**42**

In a 500 mL Schlenk flask, 2,2'-(2-bromo-1,3-phenylene)bis(1,3-dioxolane) (2.0 g, 6.6 mmol) was dissolved in dry $Et_2O$ (100 mL) and at -78 °C *n*-BuLi (1.6 M in hexane, 4.2 mL, 6.6 mmol) was added slowly. After stirring the mixture at -78 °C for 15 min, it was warmed up to 0 °C and stirred at this temperature for another 45 min. 1,10-Phenanthroline (0.8 g, 4.4 mmol) was added and the resulting brown suspension was stirred for 20 h, whilst slowly warming up to rt. The reaction was quenched by the addition of water and the aqueous phase was extracted with DCM (2x 50 mL). To the combined organic extracts was added $MnO_2$ (excess) and the black suspension was stirred for 30 min at rt. After filtration over a pad of celite, the filtrate was concentrated under reduced pressure. The residue was dissolved in a minimal amount of DCM and the product was precipitated by the addition of hexane. The solids were filtered off and dried under HV to give the desired product as a colorless powder, which was used without further purification (1.2 g, 3.0 mmol, 68%).

**ESI-MS**: *m/z* = 401.2 $[M+H]^+$ (100%).

**2,9-bis(2,6-di(1,3-dioxolan-2-yl)phenyl)-1,10-phenanthroline**

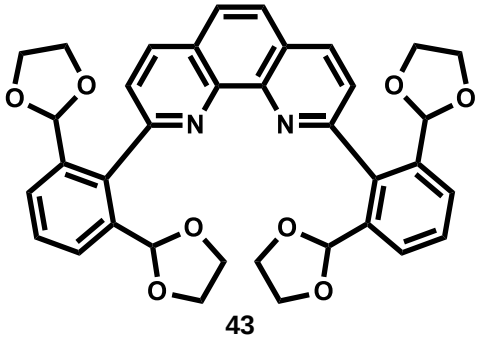

**43**

In a 100 mL Schlenk flask, 2,2'-(2-bromo-1,3-phenylene)bis(1,3-dioxolane) (684 mg, 2.3 mmol) was dissolved in dry $Et_2O$ (30 mL) and at 0 °C *n*-BuLi (1.6 M in hexane, 1.42 mL, 2.3 mmol) was added slowly. After stirring the mixture at 0 °C for 15 min 2-(2,6-di(1,3-dioxolan-2-yl)phenyl)-1,10-phenanthroline (303 mg, 0.8 mmol) was added and the resulting brown suspension was stirred for 20 h, whilst slowly warming up to rt. The reaction was quenched by the addition of water, the aqueous phase was extracted with DCM (2x 100 mL), the combined organic layers were dried over $MgSO_4$ and $MnO_2$ (excess) was added. After stirring the black suspension for 30 min at rt, it was filtered through a pad of celite and the filtrate was concentrated under reduced pressure. The residue was dissolved in a minimal amount of DCM and hexane was added to precipitate the product. The solids were filtered off and dried under HV to give the desired product as a colorless powder (232 mg, 0.4 mmol, 49%).

**$^1$H NMR** (300 MHz, $CDCl_3$): δ 8.31 (d, *J* = 8.2 Hz, 2H), 7.89 (s, 2H), 7.86 (d, *J* = 8.2 Hz, 2H), 7.73 (d, *J* = 7.8 Hz, 4H), 7.47 (t, *J* = 7.8 Hz, 2H), 4.20-3.85 (m, 16H); **ESI-MS**: *m/z* = 643.3 $[M+Na]^+$ (3%), 621.3 $[M+H]^+$ (100%).

**2-(9-(2,6-bis((hydroxyimino)methyl)phenyl)-1,10-phenanthrolin-2-yl)-3-((hydroxyimino)methyl)benzaldehyde oxime**

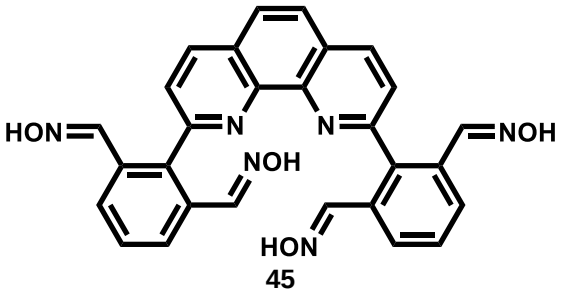

**45**

A 25 mL Schlenk flask was charged with 2,9-bis(2,6-di(1,3-dioxolan-2-yl)phenyl)-1,10-phenanthroline (132 mg, 0.21 mmol), hydroxylamine hydrochloride (369 mg, 5.32 mmol) and EtOH (5 mL). To this suspension was added aq. HCl 16% (0.84 mL, 4.25 mmol) to form a clear orange solution, which was stirred at rt for 2 h. The reaction was neutralized by the addition of aq. 1 M NaOH, whereupon a precipitate formed. To the suspension was added DCM (3 mL) and the biphasic mixture was stirred vigorously for 10 min. Filtration of the suspension and drying of the filtercake under HV yields the desired product as a grey powder (80 mg, 0.16 mmol, 75%).

**$^1$H NMR** (300 MHz, DMSO-$d_6$): δ 11.27 (s, 4H), 8.68 (d, *J* = 8.3 Hz, 2H), 8.20 (s, 2H), 7.91 (d, *J* = 7.7 Hz, 4H), 7.78 (d, *J* = 8.0 Hz, 2H), 7.59-7.50 (m, 6H); **ESI-MS**: *m/z* = 505.2 $[M+H]^+$ (100%); **Anal. calcd.** for $C_{28}H_{24}ClN_6O_6$ (M+2$H_2$O, %): C: 62.22, H: 4.48, N: 15.55; Found: C: 62.77, H: 4.45, N: 14.81.

**2,9-bis(hexahydropyrimidin-2-yl)-1,10-phenanthroline**

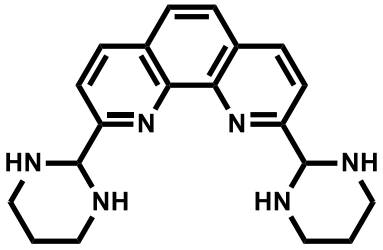

**46**

In a 25 mL Schlenk flask, 1,10-phenanthroline-2,9-dicarbaldehyde (100 mg, 0.42 mmol) was dissolved in hot MeOH (6 mL). After cooling down to rt, to the orange solution was added propane-1,3-diamine (70 µL, 0.85 mmol) and the resulting mixture was stirred for 22 h. The solvent was removed under reduced pressure, the solid residue was dissolved in a mixture of DCM and hexane and the resulting solution filtered. To the filtrate was added an excess of hexane to precipitate the product, which was filtered off and dried under HV to give the product as the dihydrate (138 mg, 0.36 mmol, 85%).

**$^1$H NMR** (300 MHz, $CDCl_3$): δ 8.24 (d, *J* = 8.3 Hz, 2H), 7.82 (d *J* = 8.3 Hz, 2H), 7.76 (s, 2H), 4.95 (s, 2H), 3.24-2.95 (m, 12H); **$^{13}$C{$^1$H} NMR** (75.5 MHz, $CDCl_3$): δ 159.8, 145.1, 137.2, 128.4, 126.4, 121.9, 75.3, 45.8, 26.5; **ESI-MS**: *m/z* = 371.2 $[M+Na]^+$ (30%), 349.3 $[M+H]^+$ (100%); **Anal. calcd.** for $C_{20}H_{28}N_6O_2$ (%): C: 62.48, H: 7.34, N: 21.86; Found: C: 63.20, H: 7.11, N: 21.73.

**1,10-phenanthroline-2,9-dicarbonitrile[68]**

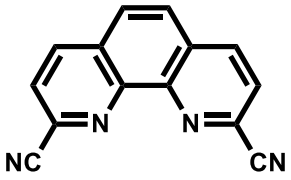

**49**

A 250 mL two neck round bottom flask, equipped with a reflux condenser, was charged with 1,10-phenanthroline-2,9-dicarbaldehyde (1.50 g, 6.4 mmol), hydroxylamine hydrochloride (0.97 g, 14.0 mmol) and dry MeCN (105 mL). To this suspension was added TEA (5.8 mL, 41.9 mmol) and the resulting mixture was heated to reflux for 3 h. After cooling down to rt, 4-methylbenzene-1-sulfonyl chloride (3.99 g, 21.0 mmol) and DBU (2.8 mL, 19.1 mmol) were added subsequently and the mixture was heated to reflux for another 21 h. The reaction mixture was filtered hot and the filtrate was concentrated under reduced pressure. The residue was suspended in MeOH and filtered. The filtercake was washed with MeOH (2x 15 mL) and dried under HV to give the desired product (0.90 g, 3.9 mmol, 62%).

**$^1$H NMR** (200 MHz, DMSO-$d_6$): δ 8.85 (d, $J$ = 8.4 Hz, 2H), 8.42 (d, $J$ = 8.6 Hz, 2H), 8.28 (s, 2H); **ESI-MS**: $m/z$ = 483.2 $[2M+Na]^+$ (25%), 461.1 $[2M+H]^+$ (45%), 253.0 $[M+Na]^+$ (2%), 231.0 $[M+H]^+$ (100%); **Anal. calcd.** for $C_{14}H_6N_4$ (%): C: 73.04, H: 2.63, N: 24.34; Found: C: 71.78, H: 2.57, N: 23.46.

**1,10-phenanthroline-2,9-bis(carboximidamide) dihydrochloride**

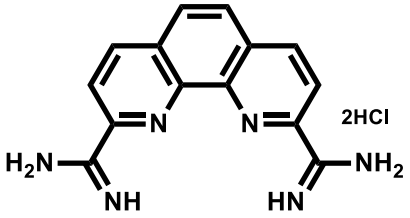

**50**

In a 50 mL two neck round bottom flask, equipped with a reflux condenser, sodium (7 mg, 0.30 mmol) was dissolved in dry MeOH (20 mL) and 1,10-phenanthroline-2,9-dicarbonitrile (350 mg, 1.52 mmol) was added. After heating this mixture to reflux for 1 h, $NH_4Cl$ (179 mg, 3.34 mmol) was added and refluxing was continued for another 2 h. The resulting suspension was filtered hot, the filtercake washed with a small amount of MeOH and dried under HV to give the desired product as a beige solid (280 mg, 0.83 mmol, 55%).

**$^1$H NMR** (200 MHz, DMSO-$d_6$): δ 9.92 (s, 6H), 8.96 (d, $J$ = 8.0 Hz, 2H), 8.84 (d, $J$ = 8.0 Hz, 2H), 8.31 (s, 2H); **ESI-MS**: $m/z$ = 529.3 $[2M-4HCl+H]^+$ (30%), 287.1 $[M-2HCl+Na]^+$ (45%), 265.1 $[M-2HCl+H]^+$ (100%), 248.1 $[M-2HCl-NH_3+H]^+$ (55%), 231.0 $[M-2HCl-2NH_3+H]^+$ (20%); **Anal. calcd.** for $C_{14}H_{14}Cl_2N_6$ (%): C: 49.87, H: 4.18, N: 24.92; Found: C: 50.10, H: 4.34, N: 24.18.

**Spiro[cyclopenta[1,2-*b*:5,4-*b*']dipyridine-5,9'-fluorene][69]**

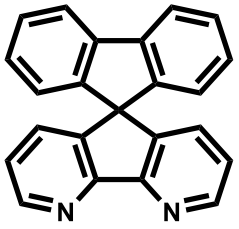

**51**

A 50 mL two neck round bottom flask, equipped with a reflux condenser, was charged with magnesium (200 mg, 8.23 mmol) and a solution of 2-iodo-1,1'-biphenyl (0.31 mL, 8.23 mmol) was in dry $Et_2O$ (5 mL) was slowly added. After complete addition, the mixture was heated to reflux for 1.5 h. After cooling down to rt, the supernatant solution was added via syringe to a solution of 5*H*-cyclopenta[1,2-*b*:5,4-*b*']dipyridin-5-one (163 mg, 0.89 mmol) in dry THF (15 mL) to give a red suspension. This mixture was heated to reflux for 2 h and was then quenched with water. The aqueous phase was extracted with DCM (2x 50 mL), the combined organic layers were dried over $MgSO_4$ and the solvent removed under reduced pressure. The residue was suspended in hexane and the precipitate filtered off. The filtercake was washed with hexane and dried under HV to give the intermediate 5-([1,1'-biphenyl]-2-yl)-5*H*-cyclopenta[1,2-*b*:5,4-*b*']dipyridin-5-ol (228 mg, 0.68 mmol, 76%), which was used

directly in the next step. **ESI-MS**: *m/z* = 337.2 $[M+H]^+$ (100%). In a 100 mL two neck round bottom flask, the intermediate (228 mg, 0.68 mmol) was dissolved in glacial AcOH (20 mL) and $H_2SO_4$ (0.25 mL, 4.69 mmol) was added. After heating the resulting orange solution to reflux for 2.5 h, the mixture was allowed to cool down to rt and ice cold water was added. Upon basification with conc. aq. NaOH, a white precipitate formed. The suspension was extracted with DCM (3x 50 mL), the combined organic extracts were dried over $MgSO_4$ and the solvent removed under reduced pressure. The residue was dried under HV to give the desired product (180 mg, 0.57 mmol, 83% based on starting intermediate).

**$^1$H NMR** (200 MHz, $CDCl_3$): δ 8.75 (t, *J* = 3.2 Hz, 2H), 7.90-7.84 (m, 2H), 7.42 (td, *J* = 7.5, 1.1 Hz, 2H), 7.20-7.09 (m, 6H), 6.76-6.70 (m, 2H); **ESI-MS**: *m/z* = 659.3 $[2M+Na]^+$ (5%), 319.2 $[M+H]^+$ (100%).

**2,8-di-sec-butylspiro[cyclopenta[1,2-*b*:5,4-*b*']dipyridine-5,9'-fluorene]**

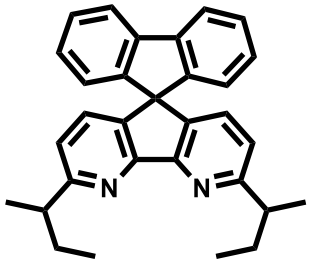


**53**

In a 25 mL Schlenk flask spiro[cyclopenta[1,2-*b*:5,4-*b*']dipyridine-5,9'-fluorene] (100 mg, 0.31 mmol) was suspended in dry toluene (10 mL) and at 0 °C was added *s*-BuLi (1.3 M in hexane, 0.73 mL, 0.94 mmol) to immediately give a deep red solution. The reaction was stirred at 0 °C for 1.5 h, was allowed to warm up to rt and stirred at this temperature for 3 h. After quenching with water, the phases were separated, the aqueous phase was extracted with DCM (2x 25 mL) and to the combined organic extracts was added $MnO_2$ (excess). The resulting black suspension was stirred at rt for 30 min, was then filtered over celite and the filtrate was concentrated under reduced pressure. The residue was purified by column chromatography (silica, hexane:EtOAc 10:1) to give the pure product as a colorless solid (15 mg, 0.04 mmol, 11%).

**$^1$H NMR** (300 MHz, $CDCl_3$): δ 7.84 (d, *J* = 7.6 Hz, 2H), 7.39 (td, *J* = 7.5, 1.0 Hz, 2H), 7.13 (t, *J* = 7.5 Hz, 2H), 6.99 (q, *J* = 8.0Hz, 4H), 6.78-6.73 (m, 2H), 3.22-3.07 (m, 2H), 1.94-1.56 (m, 4H), 1.34 (d, *J* = 7.0 Hz, 6H), 0.92 (t, *J* = 7.4 Hz, 6H); **ESI-MS**: *m/z* = 431.3 $[M+H]^+$ (100%).

## 4.2.3. Metal Complex Syntheses

**$[Cu(MeCN)_4]BF_4$[91]**

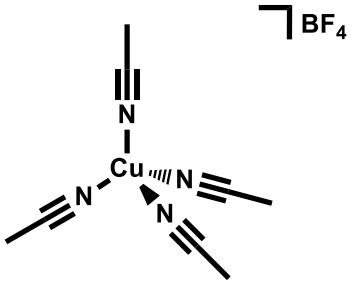


This reaction was performed with a very moist batch of $Cu(BF_4)_2$. In a 250 mL Schlenk flask $Cu(BF_4)_2$ (ca. 50 g, 196 mmol) was dissolved in MeCN (130 mL). To the blue solution was added copper powder (12.45 g, 196 mmol) and the resulting suspension was stirred at rt for 2 h. Excess copper was allowed to settle and the supernatant solution was cannulated off. The residue was washed with MeCN (2x 25 mL), the combined MeCN fractions were filtered over celite and concentrated under reduced pressure to ca. 50 mL, whereupon a white solid precipitated. To complete the precipitation $Et_2O$ (100 mL) was added and the mixture was stored overnight in the fridge under $N_2$-atmosphere. The precipitate was filtered off, washed with $Et_2O$ (2x 10 mL) and dried under HV to yield the pure product as a colorless solid (14.262 g, 45.3 mmol, 23%). The product was stored in the glove box.

**$^1$H NMR** (300 MHz, $CDCl_3$): δ 2.18 (s, 12H); **Anal. calcd.** for $C_8H_{12}BCuF_4N_4$ (%): C: 30.55, H: 3.85, N: 17.81; Found: C: 30.62, H: 3.81, N: 17.76.

**$[Cu(MeCN)_4]OTf$[92]**

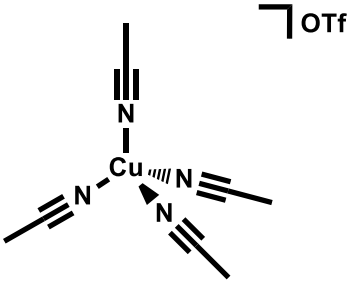


In a 100 mL Schlenk flask $Cu(OTf)_2$ (2.426 g, 6.7 mmol) was dissolved in MeCN (25 mL) and copper powder (852 mg, 13.4 mmol) was added. After stirring for 14 h at rt, the suspension was filtered over celite and the filtrate was concentrated under reduced pressure until a precipitate started to form. At this point $Et_2O$ (15 mL) was added and the mixture was cooled in the fridge for 1 h. The white precipitate was filtered off and dried briefly under HV (prolonged drying leads to an oily product). The product was obtained as a colorless solid (3.64 g, 9.7 mmol, 144%), which was allowed to dry further in the glove box.

**$^1$H NMR** (200 MHz, $CDCl_3$): δ 2.19 (s, 12H). **Anal. calcd.** for $C_9H_{12}CuF_3N_4O_3S$ (%): C: 28.69, H: 3.21, N: 14.87; Found: C: 27.31, H: 3.09, N: 14.38.

**[Cu(phen)$_2$]BF$_4$[48b]**

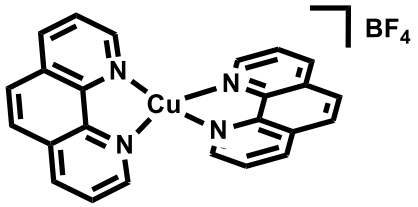


**11**

A 25 mL Schlenk flask was charged with [Cu(MeCN)$_4$]BF$_4$ (30.8 mg, 0.098 mmol) and 1,10-phenanthroline hydrate (38.8 mg, 0.196 mmol). Upon addition of MeCN (2 mL) a dark suspension was formed. After stirring at rt for 4 h, toluene (10 mL) was added and the black precipitate was filtered off. After drying under HV, the pure product was obtained as a black powder.

**$^1$H NMR** (200 MHz, acetone-$d_6$): δ 9.12 (dd, $J$ = 4.8, 1.6 Hz, 4H), 8.87 (dd, $J$ = 8.3, 1.6 Hz, 4H), 8.33 (s, 4H), 8.07 (dd, $J$ = 8.3, 4.7 Hz, 4H); **ESI-MS**: $m/z$ = 423.2 [M-BF$_4$]$^+$ (100%); **Anal. calcd.** for $C_{24}H_{16}BCuF_4N_4$ (%): C: 56.44, H: 3.16, N: 10.97; Found: C: 56.40, H: 3.13, N: 10.98.

**[Cu(dmp)$_2$]BF$_4$[48b]**

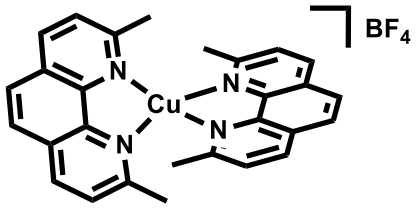


**12**

A 25 mL Schlenk flask was charged with [Cu(MeCN)$_4$]BF$_4$ (27.7 mg, 0.088 mmol) and 2,9-dimethyl-1,10-phenanthroline (36.7 mg, 0.176 mmol). Upon addition of MeCN (2 mL) a red solution was obtained, which was stirred at rt for 2 h. Then the product was precipitated by addition of toluene (10 mL). The precipitate was filtered off and dried under HV to give the pure product as a red solid.

**$^1$H NMR** (300 MHz, $CDCl_3$): δ 8.50 (d, $J$ = 8.1 Hz, 4H), 8.03 (s, 4H), 7.79 (d, $J$ = 8.1 Hz, 4H), 2.44 (s, 12H); **ESI-MS**: $m/z$ = 479.1 [M-BF$_4$]$^+$ (100%). **Anal. calcd.** for $C_{28}H_{24}BCuF_4N_4$ (%): C: 59.33, H: 4.27, N: 9.88; Found: C: 58.98, H: 4.13, N: 9.94.

**[Cu(dsbp)$_2$]BF$_4$[48b]**

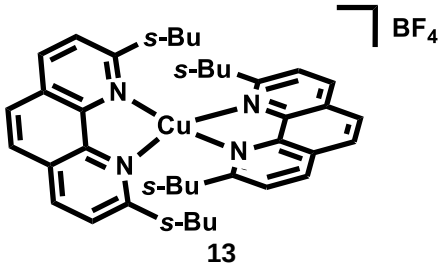


**13**

A 25 mL Schlenk flask was charged with [Cu(MeCN)$_4$]BF$_4$ (23 mg, 0.073 mmol) and 2,9-di-*sec*-butyl-1,10-phenanthroline (42.8 mg, 0.146 mmol). Upon addition of MeCN (0.5 mL) an orange solution formed, which was stirred at rt for 1 h. Afterwards $Et_2O$ (12 mL) was added and the mixture was cooled to 0 °C. The orange precipitate was filtered off and dried under HV to give the product as an orange powder (34 mg, 0.046 mmol, 63%).

**$^1$H NMR** (200 MHz, $CDCl_3$): δ 8.67-8.55 (m, 4H), 8.09 (s, 4H), 7.82-7.67 (m, 4H), 3.05-2.56 (m, 4H), 1.50-1.14 (m, 8H), 1.06-0.82 (m, 12H), 0.37-0.07 (m, 12H); **ESI-MS**: *m/z* = 647.4 $[M\text{-}BF_4]^+$ (100%).

**$[Cu(dsbdpp)_2]BF_4$[48b]**

A 50 mL Schlenk flask was charged with $[Cu(MeCN)_4]BF_4$ (35.4 mg, 0.112 mmol) and 2,9-di-*sec*-butyl-4,7-diphenyl-1,10-phenanthroline (100 mg, 0.225 mmol). Upon addition of MeCN (1 mL) a deep red solution was formed, which was stirred at rt for 3 h. The solvent was removed and the residue was dried under HV to give the product as a red powder (103 mg, 0.099 mmol, 88%).

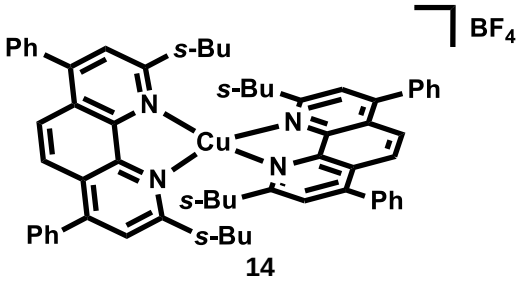

**14**

**$^1$H NMR** (200 MHz, $CDCl_3$): δ 8.09-8.07 (m, 4H), 7.73-7.57 (m, 24H), 3.25-2.82 (m, 4H), 1.68-0.80 (m, 20H), 0.52-0.24 (m, 12H); **ESI-MS**: *m/z* = 951.5 $[M\text{-}BF_4]^+$ (100%).

**$[Cu(dsbtmp)_2]BF_4$[35b]**

A 100 mL Schlenk flask was charged with $[Cu(MeCN)_4]BF_4$ (406 mg, 1.29 mmol) and 2,9-di-*sec*-butyl-3,4,7,8-tetramethyl-1,10-phenanthroline (900 mg, 2.58 mmol). Upon addition of DCM (5 mL) a dark red solution formed, which was stirred at rt for 1 h. $Et_2O$ (50 mL) was added which led to the precipitation of an orange solid. The precipitate was filtered off, was washed with $Et_2O$ and dried under HV to give the pure product as an orange powder (874 mg, 1.03 mmol, 80%).

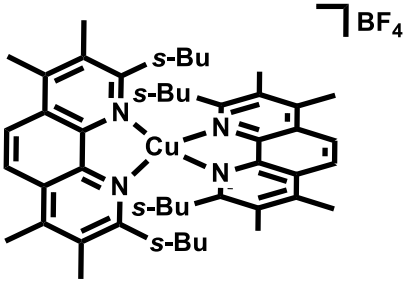

**15**

**$^1$H NMR** (300 MHz, $CDCl_3$): δ 8.21 (s, 4H), 3.68-3.12 (m, 4H), 2.82-2.76 (m, 12H), 2.57-2.48 (m, 12H), 1.68-1.20 (m, 8H), 1.12-0.76 (m, 12H), 0.21 to -0.18 (m, 12H); **ESI-MS**: *m/z* = 759.5 $[M\text{-}BF_4]^+$ (100%); **Anal. calcd.** for $C_{48}H_{64}BCuF_4N_4$ (%): C: 68.03, H: 7.61, N: 6.61; Found: C: 67.76, H: 7.42, N: 6.55.

**[Cu(dpotmp)$_2$]OTf**[48b]

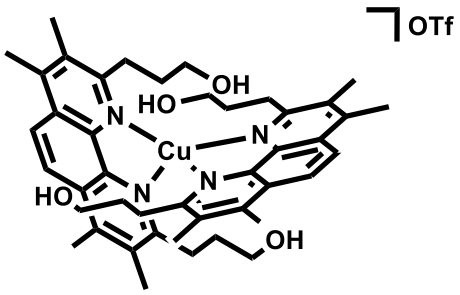


**16**

A 25 mL Schlenk flask was charged with 2,9-dipropan-3-ol-1-yl-3,4,7,8-tetramethyl-1,10-phenanthroline (5.0 mg, 14 µmol), [Cu(MeCN)$_4$]OTf (2.7 mg, 7 µmol) and DCM (3 mL) to form an orange solution. After stirring at rt for 2 h the solvent volume was reduced to ~0.5 mL and $Et_2O$ (10 mL) was added to produce an orange precipitate. The solid was filtered off and dried under HV to give the desired product (4.2 mg, 5 µmol, 77%).

**$^1$H NMR** (300 MHz, $CDCl_3$): δ 8.16 (s, 4H), 2.99-2.90 (m, 8H), 2.78 (s, 12H), 2.76-2.66 (m, 8H), 2.53 (s, 12H), 1.47-1.35 (m, 8H); **ESI-MS**: *m/z* = 765.5 [M-OTf]$^+$ (100%).

**[Cu(dsbdpSO$_3$p)$_2$]BF$_4$**

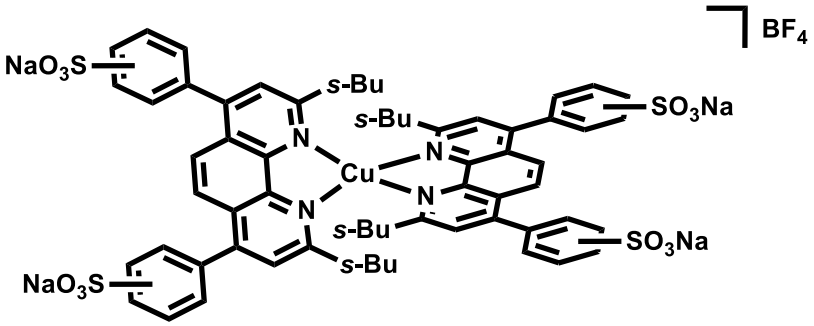


**17**

In a 25 mL Schlenk flask, sodium 2,9-di-sec-butyl-4,7-bis(sulfonatophenyl)-1,10-phenanthroline (45.4 mg, 0.070 mmol) was dissolved in water (3.5 mL) and a solution of [Cu(MeCN)$_4$]BF$_4$ in MeCN (1.75 mL) was added via cannula. The resulting dark red solution was stirred at rt overnight. Afterwards the solvent was removed under reduced pressure, the residue was dissolved in a small amount of MeOH and the solution was filtered. To the filtrate was added MeCN, which produced a precipitate, which was centrifuged off and dried under HV to give the product as a red powder (27 mg, 0.019 mmol, 53%).

**ESI-MS**: *m/z* = 301.0 [L-Na$_2$]$^{2-}$ (30%), 422.7 [M-BF$_4$Na$_4$]$^{3-}$ (100%), 625.1 [L-Na]$^-$ (20%), 645.1 [M-BF$_4$Na$_3$]$^{2-}$ (40%), 665.0 [M-L-BF$_4$Na$_2$]$^-$ (90%); **Anal. calcd.** for $C_{64}H_{72}BCuF_4N_4Na_4O_{18}S_4$ (M+6$H_2O$, %): C: 49.41, H: 4.66, N: 3.60; Found: C: 49.73, H: 4.31, N: 3.26.

**[Cu(btmopp)$_2$]BF$_4$[48b]**

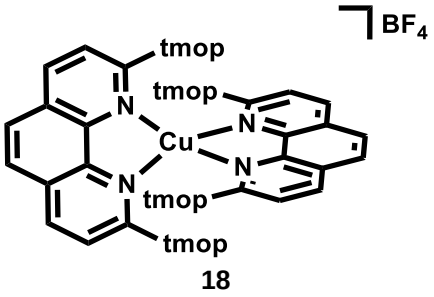

**18**

A 25 mL Schlenk flask was charged with 2,9-bis(3,4,5-trimethoxyphenyl)-1,10-phenanthroline (40 mg, 0.078 mmol), [Cu(MeCN)$_4$]BF$_4$ (12 mg, 0.039 mmol) and DCM (5 mL) to form a deep red solution. After stirring for 1 h at rt, degassed Et$_2$O (15 mL) was added, whereupon a precipitate formed. The suspension was cooled to 0 °C, the solids were filtered off and dried under HV to give the pure product as red solid (42 mg, 0.036 mmol, 92%). Crystals suitable for x-ray diffraction were grown by vapour diffusion of Et$_2$O into a concentrated DCM solution of the product.

**$^1$H NMR** (300 MHz, $CDCl_3$): δ 8.48 (d, *J* = 8.4 Hz, 4H), 8.01 (d, *J* = 8.4 Hz, 4H), 7.92 (s, 4H), 6.74 (s, 4H), 3.64 (s, 12H), 3.36 (s, 24H); **$^{13}$C{$^1$H} NMR** (75.5 MHz, $CDCl_3$): δ 157.1, 152.5, 143.7, 138.3, 137.7, 134.6, 127.9, 126.5, 125.9, 104.5, 60.8, 55.8; **ESI-MS**: *m/z* = 1087.4 [M-BF$_4$]$^+$ (100%); **Anal. calcd.** for $C_{60}H_{56}BCuF_4N_4O_{12}$ (%): C: 61.31, H: 4.80, N: 4.77; Found: C: 60.49, H: 4.71, N: 4.49.

## 4.2.4. Quencher Syntheses

**1,1'-dimethyl-[2,2'-bipyridine]-1,1'-diium tetrafluoroborate**

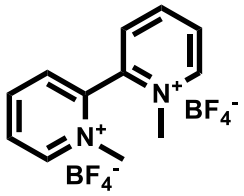


1,1'-dimethyl-[2,2'-bipyridine]-1,1'-diium iodide (1.024 g, 2.327 mmol) was dissolved in a minimal amount of water and an excess of sat. aq. NH$_4$BF$_4$ was added with stirring. A white precipitate formed, which was filtered off and washed with ice-cold water. The filtercake was dried under HV to give the pure product as a colorless crystalline solid.

**$^1$H NMR** (200 MHz, DMSO-*d*$_6$): δ 9.39 (d, *J* = 5.8 Hz, 2H), 8.88 (t, *J* = 7.2 **Anal. calcd.** for $C_{12}H_{14}B_2F_8N_2$ (%): C: 40.05, H: 3.92, N: 6.01; Found: C: 39.71, H: 3.69, N: 6.12.

**4,4',5,5'-Tetramethyl-2,2'-bipyridine[93]**

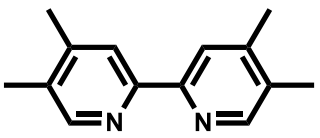


A 100 mL two neck round bottom flask equipped with a reflux condenser was charged with 3,4-dimethylpyridine (15 mL, 134 mmol) and Pd/C 5% (1 g, 134 mmol). This mixture was heated to 170 °C for 7 d, was then filtered hot through a pad of celite and the filtrate was cooled to 0 °C. A colorless precipitate

formed, which was filtered off, washed with $Et_2O$ (3x 3 mL) and dried under HV (84 mg, 0.40 mmol, 0.3%).

**$^1$H NMR** (200 MHz, $CDCl_3$): δ 8.30 (s, 2H), 8.07 (s, 2H), 2.27 (s, 6H), 2.22 (s, 6H); **ESI-MS**: *m/z* = 213.0 $[M+H]^+$ (100%).

### 2,3,12,13-Tetramethyl-6,7,8,9-tetrahydrodipyrido[1,2-*a*:2',1'-*c*][1,4]diazocine-5,10-diium bromide

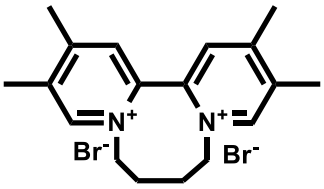


A 10 mL round bottom flask equipped with a reflux condenser was charged with 4,4',5,5'-tetramethyl-2,2'-bipyridine (42 mg, 0.198 mmol) and chlorobenzene (1 mL). The suspension was heated to 70 °C and 1,4-dibromobutane (0.12 mL, 0.989 mmol) was added. The mixture was then heated to 130 °C for 29 h. Afterwards the clear solution was cooled to 0 °C, whereupon a precipitate formed, which was filtered off and dried under HV to give the product as colorless solid (70 mg, 0.163 mmol, 83%).

**$^1$H NMR** (200 MHz, $D_2O$): δ 8.99 (s, 2H), 8.04 (s, 2H), 2.65 (s, 6H), 2.56 (s, 6H), 2.52-2.04 (m, 8H).

### 2,3,12,13-Tetramethyl-6,7,8,9-tetrahydrodipyrido[1,2-*a*:2',1'-*c*][1,4]diazocine-5,10-diium hexafluorophosphate

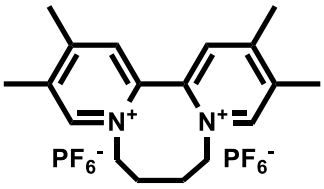


2,3,12,13-Tetramethyl-6,7,8,9-tetrahydrodipyrido[1,2-*a*:2',1'-*c*][1,4]diazocine-5,10-diium bromide (70 mg, 0.163 mmol) was dissolved in a minimal amount of water and excess of sat. aq. $NH_4PF_6$ was added, which resulted in the formation of a grey precipitate. The solid was filtered off, washed with ice-cold water (2x 2 mL) and dried under HV (64 mg, 0.115 mmol, 71%).

**Anal. calcd.** for $C_{18}H_{24}F_{12}N_2P_2$ (%): C: 38.72, H: 4.33, N: 5.02; Found: C: 38.44, H: 4.28, N: 4.99.

### 1*H*,1'*H*-2,2'-Biimidazole (BIm)[94]

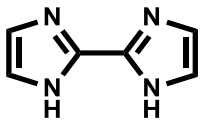


A 500 mL three neck round bottom flask, equipped with a reflux condenser and an addition funnel, was charged with $NH_4OAc$ (100 g, 1.30 mol) and water (30 mL). At 40 °C an aqueous solution of oxalaldehyde ~20% (37.2 mL, 324 mmol) was added over the course of 45 min via the addition funnel. The beige suspension was diluted with water (100 mL) and the precipitate was filtered off. The filtercake was washed subsequently with water and

acetone and was then dried under HV. The product was used without further purification (5.9 g, 44 mmol, 27%).

**$^1$H NMR** (300 MHz, DMSO-$d_6$): δ 12.73 (bs, 2H), 7.12 (s, 2H), 7.01 (s, 2H).

### 3,4,5,8,9,10-Hexahydro-2a,5a,7a,10a-tetraazadicyclopenta[*ef*,*kl*]heptalene-7a,10a-diium hexafluorophosphate ($P_2BIm(PF_6)_2$)[95]

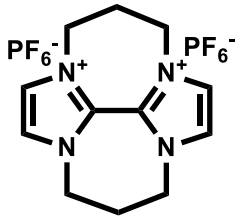


A 100 mL two neck round bottom flask was charged with BIm (1.0 g, 7.45 mmol) and DMF (10 mL). A solution of NaOH (0.6 g, 15 mmol) in water (3 mL) was added and after stirring for 5 min at rt, 1,3-dibromopropane (3.32 mL, 32.70 mmol) was added. The reaction mixture was heated to reflux for 22 h, a second portion of 1,3-dibromopropane (3.32 mL, 32.70 mmol) was added and the mixture was heated to reflux for another 23 h. After cooling down to rt, the newly formed precipitate was filtered off, washed with $Et_2O$ and dried under HV to give to product as the dibromide salt. This was dissolved in a minimal amount of water and added to sat. aq. $NH_4PF_6$ (in excess), whereupon a colorless precipitate formed. The solid was filtered off, washed with water and $Et_2O$ and was dried under HV to give the pure product as a colorless powder (2.147 g, 4.26 mmol, 57%).

**$^1$H NMR** (300 MHz, DMSO-$d_6$): δ 8.13 (s, 4H), 4.61 (t, $J$ = 5.7 Hz, 8H), 2.62-2.52 (m, 4H); **Anal. calcd.** for $C_{12}H_{16}F_{12}N_4P_2$ (%): C: 28.47, H: 3.19, N: 11.07; Found: C: 28.50, H: 3.00, N: 10.71.

### 3,4,5,6,9,10,11,12-Octahydro-2a,6a,8a,12a-tetraazadicyclopenta[*fg*,*mn*]octalene-8a,12a-diium hexafluorophosphate ($B_2BIm(PF_6)_2$)[95]

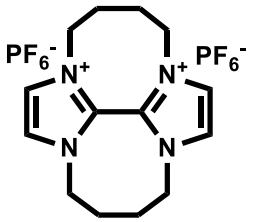


In a 250 mL two neck round bottom flask, equipped with a reflux condenser, BIm (3.0 g, 22.4 mmol) was suspended in DMF (150 mL) and a solution of NaOH (1.8 g, 45 mmol) in water (5 mL) was added. After stirring at rt for 10 min, a dark red, clear solution was formed, to which was added 1,4-dibromobutane (10.7 mL, 89 mmol). After heating to reflux for 44 h, the reaction mixture was cooled down to 0 °C and the newly formed precipitate was filtered off. The filtrate was concentrated under reduced pressure, whereupon more precipitate formed, which was filtered off as well. The combined solids were dried under HV to give the desired product as the dibromide salt (1.3 g, 3.3 mmol, 15%). This was dissolved in a minimal amount of water and added under vigorous stirring to a sat. aq. $NH_4PF_6$ (in excess), whereupon a colorless precipitate formed. The solid was filtered off, washed with water

and small amounts of EtOAc and $Et_2O$. The filtercake was dried under HV to give the pure product (1.33 g, 2.5 mmol, 11%).

**$^1$H NMR** (300 MHz, DMSO-$d_6$): δ 8.27 (s, 4H), 4.72-4.59 (m, 4H), 4.19-4.05 (m, 4H), 2.24-2.09 (m, 4H), 1.87-1.69 (m, 4H); **Anal. calcd.** for $C_{14}H_{20}F_{12}N_4P_2$ (%): C: 31.47, H: 3.77, N: 10.49; Found: C: 31.04, H: 3.76, N: 9.51.

**1*H*,1'*H*-2,2'-Bibenzo[*d*]imidazole (BBIm)[96]**

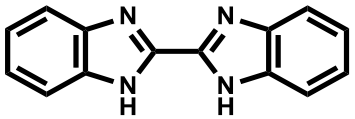

A 250 mL Schlenk flask was charged with benzene-1,2-diamine (8.65 g, 80.0 mmol) and MeOH (120 mL). At 0 °C methyl 2,2,2-trichloroacetimidate (4.95 mL, 40.0 mmol) was added, the mixture was stirred for 18 h, whilst slowly warming up to rt. The mixture was poured into water (200 mL) and the newly formed precipitate was filtered off. After washing with MeOH, the filtercake was dried under HV to give the product, which was used without further purification (7.20 g, 30.7 mmol, 77%).

**$^1$H NMR** (300 MHz, DMSO-$d_6$): δ 7.72-7.60 (m, 4H), 7.39-7.24 (m, 4H); **ESI-MS**: *m/z* = 235.0 $[M+H]^+$ (100%).

**5,6,7,12,13,14-Hexahydro-4b,7a,11b,14a-tetraazadiindeno[1,2,3-*ef*:1'2'3'-*kl*]heptalene-11b,14a-diium hexafluorophosphate ($P_2$BBIm($PF_6$)$_2$)[95a, 97]**

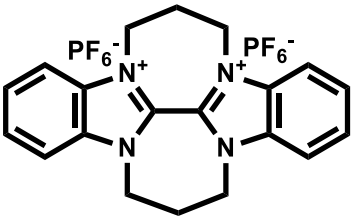

A 250 mL two neck round bottom flask, equipped with a reflux condenser, was charged with BBIm (4.0 g, 17.1 mmol), NaOH (1.50 g, 37.6 mmol) and DMF. To the resulting suspension was added 1,3-dibromopopane (10.40 mL, 102.0 mmol) and the mixture was heated to reflux for 24 h. After cooling down to rt, the reaction mixture was poured into water (500 mL), filtered over a pad of celite and the filtrate was concentrated to ~200 mL under reduced pressure. The resulting suspension was cooled to 0 °C, the precipitate was filtered off, washed with acetone and dried under HV to give the product as the dibromide salt (4.18 g, 8.8 mmol, 51%). This was dissolved in a minimal amount of water and added to sat. aq. $NH_4PF_6$ (in excess), whereupon a precipitate formed. The slightly yellow solid was filtered off, washed with water and dried under HV (2.366 g, 7.5 mmol, 44%).

**$^1$H NMR** (200 MHz, DMSO-$d_6$): δ 8.44-8.31 (m, 4H), 8.05-7.92 (m, 4H), 5.00 (t, *J* = 5.7 Hz, 8H), 2.99-2.83 (m, 4H); **Anal. calcd.** for $C_{20}H_{20}F_{12}N_4P_2$ (%): C: 39.62, H: 3.32, N: 9.24; Found: C: 38.27, H: 3.16, N: 9.23.

**5,6,7,8,13,14,15,16-Octahydro-4b,8a,12b,16a-tetraazadiindeno[1,2,3-*fg*:1',2'3'-*mn*]octalene-12b-16a-diium hexafluorophosphate ($B_2$BBIm($PF_6$)$_2$)[95a, 97]**

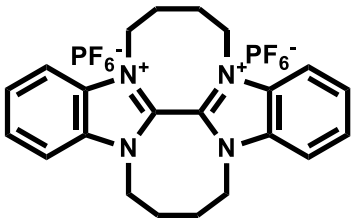


A 250 mL two neck round bottom flask, equipped with a reflux condenser, was charged with BBIm (4.0 g, 17.1 mmol), NaOH (1.5 g, 37.6 mmol) and DMF, the resulting suspension was heated to reflux for 18 h. After cooling down to rt, the mixture was poured into water (500 mL), filtered over a pad of celite and the filtrate was concentrated to dryness under reduced pressure. The residue was dissolved in a minimal amount of refluxing MeOH, the solution was filtered and the filtrate was cooled in the fridge. A crystalline solid formed overnight, which was filtered off and dried under HV to give the product as the dibromide salt (1.5 g, 4.4 mmol, 26%). 0.5 g of this were dissolved in a mixture of water (10 mL) and MeCN (16 mL) and sat. aq. $NH_4PF_6$ (in excess) was added to the resulting solution. The newly formed colorless precipitate was filtered off and dried under HV to give the pure product (438 mg, 0.7 mmol, 70% (based on dibromide starting material)). **$^1$H NMR** (200 MHz, DMSO-$d_6$): δ 8.48-8.36 (m, 4H), 8.06-7.94 (m, 4H), 5.24-5.05 (m, 4H), 4.65-4.46 (m, 4H), 2.43-2.23 (m, 4H), 2.10-1.89 (m, 4H); **Anal. calcd.** for $C_{22}H_{24}F_{12}N_4P_2$ (%): C: 41.65, H: 3.81, N: 8.83; Found: C: 40.07, H: 3.65, N: 8.85.

***N*-Methyl-4-phenylpyridinium hexafluorophosphate (MPP($PF_6$))[98]**

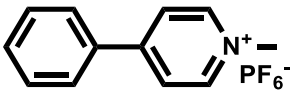


In a 100 mL Schlenk flask, 4-phenylpyridine (5.0 g, 32.2 mmol) was dissolved in MeCN (30 mL) and MeI (3.0 mL, 48.3 mmol) was added. The mixture was stirred at rt for 3 h, whereupon a precipitate formed. The solid was filtered off and washed with $Et_2O$. Upon $Et_2O$ washing, more precipitate formed in the filtrate, which was filtered off and washed with $Et_2O$. The combined filtercakes were dried under HV to give the product as the iodide salt (8.905 g, 30.0 mmol, 88%). This was dissolved in a minimal amount of water and added to sat. aq. $NH_4PF_6$ (in excess), whereupon a precipitate formed, which was filtered off and dried under HV. The crude product was suspended in EtOH (~70 mL) and at 80 °C, MeCN was added until all solids dissolved. Upon cooling to rt a crystalline solid precipitated, which was filtered off and washed with EtOH. The filtrate was stored in the fridge for 3 h, which produced more crystalline solid, which was filtered off, washed with EtOH and combined with the previous fraction. After drying under HV, the pure product was obtained as colorless crystalline solid (8.3 g, 26.2 mmol, 81%).

**$^1$H NMR** (300 MHz, DMSO-$d_6$): δ 9.01 (d, $J$ = 6.7 Hz, 2H), 8.50 (d, $J$ = 6.7 Hz, 2H), 8.11-8.02 (m, 2H), 7.69-7.60 (m, 3H), 4.33 (s, 3H); **ESI-MS**: $m/z$ = 170 $[M]^+$ (100%); **Anal. calcd.** for $C_{12}H_{12}F_6NP$ (%): C: 45.73, H: 3.84, N: 4.44; Found: C: 45.59, H: 3.90, N: 4.28.

***N*-Methyl-4-phenylpyridinium trifluoromethanesulfonate (MPP(OTf))[99]**

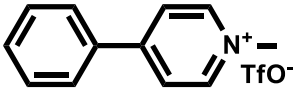


In a 50 mL Schlenk flask, 4-phenylpyridine (1.552 g, 10.0 mmol) was dissolved in DCM (10 mL) and a solution of methyl trifluoromethanesulfonate (1.097 mL, 10.0 mmol) in DCM (10 mL) was added. After stirring for 30 min at rt, $Et_2O$ (150 mL) was added to produce a colorless precipitate. The solid was filtered off, washed with $Et_2O$ and dried under HV (3.04 g, 9.5 mmol, 95%).

**$^1$H NMR** (300 MHz, DMSO-$d_6$): δ 9.01 (d, $J$ = 7.0 Hz, 2H), 8.50 (d, $J$ = 6.9 Hz, 2H), 8.11-8.03 (m, 2H), 7.68-7.60 (m, 3H), 4.33 (s, 3H); **Anal. calcd.** for $C_{13}H_{12}F_3NO_3S$ (%): C: 48.90, H: 3.79, N: 4.39; Found: C: 48.09, H: 3.53, N: 4.38.

***N*-Octyl-4-phenylpyridinium bromide ($C_8$-PPBr)**

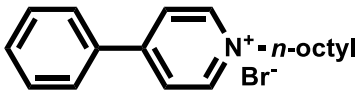


A 50 mL Young Schlenk flask was charged with 4-phenylpyridine (1.032 g, 6.65 mmol), 1-bromooctane (1.26 mL, 7.31 mmol) and toluene (10 mL). After heating this mixture to reflux for 16 h, it was allowed to cool down to rt, whereupon a colorless precipitate formed. The solid was filtered off, washed with $Et_2O$ and dried under HV. Crystallization from hot acetone yields the pure product as a colorless crystalline solid (2.097 g, 6.02 mmol, 91%).

**ESI-MS**: $m/z$ = 268.2 $[M\text{-}Br]^+$ (100%); **Anal. calcd.** for $C_{19}H_{26}BrN$ (%): C: 65.52, H: 7.52, N: 4.02; Found: C: 65.38, H: 7.54, N: 3.91.

***N*-dodecyl-4-phenylpyridinium bromide ($C_{12}$-PPBr)**


A 50 mL Young Schlenk flask was charged with 4-phenylpyridine (1.0 g, 6.4 mmol), 1-bromododecane (1.7 mL, 7.1 mmol) and toluene (10 mL). After heating this mixture to reflux for 18 h, it was allowed to cool down to rt, whereupon a colorless precipitate formed. The solid was filtered off, washed with $Et_2O$ and dried under HV to give the pure product as a colorless powder (1.1 g, 2.7 mmol, 43%).

**ESI-MS**: $m/z$ = 324.3 $[M\text{-}Br]^+$ (100%); **Anal. calcd.** for $C_{23}H_{34}BrN$ (%): C: 68.31, H: 8.47, N: 3.46; Found: C: 68.31, H: 8.53, N: 3.37.

**1-Methylpyridin-1-ium hexafluorophosphate**[95a]

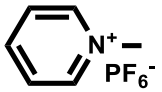

In a 50 mL Schlenk flask, pyridine (2.0 mL, 25.8 mmol) was dissolved in MeCN (10 mL) and iodomethane (2.3 mL, 37.2 mmol) was added. After stirring the mixture for 15 h at rt, a yellow solution was formed, which was slowly concentrated by a stream of nitrogen. This led to the precipitation of a solid, which was filtered off, washed with $Et_2O$ and dried under HV to give the product as the iodide salt (4.893 g, 22.1 mmol, 89%). This was dissolved in a minimal amount of water and added to sat. aq. $NH_4PF_6$, (in excess) whereupon a colorless solid precipitated, which was filtered off, washed with $Et_2O$ and dried under HV (2.931 g, 12.3 mmol, 50%).

**$^1$H NMR** (300 MHz, DMSO-$d_6$): δ 8.97 (d, $J$ = 5.7 Hz, 2H), 8.57 (t, $J$ = 7.8 Hz, 1H), 8.12 (t, $J$ = 7.1 Hz, 2H), 4.35 (s, 3H); **Anal. calcd.** for $C_6H_8F_6NP$ (%): C: 30.14, H: 3.37, N: 5.86; Found: C: 29.37, H: 3.21, N: 5.36.

**2-Methylisoquinolin-2-ium hexafluorophosphate (NMIQ($PF_6$))**[95a]

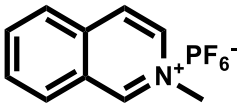

A 50 mL Schlenk flask was charged with isoquinoline (1.50 mL, 12.8 mmol) and MeOH (20 mL). At 0 °C iodomethane (3.97 mL, 63.8 mmol) was added, the mixture was allowed to warm up to rt and was stirred over the weekend. The volume was reduced to ~10 mL and $Et_2O$ was added to the mixture to form a slightly yellow precipitate. The solid was filtered off, washed with $Et_2O$ and dried under HV to give the product as the iodide salt (2.30 g, 8.5 mmol, 67%). 1 g of this was dissolved in a minimal amount of water and added to sat. aq. $NH_4PF_6$ (in excess), whereupon a colorless precipitate formed. The solid was filtered off, washed with water and dried under HV to give the pure product (0.802 g, 2.8 mmol, 75% (based on iodide starting material)).

**$^1$H NMR** (300 MHz, DMSO-$d_6$): δ 9.98 (s, 1H), 8.69 (dd, $J$ = 6.8, 1.4 Hz, 1H), 8.56 (d, $J$ = 6.9 Hz, 1H), 8.47 (d, $J$ = 8.3 Hz, 1H), 8.34 (d, $J$ = 8.2 Hz, 1H), 8.25 (ddd, $J$ = 8.3, 6.9, 1.2 Hz, 1H), 8.07 (ddd, $J$ = 8.2, 6.9, 1.2 Hz, 1H), 4.47 (s, 3H); **Anal. calcd.** for $C_{10}H_{10}F_6NP$ (%): C: 41.54, H: 3.49, N: 4.84; Found: C: 41.44, H: 3.41, N: 4.54.

**5-Methylphenanthridin-5-ium hexafluorophosphate**[95a]

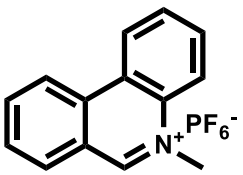

A 100 mL two neck round bottom flask, equipped with a reflux condenser, was charged with phenanthridine (1.5 g, 8.4 mmol), toluene (40 mL) and iodomethane (2.1 mL, 33.5 mmol). The mixture was stirred at 65 °C for 7 h, the newly formed precipitate

was filtered off, washed with EtOAc and dried under HV to give the product as the iodide salt (1.16 g, 3.6 mmol, 43%). This was dissolved in a mixture of water and MeCN, filtered and added to sat. aq. $NH_4PF_6$ (in excess), whereupon a slightly yellow precipitate formed. The solids were filtered off, washed subsequently with water and $Et_2O$ and dried under HV (1.16 g, 3.4 mmol, 41%).

**$^1$H NMR** (300 MHz, DMSO-$d_6$): δ 10.28 (s, 1H), 9.22-9.11 (m, 2H), 8.56 (dd, $J$ = 8.2, 3.9 Hz, 2H), 8.41 (t, $J$ = 7.8 Hz, 1H), 8.22-8.07 (m, 3H), 4.67 (s, 3H); **ESI-MS**: $m/z$ = 194.1 $[M]^+$ (100%); **Anal. calcd.** for $C_{14}H_{12}F_6NP$ (%): C: 49.57, H: 3.57, N: 4.13; Found: C: 49.38, H: 3.63, N: 4.03.

**1,1'-diphenyl-[4,4'-bipyridine]-1,1'-diium hexafluorophosphate[95a]**

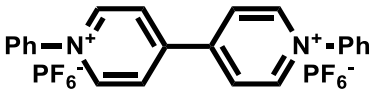


1,1'-diphenyl-[4,4'-bipyridine]-1,1'-diium chloride (1.0 g, 2.6 mmol) was dissolved in a minimal amount of water and added to sat. aq. $NH_4PF_6$ (in excess), whereupon a colorless precipitate formed. The solids were filtered off, washed with water and dried under HV to give the pure product as colorless powder (0.9 g, 1.5 mmol, 58%).

**Anal. calcd.** for $C_{22}H_{18}F_{12}N_2P_2$ (%): C: 44.02, H: 3.02, N: 4.67; Found: C: 44.09, H: 2.84, N: 4.64.

## 4.2.5. Building Block Syntheses

**(*E*)-dimethyl hex-3-enedioate[61]**

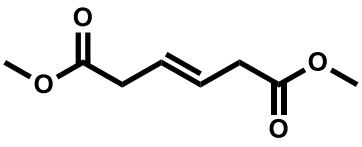


**29**

In a 250 mL two neck round bottom flask, (*E*)-hex-3-enedioic acid (4.0 g, 27.8 mmol) was suspended in MeOH (75 mL) and at 0 °C chlorotrimethylsilane (7.04 mL, 55.5 mmol) was added. The mixture was allowed to warm up to rt and was stirred for 44 h. The solution was concentrated under reduced pressure to ca. 50 mL, water (50 mL) was added and the mixture was extracted with $Et_2O$ (1x 100 mL, 2x 50 mL). The combined organic extracts were washed subsequently with sat. aq. $NaHCO_3$ and brine, were dried over $MgSO_4$ and concentrated under reduced pressure (4.04 g, 23.5 mmol, 85%).

**$^1$H NMR** (300 MHz, $CDCl_3$): δ 5.71-5.65 (m, 2H), 3.67 (s, 6H), 3.11-3.07 (m, 4H).

**(*E*)-Hex-3-ene-1,6-diol[61]**


**30**

A 250 mL two neck round bottom flask was charged with LAH (2.55 g, 67.2 mmol) and THF (100 mL). At 0 °C a

solution of (*E*)-dimethyl hex-3-enedionate (3.86 g, 22.4 mmol) in THF was added drowise. After complete addition, the mixture was stirred at rt for 2 h and was then quenched by the subsequent addition of water (2.5 mL), 2 M aq. NaOH (7.5 mL) and water (2.5 mL). The reaction mixture was heated to 70 °C, was filtered hot over a pad of celite and the filtrate was concentrated under reduced pressure. The residue was purified by column chromatography (silica, EtOAc:$Et_2O$ 1:1) to give the pure product (1.97 g, 16.9 mmol, 76%).

**$^1$H NMR** (300 MHz, $CDCl_3$): δ 5.60-5.46 (m, 2H), 3.65 (t, *J* = 6.2 Hz, 4H), 2.34-2.26 (m, 4H).

**(*E*)-2,2,3,3,12,12,13,13-octamethyl-4,11-dioxa-3,12-disilatetradec-7-ene[61]**

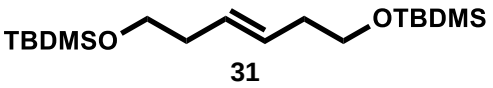

**31**

In 50 mL Schlenk flask, (*E*)-hex-3-ene-1,6-diol (1.78 g, 15.3 mmol) was dissolved in DCM and at 0 °C were added subsequently 1*H*-imidazole (5.99 g, 88.0 mmol) and *tert*-butylchlorodimethylsilane (5.99 g, 39.8 mmol), which lead to the formation of a white precipitate. The Suspension was warmed up to rt and was stirred for 2 h at this temperature. After quenching with sat. aq. $NH_4Cl$ (20 mL), the layers were separated and the aqueous phase was extracted with DCM (2x 30 mL). The combined organic extracts were washed with water, dried over $MgSO_4$ and the solvent was removed under reduced pressure (5.20 g, 15.1 mmol, 99%).

**$^1$H NMR** (300 MHz, $CDCl_3$): δ 5.50-5.43 (m, 2H), 3.61 (t, *J* = 6.9 Hz, 4H), 2.27-2.16 (m, 4H), 0.89 (s, 18H), 0.04 (s, 12H); **EI-MS**: *m/z* = 343.0 $[M-H]^+$ (5%), 286.8 $[M-tBu]^+$ (15%), 213.0 $[M-OTBDMS]^+$ (100%).

**2,2'-(2-Bromo-1,3-phenylene)bis(1,3-dioxolane)[67]**

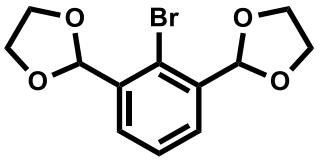

**41**

A 500 mL round bottom flask, equipped with a Dean-Stark trap, was charged with 2-bromoisophthalaldehyde (4.82 g, 22.6 mmol), 4-methylbenzenesulfonic acid (tip of a spatula), ethylene glycol (20.3 mL, 362.0 mmol) and toluene (250 mL). After heating this mixture to reflux for 20 h, it was allowed to cool down to rt and the solvent was removed under reduced pressure. The residue was taken up in a mixture of DCM (60 mL) and $Et_2O$ (60 mL), was washed with sat. aq. $Na_2CO_3$, the organic layer was dried over $MgSO_4$ and the solvent was removed under reduced pressure. The residue was dried under HV to give the desired product as a colorless powder (6.63 g, 22.0 mmol, 97%).

**$^1$H NMR** (300 MHz, $CDCl_3$): δ 7.62 (d, *J* = 7.7 Hz, 2H), 7.40-7.33 (m, 1H), 6.19 (s, 2H), 4.19-4.02 (m, 8H); **ESI-MS**: *m/z* = 323.0 $[M+Na]^+$ (100%).

## 4.3. Crystallographic Tables

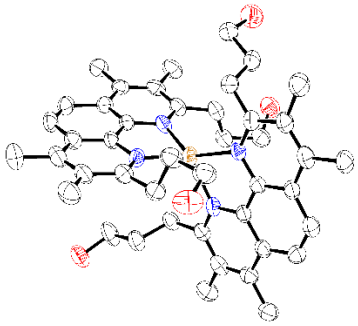

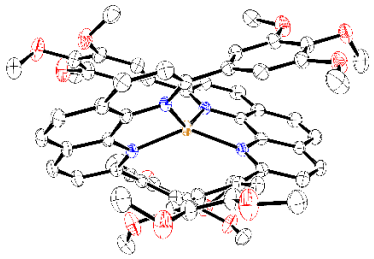

| Compound # | **16** | **18** |
|---|---|---|
| | jw211016o | jw050115 |
| Empirical formula | $C_{46}H_{57}Cl_3CuF_3N_4O_7S$ | $C_{60}H_{56}BCuF_4N_4O_{12}$ |
| Diffractometer | SuperNova, Dual, Cu at zero, Atlas | Xcalibur Ruby |
| Wavelength [Å] | 1.54184 | 0.71073 |
| Formula weight | 1036.90 | 1175.43 |
| Crystal system | Orthorhombic | Orthorhombic |
| Space group | $P2_12_12_1$ | Ibca |
| a [Å] | 11.1493(2) | 14.2175(7) |
| b [Å] | 25.6982(7) | 20.3621(9) |
| c [Å] | 33.0161(9) | 37.1609(12) |
| α [°] | 90 | 90 |
| β [°] | 90 | 90 |
| γ [°] | 90 | 90 |
| Volume [$Å^3$] | 9459.7(4) | 10758.0(8) |
| Z | 8 | 8 |
| Density (calculated) [$Mg/m^3$] | 1.456 | 1.451 |
| Absorption coefficient [$mm^{-1}$] | 3.184 | 0.490 |
| F(000) | 4320 | 4880 |
| Crystal size [$mm^3$] | 0.370 x 0.060 x 0.010 | 0.330 x 0.280 x 0.060 |
| Crystal description | red needle | dark red plate |
| Theta range for data collection [°] | 3.182 to 76.918 | 2.804 to 30.508 |
| Index ranges | -8 ≤ h ≤ 14<br>-32 ≤ k ≤ 30<br>-30 ≤ l ≤ 41 | -19 ≤ h ≤ 20<br>-29 ≤ k ≤ 17<br>-53 ≤ l ≤ 50 |
| Reflections collected | 51968 | 31956 |
| Independent reflections | 19644 [R(int) = 0.0696] | 8211 [R(int) = 0.0504] |
| Reflections observed | 14901 | 5486 |
| Criterion for observation | I > 2(I) | I > 2(I) |
| Completeness to theta | 99.9 % to 67.684° | 99.9 % to 25.242° |
| Absorption correction | Semi-empirical from equivalents | Semi-empirical from equivalents |
| Max. and min. transmission | 1.00000 and 0.59561 | 1.00000 and 0.72788 |
| Data / restraints / parameters | 19644 / 2 / 1198 | 8211 / 0 / 377 |
| Goodness-of-fit on $F^2$ | 1.065 | 1.024 |
| Final R indices [I>2sigma(I)] | R1 = 0.0855, wR2 = 0.2372 | R1 = 0.0497, wR2 = 0.1151 |
| R indices (all data) | R1 = 0.1048, wR2 = 0.2645 | R1 = 0.0839, wR2 = 0.1343 |
| Absolute structure parameter | 0.46(4) | - |
| Largest diff. peak and hole [$e.Å^{-3}$] | 1.521 and -1.874 | 0.724 and -0.443 |

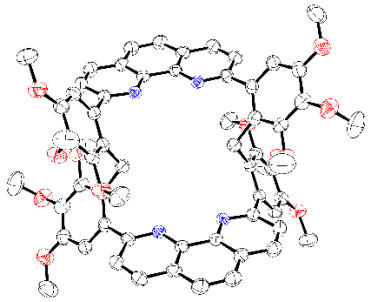

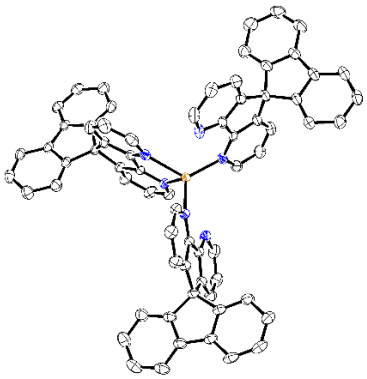

| Compound # | **39** | [Cu(**51**)$_3$]BF$_4$ |
|---|---|---|
| | jw290815o | jw251016o |
| Empirical formula | $C_{65.2}H_{62.4}Cl_{6.4}N_4O_{12}$ | $C_{69}H_{42}BCuF_4N_6$ |
| Diffractometer | SuperNova, Dual, Cu at zero, Atlas | Agilent SuperNova dual radiation CCD |
| Wavelength [Å] | 1.54184 | 0.71073 |
| Formula weight | 1320.87 | 1105.43 |
| Crystal system | Trigonal | Tetragonal |
| Space group | R-3 | $I4_1/acd$ |
| a [Å] | 37.3698(4) | 24.56340(19) |
| b [Å] | 37.3698(4) | 24.56340(19) |
| c [Å] | 12.31520(15) | 35.5497(4) |
| α [°] | 90 | 90 |
| β [°] | 90 | 90 |
| γ [°] | 120 | 90 |
| Volume [Å$^3$] | 14894.1(3) | 21449.3(4) |
| Z | 9 | 16 |
| Density (calculated) [Mg/m$^3$] | 1.325 | 1.369 |
| Absorption coefficient [mm$^{-1}$] | 3.032 | 0.472 |
| F(000) | 6178 | 9088 |
| Crystal size [mm$^3$] | 0.200 x 0.150 x 0.090 | 0.220 x 0.210 x 0.130 |
| Crystal description | colourless prism | orange prism |
| Theta range for data collection [°] | 2.365 to 76.550 | 2.829 to 30.920 |
| Index ranges | -47 ≤ h ≤ 46<br>-46 ≤ k ≤ 47<br>-15 ≤ l ≤ 15 | -16 ≤ h ≤ 32<br>-14 ≤ k ≤ 34<br>-48 ≤ l ≤ 48 |
| Reflections collected | 62586 | 32357 |
| Independent reflections | 6952 [R(int) = 0.0289] | 7845 [R(int) = 0.0213] |
| Reflections observed | 6037 | 6276 |
| Criterion for observation | I > 2(I) | I > 2(I) |
| Completeness to theta | 100.0 % to 67.684° | 99.9 % to 25.242° |
| Absorption correction | Semi-empirical from equivalents | Semi-empirical from equivalents |
| Max. and min. transmission | 1.00000 and 0.79816 | 1.00000 and 0.89383 |
| Data / restraints / parameters | 6952 / 0 / 430 | 7845 / 3 / 372 |
| Goodness-of-fit on F$^2$ | 1.202 | 1.038 |
| Final R indices [I>2sigma(I)] | R1 = 0.0942, wR2 = 0.3477 | R1 = 0.0561, wR2 = 0.1605 |
| R indices (all data) | R1 = 0.1006, wR2 = 0.3683 | R1 = 0.0704, wR2 = 0.1722 |
| Absolute structure parameter | - | - |
| Largest diff. peak and hole [e.Å$^{-3}$] | 0.722 and -1.660 | 1.274 and -1.179 |

# 5. References


[1] IEA, *Key world energy statistics* **2016**.

[2] This was estimated from the impact energy of the meteor being equivalent to ~10 megatons TNT (https://en.wikipedia.org/wiki/Meteor_Crater, accessed on 29.11.2016) and 1 Mtoe being equivalent to ~10 megatons TNT.

[3] https://wolframalpha.com/input/?i=573+exajoules+to+GWh, accessed on 29.11.2016.

[4] Mauna Loa Observatory.

[5] a) United Nations Framework Convention on Climate Change, *Paris Agreement* **2015**; b) A. Borgschulte, *Front. Energy Res.* **2016**, *4*.

[6] a) V. Balzani, A. Credi, M. Venturi, *ChemSusChem* **2008**, *1*, 26-58; b) R. Schlögl, *ChemSusChem* **2010**, *3*, 209-222.

[7] a) N. Armaroli, V. Balzani, *Angew. Chem.* **2007**, *119*, 52-67; b) S. Styring, *Faraday Discuss.* **2012**, *155*, 357-376.

[8] https://en.wikipedia.org/wiki/Energy_density, accessed on 21.11.2016.

[9] https://empa.ch/web/s604/move-700bar, accessed on 22.11.2016.

[10] G. A. Olah, *Angew. Chem. Int. Ed.* **2005**, *44*, 2636-2639.

[11] S. W. Gersten, G. J. Samuels, T. J. Meyer, *J. Am. Chem. Soc.* **1982**, *104*, 4029-4030.

[12] a) J. D. Blakemore, R. H. Crabtree, G. W. Brudvig, *Chem. Rev.* **2015**, *115*, 12974-13005; b) S. Berardi, S. Drouet, L. Francas, C. Gimbert-Surinach, M. Guttentag, C. Richmond, T. Stoll, A. Llobet, *Chem. Soc. Rev.* **2014**, *43*, 7501-7519.

[13] a) A. R. Parent, K. Sakai, *ChemSusChem* **2014**, *7*, 2070-2080; b) F. Evangelisti, R. Güttinger, R. Moré, S. Luber, G. R. Patzke, *J. Am. Chem. Soc.* **2013**, *135*, 18734-18737.

[14] a) H. Lv, Y. V. Geletii, C. Zhao, J. W. Vickers, G. Zhu, Z. Luo, J. Song, T. Lian, D. G. Musaev, C. L. Hill, *Chem. Soc. Rev.* **2012**, *41*, 7572-7589; b) P.-E. Car, M. Guttentag, K. K. Baldridge, R. Alberto, G. R. Patzke, *Green Chem.* **2012**, *14*, 1680-1688; c) F. Evangelisti, P.-E. Car, O. Blacque, G. R. Patzke, *Catal. Sci. Technol.* **2013**, *3*, 3117-3129; d) M. Orlandi, R. Argazzi, A. Sartorel, M. Carraro, G. Scorrano, M. Bonchio, F. Scandola, *Chem. Commun.* **2010**, *46*, 3152-3154.

[15] J. D. Blakemore, N. D. Schley, D. Balcells, J. F. Hull, G. W. Olack, C. D. Incarvito, O. Eisenstein, G. W. Brudvig, R. H. Crabtree, *J. Am. Chem. Soc.* **2010**, *132*, 16017-16029.

[16] T. Nakazono, A. R. Parent, K. Sakai, *Chem. Commun.* **2013**, *49*, 6325-6327.

[17] T. Zhang, C. Wang, S. Liu, J.-L. Wang, W. Lin, *J. Am. Chem. Soc.* **2014**, *136*, 273-281.

[18] M. Kirch, J.-M. Lehn, J.-P. Sauvage, *Helv. Chim. Acta* **1979**, *62*, 1345-1384.

[19] a) E. D. Cline, S. E. Adamson, S. Bernhard, *Inorg. Chem.* **2008**, *47*, 10378-10388; b) S. Fukuzumi, T. Kobayashi, T. Suenobu, *Angew. Chem. Int. Ed.* **2011**, *50*, 728-731; c) T. Stoll, M. Gennari, I. Serrano, J. Fortage, J. Chauvin, F. Odobel, M. Rebarz, O. Poizat, M. Sliwa, A. Deronzier, M.-N. Collomb, *Chem. Eur. J.* **2013**, *19*, 782-792.

[20] K. Sakai, H. Ozawa, *Coord. Chem. Rev.* **2007**, *251*, 2753-2766.

[21] a) W. T. Eckenhoff, R. Eisenberg, *Dalton Trans.* **2012**, *41*, 13004-13021; b) N. Queyriaux, R. T. Jane, J. Massin, V. Artero, M. Chavarot-Kerlidou, *Coord. Chem. Rev.* **2015**, *304–305*, 3-19; c) M. Wang, L. Chen, L. Sun, *Energy Environ. Sci.* **2012**, *5*, 6763-6778.

[22] a) B. Probst, A. Rodenberg, M. Guttentag, P. Hamm, R. Alberto, *Inorg. Chem.* **2010**, *49*, 6453-6460; b) B. Probst, M. Guttentag, A. Rodenberg, P. Hamm, R. Alberto, *Inorg. Chem.* **2011**, *50*, 3404-3412; c) M. Guttentag, A. Rodenberg, R. Kopelent, B. Probst, C. Buchwalder, M. Brandstätter, P. Hamm, R. Alberto, *Eur. J. Inorg. Chem.* **2012**, *2012*, 59-64.

[23] a) C. Bachmann, M. Guttentag, B. Spingler, R. Alberto, *Inorg. Chem.* **2013**, *52*, 6055-6061; b) M. Guttentag, A. Rodenberg, C. Bachmann, A. Senn, P. Hamm, R. Alberto, *Dalton Trans.* **2013**, *42*, 334-337; c) C. Bachmann, B. Probst, M. Guttentag, R. Alberto, *Chem. Commun.* **2014**, *50*, 6737-6739; d) A. Rodenberg, M. Orazietti, B. Probst, C. Bachmann, R. Alberto, K. K. Baldridge, P. Hamm, *Inorg. Chem.* **2015**, *54*, 646-657; e) E. Joliat, S. Schnidrig, B. Probst, C. Bachmann, B. Spingler, K. K. Baldridge, F. von Rohr, A. Schilling, R. Alberto, *Dalton Trans.* **2016**, *45*, 1737-1745.

[24] a) A. Juris, V. Balzani, F. Barigelletti, S. Campagna, P. Belser, A. von Zelewsky, *Coord. Chem. Rev.* **1988**, *84*, 85-277; b) T. J. Meyer, *Pure Appl. Chem.* **1986**, *58*, 1193-1206.

[25] a) P. Du, K. Knowles, R. Eisenberg, *J. Am. Chem. Soc.* **2008**, *130*, 12576-12577; b) R. Okazaki, S. Masaoka, K. Sakai, *Dalton Trans.* **2009**, 6127-6133; c) W.-G. Wang, F. Wang, H.-Y. Wang, C.-H. Tung, L.-Z. Wu, *Dalton Trans.* **2012**, *41*, 2420-2426.

[26] a) B. F. DiSalle, S. Bernhard, *J. Am. Chem. Soc.* **2011**, *133*, 11819-11821; b) F. Gärtner, D. Cozzula, S. Losse, A. Boddien, G. Anilkumar, H. Junge, T.

Schulz, N. Marquet, A. Spannenberg, S. Gladiali, M. Beller, *Chem. Eur. J.* **2011**, *17*, 6998-7006; c) F. Gärtner, S. Denurra, S. Losse, A. Neubauer, A. Boddien, A. Gopinathan, A. Spannenberg, H. Junge, S. Lochbrunner, M. Blug, S. Hoch, J. Busse, S. Gladiali, M. Beller, *Chem. Eur. J.* **2012**, *18*, 3220-3225; d) D. N. Chirdon, W. J. Transue, H. N. Kagalwala, A. Kaur, A. B. Maurer, T. Pintauer, S. Bernhard, *Inorg. Chem.* **2014**, *53*, 1487-1499.

[27] a) B. Probst, C. Kolano, P. Hamm, R. Alberto, *Inorg. Chem.* **2009**, *48*, 1836-1843; b) W. Jiang, J. Liu, C. Li, *Inorg. Chem. Commun.* **2012**, *16*, 81-85; c) M. Oberholzer, B. Probst, D. Bernasconi, B. Spingler, R. Alberto, *Eur. J. Inorg. Chem.* **2014**, *2014*, 3002-3009.

[28] T. Lazarides, T. McCormick, P. Du, G. Luo, B. Lindley, R. Eisenberg, *J. Am. Chem. Soc.* **2009**, *131*, 9192-9194.

[29] Z. Han, W. R. McNamara, M.-S. Eum, P. L. Holland, R. Eisenberg, *Angew. Chem. Int. Ed.* **2012**, *51*, 1667-1670.

[30] M. Natali, R. Argazzi, C. Chiorboli, E. Iengo, F. Scandola, *Chem. Eur. J.* **2013**, *19*, 9261-9271.

[31] T. Lazarides, M. Delor, I. V. Sazanovich, T. M. McCormick, I. Georgakaki, G. Charalambidis, J. A. Weinstein, A. G. Coutsolelos, *Chem. Commun.* **2014**, *50*, 521-523.

[32] a) A.-M. Manke, K. Geisel, A. Fetzer, P. Kurz, *Phys. Chem. Chem. Phys.* **2014**, *16*, 12029-12042; b) L. Mintrop, J. Windisch, C. Gotzmann, R. Alberto, B. Probst, P. Kurz, *J. Phys. Chem. B* **2015**, *119*, 13698-13706.

[33] a) K. A. Brown, S. Dayal, X. Ai, G. Rumbles, P. W. King, *J. Am. Chem. Soc.* **2010**, *132*, 9672-9680; b) M. L. Tang, D. C. Grauer, B. Lassalle-Kaiser, V. K. Yachandra, L. Amirav, J. R. Long, J. Yano, A. P. Alivisatos, *Angew. Chem. Int. Ed.* **2011**, *50*, 10203-10207; c) F. Wang, W.-G. Wang, X.-J. Wang, H.-Y. Wang, C.-H. Tung, L.-Z. Wu, *Angew. Chem. Int. Ed.* **2011**, *50*, 3193-3197; d) Z. Han, F. Qiu, R. Eisenberg, P. L. Holland, T. D. Krauss, *Science* **2012**, *338*, 1321-1324; e) J. Huang, K. L. Mulfort, P. Du, L. X. Chen, *J. Am. Chem. Soc.* **2012**, *134*, 16472-16475; f) Z.-J. Li, X.-B. Li, J.-J. Wang, S. Yu, C.-B. Li, C.-H. Tung, L.-Z. Wu, *Energy Environ. Sci.* **2013**, *6*, 465-469.

[34] A. Edel, P. A. Marnot, J. P. Sauvage, *New J. Chem.* **1984**, *8*, 495-498.

[35] a) R. S. Khnayzer, C. E. McCusker, B. S. Olaiya, F. N. Castellano, *J. Am. Chem. Soc.* **2013**, *135*, 14068-14070; b) C. E. McCusker, F. N. Castellano, *Inorg. Chem.* **2013**, *52*, 8114-8120.

[36] S. Garakyaraghi, P. D. Crapps, C. E. McCusker, F. N. Castellano, *Inorg. Chem.* **2016**, *55*, 10628-10636.

[37] a) S.-P. Luo, E. Mejía, A. Friedrich, A. Pazidis, H. Junge, A.-E. Surkus, R. Jackstell, S. Denurra, S. Gladiali, S. Lochbrunner, M. Beller, *Angew. Chem. Int. Ed.* **2013**, *52*, 419-423; b) S. Fischer, D. Hollmann, S. Tschierlei, M. Karnahl, N. Rockstroh, E. Barsch, P. Schwarzbach, S.-P. Luo, H. Junge, M. Beller, S. Lochbrunner, R. Ludwig, A. Brückner, *ACS Catal.* **2014**, *4*, 1845-1849; c) M. Karnahl, E. Mejía, N. Rockstroh, S. Tschierlei, S.-P. Luo, K. Grabow, A. Kruth, V. Brüser, H. Junge, S. Lochbrunner, M. Beller, *ChemCatChem* **2014**, *6*, 82-86; d) M. Heberle, S. Tschierlei, N. Rockstroh, M. Ringenberg, W. Frey, H. Junge, M. Beller, S. Lochbrunner, M. Karnahl, *Chem. Eur. J.* **2016**, early view article, DOI: 10.1002/chem.201604005.

[38] a) G. Tartarini, *Gazz. Chim. Ital.* **1933**, *63*, 597 - 600; b) W. W. Brandt, F. P. Dwyer, E. D. Gyarfas, *Chem. Rev.* **1954**, *54*, 959-1017.

[39] G. F. Smith, W. H. McCurdy, *Anal. Chem.* **1952**, *24*, 371-373.

[40] a) D. R. McMillin, M. T. Buckner, B. T. Ahn, *Inorg. Chem.* **1977**, *16*, 943-945; b) B.-T. Ahn, D. R. McMillin, *Inorg. Chem.* **1978**, *17*, 2253-2258.

[41] M. W. Blaskie, D. R. McMillin, *Inorg. Chem.* **1980**, *19*, 3519-3522.

[42] a) C. C. Phifer, D. R. McMillin, *Inorg. Chem.* **1986**, *25*, 1329-1333; b) A. K. Ichinaga, J. R. Kirchhoff, D. R. McMillin, C. O. Dietrich-Buchecker, P. A. Marnot, J. P. Sauvage, *Inorg. Chem.* **1987**, *26*, 4290-4292; c) C. T. Cunningham, K. L. H. Cunningham, J. F. Michalec, D. R. McMillin, *Inorg. Chem.* **1999**, *38*, 4388-4392.

[43] a) T. J. Penfold, S. Karlsson, G. Capano, F. A. Lima, J. Rittmann, M. Reinhard, M. H. Rittmann-Frank, O. Braem, E. Baranoff, R. Abela, I. Tavernelli, U. Rothlisberger, C. J. Milne, M. Chergui, *J. Phys. Chem. A* **2013**, *117*, 4591-4601; b) M. W. Mara, K. A. Fransted, L. X. Chen, *Coord. Chem. Rev.* **2015**, *282–283*, 2-18; c) M. Iwamura, S. Takeuchi, T. Tahara, *Acc. Chem. Res.* **2015**, *48*, 782-791; d) G. Capano, U. Rothlisberger, I. Tavernelli, T. J. Penfold, *J. Phys. Chem. A* **2015**, 7026-7037.

[44] a) C. O. Dietrich-Buchecker, J. P. Sauvage, J. P. Kintzinger, *Tetrahedron Lett.* **1983**, *24*, 5095-5098; b) M. Cesario, C. O. Dietrich-Buchecker, J. Guilhem, C. Pascard, J. P. Sauvage, *J. Chem. Soc., Chem. Commun.* **1985**, 244-247; c) C. O. Dietrich-Buchecker, J. F. Nierengarten, J. P. Sauvage, N. Armaroli, V. Balzani, L. De Cola, *J. Am. Chem. Soc.* **1993**, *115*, 11237-11244; d) J. P. Collin,

P. Gaviña, J. P. Sauvage, *New J. Chem.* **1997**, *21*, 525-528; e) P. Mobian, J.-P. Collin, J.-P. Sauvage, *Tetrahedron Lett.* **2006**, *47*, 4907-4909.

[45] a) A. K. I. Gushurst, D. R. McMillin, C. O. Dietrich-Buchecker, J. P. Sauvage, *Inorg. Chem.* **1989**, *28*, 4070-4072; b) P. Federlin, J.-M. Kern, A. Rastegar, C. Dietrich-Buchecker, P. A. Marnot, J. P. Sauvage, *New J. Chem.* **1990**, *14*, 9-12; c) N. Armaroli, M. A. J. Rodgers, P. Ceroni, V. Balzani, C. O. Dietrich-Buchecker, J.-M. Kern, A. Bailal, J.-P. Sauvage, *Chem. Phys. Lett.* **1995**, *241*, 555-558.

[46] E. Mejía, S.-P. Luo, M. Karnahl, A. Friedrich, S. Tschierlei, A.-E. Surkus, H. Junge, S. Gladiali, S. Lochbrunner, M. Beller, *Chem. Eur. J.* **2013**, *19*, 15972-15978.

[47] https://nobelprize.org/nobel_prizes/chemistry/laureates/2016/, accessed on 30.11.2016.

[48] a) C. O. Dietrick-Buchecker, P. A. Marnot, J. P. Sauvage, *Tetrahedron Lett.* **1982**, *23*, 5291-5294; b) A. J. Pallenberg, K. S. Koenig, D. M. Barnhart, *Inorg. Chem.* **1995**, *34*, 2833-2840.

[49] a) V. Kalsani, H. Ammon, F. Jäckel, J. P. Rabe, M. Schmittel, *Chem. Eur. J.* **2004**, *10*, 5481-5492; b) D. H. Hua, A. Verma, *Tetrahedron Lett.* **1985**, *26*, 547-550; c) M. Vitale, G. Prestat, D. Lopes, D. Madec, C. Kammerer, G. Poli, L. Girnita, *J. Org. Chem.* **2008**, *73*, 5795-5805.

[50] J. M. Mathis, A. J. Pallenberg, *Synth. Commun.* **1997**, *27*, 2943-2951.

[51] S. Knapp, A. F. Trope, M. S. Theodore, N. Hirata, J. J. Barchi, *J. Org. Chem.* **1984**, *49*, 608-614.

[52] M. Ruthkosky, F. N. Castellano, G. J. Meyer, *Inorg. Chem.* **1996**, *35*, 6406-6412.

[53] a) M. Schmittel, U. Lüning, M. Meder, A. Ganz, C. Michel, M. Herderich, *Heterocycl. Commun.* **1997**, *3*, 493; b) M. Sandroni, M. Kayanuma, A. Planchat, N. Szuwarski, E. Blart, Y. Pellegrin, C. Daniel, M. Boujtita, F. Odobel, *Dalton Trans.* **2013**, *42*, 10818-10827.

[54] a) B. A. Gandhi, O. Green, J. N. Burstyn, *Inorg. Chem.* **2007**, *46*, 3816-3825; b) O. Green, B. A. Gandhi, J. N. Burstyn, *Inorg. Chem.* **2009**, *48*, 5704-5714.

[55] a) C. Dietrich-Buchecker, J.-P. Sauvage, *Tetrahedron* **1990**, *46*, 503-512; b) A. Livoreil, C. O. Dietrich-Buchecker, J.-P. Sauvage, *J. Am. Chem. Soc.* **1994**, *116*, 9399-9400.

[56] a) A. Gradillas, J. Pérez-Castells, *Angew. Chem. Int. Ed.* **2006**, *45*, 6086-6101; b) P. L. Ng, J. N. Lambert, *Synlett* **1999**, *1999*, 1749-1750; c) J. Tae, Y.-K. Yang, *Org. Lett.* **2003**, *5*, 741-744; d) T. Ueda, N. Kanomata, H. Machida, *Org. Lett.*

**2005**, *7*, 2365-2368; e) B. Mohr, J.-P. Sauvage, R. H. Grubbs, M. Weck, *Angew. Chem.* **1997**, *109*, 1365-1367; f) M. Weck, B. Mohr, J.-P. Sauvage, R. H. Grubbs, *J. Org. Chem.* **1999**, *64*, 5463-5471.

[57] H. C. Guo, R. H. Zheng, H. J. Jiang, *Org. Prep. Proced. Int.* **2012**, *44*, 392-396.

[58] T. Ishi-i, R. Hirashima, N. Tsutsumi, S. Amemori, S. Matsuki, Y. Teshima, R. Kuwahara, S. Mataka, *J. Org. Chem.* **2010**, *75*, 6858-6868.

[59] R. Ziessel, J. Suffert, M.-T. Youinou, *J. Org. Chem.* **1996**, *61*, 6535-6546.

[60] M. Sjoegren, S. Hansson, P. O. Norrby, B. Aakermark, M. E. Cucciolito, A. Vitagliano, *Organometallics* **1992**, *11*, 3954-3964.

[61] S. Hoppen, S. Bäurle, U. Koert, *Chem. Eur. J.* **2000**, *6*, 2382-2396.

[62] A. Abushamleh, H. Goodwin, *Aust. J. Chem.* **1980**, *33*, 2171-2179.

[63] X. Fang, J. G. Watkin, B. P. Warner, *Tetrahedron Lett.* **2000**, *41*, 447-449.

[64] a) F. Colombo, G. Cravotto, G. Palmisano, A. Penoni, M. Sisti, *Eur. J. Org. Chem.* **2008**, *2008*, 2801-2807; b) G. W. Kabalka, M.-L. Yao, S. Borella, *J. Am. Chem. Soc.* **2006**, *128*, 11320-11321; c) H. Mayr, G. Gorath, *J. Am. Chem. Soc.* **1995**, *117*, 7862-7868; d) T. Saito, Y. Nishimoto, M. Yasuda, A. Baba, *J. Org. Chem.* **2006**, *71*, 8516-8522.

[65] a) L. H. Baekeland, *J. Ind. Eng. Chem.* **1913**, *5*, 506-511; b) A. Baeyer, *Ber. Dtsch. Chem. Ges.* **1872**, *5*, 1094-1100; c) C. D. Gutsche, *Acc. Chem. Res.* **1983**, *16*, 161-170.

[66] K. E. Krakowiak, J. S. Bradshaw, W. Jiang, N. K. Dalley, G. Wu, R. M. Izatt, *J. Org. Chem.* **1991**, *56*, 2675-2680.

[67] T. Toyoshima, S. Yoshida, S. Watanabe, *Tetrahedron* **2013**, *69*, 1904-1911.

[68] S. Tai, N. J. Williams, J. D. Carrick, *J. Heterocycl. Chem.* **2016**, *53*, 307-312.

[69] K.-T. Wong, R.-T. Chen, F.-C. Fang, C.-c. Wu, Y.-T. Lin, *Org. Lett.* **2005**, *7*, 1979-1982.

[70] H.-F. Chen, W.-Y. Hung, S.-W. Chen, T.-C. Wang, S.-W. Lin, S.-H. Chou, C.-T. Liao, H.-C. Su, H.-A. Pan, P.-T. Chou, Y.-H. Liu, K.-T. Wong, *Inorg. Chem.* **2012**, *51*, 12114-12121.

[71] a) M. Meyer, A.-M. Albrecht-Gary, C. O. Dietrich-Buchecker, J.-P. Sauvage, *Inorg. Chem.* **1999**, *38*, 2279-2287; b) E. Riesgo, Y.-Z. Hu, F. Bouvier, R. P. Thummel, *Inorg. Chem.* **2001**, *40*, 2541-2546.

[72] N. Armaroli, G. Accorsi, F. Cardinali, A. Listorti, in *Photochemistry and Photophysics of Coordination Compounds I* (Eds.: V. Balzani, S. Campagna), Springer Berlin Heidelberg, Berlin, Heidelberg, **2007**, pp. 69-115.

[73] a) J. R. Kirchhoff, R. E. Gamache, M. W. Blaskie, A. A. Del Paggio, R. K. Lengel, D. R. McMillin, *Inorg. Chem.* **1983**, *22*, 2380-2384; b) D. Felder, J.-F. Nierengarten, F. Barigelletti, B. Ventura, N. Armaroli, *J. Am. Chem. Soc.* **2001**, *123*, 6291-6299; c) M. S. Asano, K. Tomiduka, K. Sekizawa, K. Yamashita, K. Sugiura, *Chem. Lett.* **2010**, *39*, 376-378.

[74] a) R. Englman, J. Jortner, *Mol. Phys.* **1970**, *18*, 145-164; b) K. F. Freed, J. Jortner, *J. Chem. Phys.* **1970**, *52*, 6272-6291; c) J. V. Caspar, E. M. Kober, B. P. Sullivan, T. J. Meyer, *J. Am. Chem. Soc.* **1982**, *104*, 630-632.

[75] G. Accorsi, N. Armaroli, C. Duhayon, A. Saquet, B. Delavaux-Nicot, R. Welter, O. Moudam, M. Holler, J.-F. Nierengarten, *Eur. J. Inorg. Chem.* **2010**, *2010*, 164-173.

[76] a) M. K. Eggleston, D. R. McMillin, K. S. Koenig, A. J. Pallenberg, *Inorg. Chem.* **1997**, *36*, 172-176; b) M. A. Masood, P. S. Zacharias, *J. Chem. Soc., Dalton Trans.* **1991**, 111-114; c) M. T. Miller, P. K. Gantzel, T. B. Karpishin, *Inorg. Chem.* **1999**, *38*, 3414-3422; d) G. Sanna, M. I. Pilo, M. A. Zoroddu, R. Seeber, S. Mosca, *Inorg. Chim. Acta* **1993**, *208*, 153-158; e) M. Magni, A. Colombo, C. Dragonetti, P. Mussini, *Electrochim. Acta* **2014**, *141*, 324-330.

[77] F. Kanoufi, Y. Zu, A. J. Bard, *J. Phys. Chem. B* **2001**, *105*, 210-216.

[78] H. Sun, M. Z. Hoffman, *J. Phys. Chem.* **1994**, *98*, 11719-11726.

[79] C. Creutz, *Inorg. Chem.* **1981**, *20*, 4449-4452.

[80] a) K. L. Cunningham, D. R. McMillin, *Inorg. Chem.* **1998**, *37*, 4114-4119; b) K. L. Cunningham, C. R. Hecker, D. R. McMillin, *Inorg. Chim. Acta* **1996**, *242*, 143-147.

[81] P. Wardman, *J. Phys. Chem. Ref. Data* **1989**, *18*, 1637-1755.

[82] M. A. Oturan, P. Dostert, M. S. Benedtti, J. Moiroux, A. Anne, M. B. Fleury, *J. Electroanal. Chem.* **1988**, *242*, 171-179.

[83] G. R. Fulmer, A. J. M. Miller, N. H. Sherden, H. E. Gottlieb, A. Nudelman, B. M. Stoltz, J. E. Bercaw, K. I. Goldberg, *Organometallics* **2010**, *29*, 2176-2179.

[84] Oxford Diffraction Ltd. CrysAlis$^{Pro}$ Software system, 171.32; Oxford, UK, **2007**.

[85] A. Altomare, M. C. Burla, M. Camalli, G. L. Cascarano, C. Giacovazzo, A. Guagliardi, A. G. G. Moliterni, G. Polidori, R. Spagna, *J. Appl. Crystallogr.* **1999**, *32*, 115-119.

[86] G. Sheldrick, *Acta. Crystallogr., Sect. A* **2008**, *64*, 112-122.

[87] L. Farrugia, *J. Appl. Crystallogr.* **2012**, *45*, 849-854.

[88] J. Huang, O. Buyukcakir, M. W. Mara, A. Coskun, N. M. Dimitrijevic, G. Barin, O. Kokhan, A. B. Stickrath, R. Ruppert, D. M. Tiede, J. F. Stoddart, J.-P. Sauvage, L. X. Chen, *Angew. Chem. Int. Ed.* **2012**, *51*, 12711-12715.

[89] C. J. Chandler, L. W. Deady, J. A. Reiss, *J. Heterocycl. Chem.* **1981**, *18*, 599-601.

[90] F. W. Lewis, L. M. Harwood, M. J. Hudson, M. G. B. Drew, J. F. Desreux, G. Vidick, N. Bouslimani, G. Modolo, A. Wilden, M. Sypula, T.-H. Vu, J.-P. Simonin, *J. Am. Chem. Soc.* **2011**, *133*, 13093-13102.

[91] B. J. Hathaway, D. G. Holah, J. D. Postlethwaite, *J. Chem. Soc.* **1961**, 3215-3218.

[92] J. K. Irangu, R. B. Jordan, *Inorg. Chem.* **2003**, *42*, 3934-3942.

[93] G. A. Mines, M. J. Bjerrum, M. G. Hill, D. R. Casimiro, I. J. Chang, J. R. Winkler, H. B. Gray, *J. Am. Chem. Soc.* **1996**, *118*, 1961-1965.

[94] J.-C. Xiao, B. Twamley, J. n. M. Shreeve, *Org. Lett.* **2004**, *6*, 3845-3847.

[95] a) P. Bolduc, A. Jacques, S. K. Collins, *J. Am. Chem. Soc.* **2010**, *132*, 12790-12791; b) R. P. Thummel, V. Goulle, B. Chen, *J. Org. Chem.* **1989**, *54*, 3057-3061.

[96] J. Yin, R. L. Elsenbaumer, *J. Org. Chem.* **2005**, *70*, 9436-9446.

[97] Z. Shi, R. P. Thummel, *J. Org. Chem.* **1995**, *60*, 5935-5945.

[98] A. Deutman, T. Woltinge, J. Smits, R. De Gelder, J. Elemans, R. Nolte, A. Rowan, *Molecules* **2014**, *19*, 5278.

[99] T. Michael Bockman, J. K. Kochi, *J. Phys. Org. Chem.* **1997**, *10*, 542-562.

## Acknowledgements

First, I would like to thank Prof. Dr. Roger Alberto for accepting me as a PhD student and for his never-ending interest and joy in the project. By permanently providing new ideas from his very creative and very knowledgeable mind, he made the work challenging but also enjoyable.

A big thanks goes to Dr. Benjamin Probst, who introduced me to all aspects in the field of photocatalytic water splitting, from theoretical concepts to the practical details in the lab. Being the $H_2$ sub-group leader, he was the first person to contact with any issues and provided excellent guidance throughout the thesis.

Further thanks go to Prof. Dr. Greta Patzke and Prof. Dr. Peter Hamm, not only for being my co-examiners, but also for great support from their groups with measurements and other things that contributed to this work.

I would also like to thank Prof. Dr. Thomas Ward from the University of Basel for being my external referee.

I am also very grateful to all former and present members of the $H_2$ sub-group: Mathias Mosberger and Dr. Benjamin Probst from my lab, Stephan Schnidrig, Evelyne Joliat, Miriam Oberholzer, Cyril Bachmann, Miguel Guttentag, Dr. Craig Richmond, Dr. Chunhua Cui, Nicola Weder and Peter Müller. Everyone contributed to a very comfortable working environment and we had great times together at retreats, conferences, summer schools and many other occasions.

Margherita Orazietti generously helped me with measuring and interpreting transient absorption spectra, which is a big part of this thesis. Thank you!

Many thanks go to all the people, who helped me with any kind of measurements: Prof. Dr. Bernhard Spingler for single crystal X-ray analysis, Heinz Spring for elemental analysis, Dr. Thomas Fox for NMR measurements, Dr. Ferdinand Wild and Roger Jacot for SEM/EDX measurements.

Special thanks go to Hanspeter Stalder and Serkan Sariyildiz from the workshop, who professionally built and repaired many of our custom setups.

Moreover, the administrative staff was always of great help, especially Dr. Valeria Mozzetti Rohrseitz, organising all things concerning the LightChEC consortium, as well as Ramona Erni, not only helpful with bureaucracy, but also in charge of the coffee maker.

I would also like to thank Prof. Dr. Philipp Kurz and Luise Mintrop from the University of Freiburg, for approaching us with a collaborative proposal that ultimately led to a joint publication.

I am very grateful to Dr. Rino Schwenk, overseeing my master thesis, as well as Dr. Serena Fantasia and Dr. Michelangelo Scalone, supervising my industrial internship at Roche. With all of them, I gathered my first experiences in chemical research and was thereby encouraged to start a PhD.

Many thanks also go to all the students that conducted some if their practical courses in our group and therefore contributed a lot to our research: Jonathan Lamprecht, Maria Keel, Severin Koch, Jolanda Minder, Eliane Weiss and Amber de Bruijn.

Numerous other people from the University and from elsewhere contributed in many different ways to this thesis. I would like to thank them all.

For financial support, I would like to thank the University of Zurich, the URPP LightChEC and the graduate school CMSZH.

I would like to thank my friends from the university, from the sports club, from the Kanti, from the ETH and all others, for helping to keep my life balanced at all – not always easy – times.

The greatest thanks go to my family! My parents, Helen and Kari Windisch, as well as my brother Sebastian Windisch. They always supported me with their love and motivated me to keep going in difficult situations.

# Curriculum Vitae

## Personal Data

| | |
|---|---|
| **Surname** | Windisch |
| **First Name** | Johannes |
| **Date of Birth** | 18.07.1987 |
| **Place of Origin** | Densbüren AG |
| **E-Mail** | j.wind@gmx.ch |

## Education

| | |
|---|---|
| **Jan 2013 – Jan 2017** | PhD Thesis in the group of Prof. Roger Alberto, University of Zurich, Switzerland |
| **Apr 2012 – Dec 2012** | Various vacation jobs and travelling |
| **Oct 2011 – Apr 2012** | Industrial Internship at F. Hoffmann - La Roche AG (Basel) |
| **Oct 2011** | Master graduation<br>Master thesis in the group of Prof. A. Togni: *"Josiphos-type Ligands Bearing P-Stereogenic Trifluoromethylphosphines and their Application in Asymmetric Catalysis"* |
| **Oct 2006 – Oct 2011** | Chemistry Studies at Swiss Federal Institute of Technology, ETH Zürich, Switzerland |
| **2006** | Matura graduation with a focus on chemistry and biology |
| **1999 – 2006** | Kantonsschule Olten, Switzerland |

## List of Publications

- *"General Scheme for Oxidative Quenching of a Copper Bis-Phenanthroline Photosensitizer for Light-Driven Hydrogen Production"*, J. Windisch, M. Orazietti, P. Hamm, R. Alberto, B. Probst, *ChemSusChem* **2016**, *9*, 1719-1726.
- *"$Sn^{IV}$ Metalloporphyrin / $Co^{III}$ Complex: An All-Abundant-Element System for the Photocatalytic Production of $H_2$ in Aqueous Solution"*, L. Mintrop, J. Windisch, C. Gotzmann, R. Alberto, B. Probst, P. Kurz, *J. Phys. Chem. B* **2015**, *119*, 13698-13706.
- *"Ligandless Copper-Catalyzed Coupling of Heteroaryl Bromides with Gaseous Ammonia"*, S. Fantasia, J. Windisch, M. Scalone, *Adv. Synth. Catal.* **2013**, *355*, 627-631.

## Conference Contributions

### Oral Presentation

- *"General Scheme for Oxidative Quenching of a Copper Bis-Phenanthroline Photosensitizer for Light-Driven Hydrogen Production"*, 21st International Conference on Photochemical Conversion and Storage of Solar Energy (IPS-21), St. Petersburg, Russia, **2016**.

### Poster Presentations

- *"General Scheme for Oxidative Quenching of a Copper Bis-Phenanthroline Photosensitizer for Light-Driven Hydrogen Production"*, SwissPEC Symposium, Lausanne, Switzerland, **2016**.
- *"General Scheme for Oxidative Quenching of a Copper Bis-Phenanthroline Photosensitizer for Light-Driven Hydrogen Production"*, SCS Fall Meeting, Zürich, Switzerland, **2016**.
- *"Using Oxidative Quenching of a Copper Photosensitizer for Light-Driven Hydrogen Production"*, 1st International Solar Fuels Conference (ISF-1), Uppsala, Sweden, **2015**.
- *"Using Oxidative Quenching of a Copper Photosensitizer for Light-Driven Hydrogen Production"*, SCS Fall Meeting, Lausanne, Switzerland, **2015**.
- *"Synthesis of a Phenanthroline Based Tetrahedral Cage Ligand"*, LightChEC Summer School, Les Diablerets, Switzerland, **2014**.

# Appendix I

ChemPubSoc Europe

DOI: 10.1002/cssc.201600422

CHEMSUSCHEM Full Papers

# General Scheme for Oxidative Quenching of a Copper Bis-Phenanthroline Photosensitizer for Light-Driven Hydrogen Production

J. Windisch, M. Orazietti, P. Hamm, R. Alberto,* and B. Probst*[a]

A new, general reaction scheme for photocatalytic hydrogen production is presented based on oxidative quenching of a homoleptic copper(I) bis-1,10-phenanthroline photosensitizer (PS) by 1-methyl-4-phenyl-pyridinium ($MPP^+$) as the electron relay and subsequent regeneration of the so formed copper(II) complex by a sacrificial electron donor. Electron transfer from the relay to various cobalt based water reduction catalysts and subsequent $H_2$ production was shown to close the catalytic cycle. Transient absorption experiments unambiguously confirmed the proposed pathway, both the oxidative quenching and subsequent regeneration of oxidized PS. Photocatalytic test runs further confirmed the role of $MPP^+$ and up to 10 turnovers were achieved in the relay. The performance limiting factor of the system was shown to be the decomplexation of the copper PS. Quantum yields of the system were 0.03 for $H_2$ production, but 0.6 for $MPP^•$ formation, clearly indicating that unproductive pathways still prevail.

## Introduction

The direct conversion of solar energy into storable fuel is currently a major research challenge.[1] If this can be achieved in an efficient manner, a sustainable and almost inexhaustible source of energy would be provided. To reach this goal, a lot of effort has been devoted to the development of artificial photosynthetic systems that allow for the conversion of solar energy into chemical energy by water splitting (i.e., into $H_2$ and $O_2$).[2] Because a full water splitting system is very complex to study, the research usually focuses on either the oxidative[3] or the reductive[4] half reaction using sacrificial reagents. Our group is mainly engaged in studying three component systems for the reductive part of the reaction, consisting of a photosensitizer (PS), water reduction catalyst (WRC) and a sacrificial electron donor (D).[5] Common photosensitizers include late transition metal complexes based on ruthenium,[6] rhenium,[5,7] platinum[8] or iridium.[9] To make a water splitting system commercially viable, these rare and expensive noble metals should be replaced by cheaper and more abundant materials, as was already demonstrated in the case of Eosin Y,[10] fluorescein,[11] Al-,[12] Zn-[13] and Sn-porphyrins[14] as well as quantum dots.[15] Copper based chromophores, in particular copper(I) bis-1,10-phenanthroline complexes represent another very attractive alternative. The photoredox activity of these compounds was described by McMillin et al.[16] in 1977 and since then various studies have led to a profound knowledge and understanding of their properties.[17] Most recently, ultrafast spectroscopy revealed a lot of detail about the very early processes after light excitation on the femto- to picosecond timescale.[18]

In 1984 Sauvage et al. investigated copper(I) bis-1,10-phenanthroline complexes for proton reduction using $TiO_2$ supported platinum as a WRC.[19] More recently, Castellano et al. presented a copper(I) bis-1,10-phenanthroline complex ($[Cu(dsbtmp)_2]^+$, see Scheme 1) with very promising photophysical properties, which was also applied in photocatalytic hydrogen evolution with $[Co^{III}(dmgH)_2(py)Cl]$ (dmgH = dimethylglyoximate, py = pyridine) as a WRC.[20] Oxidative quenching of the PS by $Co^{III}$ was observed with a quench constant $k_q = 7.2 \times 10^9\ L\,mol^{-1}\,s^{-1}$, followed by a proposed second reduction of the WRC ($Co^{II}/Co^{I}$) through a very slow oxidative quenching step or through disproportionation. The group of Beller developed heteroleptic copper(I) complexes composed of a 1,10-phenanthroline ligand as well as a bidentate phosphine ligand ($[Cu(PP)(NN)]^+$, see Scheme 1).[21] Reductive quenching by triethylamine (TEA), as well as oxidative quenching by an iron carbonyl-based WRC ($[Fe_3(CO)_{12}]$) was observed and hydrogen was proposed to evolve through both pathways.[21c] Although the $[Cu(PP)(NN)]^+$-type complexes only absorb a limited amount of visible light, their ability to be reductively quenched greatly facilitates the replacement of rhenium or ruthenium photosensitizers in current systems, which mostly operate through the reductive quenching pathway. However, there are only a few examples of reductive quenching of copper(I) bis-1,10-phenanthrolines employing methyl substituted ferrocenes.[22] Instead, the oxidative pathway is preferred, which can be readily understood when comparing the excited state redox potentials, as shown in Figure 1. Relative to heteroleptic $[Cu(PP)(NN)]^+$, $[Ru(bpy)_3]^{2+}$ or $[ReNCS(CO)_3bpy]$ (bpy: bipyridine, see Scheme 1), both potentials of

[a] J. Windisch, M. Orazietti, Prof. P. Hamm, Prof. R. Alberto, Dr. B. Probst
Department of Chemistry
University of Zurich
Winterthurerstrasse 190, 8049 Zurich (Switzerland)
E-mail: benjamin.probst@uzh.ch

Supporting Information and the ORCID identification number(s) for the author(s) of this article can be found under http://dx.doi.org/10.1002/cssc.201600422.

ChemPubSoc Europe

CHEMSUSCHEM Full Papers

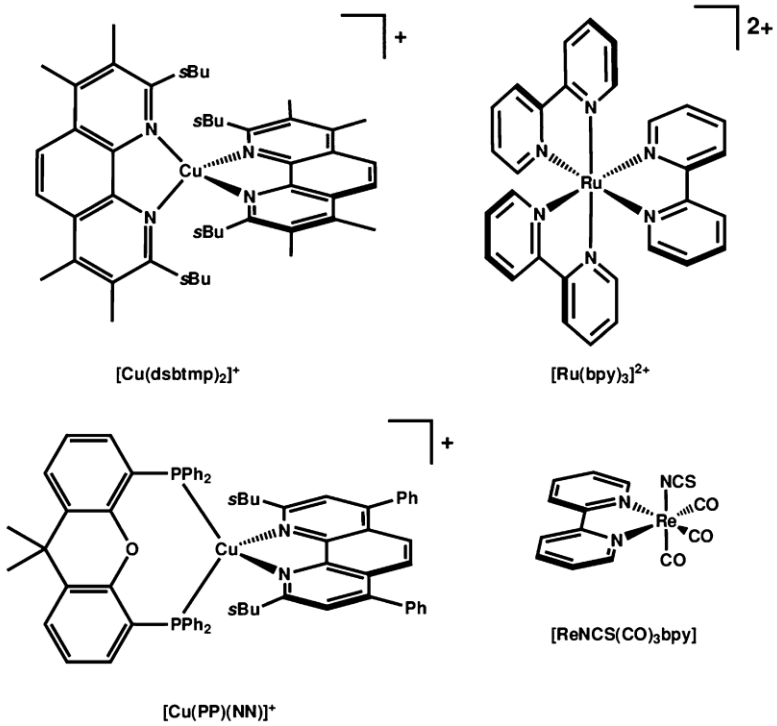


**Scheme 1.** Molecular structures of homo- and heteroleptic copper(I) PSs as well as Ru- and Re-based PSs.

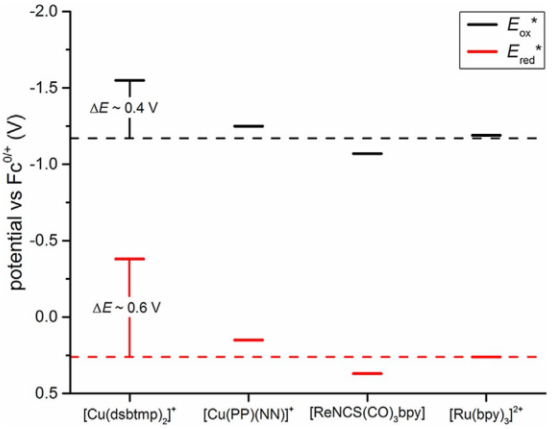


**Figure 1.** Comparison of excited state redox potentials for different photosensitizers. Dashed lines indicate the average excited state potentials of $[Cu(PP)(NN)]^+$,[21a] $[ReNCS(CO)_3bpy]$ and $[Ru(bpy)_3]^{2+}$.[24]

$[Cu(dsbtmp)_2]^+$ are cathodically shifted, thus making homoleptic 1,10-phenanthroline complexes of $Cu^I$ better electron donors but much worse acceptors in their excited state.[23]

To take full advantage of these excited state properties, the goal of this work was to find a suitable oxidative quencher for the copper photosensitizer $[Cu(dsbtmp)_2]^+$ developed by Castellano et al. in 2013.[20a] Specifically, we want to directly exploit the very high reducing power of the excited state and store this energy in molecular hydrogen through proton reduction. A generally applicable method was sought, consisting of an acceptor relay between PS and the WRC. If potentials are tuned well, only a few hundred millivolts would be needed to drive the relay system, allowing a much more general approach in applying homoleptic Cu bis-diimine PSs than if the WRC was used as an oxidative quencher. Furthermore, if oxidative quenching is used to drive proton reduction, the catalytic cycle in PS can then be closed by the oxidation reaction of $PS^+$ with a donor, which 1) occurs at higher potentials than for the excited PS (in the reductive pathway) and 2) leaves more time for the reaction because the excited state is not involved.

## Results and Discussion

A detailed comparison of selected properties of different photosensitizers (Table 1) helped to identify a suitable catalytic system. The main visible absorption for all shown photosensitizers is characterized by an intense metal-to-ligand charge-transfer band. Both, $[Cu(dsbtmp)_2]^+$ and $[Ru(bpy)_3]^{2+}$, feature very similar absorption properties with the position of the absorption maximum at approximately 450 nm. In contrast, the maxima for the rhenium and heteroleptic copper photosensitizer are blueshifted by about 70 nm, clearly minimizing the overlap with solar irradiation. Another important property of dyes for the application in homogeneous photocatalysis is their excited state lifetime ($\tau_0$). It should be at least long enough to allow for diffusional controlled reactions.

ChemPubSoc Europe

CHEMSUSCHEM Full Papers

**Table 1.** Photo- and electrochemical data of four selected PSs in DMF. All potentials are given versus $Fc/Fc^+$.

| Compound | $\lambda_{abs}$ [nm] | $\varepsilon$ [$L\,mol^{-1}\,cm^{-1}$] | $\lambda_{em}$ [nm] | $\tau_0$ [ns] | $E_{ox}$ [V] | $E_{red}$ [V] | $E^*_{ox}$ [a] [V] | $E^*_{red}$ [a] [V] |
|---|---|---|---|---|---|---|---|---|
| $[Cu(dsbtmp)_2]^+$ | 444 | 5060 | 627 | 1090 | 0.43[d] | −2.36 | −1.55 | −0.38 |
| $[Cu(PP)(NN)]^+$ [b] | 387 | 4849 | 546 | 5410 | 1.02[d] | −2.12 | −1.25 | 0.15 |
| $[ReNCS(CO)_3bpy]$ | 376 | 2760 | 602 | 25.5 | 0.99[d] | −1.69 | −1.07 | 0.37 |
| $[Ru(bpy)_3]^{2+}$ [c] | 454 | 12700 | 620 | 912 | 0.81 | −1.74 | −1.19 | 0.26 |

[a] Minimal excited state potentials were estimated as $E^*_{ox/red} = E_{ox/red} \pm E_{00,min}$ ($E_{00,min}$ is the emission energy at maximum intensity). [b] In MeCN from ref. [21a]. [c] Lifetime from Ref. [25] and redox potentials from Ref. [24]. [d] Irreversible wave, cathodic peak potential $E_{pc}$ given.

$[ReNCS(CO)_3bpy]$ has a relatively short lifetime, and therefore, a large excess of sacrificial reagent is usually necessary to promote photocatalytic hydrogen evolution.[5g] With lifetimes of approximately 1 μs and as high as 54 μs, the excited state energy of the other photosensitizers is harvested much more easily.

The most distinct feature of $[Cu(dsbtmp)_2]^+$ and homoleptic copper(I) bis-1,10-phenanthroline complexes in general, is their excited state redox potentials. Compared to other photosensitizers, the excited state is harder to reduce but more easily oxidized. Therefore, it seems clear to take advantage of the high reducing power of the excited state and choose the oxidative quenching pathway for photocatalytic hydrogen production. As opposed to reductive quench pathways, the nature and concentration of the electron donor should allow for more flexibility in the oxidative quenching pathway because now regeneration only involves the oxidized dye and no longer the excited state. WRCs could take the role of the oxidative quencher, as reported before,[20b] but to make the scheme generally applicable, an additional oxidative quencher was sought.

### Oxidative quenching of copper

An ideal oxidative quencher for the envisioned system can be characterized by three main properties: 1) the reduction should be fully reversible, or the reduced species should at least be long lived enough to allow for electron transfer to a WRC; 2) the quench reaction should proceed with a high cage escape yield; and 3) the reduction potential should be close to the excited state potential of the photosensitizer, so that most of the stored energy is conserved. However, to still guarantee a fast quenching reaction, a small energy loss can be accepted.

To identify such a quencher for $[Cu(dsbtmp)_2]^+$ with these properties, various electron acceptors with different reduction potentials (−0.6 to −1.7 V vs. ferrocene/ferrocenium ($Fc^{0/+}$)) were tested (Scheme 2). Plots of quencher potential versus quench rate (Figure 2) have a typical half parabola shape as expected from the Marcus theory of electron transfer in the normal region.[26] This dependency indicates that the quench reaction is likely to be oxidative in nature rather than energy transfer. Towards anodic potentials, the quench rate approaches the diffusional limit, whereas in the cathodic region, in which the potential of the quencher and excited state are similar, the reaction rate slows down drastically. In our analysis only two quenchers offer a fast reaction with minimal energy loss: $NMIQ^+$ (anodic peak potential $E_{pa} = -1.52$ V) and 1-methyl-4-phenyl-pyridinium ($MPP^+$, $E_{1/2} = -1.61$ V). The cyclic voltammogram ($1\,V\,s^{-1}$) of $NMIQ^+$ indicates irreversibility, whereas a reversible process is found for $MPP^+$ at scan rates $\geq 1\,V\,s^{-1}$. Below this scan rate, partial irreversibility of the cyclic voltammetry response and a new peak in the anodic scan indicates dimerization, in agreement with literature reports, according to Equations (1) and (2):[27]

$$MPP^+ + e^- \rightleftharpoons MPP^\bullet, \quad E_{1/2} = -1.61\ V \tag{1}$$

$$2\,MPP^\bullet \underset{k_{-1}}{\overset{k_1}{\rightleftharpoons}} (MPP)_2, \quad K_{dim} = \frac{k_1}{k_{-1}}. \tag{2}$$

In acetonitrile solvent, the dimerization rate constant $k_1$ was estimated to be $175\,L\,mol^{-1}\,s^{-1}$ and the equilibrium constant $K_{dim} = 720\,L\,mol^{-1}$.[27b] Spectroelectrochemistry on the first reduction wave gives two new absorption maxima at 540 nm and 365 nm, characteristic for the radical, and a shoulder at

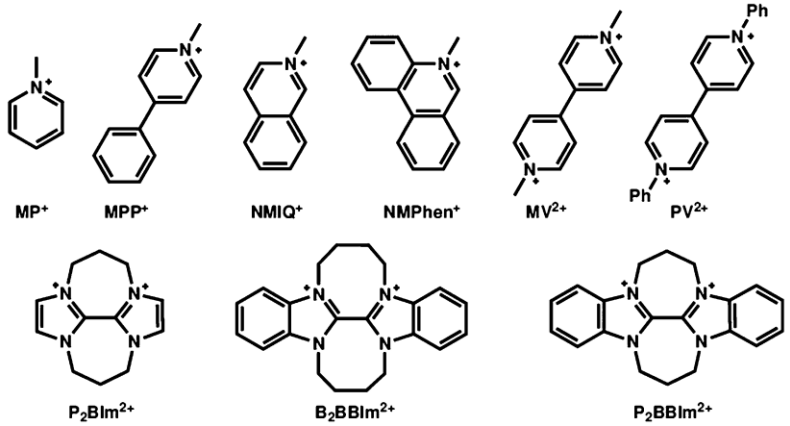


**Scheme 2.** Molecular structures of different electron acceptors tested as oxidative quenchers in this study.

ChemPubSoc Europe

CHEMSUSCHEM Full Papers

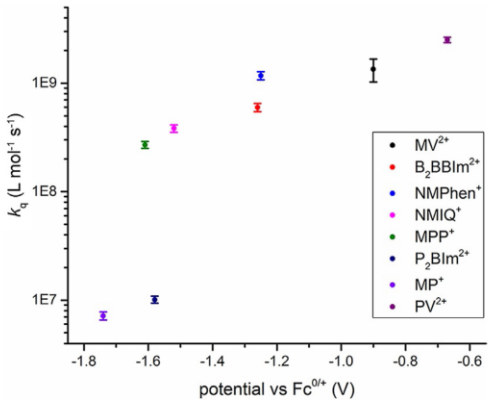


**Figure 2.** Reduction potential (V vs. $Fc^+/Fc$) of different electron acceptors versus the quench rate constant ($k_q$) for reaction with excited $[Cu(dsbtmp)_2]^+$. Quench rate constants were determined from the emission lifetimes of 0.1 mM $[Cu(dsbtmp)_2]^+$ in degassed DMF at different quencher concentrations ($1/\tau = k_q \times [Q] + 1/\tau_0$; $\tau_0$ is the lifetime in the absence of quenchers, $k_q$ is the bimolecular quench constant, $\tau$ is the photosensitizer lifetime in the presence of quencher and [Q] is the quencher concentration).

400 nm, assigned to the dimer, which becomes more intense at higher concentrations of the radical $MPP^•$ (see Figure S1, Supporting Information). On the basis of the above results, we estimate equilibrium concentrations of $[MPP^•]$ and $[(MPP)_2]$ of 1.14 and 0.93 mM, respectively, at 3 mM $[MPP^+]$, and thus $\varepsilon_{540nm} = 1200 \pm 200\ L\,mol^{-1}\,cm^{-1}$ and $\varepsilon_{365nm} = 7400 \pm 1200\ L\,mol^{-1}\,cm^{-1}$. After re-oxidation, the initial absorption spectrum is almost perfectly recovered (see Figure S1 and S2), suggesting the clean transformation of $MPP^+$ into $MPP^•$/dimer and vice versa. $MPP^+$ thus fulfills the required properties to be incorporated into a photocatalytic system using the oxidative quenching pathway and was therefore chosen for further investigation.

### Photocatalysis

Investigations in photocatalytic experiments indeed confirmed the evolution of hydrogen when $MPP^+$ was used as an oxidative quencher in a system with $[Cu(dsbtmp)_2]^+$ as the photosensitizer, $[Co(DOH)Br_2]$ (see Scheme 3) as the WRC, triethanolamine (TEOA) as sacrificial electron donor and triethanolammonium tetrafluoroborate ($[HTEOA]BF_4$) as the proton source in dimethylformamide (DMF). Hydrogen was not detected in blank experiments without $MPP^+$ or any of the other components. Although the quantum yield for $H_2$ production is $<4\%$ for all concentrations of $MPP^+$ tested, it correlates well with the calculated maximum quench yield as a function of $MPP^+$ concentration (Figure 3). When quantum yields were corrected for maximal possible quench rates ($\Phi_{q,max}$; see Figure S11), a constant corrected quantum yield ($\Phi_{corr}$) of approximately 4% was obtained, indicating a significant loss channel independent of $MPP^+$ concentration. Also, the $[Co(DOH)Br_2]$ WRC would allow for a much faster hydrogen evolution reaction, as seen using $[Ru(bpy)_3]^{2+}$ or $[ReNCS(CO)_3bpy]$ as PS (see Figure S5), indicating a limitation in the $[Cu(dsbtmp)_2]^+/MPP^+$ system. Time resolved spectroscopy on the initial electron transfer steps was conducted to shed light on the issue, as described in the mechanistic investigations section below.

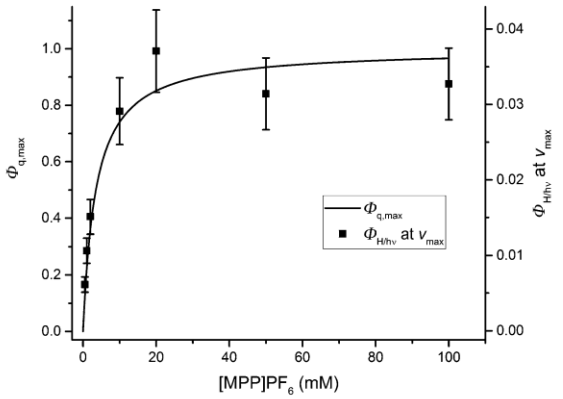


**Figure 3.** Calculated maximum quench yields as a function of $[MPP]PF_6$ concentration (left, full line; $\Phi_{q,max} = k_q \times [Q]/(k_q \times [Q] + \tau_0^{-1})$; $k_q$ is the bimolecular quench constant, [Q] the quencher concentration and $\tau_0$ the photosensitizer lifetime in the absence of quenchers) and experimentally determined quantum yields at maximum $H_2$ evolution rates (right, squares; $\Phi_{H/hv} = 2 \times v_{max}/q_p$; DMF, 0.5 mM $[Cu(dsbtmp)_2]BF_4$, 0.23 mM $[Co(DOH)Br_2]$, 1 M TEOA, 0.1 M $HBF_4$, $[MPP]PF_6$ varied from 0.5–100 mM, total volume of 8 mL, irradiation with a 450 nm light-emitting diode (LED) at a constant photon flux of $q_p = 0.3 \pm 0.04\ \mu E\,s^{-1}$).

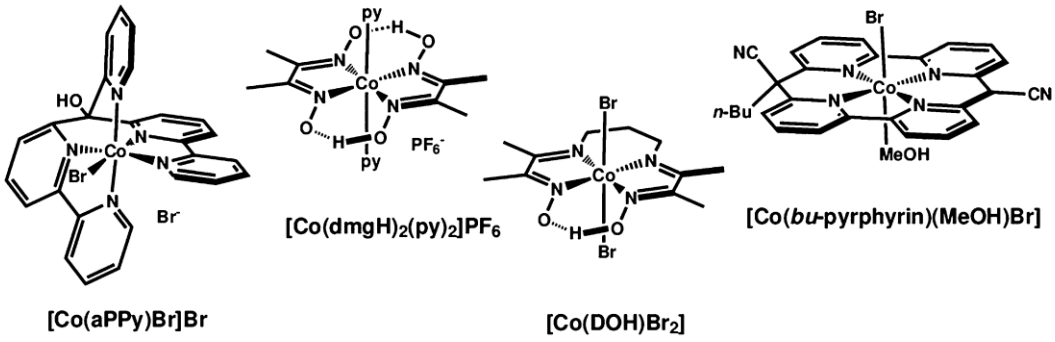


**Scheme 3.** Molecular structures of the applied Co-based WRCs.

ChemPubSoc Europe

CHEMSUSCHEM Full Papers

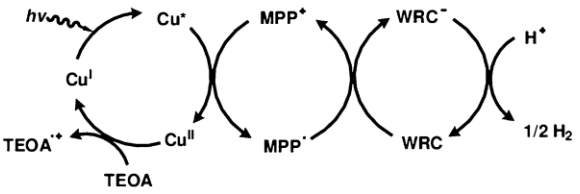


**Scheme 4.** Proposed reaction sequence for the presented system.

Clearly, at low $MPP^+$ concentrations oxidative quenching is limiting the quantum yield. Conversely, the total amounts of $H_2$ produced did not vary greatly between different [$MPP^+$], indicating that the stability of the system is not limited by the electron relay. Up to 9.7 ± 1.2 turnovers in $MPP^+$ were possible. Thus, a concentration of 10 mM [MPP]$PF_6$ is sufficient for catalysis, whereas oxidative quenching is rate limiting below a concentration of 10 mM. This confirmed that $MPP^+$ indeed plays the role of the electron relay in the system, as depicted in Scheme 4.

To elucidate the versatility of this newly developed photosensitizer/quencher combination, different cobalt based WRCs (Scheme 3) were applied to the optimized system. As shown in Figure 4, some evolution of hydrogen could be detected in all cases. Blank experiments were conducted to determine if all the components are needed. Notably, the system using [$Co^{III}$(dmgH)$_2$(py)$_2$]$PF_6$ as a WRC did not show any detectable $H_2$ production in the absence of $MPP^+$, in contrast to a similar system reported by Castellano et al., which showed hydrogen production by oxidative quenching of the same PS using [$Co^{III}$(dmgH)$_2$pyCl] (220 μM PS, 220–500 μM [$Co^{III}$(dmgH)$_2$pyCl], acetonitrile MeCN/$H_2O$, 1:1, 70 mM dimethyl-*p*-toluidine, pH 6).[20b] This indicates that a slight change in the reaction conditions, or the axial ligands on the WRC, prevents the direct oxidative quench pathway. It is well-known that in the case of the oxime compounds, reduction to $Co^I$ is sufficient for $H_2$ evolution to occur,[5h,28] whereas reduction to a formal $Co^0$ is required in the case of the polypyridines.[5a,24] In the case of [$Co^{III}$(dmgH)$_2$(py)$_2$]$PF_6$ and [$Co^{III}$(DOH)$Br_2$], the potential of $MPP^•$ (−1.61 V vs. ($Fc^{+/0}$)) is sufficient to access the catalytically active $Co^I$ species, whereas in the case of [$Co^{II}$(aPPy)Br]Br and [$Co^{II}$(*bu*-pyrphyrin)(MeOH)Br], it is not (by 270 and 210 mV, respectively; Table 2). The active form of the catalyst most likely forms by disproportionation of the respective $Co^I$,[5i] thus explaining the low observed rates.

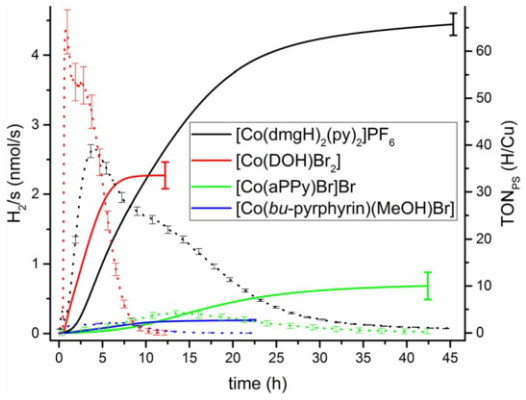


**Figure 4.** Hydrogen evolution rate ($H_2$/s, dotted lines) and $TON_{PS}$ (solid lines) over time of different cobalt based WRCs. Conditions: DMF, 0.5 mM [Cu(dsbtmp)$_2$]$BF_4$, 10 mM [MPP]$PF_6$, 1 M TEOA, 0.1 M $HBF_4$, different WRC concentrations (0.5 mM [Co(dmgH)$_2$(py)$_2$]$PF_6$, 0.23 mM [Co(DOH)$Br_2$], 50 μM [Co(aPPy)Br]Br, 10 μM [Co(*bu*-pyrphyrin)(MeOH)Br]). Irradiation with a 450 nm LED at a constant photon flux of 0.3 ± 0.04 μE $s^{-1}$.

**Table 2.** Reduction potentials of WRCs (DMF, 0.1 M [TBA]($PF_6$), V vs. $Fc^{+/0}$).

| Compound | $E_{red}$ ($Co^{III/II}$) [V] | $E_{red}$ ($Co^{II/I}$) [V] | $E_{red}$ ($Co^{I/0}$) [V] |
|---|---|---|---|
| [Co(dmgH)$_2$(py)$_2$]$PF_6$ | −0.78[c] | −1.53 | – |
| [Co(DOH)$Br_2$][a] | −0.57 | −1.11 | – |
| [Co(aPPy)Br]Br | – | −1.40 | −1.89 |
| [Co(*bu*-pyrphyrin)(MeOH)Br][b] | −0.26 | −1.12 | −1.82 |

[a] In MeCN.[28] [b] Ref. [24]. [c] Partial reversibility at high scan rates (≥ 10 $V s^{-1}$).

Decomplexation of [Cu(dsbtmp)$_2$]$^+$ seems to be a major deactivation pathway limiting the stability of the system, as shown below. In almost all catalytic runs the formation of a black precipitate accompanied by discoloration of the reaction solution was observed. In one case the solid was isolated and identified as elemental copper (SEM/energy-dispersive X-ray spectroscopy, Figure S10). Interestingly, the precipitate redissolved upon stirring the used reaction solution in air and the original orange color of the solution was recovered. Hydrogen evolution was restored from a used catalysis solution that had ceased $H_2$ production after the PS was regenerated using air without the addition of any fresh components. This indicated that photosensitizer stability limited the system through decomplexation and subsequent formation of elemental copper. Confirmation of this was found in comparative experiments employing the established rhenium and ruthenium based photosensitizers, in which a superior stability of the system was found (see Figure S4), indicating that [Co(DOH)$Br_2$] allows for more turnover under otherwise identical conditions. Conversely, the turnover number of the PS ($TON_{PS}$) increased from 33 to 65 when using [Co(dmgH)$_2$(py)$_2$]$^+$ instead of [Co(DOH)$Br_2$] (Figure 4), and was roughly halved by going from 0.5 mM to 1 mM PS (see Figure S3). However, the addition of an excess of phenanthroline ligand (dsbtmp, 5 mM) prevents, or at least diminishes the formation of the precipitate, as no decoloration or turbidity of the solution is observed anymore, allowing for an increase in $TON_{PS}$ from 34 ± 3 to 113 ± 9 (H/Cu, Figure S6). Even though HPLC analysis of [Cu(dsbtmp)$_2$]$BF_4$ in DMF always showed partial decomplexation, no formation of elemental copper was observed in the absence of catalytic conditions, indicating that $Cu^0$ is not formed by disproportionation. In line with this assignment, addition of MeCN to stabilize $Cu^I$ did not change the catalytic performance. Instead, we hypothesize a reduction of the solvated $Cu^I$ by photogenerated reducing equivalents (e.g. MPP radicals, or TEOA decomposition products). In summary, decomplexation of [Cu(dsbtmp)$_2$]$^+$ and subsequent




X

ChemPubSoc Europe

CHEMSUSCHEM Full Papers

reduction seems to limit catalysis in DMF/TEOA/[HTEOA](BF$_4$) mixtures. These findings are in contrast to the report of Castellano et al., in which the limitation of the system's stability was identified to be the WRC, restricting the TONs in PS to a maximum of approximately 70 (H/Cu; ≈360 after six recycling runs, in MeCN/H$_2$O).[20b] The group of Beller showed a stabilization of the heteroleptic [Cu(PP)(NN)]$^+$ PS by immobilization on TiO$_2$ and encapsulation in a plasma-polymerized allylamine layer, improving the maximum TONs from 1500 (H/Cu) in the homogeneous system to 2500 (H/Cu) in the heterogeneous system.[21d]

### Mechanistic investigations

Transient absorption experiments in the nanosecond to millisecond timescale unambiguously confirmed the proposed reaction sequence and allowed for a better understanding of the observed quantum yields in photocatalytic experiments. Upon excitation at 355 nm (6 ns pulse width), we observed prompt formation of the triplet excited state of the copper photosensitizer ($\tau = 1.1 \pm 0.1$ μs), which is characterized by a ground state bleach at 450 nm, as well as two new absorption bands at 540 nm and 580 nm (Figure 5, red trace), in line with literature reports.[20a] With the addition of MPP$^+$ (10 mM), quenching of the excited state was found at 295 ns, giving a bimolecular rate constant of $k_q = 2.6 \pm 0.1 \times 10^8$ L mol$^{-1}$ s$^{-1}$ (average of several experiments at varying [MPP$^+$], see Figure S7). A new absorption was observed with a maximum at 540 nm, which corresponds well with the spectrum of MPP$^•$ and oxidized PS (Figure 5 and confirmed the oxidative nature of the quenching process. By coincidence, both the excited PS and MPP$^•$ possess an absorption peak at 540 nm, however the two species are clearly distinguishable by their other absorption features (compare the red trace and green/blue trace in Figure 5). Because oxidized [Cu(dsbtmp)$_2$]$^+$ absorbs only very weakly at 540 nm,[18e] this wavelength was used to calculate the concentration of MPP$^•$. Its disappearance could be fitted to second order kinetics, giving a rate constant for the recombination with oxidized PS of $k_{rec} = 7.2 \pm 1.2 \times 10^8$ L mol$^{-1}$ s$^{-1}$ (average of several experiments at varying [MPP$^+$] and laser power, Figure S8). Upon addition of TEOA (1 M), the same spectral signature of MPP$^•$ and oxidized PS appears, but only the latter decays during the first microsecond owing to reaction with TEOA ($k_{TEOA} = 1.3 \pm 0.1 \times 10^6$ L mol$^{-1}$ s$^{-1}$, Figure S9). After 5 μs MPP$^•$ is formed with a cage escape yield $\Phi_{cage} \approx 0.6$, after 10 ms the absorption of the radical has clearly diminished but was still present with an estimated quantum yield of 0.2 (Figure 5, 10 ms). Between 1 and 10 μs recombination of MPP$^•$ with oxidized PS competes with regeneration of the latter by TEOA, causing the yield to drop from 0.6 to 0.3. This is in line with the observation that a higher yield of MPP$^•$ results at higher [TEOA]. On the millisecond timescale side reactions with decomposition products of oxidized TEOA likely interfere with MPP < MI, as seen before,[5i] causing the yield of MPP$^•$ to stabilize at 0.2 after 10 ms. As the spectrum of the radical is unaffected up to the millisecond timescale, and no effect of MPP$^•$ concentration is observed, dimerization is excluded, in line with literature observations [see Equation (2), $k_1 = 175$ L mol$^{-1}$ s$^{-1}$].[27b] Thus, electron transfer from the excited photosensitizer to the quencher occurs very fast and efficiently, whereas electron back-transfer is only partially inhibited owing to regeneration of the oxidized PS by an excess of TEOA.

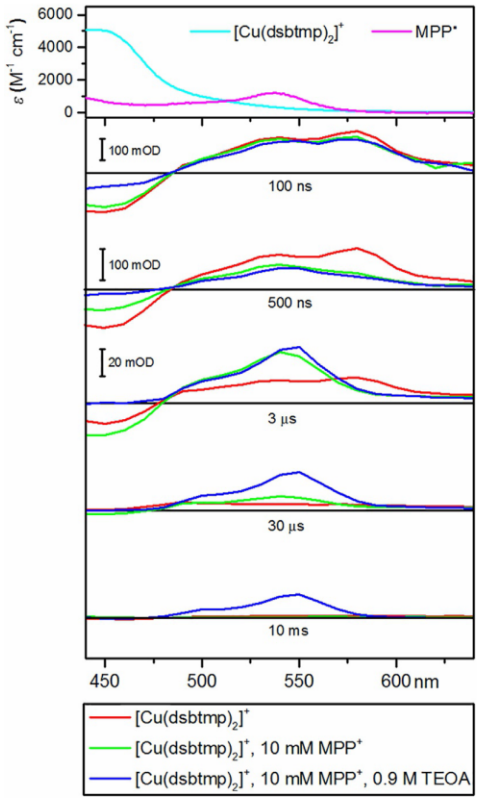


**Figure 5.** Summary of ground state and transient absorption spectra. All spectra were recorded in Ar-degassed DMF; laser excitation at 355 nm; Top: ground state absorption spectra of [Cu(dsbtmp)$_2$]BF$_4$ (cyan) and electrochemically produced MPP$^•$ (magenta). Below: transient absorption spectra at the given time delays of 0.5 mM [Cu(dsbtmp)$_2$]BF$_4$ (red), 0.5 mM [Cu(dsbtmp)$_2$]BF$_4$ and 10 mM [MPP]PF$_6$ (green), 0.5 mM [Cu(dsbtmp)$_2$]BF$_4$ and 10 mM [MPP]PF$_6$ with 1 M TEOA and 0.1 M HBF$_4$ (blue).

The same electron transfer sequence is expected to occur in the presence of a WRC, with subsequent electron transfer from MPP$^•$ to the WRC in the microsecond timescale.[5d,g,i,13,29] Additionally, any WRC can in principle oxidatively quench the PS's excited state,[20b,21] provided that it is thermodynamically allowed and that energy transfer does not dominate.[30,5a,f,h] The quantum yields for MPP$^•$ formation and hydrogen evolution (<0.03) differ significantly, indicating further limitations. The accumulation of reduced WRC, as required for most catalysts, most likely competes with TEOA for Cu$^{II}$ regeneration, thus limiting the overall yield. In summary, the combination of [Cu(dsbtmp)$_2$]$^+$, the electron acceptor MPP$^+$ and the sacrificial reductant TEOA increases the lifetime of the charge-separated state from approximately 1 μs to >10 ms, temporarily storing the absorbed energy in the form of an organic radical before it is passed on to a WRC.

ChemPubSoc Europe

CHEMSUSCHEM Full Papers

## Conclusions

The copper based photosensitizer (PS) $[Cu(dsbtmp)_2]^+$ (dsbtmp = 2,9-di-*sec*-butyl-1,10-phenanthroline) can be applied in a new reaction scheme for photocatalytic proton reduction using 1-methyl-4-phenyl-pyridinium ($MPP^+$) as oxidative quencher and triethanolamine (TEOA) as sacrificial reductant for the regeneration of the oxidized PS. The generated $MPP^•$ serves as an electron donor for several water reduction catalysts. This generates a quite general catalysis scheme for copper-based PSs. The turnover number (TON) (34 ± 3) in copper still leaves a lot of room for improvement as the stability of the catalytic reaction was clearly shown to be limited by the PS. Moreover, decomplexation of the PS and subsequent reduction to $Cu^0$ was observed, thus limiting the overall system stability. Stabilization of the PS consequently resulted in a drastically improved TON of 113 ± 9 in the PS, thus unambiguously confirming the stability limitation of the PS.

The development of more robust and water soluble copper bis-phenanthroline coordination complexes seems necessary and promising, provided that the excellent photophysical properties of $[Cu(dsbtmp)_2]^+$ can be maintained. This work opens the door for other strategies such as attachment of an electron acceptor to the backbone of the copper PS, which would allow for charge transfer even in the case of short lived PSs. Moreover, alternative electron acceptors must be identified, which could help to increase the quantum yield of the reaction. Conversely, integration of an (intermediate) electron donor in the PS structure would help to diminish the losses associated with the regeneration of the oxidized PS.

## Experimental Section

**Materials**: All commercially available chemicals were purchased at the highest available purity from Acros, Fluorochem, Sigma Aldrich, or TCI and used without further purification. The following materials were prepared according to known literature procedures: $[Co(dmgH)_2(py)_2]PF_6$,[31] $[Co(DOH)Br_2]$,[5f] [Co(aPPy)Br]Br,[5a] [Co(*bu*-pyrphyrin)(MeOH)Br].[24] 1*H*,1′*H*-2,2′-biimidazole (Blm)[32] and 1*H*,1′*H*-2,2′-bibenzo[d]imidazole (BBlm)[33] were used as precursors for the synthesis of the intermediates $[P_2Blm]Br_2$,[34] $[P_2BBlm]Br_2$ and $[B_2BBlm]Br_2$[35]. $[MP]PF_6$, $[NMIQ]PF_6$ and $[NMPhen]PF_6$,[36] $[MPP]PF_6$.[37] Counter ion exchange of intermediates $[P_2Blm]Br_2$, $[P_2BBlm]Br_2$ and $[B_2BBlm]Br_2$ as well as commercially available $[PV]Br_2$ to the corresponding $PF_6$-salts was performed similar to Collins et al..[36]

**Spectroscopy**: UV/Vis spectra were recorded on a Varian Cary 50 Scan in 1 cm quartz cuvettes and steady state luminescence spectra were recorded on a PerkinElmer LS50B in 1 cm quartz cuvettes.

**Electrochemistry**: Electrochemical measurements were performed in nitrogen degassed DMF using $[TBA]PF_6$ (TBA = tetrabutylammonium) as the supporting electrolyte. A Methrom 757 VA Computrace electrochemical analyzer was used with a glassy carbon working electrode ($d$ = 2 mm), a Pt auxiliary electrode and a Ag/AgCl reference electrode. All potentials were referenced to Fc as an internal standard and are given versus $Fc/Fc^+$.

**Excited state lifetimes**: Luminescence lifetime measurements were performed on an Edinburgh Instrument LP920 K system equipped with a pumped Q-switched Nd:YAG laser (Continuum Surelite), monochromator (Czerny–Turner with triple grating turret, 300 mm focal length) and a photomultiplier tube. Data analysis was performed using either the F900 package provided by Edinburgh Instruments or Origin by OriginLab Corporation.

**Transient absorption spectroscopy**: A home-constructed flash photolysis setup used a frequency-tripled Nd:YAG laser for sample excitation (355 nm, 6 ns pulse duration) and a two monochromator setup for single-wavelength detection to minimize the sample's exposure to probe light and remove most of the phosphorescence emitted by the photosensitizer.[5i] A white-light LED was used as a light source. The probe light was detected with an amplified silicon photodiode (Hamamatsu S3883, spectral response 320–1000 nm, bandwidth 300 MHz) and the signal was digitized with a transient recorder (125 MHz bandwidth, 200 MS $s^{-1}$, 16 bit resolution). The instrument can cover a range from 440 to 890 nm with a spectral resolution of approximately 10 nm and a time resolution of 30 ns. The maximum measurement time extends into the seconds range. Experiments were performed in a cuvette with a 2 mm path length.

**Hydrogen evolution measurements**: Gas chromatograms were recorded using either an automated Bruker GC-450 or GC-456 gas chromatograph with argon as carrier gas and a 3 m × 2 mm packed molecular sieve 13X 80–100 column. The column and reference gas flow (Ar) was set to 20 mL $min^{-1}$. The oven was operated isothermally at 100 °C. An argon flow of 6 mL $min^{-1}$ (adjusted with a manual flow controller (Porter, 100) or an onboard electronic flow control device for the GC-456 and referenced with a F-200CV-002 from Bronkhorst) was passed through the reaction mixture and into the GC, in which 100 µL gas samples were automatically injected at defined time intervals (usually 5 min) using a 6-Port 2-Position Valve from Vicci. The gases were detected using a thermal conductivity detector operated at 150 °C (retention time was ≈1 min for $H_2$). Calibration was achieved by mixing Ar and $H_2$ in known ratios with two mass flow controllers (Bronkhorst, F-201CV-200 for Ar and F-200CV-002 for $H_2$, 0.51 % $H_2$ in Ar (Pangas)). This setup allowed the detection of $H_2$ down to minimum mole fractions of $2\times10^{-5}$ and $2\times10^{-6}$ for GC-450 and GC-456, respectively. At Ar flows of 6 mL $min^{-1}$ through the reaction the detection limit was $H_2/s \geq 1\cdot10^{-10}$ and $\geq 1\cdot10^{-11}$ mol $s^{-1}$ for GC-450 and GC-456, respectively.

## Acknowledgements

*We wish to thank J. P. Sauvage for valuable discussions and his motivation to work with copper bis-phenantholine photosensitizers and the group of F. N. Castellano for the development of the very useful $[Cu(dsbtmp)_2]^+$ photosensitizer. We acknowledge the University of Zurich, the Swiss National Science Foundation (Grant CRSII2_160801/1) and the University of Zurich (URPP LightChEC) for financial support.*

**Keywords:** copper · oxidative quenching · photocatalysis · reaction mechanisms · time-resolved spectroscopy

[1] a) N. S. Lewis, D. G. Nocera, *Proc. Natl. Acad. Sci. USA* **2006**, *103*, 15729–15735; b) N. Armaroli, V. Balzani, *Angew. Chem. Int. Ed.* **2007**, *46*, 52–66; *Angew. Chem.* **2007**, *119*, 52–67.

[2] a) E. S. Andreiadis, M. Chavarot-Kerlidou, M. Fontecave, V. Artero, *Photochem. Photobiol.* **2011**, *87*, 946–964; b) V. Artero, M. Chavarot-Kerlidou, M. Fontecave, *Angew. Chem. Int. Ed.* **2011**, *50*, 7238–7266; *Angew. Chem.* **2011**, *123*, 7376–7405.

[3] a) D. J. Wasylenko, R. D. Palmer, C. P. Berlinguette, *Chem. Commun.* **2013**, *49*, 218–227; b) A. Sartorel, M. Bonchio, S. Campagna, F. Scandola, *Chem. Soc. Rev.* **2013**, *42*, 2262–2280; c) J. D. Blakemore, R. H. Crabtree, G. W. Brudvig, *Chem. Rev.* **2015**, *115*, 12974–13005.

ChemPubSoc Europe

CHEMSUSCHEM Full Papers

[4] a) S. Losse, J. G. Vos, S. Rau, *Coord. Chem. Rev.* **2010**, *254*, 2492 – 2504; b) N. Queyriaux, R. T. Jane, J. Massin, V. Artero, M. Chavarot-Kerlidou, *Coord. Chem. Rev.* **2015**, *304 – 305*, 3 – 19; c) A. Zarkadoulas, E. Koutsouri, C. Kefalidi, C. A. Mitsopoulou, *Coord. Chem. Rev.* **2015**, *304 – 305*, 55 – 72; d) W. T. Eckenhoff, R. Eisenberg, *Dalton Trans.* **2012**, *41*, 13004 – 13021; e) J. R. McKone, S. C. Marinescu, B. S. Brunschwig, J. R. Winkler, H. B. Gray, *Chem. Sci.* **2014**, *5*, 865 – 878; f) J. W. Jurss, R. S. Khnayzer, J. A. Panetier, K. A. El Roz, E. M. Nichols, M. Head-Gordon, J. R. Long, F. N. Castellano, C. J. Chang, *Chem. Sci.* **2015**, *6*, 4954 – 4972; g) R. S. Khnayzer, V. S. Thoi, M. Nippe, A. E. King, J. W. Jurss, K. A. El Roz, J. R. Long, C. J. Chang, F. N. Castellano, *Energy Environ. Sci.* **2014**, *7*, 1477 – 1488.

[5] a) C. Bachmann, M. Guttentag, B. Spingler, R. Alberto, *Inorg. Chem.* **2013**, *52*, 6055 – 6061; b) C. Bachmann, B. Probst, M. Guttentag, R. Alberto, *Chem. Commun.* **2014**, *50*, 6737 – 6739; c) M. Guttentag, A. Rodenberg, C. Bachmann, A. Senn, P. Hamm, R. Alberto, *Dalton Trans.* **2013**, *42*, 334 – 337; d) M. Guttentag, A. Rodenberg, R. Kopelent, B. Probst, C. Buchwalder, M. Brandstätter, P. Hamm, R. Alberto, *Eur. J. Inorg. Chem.* **2012**, 59 – 64; e) M. Oberholzer, B. Probst, D. Bernasconi, B. Spingler, R. Alberto, *Eur. J. Inorg. Chem.* **2014**, 3002 – 3009; f) B. Probst, M. Guttentag, A. Rodenberg, P. Hamm, R. Alberto, *Inorg. Chem.* **2011**, *50*, 3404 – 3412; g) B. Probst, C. Kolano, P. Hamm, R. Alberto, *Inorg. Chem.* **2009**, *48*, 1836 – 1843; h) B. Probst, A. Rodenberg, M. Guttentag, P. Hamm, R. Alberto, *Inorg. Chem.* **2010**, *49*, 6453 – 6460; i) A. Rodenberg, M. Orazietti, B. Probst, C. Bachmann, R. Alberto, K. K. Baldridge, P. Hamm, *Inorg. Chem.* **2015**, *54*, 646 – 657.

[6] A. Juris, V. Balzani, F. Barigelletti, S. Campagna, P. Belser, A. von Zelewsky, *Coord. Chem. Rev.* **1988**, *84*, 85 – 277.

[7] W. Jiang, J. Liu, C. Li, *Inorg. Chem. Commun.* **2012**, *16*, 81 – 85.

[8] a) P. Du, K. Knowles, R. Eisenberg, *J. Am. Chem. Soc.* **2008**, *130*, 12576 – 12577; b) R. Okazaki, S. Masaoka, K. Sakai, *Dalton Trans.* **2009**, 6127 – 6133; c) W.-G. Wang, F. Wang, H.-Y. Wang, C.-H. Tung, L.-Z. Wu, *Dalton Trans.* **2012**, *41*, 2420 – 2426.

[9] a) B. F. DiSalle, S. Bernhard, *J. Am. Chem. Soc.* **2011**, *133*, 11819 – 11821; b) F. Gärtner, D. Cozzula, S. Losse, A. Boddien, G. Anilkumar, H. Junge, T. Schulz, N. Marquet, A. Spannenberg, S. Gladiali, M. Beller, *Chem. Eur. J.* **2011**, *17*, 6998 – 7006; c) F. Gärtner, S. Denurra, S. Losse, A. Neubauer, A. Boddien, A. Gopinathan, A. Spannenberg, H. Junge, S. Lochbrunner, M. Blug, S. Hoch, J. Busse, S. Gladiali, M. Beller, *Chem. Eur. J.* **2012**, *18*, 3220 – 3225; d) D. N. Chirdon, W. J. Transue, H. N. Kagalwala, A. Kaur, A. B. Maurer, T. Pintauer, S. Bernhard, *Inorg. Chem.* **2014**, *53*, 1487 – 1499.

[10] T. Lazarides, T. McCormick, P. Du, G. Luo, B. Lindley, R. Eisenberg, *J. Am. Chem. Soc.* **2009**, *131*, 9192 – 9194.

[11] Z. Han, W. R. McNamara, M.-S. Eum, P. L. Holland, R. Eisenberg, *Angew. Chem. Int. Ed.* **2012**, *51*, 1667 – 1670; *Angew. Chem.* **2012**, *124*, 1699 – 1702.

[12] M. Natali, R. Argazzi, C. Chiorboli, E. Iengo, F. Scandola, *Chem. Eur. J.* **2013**, *19*, 9261 – 9271.

[13] T. Lazarides, M. Delor, I. V. Sazanovich, T. M. McCormick, I. Georgakaki, G. Charalambidis, J. A. Weinstein, A. G. Coutsolelos, *Chem. Commun.* **2014**, *50*, 521 – 523.

[14] A.-M. Manke, K. Geisel, A. Fetzer, P. Kurz, *Phys. Chem. Chem. Phys.* **2014**, *16*, 12029 – 12042.

[15] a) K. A. Brown, S. Dayal, X. Ai, G. Rumbles, P. W. King, *J. Am. Chem. Soc.* **2010**, *132*, 9672 – 9680; b) M. L. Tang, D. C. Grauer, B. Lassalle-Kaiser, V. K. Yachandra, L. Amirav, J. R. Long, J. Yano, A. P. Alivisatos, *Angew. Chem. Int. Ed.* **2011**, *50*, 10203 – 10207; *Angew. Chem.* **2011**, *123*, 10385 – 10389; c) F. Wang, W.-G. Wang, X.-J. Wang, H.-Y. Wang, C.-H. Tung, L.-Z. Wu, *Angew. Chem. Int. Ed.* **2011**, *50*, 3193 – 3197; *Angew. Chem.* **2011**, *123*, 3251 – 3255; d) J. Huang, K. L. Mulfort, P. Du, L. X. Chen, *J. Am. Chem. Soc.* **2012**, *134*, 16472 – 16475; e) Z. Han, F. Qiu, R. Eisenberg, P. L. Holland, T. D. Krauss, *Science* **2012**, *338*, 1321 – 1324; f) Z.-J. Li, X.-B. Li, J.-J. Wang, S. Yu, C.-B. Li, C.-H. Tung, L.-Z. Wu, *Energy Environ. Sci.* **2013**, *6*, 465 – 469.

[16] D. R. McMillin, M. T. Buckner, B. T. Ahn, *Inorg. Chem.* **1977**, *16*, 943 – 945.

[17] a) N. Armaroli, *Chem. Soc. Rev.* **2001**, *30*, 113 – 124; b) N. Armaroli, G. Accorsi, F. Cardinali, A. Listorti in *Photochemistry and Photophysics of Coordination Compounds I, Vol. 280* (Eds.: V. Balzani, S. Campagna), Springer, Berlin, **2007**, pp. 69 – 115; c) M. S. Lazorski, F. N. Castellano, *Polyhedron* **2014**, *82*, 57 – 70.

[18] a) M. W. Mara, K. A. Fransted, L. X. Chen, *Coord. Chem. Rev.* **2015**, *282 – 283*, 2 – 18; b) M. Iwamura, S. Takeuchi, T. Tahara, *Acc. Chem. Res.* **2015**, *48*, 782 – 791; c) T. J. Penfold, S. Karlsson, G. Capano, F. A. Lima, J. Rittmann, M. Reinhard, M. H. Rittmann-Frank, O. Braem, E. Baranoff, R. Abela, I. Tavernelli, U. Rothlisberger, C. J. Milne, M. Chergui, *J. Phys. Chem. A* **2013**, *117*, 4591 – 4601; d) G. Capano, U. Rothlisberger, I. Tavernelli, T. J. Penfold, *J. Phys. Chem. A* **2015**, *119*, 7026 – 7037; e) S. Garakyaraghi, E. O. Danilov, C. E. McCusker, F. N. Castellano, *J. Phys. Chem. A* **2015**, *119*, 3181 – 3193.

[19] A. Edel, P. A. Marnot, J. P. Sauvage, *Nouv. J. Chim.* **1984**, *8*, 495 – 498.

[20] a) C. E. McCusker, F. N. Castellano, *Inorg. Chem.* **2013**, *52*, 8114 – 8120; b) R. S. Khnayzer, C. E. McCusker, B. S. Olaiya, F. N. Castellano, *J. Am. Chem. Soc.* **2013**, *135*, 14068 – 14070.

[21] a) E. Mejía, S.-P. Luo, M. Karnahl, A. Friedrich, S. Tschierlei, A.-E. Surkus, H. Junge, S. Gladiali, S. Lochbrunner, M. Beller, *Chem. Eur. J.* **2013**, *19*, 15972 – 15978; b) S.-P. Luo, E. Mejía, A. Friedrich, A. Pazidis, H. Junge, A.-E. Surkus, R. Jackstell, S. Denurra, S. Gladiali, S. Lochbrunner, M. Beller, *Angew. Chem. Int. Ed.* **2013**, *52*, 419 – 423; *Angew. Chem.* **2013**, *125*, 437 – 441; c) S. Fischer, D. Hollmann, S. Tschierlei, M. Karnahl, N. Rockstroh, E. Barsch, P. Schwarzbach, S.-P. Luo, H. Junge, M. Beller, S. Lochbrunner, R. Ludwig, A. Brückner, *ACS Catal.* **2014**, *4*, 1845 – 1849; d) M. Karnahl, E. Mejía, N. Rockstroh, S. Tschierlei, S.-P. Luo, K. Grabow, A. Kruth, V. Brüser, H. Junge, S. Lochbrunner, M. Beller, *ChemCatChem* **2014**, *6*, 82 – 86.

[22] a) K. L. Cunningham, C. R. Hecker, D. R. McMillin, *Inorg. Chim. Acta* **1996**, *242*, 143 – 147; b) K. L. Cunningham, D. R. McMillin, *Inorg. Chem.* **1998**, *37*, 4114 – 4119.

[23] In addition to the thermodynamic restriction on reductive quenching, a kinetic barrier can also be present, which arises from an innersphere reorganization. This effect is very pronounced if the 2,9-substituents on the phenanthroline ligand allow for strong distortions of the complex, as was shown for $[Cu(dpp)_2]^+$ (dpp = 2,9-diphenyl-1,10-phenanthroline), which has a self-exchange rate of about $10^5\,L\,mol^{-1}\,s^{-1}$ for reductive quenching. However, the self-exchange rate increases to $2\times 10^8\,L\,mol^{-1}\,s^{-1}$ for $[Cu(dipp)_2]^+$ (dipp = 2,9-diisopropyl-1,10-phenanthroline) owing to its more rigid structure. Similarly, only a marginal kinetic barrier is expected for $[Cu(dsbtmp)_2]^+$.

[24] E. Joliat, S. Schnidrig, B. Probst, C. Bachmann, B. Spingler, K. K. Baldridge, F. von Rohr, A. Schilling, R. Alberto, *Dalton Trans.* **2016**, *45*, 1737 – 1745.

[25] J. V. Caspar, T. J. Meyer, *J. Am. Chem. Soc.* **1983**, *105*, 5583 – 5590.

[26] a) R. A. Marcus, *J. Chem. Phys.* **1956**, *24*, 966 – 978; b) R. A. Marcus, *J. Chem. Phys.* **1956**, *24*, 979 – 989; c) R. A. Marcus, *J. Chem. Phys.* **1957**, *26*, 867 – 871.

[27] a) K. Akiyama, S. Kubota, Y. Ikegami, *Chem. Lett.* **1981**, *10*, 469 – 472; b) M. A. Oturan, P. Dostert, M. S. Benedtti, J. Moiroux, A. Anne, M. B. Fleury, *J. Electroanal. Chem.* **1988**, *242*, 171 – 179.

[28] P.-A. Jacques, V. Artero, J. Pécaut, M. Fontecave, *Proc. Natl. Acad. Sci. USA* **2009**, *106*, 20627 – 20632.

[29] a) E. Deponti, A. Luisa, M. Natali, E. Iengo, F. Scandola, *Dalton Trans.* **2014**, *43*, 16345 – 16353; b) R. Gueret, C. E. Castillo, M. Rebarz, F. Thomas, A.-A. Hargrove, J. Pécaut, M. Sliwa, J. Fortage, M.-N. Collomb, *J. Photochem. Photobiol. B* **2015**, *152*, 82 – 94; c) C. Bachmann, B. Probst, M. Oberholzer, T. Fox, R. Alberto, *Chem. Sci.* **2016**, *7*, 436 – 445.

[30] In our experience, oxidative quenching of excited states by a WRC is difficult. We always found rather low to zero cage escape yields for the first reduction, whereas the second reduction is very difficult to assess at all owing to the inherent instability of one electron reduced WRCs (e.g., $Co^{I}$ species).

[31] B. Probst, PhD thesis, University of Zurich (Switzerland), **2010**.

[32] J.-C. Xiao, B. Twamley, J. n. M. Shreeve, *Org. Lett.* **2004**, *6*, 3845 – 3847.

[33] J. Yin, R. L. Elsenbaumer, *J. Org. Chem.* **2005**, *70*, 9436 – 9446.

[34] R. P. Thummel, V. Goulle, B. Chen, *J. Org. Chem.* **1989**, *54*, 3057 – 3061.

[35] Z. Shi, R. P. Thummel, *J. Org. Chem.* **1995**, *60*, 5935 – 5945.

[36] P. Bolduc, A. Jacques, S. K. Collins, *J. Am. Chem. Soc.* **2010**, *132*, 12790 – 12791.

[37] A. Deutman, T. Woltinge, J. Smits, R. De Gelder, J. Elemans, R. Nolte, A. Rowan, *Molecules* **2014**, *19*, 5278.

Received: March 31, 2016
Published online on May 25, 2016

CHEMISTRY & SUSTAINABILITY
CHEMSUSCHEM
ENERGY & MATERIALS

Supporting Information

# General Scheme for Oxidative Quenching of a Copper Bis-Phenanthroline Photosensitizer for Light-Driven Hydrogen Production

J. Windisch, M. Orazietti, P. Hamm, R. Alberto,* and B. Probst*[a]

cssc_201600422_sm_miscellaneous_information.pdf

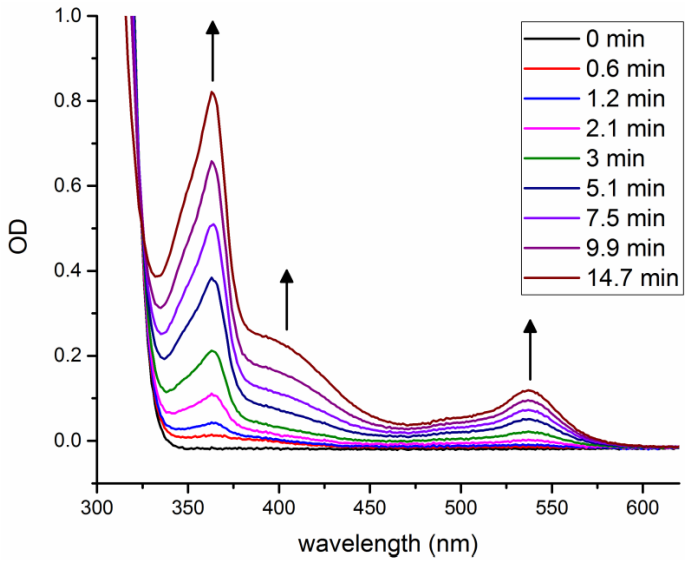


**Figure S1:** UV/Vis spectroelectrochemical analysis of $MPP^+$, scanning from 0 V to -1.3 V (vs Ag/AgCl). Conditions: DMF, 3 mM $MPP(PF_6)$, 0.1 M $TBAPF_6$, in an OTTLE cell with 1 mm pathlength using a Pt-gauze working electrode, Pt-wire counter electrode and Ag/AgCl reference electrode. Estimated equilibrium concentrations of $[MPP^{\cdot}]$ and $[(MPP)_2]$ are 1.14 and 0.93 mM, respectively,[1] and thus $\varepsilon_{540nm}$ = 1200 ± 200 $M^{-1}$ $cm^{-1}$ and $\varepsilon_{365}$ = 7400 ± 1200 $M^{-1}$ $cm^{-1}$.

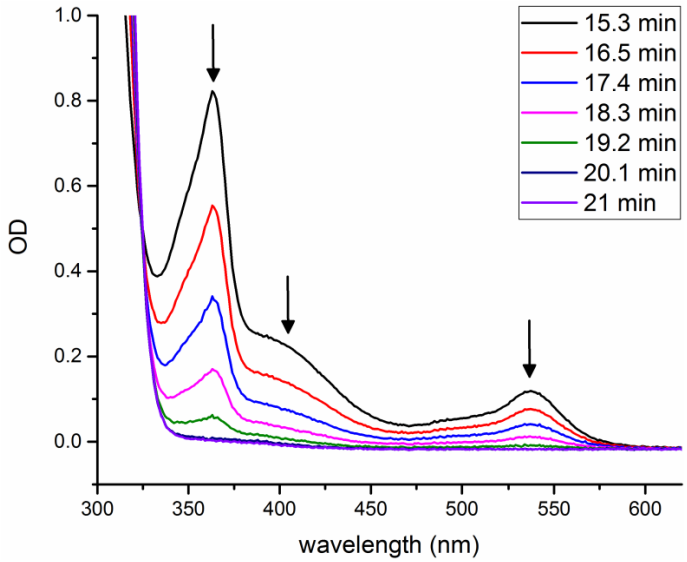


**Figure S2:** UV/Vis spectroelectrochemical analysis of $MPP^+$, scanning from -1.3 V to 0 V (vs Ag/AgCl). Conditions: DMF, 3 mM $MPP(PF_6)$, 0.1 M $TBAPF_6$, in an OTTLE cell with 1 mm pathlength using a Pt-gauze working electrode, Pt-wire counter electrode and Ag/AgCl reference electrode.

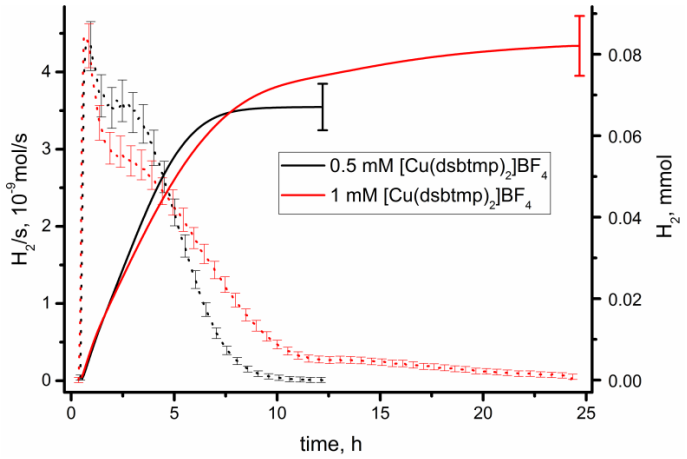


**Figure S3:** TONs of the photosensitizer plotted over time at different [PS]. Conditions: DMF, 0.23 mM [Co(DOH)$Br_2$], 10 mM [MPP]$PF_6$, 1 M TEOA, 0.1 M $HBF_4$, different [PS] according to the legend. Irradiation with a 450 nm LED at a constant photonflux of 0.3 ± 0.04 µE $s^{-1}$

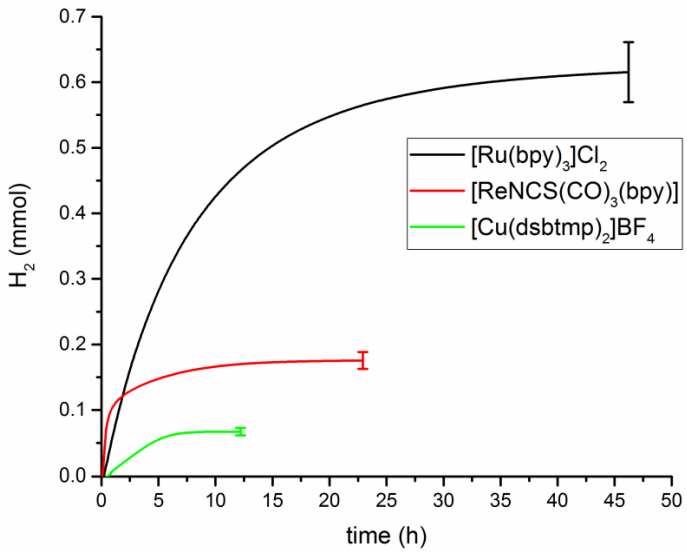


**Figure S4:** Comparison of the total amount of evolved hydrogen for different photosensitizers with [Co(DOH)$Br_2$] in DMF. Conditions: DMF, 0.5 mM PS, 0.23 mM [Co(DOH)$Br_2$], 1 M TEOA, 0.1 M $HBF_4$, additionally 10 mM [MPP]$PF_6$ in case of the Cu-PS. Irradiation with a 450 nm LED for Ru- and Cu-PS, irradiation with a 390 nm LED for the Re-PS at a constant photonflux of 0.3 ± 0.04 µE $s^{-1}$.

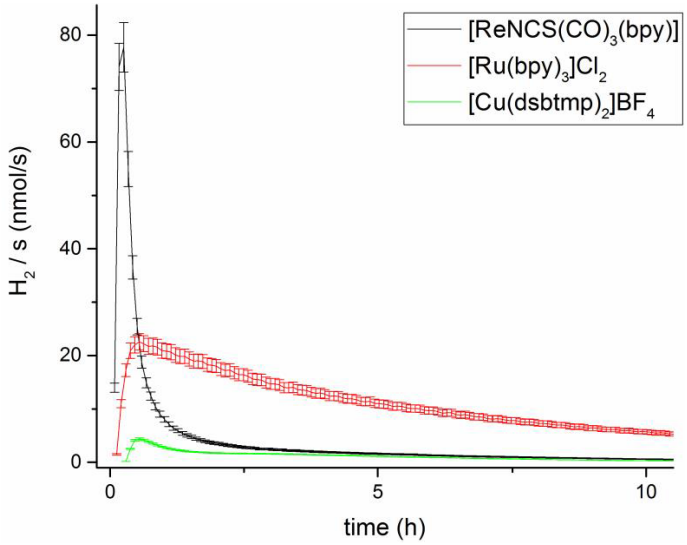


**Figure S5:** Comparison of the rate of hydrogen evolution for different photosensitizers with [Co(DOH)$Br_2$] in DMF. Conditions: DMF, 0.5 mM PS, 0.23 mM [Co(DOH)$Br_2$], 1 M TEOA, 0.1 M $HBF_4$, additionally 10 mM [MPP]$PF_6$ in case of the Cu-PS. Irradiation with a 450 nm LED for Ru- and Cu-PS, irradiation with a 390 nm LED for the Re-PS at a constant photonflux of 0.3 ± 0.04 µE $s^{-1}$.

**Table S1:** Reduction potentials of the investigated electron acceptors. All potentials were measured in DMF and are given vs the Fc/Fc+ couple.

| Quencher | $E_{red1}$ | $E_{red2}$ |
|---|---|---|
| $PV^{2+}$ | -0.67 | -0.95 |
| $MV^{2+}$ (ref [2]) | -0.90[a] | -1.28[a] |
| $B_2BBIm^{2+}$ | -1.26[a] | -1.44[a] |
| $NMPhen^{+}$ | -1.25[b] | n.a. |
| $NMIQ^{+}$ | -1.52[b] | n.a. |
| $MPP^{+}$ | -1.61[a] | n.a. |
| $P_2BIm^{2+}$ | -1.58[c] | -1.72[c] |
| $MP^{+}$ | -1.74[b] | n.a. |

[a]: reversible half-wave potential; [b]: cathodic/anodic peak potential of the irreversible reduction; [c]: determined as the peak potential from Gaussian fitting of the DP voltammogram, since the two reversible reductions are very closely spaced.

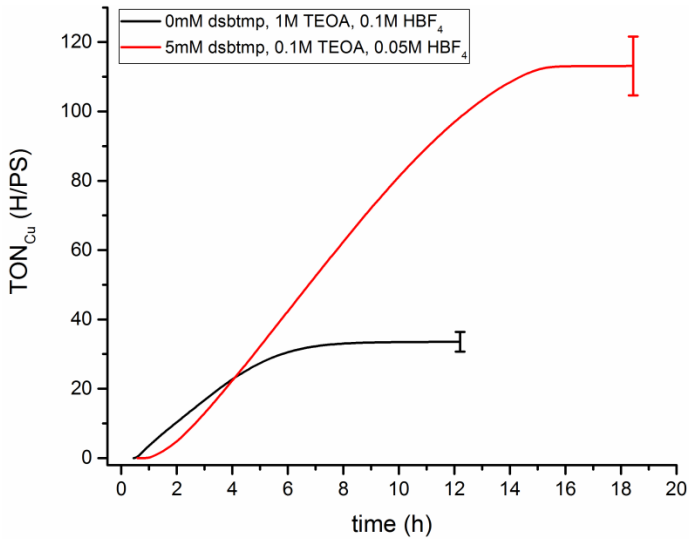


**Figure S6:** $TON_{Cu}$ over time, showing the effect of excess dsbtmp-ligand. Conditions: DMF, 0.5 mM $[Cu(dsbtmp)_2]BF_4$, 10 mM $[MPP]PF_6$, 0.23 mM $[Co(DOH)Br_2]$, varying concentrations of TEOA, $HBF_4$ and dsbtmp according to the legend. Irradiation with a 450 nm LED at a constant photonflux of 0.3 ± 0.04 µE $s^{-1}$.

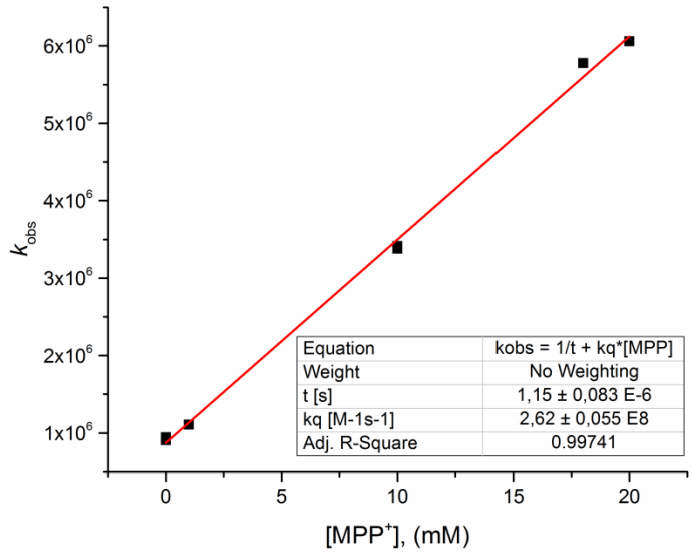


**Figure S7:** First order analysis for the oxidative quenching of excited $[Cu(dsbtmp)_2]BF_4$ (0.5 mM, 355 nm excitation) by varying concentrations of $MPP^+$ according to $1/\tau = k_q \cdot [MPP^+] + 1/\tau_0$ ($\tau_0$ is the lifetime in the absence of $MPP^+$, $k_q$ the bimolecular quench constant, $\tau$ the photosensitizer lifetime in the presence of $MPP^+$ and $[MPP^+]$ the quencher concentration; Ar degassed DMF solutions; either luminescence emission decay at 630 nm or transient absorption decay at 590).

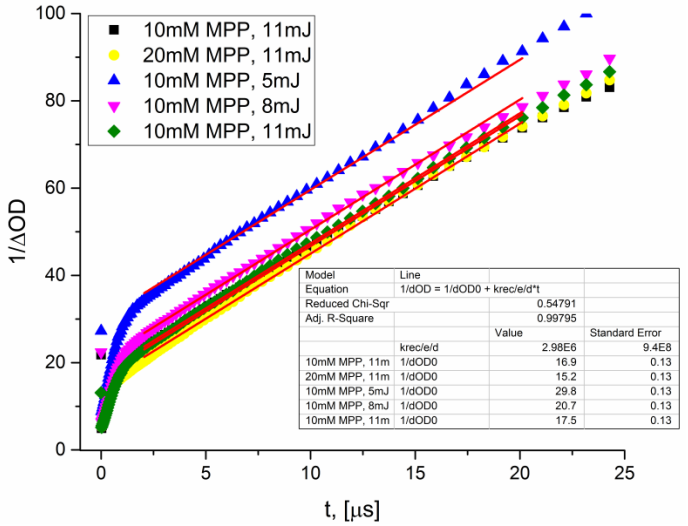


**Figure S8:** Second order analysis of the recombination reaction between oxidised $[Cu(dsbtmp)_2]BF_4$ (0.5 mM) and reduced $MPP^+$, according to $1/\Delta OD = k_{rec}/\varepsilon_{540}/d \cdot t + 1/\Delta OD_0$ ($\varepsilon_{540}$ = 1200 ± 200, d = 0.2 cm) for varying [$MPP^+$] and laser power (see legend), as observed at 540 nm after excitation at 355 nm. $k_{rec}$ = 7.2 ± 1.2 × $10^8$ $M^{-1}$ $s^{-1}$.

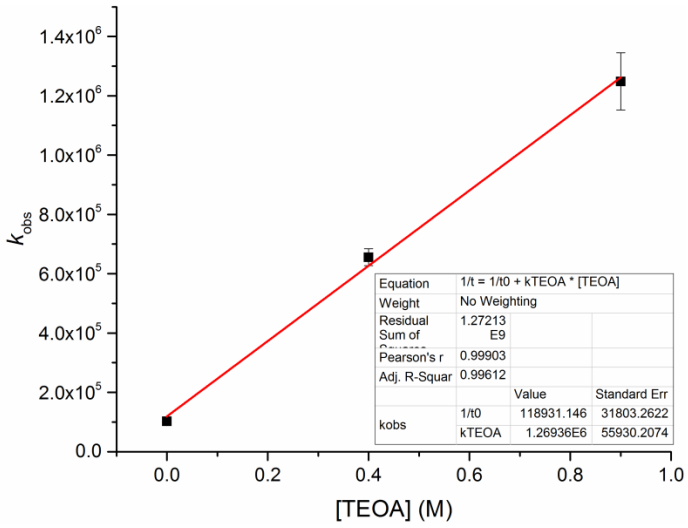


**Figure S9:** First order analysis of the regeneration reaction between oxidised $[Cu(dsbtmp)_2]BF_4$ (0.5 mM) and TEOA, according to $1/\tau = k_{TEOA} \cdot [TEOA] + 1/\tau_0$, observed at 450 nm after excitation at 355 nm. $k_{TEOA}$ = 1.3 ± 0.1× $10^6$ $M^{-1}$ $s^{-1}$.

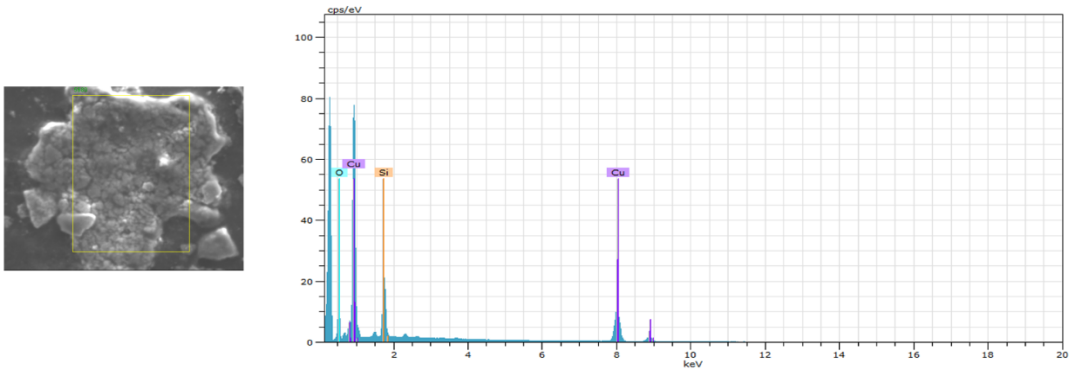


**Figure S10:** SEM-picture (left) and EDX spectrum (right) of the black precipitate observed after photocatalysis (0.5 mM $[Cu(dsbtmp)_2]BF_4$, 0.23 mM $[Co(DOH)Br_2]$, 10 mM $[MPP]PF_6$, 0.1 M TEOA, 50 mM $HBF_4$, 450 nm, DMF).

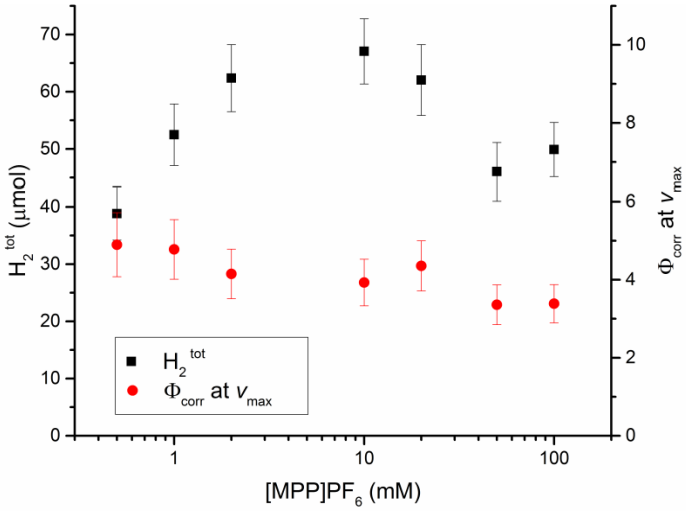


**Figure S11:** Total amount of evolved hydrogen and quantum yields $\Phi_{corr}$ at the maximum $H_2$ evolution rate ($v_{max}$) as a function of quencher concentration. The quantum yields at the maximum $H_2$ evolution rate were calculated according to $v_{max}/(q_p \times \Phi_{q,max})$; $v_{max}$ is the maximum hydrogen evolution rate, $q_p$ the photon flux (0.3 ± 0.04 µE $s^{-1}$) and $\Phi_{q,max}$ the calculated maximum quench yield. Conditions: DMF, 0.5 mM $[Cu(dsbtmp)_2]BF_4$, 0.23 mM $[Co(DOH)Br_2]$, 1 M TEOA, 0.1 M $HBF_4$, $[MPP]PF_6$ varied from 0.5 - 100 mM, total volume of 8 mL, irradiation with a 450 nm LED.

**Table S2:** Elemental composition of the black precipitate observed after photocatalysis, as calculated from the EDX-spectrum.

| Element | AN | Series | Unn. C [wt.%] | Norm. C [wt.%] | Atom. C [at.%] | Error [wt.%] |
|---|---|---|---|---|---|---|
| O | 8 | K-Series | 8.56 | 13.20 | 33.60 | 1.0 |
| Si | 14 | K-Series | 8.64 | 13.34 | 19.34 | 0.4 |
| Cu | 29 | K-Series | 47.61 | 73.46 | 47.07 | 1.4 |
| | | **Total** | 64.81 | 100.00 | 100.00 | |

## References

[1] M. A. Oturan, P. Dostert, M. S. Benedtti, J. Moiroux, A. Anne, M. B. Fleury, *J. Electroanal. Chem.* **1988**, *242*, 171-179.
[2] M. Jonsson, A. Houmam, G. Jocys, D. D. M. Wayner, *J. Chem. Soc., Perkin Trans. 2* **1999**, 425-430.